Effects of nonlinear quantum electrodynamics on the interaction of extremely intensive laser pulses and high-current beams of ultrarelativistic particles with matter

Inaugural dissertation

for the attainment of the title of doctor
in the Faculty of Mathematics and Natural Sciences
at the Heinrich Heine University Düsseldorf

presented by

Alexander Samsonov
from Nizhny Novgorod

Düsseldorf, April 2024

from the institute for Theoretical Physics I
at the Heinrich Heine University Düsseldorf

Published by permission of the
Faculty of Mathematics and Natural Sciences at
Heinrich Heine University Düsseldorf

Supervisor: Prof. Dr. Alexander Pukhov
Co-supervisor: Prof. Dr. Carsten Müller

Date of the oral examination: 09/04/2024

Abstract

Record field strengths are expected to be achieved using multi-petawatt femtosecond lasers or high-current beams of ultrarelativistic particles on the next generation of accelerators in the near future. This will make it feasible to experimentally investigate interaction of matter and strong fields. The nonlinear regime of quantum electrodynamics (QED) can be achieved during such an interaction, leading to manifestation of new effects. These effects, which include, e.g. production of electron-positron pairs, were theoretically predicted a long time ago, although have not yet been observed experimentally. Investigation of the impact of nonlinear QED processes on the behavior of matter is one of the frontiers of theoretical physics nowadays and is far from being complete. In this thesis, we aim to further extend the understanding of processes in strong fields.

In the first part of the work, general properties of particle motion under effect of extreme radiation reaction are investigated. It is shown that particles are attracted to some asymptotic trajectories, which can be found from reduced motion equations. One of the implications of such behavior is the periodicity of particle trajectories in a large class of field configurations. This can explain an effect of radiative trapping of particles in a region of strong field. A general method for approximate solution of the motion equations with account of radiation reaction is proposed. Utilizing this method, several known solutions are reproduced.

In the second part of the work, a new effect is discovered and described, namely development of self-sustained QED cascade in field of a single plane wave. It is demonstrated that dense electron-positron plasma is able to alter propagation of a strong plane wave. This results in a field configuration, which is favorable for production and multiplication of electron-positron pairs. Ultimately, this leads to a steady expansion of the electron-positron plasma towards the laser radiation until the latter is completely absorbed. It is shown that dense enough electron-positron plasma can be initially produced, e.g. during interaction of an extremely intensive plane wave with a thin stationary solid target.

In the third part of the work, impact of QED processes on interaction of high-current beams of ultrarelativistic particles with matter is considered. First, a model for calculation of disruption parameter in beam-beam collision with account of beamstrahlung is developed. Second, an efficient generation of gamma radiation in the interaction of a dense electron beam with a thick plasma target is demonstrated. A model is developed for calculating the efficiency of conversion of the beam energy to the energy of gamma radiation. Finally, an alternative numerical scheme for solving Maxwell's equations on a rectangular grid is developed, which facilitates to sufficiently suppress numerical Cherenkov instability, present in the commonly used schemes.

Zusammenfassung

Es wird erwartet, dass mittels Multi-Petawatt-Femtosekunden-Lasern oder ultrarelativistischen Teilchenstrahlen hoher Stromstärke Rekord-Feldstärken in der nächsten Generation an Beschleunigern erzielt werden. Dies wird es möglich machen, experimentell die Wechselwirkung von Materie und starken Feldern zu untersuchen. Das nicht-lineare Regime der Quantenelektrodynamik (QED) kann durch solche Wechselwirkungen erreicht werden, und führt zur Manifestierung neuer Effekte. Diese Effekte, welche z.B. die Produktion von Elektronen-Positronen-Paaren einschließen, wurden vor langer Zeit theoretisch vorhergesagt, aber bislang nicht experimentell beobachtet. Die Untersuchung des Einflusses nicht-linearer QED-Effekte auf das Verhalten von Materie ist Gegenstand aktueller Forschung in der theoretischen Physik und noch lange nicht abgeschlossen. In dieser Dissertation wollen wir das Verständnis dieser Prozesse in starken Feldern erweitern.

Im ersten Teil der Arbeit werden generelle Eigenschaften der Teilchen-Bewegung unter dem Einfluss extremer Strahlungsrückwirkung untersucht. Es wird gezeigt, dass die Teilchen sich auf asymptotische Trajektorien hingezogen werden, welche durch die reduzierten Bewegungsgleichungen gefunden werden können. Eine Konsequenz dieses Verhaltens ist die Periodizität der Teilchenbahnen für eine große Klasse an Feld-Konfigurationen. Dies erlaubt eine Erklärung des Strahlungseinfangs von Teilchen in einer Region mit starkem Feld. Eine allgemeine Methode für eine Näherungs-Lösung der Bewegungsgleichungen unter Berücksichtigung der Strahlungsrückwirkung wird vorgestellt. Mithilfe dieser Methode können mehrere bekannte Ergebnisse reproduziert werden.

Im zweiten Teil der Arbeit wird ein neuer Effekt entdeckt und beschrieben, nämlich die Entwicklung einer selbst-erhaltenden QED-Kaskade im Feld einer einzelnen ebenen Welle. Es wird gezeigt, dass ein dichtes Elektronen-Positronen-Plasma dazu in der Lage ist, die Propagation einer starken ebenen Welle zu verändern. Dies resultiert in einer Feldkonfiguration, welche für die Produktion und Vervielfachung von Elektronen-Positronen-Paaren hilfreich ist. Letztlich führt dies zu einer stetigen Expansion des Elektronen-Positronen-Plasmas in Richtung der Laser-Strahlung bis letztere vollständig absorbiert wird. Es wird gezeigt, dass ein Elektronen-Positronen-Plasma von hinreichender Dichte erzeugt werden kann, z.B. währender der Wechselwirkung einer extrem starken ebene Welle mit einem dünnen, stationären Festkörper-Target.

Im dritten Teil der Arbeit wird der Einfluss von QED-Prozessen auf die Wechselwirkung von ultra-relativistischen Teilchenstrahlen hoher Stromstärke mit Materie untersucht. Zunächst wird ein Modell zur Berechnung des Disruption-Parameters in Beam-Beam-Kollisionen unter Berücksichtigung von Beam-Strahlung entwickelt. Zweitens wird gezeigt, dass Gammastrahlung in der Wechselwirkung eines dichten Elektronenstrahls mit einem dicken Plasma-Target effizient erzeugt werden kann. Letztlich wird ein alternatives numerisches Schema zur Lösung der Maxwell-Gleichungen auf einem rechteckigen Gitter entwickelt, welches es erlaubt, die numerische Cherenkov-Instabilität zu unterdrücken, welche in konventionellen Schemata präsent ist.

Contents

Chapter 1

Introduction

1.1 Motivation

Quantum electrodynamics (QED), which describes the interaction of charged particles and electromagnetic (EM) field, is currently the most accurate physical theory in terms of experimental confirmation of its predictions. However, a number of analytical results of nonlinear QED, the main of which is the production of electron-positron pairs from vacuum (the Sauter-Schwinger effect) [1, 2] in a strong constant field, were first made back in the 1930s but have not yet been experimentally confirmed. With the expected commissioning of a new generation of multipetawatt and subexawatt laser facilities in the coming years, such as ELI [3], Apollon [4], SULF [5], SEL [6], XCELS [7], etc., experimental study of the interaction of radiation with matter in the regime of extreme intensity will become available, which opens up new possibilities for observing the effects of *strong-field* QED. For determining which field is strong according to QED, four Lorentz-invariant parameters are responsible: a_0, $\mathscr{F}$, $\mathscr{G}$, χ.

The parameter a_0 — the classical nonlinearity parameter — determines the dimensionless amplitude of the external EM field and the significance of relativistic effects

$$a_0 = \frac{e}{mc}\sqrt{-A_\mu A^\mu} \equiv \frac{eE_0}{mc\omega} \approx 0.85\sqrt{I[10^{18}\,\mathrm{W/cm^2}]}\lambda[\mu\mathrm{m}], \tag{1.1}$$

where m and $e > 0$ — the mass and absolute value of the electron charge, respectively, c — the speed of light, A_μ — vector potential of the EM field, E_0 and ω — characteristic magnitude and frequency of EM field variation, respectively. For $a_0 > 1$, the motion of charged particles becomes relativistic. The progress of laser technology in the 20th century made it possible to implement Veksler's idea of coherent acceleration of particles [8] by generating high accelerating gradients in plasma during the propagation of intense laser radiation in it. Currently, laser acceleration of electrons [9–18], ions [19–27] and even positrons [28–31] is regarded as one of the most promising alternatives to classical accelerators and one of the most important goals in both experimental and theoretical physics.

The parameters $\mathcal{F}$ and $\mathcal{G}$ determine the interaction of the EM field with the quantum *vacuum* and are defined as follows

$$\mathcal{F} = \frac{E^2 - B^2}{E_S^2}, \tag{1.2}$$

$$\mathcal{G} = \frac{\mathbf{E} \cdot \mathbf{B}}{E_S^2}, \tag{1.3}$$

where $E_S = m^2c^3/e\hbar$ is a critical field of QED or Sauter-Schwinger field [32, 33], $\hbar$ — Planck's constant. Production of electron-positron pairs from vacuum is exponentially suppressed at $|\mathcal{F}| \lesssim 1$, which explains the difficulty of its experimental observation. At the same time, for example, vacuum birefringence [34–37], which is also one of the earliest predictions of QED, and which is determined by the quantities $\mathcal{F}$ and $\mathcal{G}$, is confirmed in experiments in the region of $|\mathcal{F}| \ll 1$ both indirectly [38, 39] and directly [40]. Note that the fields of laser pulses and charged particle beams (see below) are crossed, so the values of the parameters $\mathcal{F}$ and $\mathcal{G}$ are close to zero in such configurations. In what follows, it will always be assumed that $\mathcal{F} = \mathcal{G} = 0$.

Finally, the parameter χ determines the significance of purely quantum effects in the interaction of the EM field with particles

$$\chi = \frac{e\hbar\sqrt{-\left(F_{\mu\nu}p^\nu\right)^2}}{m^3c^4} = \frac{1}{E_S mc}\sqrt{\left(\frac{\varepsilon}{c}\mathbf{E} + \mathbf{p} \times \mathbf{B}\right)^2 - (\mathbf{pE})^2}, \tag{1.4}$$

where $F_{\mu\nu} = \partial_\mu A_\nu - \partial_\nu A_\mu$ — EM field tensor, ε and $\mathbf{p}$ — energy and momentum of the particle respectively. This expression can be written for photons in a similar way, taking into account that $\varepsilon = \hbar\omega$, $p^\nu = \hbar k^\nu$. Here it is necessary to point out an important distinction between the quantum description of the EM field as a collection of photons and the classical description in terms of field strengths. At large occupation numbers, the quantum description coincides with the classical one, so relatively strong external fields are described classically, and single photons produced as a result of QED processes are described using the quantum approach itself. Moreover, the interaction of electrons (and positrons) with a strong classical field ($a_0 > 1$) in QED must be taken into account nonperturbatively, i.e. in all orders of perturbation theory, which is done using the Furry picture [41] and the use of Volkov functions to describe the state of electrons [42] (the specifics of this method is described in more detail, for example, in the recent review [43]). The classical external field also often differs significantly from the photons produced by the particles radiating in this external field from the spectral point of view. Thus, extremely strong EM fields are currently available mainly in the optical range $\hbar\omega_L \sim 1$ eV, while the characteristic frequency of particle radiation in such a field, which can be estimated from synchrotron formulas as $\hbar\omega \sim \gamma^3\hbar\omega_L$, usually lies in the X-ray or even gamma range.

In the $\chi > 1$ regime, quantum processes leading to the production of electron-positron pairs become probable. These include, for example, the Breit-Wheeler process [44], in which a hard photon «decays» into an electron-positron pair, and the so-called *trident* process [45], in which an electron or positron emits a virtual photon, which decays into an electron-positron pair (see Fig. 1.1). Note that the probability of the Breit-Wheeler process significantly exceeds the probability of the trident process in the region of high intensities [46], so the latter will not be taken into account in this thesis. These processes are exponentially suppressed at $\chi \lesssim 1$ and are in many respects similar to the pro-

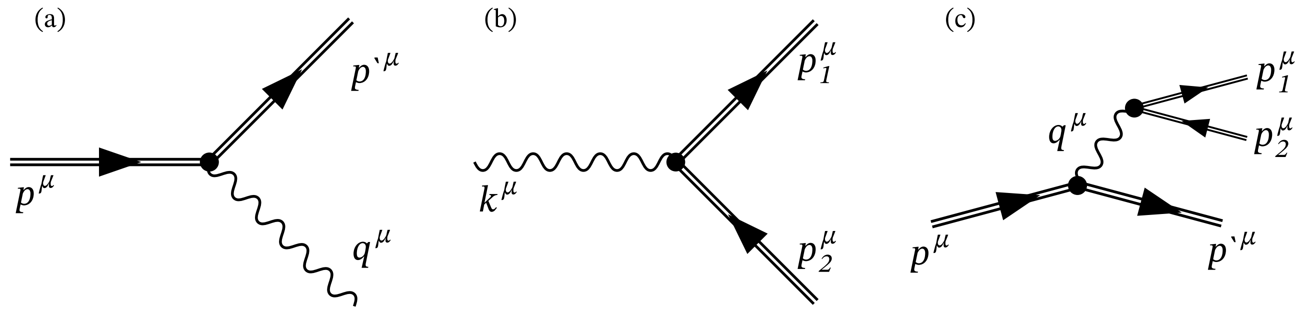

Figure 1.1: Some QED processes in an external field. (a) Compton scattering, (b) Breit-Wheeler process, (c) trident process. The double straight line corresponds to the «dressed» state of an electron in an external field, described by the Volkov function (see text).

cess of formation of electron-positron pairs by the Sauter-Schwinger mechanism. However, even in this regime, when the production of electron-positron pairs is suppressed, the interaction of charged particles with the EM field can change significantly due to effect of *radiation reaction*. The very fact that charged particles experience a recoil force from their own radiation has been known for more than a century and was originally described in the framework of classical electrodynamics. However, it led to the inconsistency of the concept of an electron as a point object and marked the applicability limit of the classical ED, which can be determined by the condition $E_{\text{cl}} = m^2c^4/e^3 = E_{\text{S}}/\alpha$. A field of such intensity is created by an electron at a distance of its classical radius $r_e = e^2/mc^2$. Note that it is $1/\alpha \approx 137$ times greater than the critical field of QED, so quantum effects appear «earlier» than classical ED becomes self-contradictory. Quantum electrodynamics describes the emission of photons by electrons in a consistent manner and, as expected, coincides with the results of classical ED in the classical limit $\chi \ll 1$. Of particular interest, however, is the modification of the emission spectrum and the significant recoil effect in the $\chi \sim 1$ regime, which has not yet been practically studied experimentally. Until recently, there was only one example from the 1990s, namely the E-144 experiment at the SLAC accelerator, where an electron beam with an energy of 46.6 GeV interacted with a laser pulse with an intensity of $I \sim 10^{18}$ W/cm^2 ($a_0 \lesssim 1$, $\chi \ll 1$), producing high-energy photons and electron-positron pairs [47, 48]. Recently, conceptually similar experiments were carried out at the Astra Gemini facility, where one laser pulse was used to accelerate electrons, and the second one for scattering the accelerated electrons [49, 50]. It is important to note that despite the undeniable value of these experiments, their results contain a certain level of uncertainty, which does not yet allow us to confidently confirm the QED predictions in the $\chi \sim 1$ regime. Due to the development of technologies of both laser facilities and accelerators, new experiments in strong field physics are expected in the near future, in particular, the direct successor of the E-144 experiment — experiment E-320, which is expected to achieve a sufficiently quantum regime of interaction [51] ($a_0 > 1$, $\chi > 1$). Meanwhile, the number of theoretical studies is rapidly growing, predicting new effects caused by the effect of radiation reaction on collective processes during the interaction of radiation of extreme intensity with matter. These effects are extremely various and they include, for example, alteration of the particle acceleration mechanisms [52–61], radiative trapping of particles [62–67], extremely efficient absorption of laser radiation [68], relativistic transparency suppression [69, 70], inverse Faraday effect [71–74], particle polarization [75–85] and many others. Strong radiative losses can also have a significant effect on the dynamics of particles in various astrophysical environments, and in particular, they can determine the upper limit of the energy of accelerated particles [86–88], the dynamics of the pulsar magnetosphere [89, 90], the character of magnetic reconnection [91, 92], etc.

In the $\chi \gtrsim 1$ regime, it is assumed that the behavior of matter in extreme EM fields in a vast number of configurations is largely determined by the development of *quantum-electrodynamic cascades* [46, 93–105]. The essence of the QED cascade is the emission of hard photons by ultrarelativistic particles as a result of nonlinear Compton scattering and the subsequent «decay» of the former into electron-positron pairs as a result of the Breit-Wheeler process[1]. Secondary particles also become involved in the formation of the next generation of pairs, which leads to an avalanche-like increase in the total number of particles. The development of such cascades is qualitatively similar to another physical process — avalanche-like ionization during a gas breakdown [106]. An active study of microwave breakdown in gases revealed a rather complex dynamics of this process, accompanied by the formation of plasma and the generation of breakdown waves [107, 108]. The analogy between pair production in vacuum and gas ionization, or between *vacuum breakdown* as a result of the development of a QED cascade and gas breakdown, has a deep physical justification [96, 109, 110]. It is also believed that the development of QED cascades plays an important role in various astrophysical phenomena, such as cosmic showers [111], gamma flashes [112], processes in the pulsar magnetosphere [113–116] and others. The diversity and complexity of the electron-positron plasma structures formed as a result of QED cascade development explains their active research, which is far from being completed.

Laboratory modeling of astrophysical processes (*laboratory astrophysics*) through the use of extremely intense lasers is one of the most demanded but also extremely non-trivial problems of experimental physics nowadays [117]. This is largely due to the fact that the key role in such processes is played by the interaction of particle flows with each other, which must be first created in a controlled way in the interaction of laser radiation and matter. In this regard, alternative possibilities are also being explored, for example, the use of colliders, which are the main research tool in the field of elementary particle physics, and which are based on the head-on collision of beams of high-energy charged particles. Currently, there are several projects aimed at building high-energy lepton colliders with record parameters, such as ILC [118] and CLIC [119]. Relatively recently, plasma acceleration has been considered as an attractive alternative method for creating linear colliders with a large acceleration gradient [120]. Strong EM fields can be generated in the interaction region of such colliders, which makes it possible to manifest such effects as *disruption* of beams [121–123], *beamstrahlung* [124–126], the production of secondary electron-positron pairs [127, 128], and even the effects of *nonperturbative* strong-field QED [129, 130]. Since the achievement of ever-increasing

[1]As noted above, the formation of an electron-positron pair is also possible directly from electrons or positrons in an external field as a result of the trident process.

radiation intensities at laser facilities imposes increasingly stringent requirements on contrast, stability, and beam quality, which have not yet been achieved in practice [131], high-current high-energy colliders, which are characterized by high beam quality and stability, can become an attractive «laserless» alternative for experiments in the field of strong-field physics. In this context, the most actively discussed project is FACET-II, dedicated to the study of plasma acceleration [51, 129, 132, 133].

Thus, the study of the physics of strong fields is of both fundamental interest and practical importance. The aim of the present thesis is to further push understanding of effects of nonlinear QED on behavior of matter in strong fields by investigating multiple related problems listed below.

1.2 Outline

In chapter 2, a theory of the motion of charged particles in strong fields in the strongly radiation-dominated regime is developed. The general properties of particle motion are determined according to the developed theory. A general method for solving motion equations with account of radiation reaction is proposed based on the developed theory. It is applied to various configurations of the electromagnetic field. The region of applicability of the method is determined, in particular, by comparing the results obtained analytically and with numerical methods.

In chapter 3, the interaction of a laser pulse of extreme intensity with a solid target is studied using numerical simulation. The key features and mechanism of the development of a QED cascade during such an interaction are determined. An analytical model for the development of such a cascade is developed. The accuracy of the developed model is determined by comparison with the results of numerical simulations.

In chapter 4, the influence of the radiation reaction on the process of focusing of ultrarelativistic particle beams during their head-on collision is studied. A model is developed for calculation of the disruption parameter with account of radiation reaction. The obtained analytical results are compared with the results of numerical simulations. Second, the process of generation of gamma radiation during the interaction of a high-current beam of ultrarelativistic electrons with a plasma target is studied using numerical simulation. A model is developed for calculation of the efficiency of beam energy conversion into gamma radiation energy. The beam parameters are determined for the FACET-II facility, which are optimal from the point of view of gamma radiation generation. Finally, a numerical scheme for solving Maxwell's equations on a regular grid with suppressed numerical Cherenkov instability is developed.

An overview of the results of the thesis is given in chapter 5.

1.3 List of publications

1.3.1 Publications in peer-reviewed journals

The specific contributions are given at the end of the summary of each chapter.

[A1] A. S. Samsonov, E. N. Nerush, and I. Yu. Kostyukov, "*Asymptotic electron motion in the strongly-radiation-dominated regime*", Physical Review A **98**, 053858 (2018).

[A2] A. S. Samsonov, E. N. Nerush, and I. Yu. Kostyukov, "*Laser-driven vacuum breakdown waves*", Scientific reports **9**, 11133 (2019).

[A3] A. Samsonov, A. Pukhov, and I. Kostyukov, "*Superluminal phase velocity approach for suppression of Numerical Cherenkov Instability in Maxwell solver*", Journal of Physics: Conference Series **1692**, 012002 (2020).

[A4] A. S. Samsonov, I. Yu. Kostyukov, and E. N. Nerush, "*Hydrodynamical model of QED cascade expansion in an extremely strong laser pulse*", Matter and Radiation at Extremes **6**, 034401 (2021).

[A5] A. S. Samsonov, E. N. Nerush, and I. Yu. Kostyukov, "*Effect of electron–positron plasma production on the generation of a magnetic field in laser-plasma interactions*", Quantum Electronics **51**, 861 (2021).

[A6] A. S. Samsonov, E. N. Nerush, I. Yu. Kostyukov, M. Filipovic, C. Baumann, and A. Pukhov, "*Beamstrahlung-enhanced disruption in beam-beam interaction*", New Journal of Physics **23**, 103040 (2021).

[A7] M. Filipovic, C. Baumann, A. Pukhov, A. S. Samsonov, and I. Yu. Kostyukov, "*Effect of transverse displacement of charged particle beams on quantum electrodynamic processes during their collision*", Quantum Electronics **51**, 807 (2021).

[A8] A. S. Samsonov and I. Yu. Kostyukov, "*Simulation of Gamma-Ray Generation in Interaction of High-Current Ultrarelativistic Particle Beams with Plasma*", Optics and Spectroscopy **130**, 219–223 (2022).

[A9] A. S. Samsonov, E. N. Nerush, and I. Yu. Kostyukov, "*High-order corrections to the radiation-free dynamics of an electron in the strongly radiation-dominated regime*", Matter and Radiation at Extremes **8**, 014402 (2022).

[A10] A. S. Samsonov, I. Yu. Kostyukov, M. Filipovic, and A. Pukhov, "*Generation of electron–positron pairs upon grazing incidence of a laser pulse on a foil*", Bulletin of the Lebedev Physics Institute **50**, S693–S699 (2023).

[A11] A. S. Samsonov and I. Yu. Kostyukov, "*Acceleration of ions by the force of radiation pressure during the interaction of an extremely intense pulse of circularly polarized laser radiation with a solid target*", Bulletin of the Lebedev Physics Institute **50**, S749–S754 (2023).

[A12] M. A. Serebryakov, A. S. Samsonov, E. N. Nerush, and I. Yu. Kostyukov, “*Abnormal absorption of extremely intense laser pulses in relatively underdense plasmas*”, Physics of Plasmas **30**, 113303 (2023).

1.3.2 Proceedings

[B1] A. S. Samsonov, I. Yu. Kostyukov, and E. N. Nerush, “*e^-e^+ cushion formation in the interaction of extremely intensive radiation with solid target*”, in *VII International Conference «Frontiers of Nonlinear Physics»* (2019), pp. 161–163.

[B2] A. S. Samsonov, I. Yu. Kostyukov, and E. N. Nerush, “*Analytical model of the QED cascade development in the plane wave*”, in *IV International Conference on Ultrafast Optical Science «UltrafastLight-2020»* (2020), p. 51.

[B3] A. S. Samsonov, E. N. Nerush, and I. Yu. Kostyukov, “*Advances in the asymptotic description of the electron motion in the strongly radiation-dominated regime*”, in *47th EPS conference on plasma physics «EPS 2021»* (2021), pp. 976–979.

[B4] A. S. Samsonov, E. N. Nerush, and I. Yu. Kostyukov, “*Effect of e^+e^- pair production on generation of magnetic field driven by radiation reaction*”, in *V International Conference on Ultrafast Optical Science «UltrafastLight-2021»* (2021), p. 35.

[B5] A. S. Samsonov, I. Yu. Kostyukov, E. N. Nerush, M. Filipovic, C. Baumann, and A. Pukhov, “*Effect of Radiation Reaction on Collective Processes in Collision of High-Current Ultrarelativistic Beams of Particles*”, in *29th annual International Laser Physics Workshop* (2021).

[B6] A. S. Samsonov, I. Yu. Kostyukov, and E. N. Nerush, “*Features of the Electron Motion in the Strongly Radiation-Dominated Regime*”, in *18th International Workshop Complex Systems of Charged Particles and Their Interactions with Electromagnetic Radiation «CSCPIER-2022»* (2022).

[B7] A. S. Samsonov, I. Yu. Kostyukov, and E. N. Nerush, “*Features of the Electron Motion in the Strongly Radiation-Dominated Regime*”, in *30th annual International Laser Physics Workshop* (2022).

[B8] A. S. Samsonov and A. Pukhov, “*Electron motion in relativistically strong plane waves*”, in *31th annual International Laser Physics Workshop* (2023).

[B9] A. S. Samsonov, M. Filipovic, I. Yu. Kostyukov, and A. Pukhov, “*Generation of electron-positron pairs in interaction of multiple laser pulses with a foil at grazing angle*”, in *5th Conference on Extremely High Intensity Laser Physics* (2023).

Chapter 2

Properties of charged particles motion in extremely strong electromagnetic fields

2.1 Introduction

At present, the most complete answer to the question about the nature of radiation reaction is given by quantum electrodynamics. With the help of this theory, for example, the probability of emission of a photon with a given energy by an electron can be calculated [32, 33]. Despite the fact that the description of the radiation process using QED is the most accurate, it most often cannot be applied directly to practical problems involving complex interaction of radiation with matter. This is due to the fact that the final analytical expressions in QED can be obtained for the probabilities of transitions between some quasi-stationary electron states, most often described using Volkov functions [42]. To describe a dynamic problem in which the electron states and the EM field evolve, it is necessary to self-consistently solve the non-stationary Dirac equation and the Maxwell equations, which is usually impossible, at least from a practical point of view. However, under certain conditions, this procedure turns out to be redundant and the task is greatly simplified. The first parameter responsible for the fulfillment of one of these conditions is the dimensionless amplitude of the EM field a_0

$$a_0 = \frac{eE_0}{mc\omega}, \tag{2.1}$$

where m and $e > 0$ are the mass and absolute value of the electron charge, respectively, E_0 and ω are characteristic value and frequency of change of the EM field, respectively.

In the regime $a_0 \gg 1$, the characteristic radiation formation length λ_f in most field configurations can be estimated as $\lambda/a_0 \ll \lambda$, where $\lambda = 2\pi c/\omega$, i.e. individual acts of emission of a photon by an electron occur almost instantaneously, compared to the characteristic time of the change of the EM field. Thus, the EM fields can be considered constant over the radiation formation length. In the literature, this approximation is often called *locally constant field approximation* (LCFA) [32, 33, 134, 135]. In this approximation, the probability and emission spectrum depend on a single QED parameter χ defined as follows

$$\chi = \frac{\gamma}{E_S}\sqrt{(\mathbf{E} + \mathbf{v} \times \mathbf{B})^2 - (\mathbf{vE})^2}, \tag{2.2}$$

where γ and $\mathbf{v}$ are the Lorentz factor and the electron velocity normalized to c, respectively, $\mathbf{E}$ and $\mathbf{B}$ are the electric and the magnetic fields respectively, $E_S = m^2c^3/e\hbar$ is the critical field of QED or Sauter-Schwinger field [32], $\hbar$ is Planck's constant. In the classical ($\chi \ll 1$) or essentially quantum ($\chi \gg 1$) regimes, the probability can be approximately calculated as follows

$$W_{\text{rad}} \approx \alpha \frac{mc^2}{\gamma\hbar} \times \begin{cases} 1.44\chi, & \chi \ll 1, \\ 1.46\chi^{2/3}, & \chi \gg 1, \end{cases} \tag{2.3}$$

where $\alpha = e^2/\hbar c$ is the fine structure constant. Note that various approaches have been proposed for calculating the emission probability beyond the LCFA approximation [136–141]. Within the framework of LCFA, the characteristic distance that an ultrarelativistic electron travels between two successive emission λ_W can be estimated as c/W_{rad}, which in both classical and quantum regimes is at least $1/\alpha \approx 137$ times greater than the radiation formation length. The ratio of the electron mean free path λ_W to the characteristic wavelength of the EM field can be estimated as follows

$$\frac{\lambda_W}{\lambda} \approx \frac{1}{\alpha a_0} \times \begin{cases} 1, & \chi \ll 1, \\ \chi^{1/3}, & \chi \gg 1. \end{cases} \tag{2.4}$$

Note, however, that the mean free path actually depends on the energy of the emitted photon [142], and the given estimate may be inaccurate for $\chi \gtrsim 10$. Since the condition $\chi \lesssim 10$ is certainly satisfied for the experiments expected in the near future, the characteristic scales in the problem under consideration are in the following hierarchy

$$\lambda_f \ll \lambda_W \ll \lambda. \tag{2.5}$$

This inequality can be interpreted in such a way that the electron moves classically between short but frequent emission events. In this case, the effect of recoil from radiation can be approximately taken into account in the form of some additional continuous force acting on the particle, i.e. the equations of motion can be written in the following form

$$\frac{\mathrm{d}\mathbf{p}}{\mathrm{d}t} = -\mathbf{E} - \mathbf{v} \times \mathbf{B} - F_{\text{rr}}\mathbf{v}, \tag{2.6}$$

$$\frac{\mathrm{d}\gamma}{\mathrm{d}t} = -\mathbf{vE} - F_{\text{rr}}v^2, \tag{2.7}$$

where the electron momentum $\mathbf{p}$ is normalized to mc, time t — to $1/\omega$, electric and magnetic fields — to $mc\omega/e$, F_{rr} — total radiation power normalized by $mc^2\omega$ and given by

$$F_{\text{rr}} = \frac{\alpha a_{\text{S}}}{3\sqrt{3}\pi} \int_0^\infty \frac{4u^3 + 5u^2 + 4u}{(1+u)^4} K_{2/3}\left(\frac{2u}{3\chi}\right) \mathrm{d}u, \tag{2.8}$$

where $a_{\text{S}} = eE_{\text{S}}/mc\omega \equiv mc^2/\hbar\omega$ is normalized Sauter-Schwinger field, K_ν — modified Bessel function of the second kind. In limiting cases, this expression is greatly simplified

$$F_{\text{rr}} \approx \alpha a_{\text{S}} \times \begin{cases} 0.67\chi^2, & \chi \ll 1, \\ 0.37\chi^{2/3}, & \chi \gg 1. \end{cases} \tag{2.9}$$

Such an approach to describing the dynamics of an electron taking into account radiation reaction is often called *semiclassical* in the literature [143–147], because the approximation of a continuous classical force of radiative friction is used, however, its magnitude is calculated based on the results of QED. It is important to note that in the essentially quantum regime ($\chi \gg 1$) a single emitted photon can take a significant fraction of the electron energy. And since the radiation process is stochastic by its nature, the electrons located in an infinitely small phase volume at some point in time, can significantly diverge in the phase space after a finite time. In this case, the equations written above (2.6)–(2.7) describe the zeroth moment of the electron distribution function, or the trajectory of their center of mass. Effects caused by the probabilistic nature of radiation, such as straggling and quenching [147–150], lead to diffusion of the distribution function and, accordingly, cannot be described in a semiclassical approach. In this case, the dynamics of electrons can be described using higher moments of the distribution function. Such an approach was, for example, used to calculate the average value and dispersion of the energy of particles in various configurations in publications [146, 151, 152]. In the opposite limit, $\chi \lesssim 1$, the recoil from the radiation of a single photon is small and the continuous force approximation is justified.

Another important consideration in research of effect of radiation reaction is its dependence on the internal degree of freedom of the electron — spin. Strictly speaking quasi-classical limit of the Dirac equation leads to motion equations where both orbital motion of the electron and evolution of its spin are coupled. In particular, one should add the Stern-Gerlach force [153] in the equation for the electron momentum and describe spin dynamics via Thomas-Bargmann-Michel-Telegdi (T-BMT) [154, 155] equation. Note, that although the latter is strictly valid in homogeneous EM fields, it still can be used in heterogeneous fields if the Stern-Gerlach force can be neglected [156]. One can estimate that the ratio between the Stern-Gerlach force and the Lorentz force is of the order of $\hbar\omega/mc^2$, thus for optical frequencies ($\hbar\omega \sim 1\,\text{eV}$) the former can be neglected with a large margin of accuracy. In that case spin dynamics is decoupled from the electron orbital motion and can be calculated after the electron trajectory is found. Radiation reaction can again couple spin dynamics and electron orbital motion, since radiation probabilities depend on spin of the electron (and polarization of the emitted photon). Note that an order of magnitude estimates made above where radiation probabilities are averaged over initial and summed over final polarization states of the electron remain valid. Although in a certain scenarios assuming that electrons are generally not polarized can be invalid, since radiation probabilities of spin up and spin down electron are different. Resolving electron polarization can lead to effects such as significant increase of pair production during QED cascade development [157], production of polarized high-energy particles [15, 80], spatially-inhomogeneous polarization [84], etc. In this work, such effects caused by spin dynamics are not covered.

It turns out that the problem of the dynamics of an electron in an EM field, taking into account radiation reaction, can be simplified even further. In particular, under certain conditions, the radiation reaction can be taken into account implicitly, i.e. without including additional terms in the motion equations. To understand the reason for the possibility of such a simplification, let us briefly consider the well-known problem of the motion of a relativistic electron in a uniform constant EM field without taking into account radiation reaction [158]. The simplest way to solve this problem is to transform to the reference frame K', where the electric and magnetic fields become parallel or one of them is absent. Assume for definiteness that in K' the fields are directed along the z' axis. Let us omit from consideration a particular case of a purely magnetic configuration $\mathbf{E} \cdot \mathbf{B} = 0$, $B > E$, in which an electron in K' rotates in a magnetic field. In a more general case, when there is an electric field in K', the electron also rotates in the $x'y'$ plane (if the magnetic field is nonzero) and is constantly accelerating along the z' axis. Thus, in K' the trajectory of an electron is a helix with a monotonously increasing step and decreasing radius, and a longitudinal velocity approaching the speed of light. The asymptotic limit of such a trajectory is a straight line along the z' axis along which the electron moves at the speed of light. Accounting for the radiation reaction in this case does not qualitatively change the result obtained. It is easy to show that the radiation reaction leads to a gradual decrease of the electron momentum in the plane of rotation $x'y'$ and slows down the growth of the longitudinal momentum[1]. However, the electron trajectory also asymptotically tends to a straight line along the z' axis, i.e. in fact, this statement does not depend on taking into account the radiation reaction. According to the Lorentz transformation, in the laboratory reference frame the asymptotic trajectory is also a straight line along some direction $\mathbf{v}_0$. The characteristic time τ_v, during which the electron trajectory approaches the asymptotic, can be estimated as $\gamma_0 mc/eE$, where γ_0 is the initial electron energy, and E is the strength of the electric field. Since this asymptotic direction $\mathbf{v}_0$ is determined only by the relation between the electric and magnetic fields, it can be constructed at each time instant at each point in space, even if the EM field is inhomogeneous and non-constant. If the characteristic frequency of the EM field variation is equal to ω, then the locally given direction $\mathbf{v}_0$ also changes with the same frequency. Without taking into account the radiation reaction in an alternating EM field, the characteristic energy of an electron can be estimated as $\gamma \sim eE/mc\omega \equiv a_0$. So the timescale at which the electron velocity aligns with the local asymptotic direction $\mathbf{v}_0$ is of the same order of magnitude as the timescale of the EM field variation: $\tau_v \sim 1/\omega$. Thus, the relation between the electron velocity vector and the local asymptotic direction can be arbitrary. However, in the *strongly radiation-dominated* regime, the last statement is not accurate. This is due to the fact that in such a regime the relation between the electron energy and the dimensionless amplitude

[1] An identical result is predicted by the exact solution of the problem of electron motion in a constant homogeneous EM field with account of radiation reaction found in Ref. [159].

of the EM field is determined by the inequality $\gamma \ll a_0$. Because of this, the EM field orients the electron velocity vector towards the local asymptotic direction during a time interval much shorter than the timescale at which EM field varies itself. Thus, for an approximate description of the dynamics of an electron in an EM field under conditions of extreme radiation losses, we can assume that the electron velocity is determined by the asymptotic direction $\mathbf{v}_0$, which depends only on the local configuration of the EM field, and thus reduce the order of the motion equations. In the next section, the above qualitative procedure is derived mathematically rigorously.

2.2 Asymptotic particle dynamics in strongly radiation-dominated regime

Let us proceed to the construction of an asymptotic theory of electron motion in the strongly radiation-dominated regime. To do this, consider the equation of motion of an electron in an external EM field, taking into account radiation reaction using a semiclassical approach, written with respect to its velocity $\mathbf{v}$ and energy γ

$$\frac{\mathrm{d}\gamma}{\mathrm{d}t} = -\mathbf{v}\mathbf{E} - F_{\mathrm{rr}}v^2, \tag{2.10}$$

$$\frac{\mathrm{d}\mathbf{v}}{\mathrm{d}t} = -\frac{1}{\gamma}\left(\mathbf{E} + \mathbf{v}\times\mathbf{B} - \mathbf{v}\left(\mathbf{v}\mathbf{E}\right) + \frac{F_{\mathrm{rr}}\mathbf{v}}{\gamma^2}\right) \equiv -\frac{\mathbf{F}_\perp}{\gamma}. \tag{2.11}$$

Since radiation reaction can significantly alter the dynamics of only ultrarelativistic particles ($\gamma \gg 1$), the last term in (2.11) can be omitted. The equations written above have a formal stationary solution $\mathbf{v}_0$, which corresponds to the vanishing of the transverse force acting on the electron and, correspondingly, to the vanishing of radiation reaction. Because of the latter property, this solution is called *radiation-free direction* (RFD). It is found from the following equation

$$\mathbf{E} + \mathbf{v}_0\times\mathbf{B} - \mathbf{v}_0\left(\mathbf{v}_0\mathbf{E}\right) = 0. \tag{2.12}$$

Note first that the solution of this equation always exists and it can be either calculated algebraically or constructed geometrically [160]. Let us construct an algebraic solution of the equation (2.12).

In the special case of the fulfillment of the equalities $\mathbf{E}\cdot\mathbf{B} = 0$ and $B > E$, according to the Lorentz transformations, there exists a reference frame K' in which the field is purely magnetic. Moreover, in K' the magnetic field $\mathbf{B}'$ is parallel to the magnetic field $\mathbf{B}$ in the laboratory frame K. In the reference frame K', the electron trajectory is a helix with an axis parallel to the direction of the magnetic field $\mathbf{B}'$. The corresponding drift velocity of an electron in the laboratory reference frame is the velocity of K' relative to K and can be found as follows

$$\mathbf{E} + \mathbf{v}_0\times\mathbf{B} = 0. \tag{2.13}$$

Note that the equation (2.13) does not depend on the velocity component along the magnetic field, so it can be chosen arbitrarily, limited only by the condition $|\mathbf{v}_0| < 1$. As an example, here is a solution that satisfies the condition $\mathbf{v}_0 \cdot \mathbf{B} = 0$

$$\mathbf{v}_0 = \frac{\mathbf{E} \times \mathbf{B}}{B^2}. \tag{2.14}$$

As will be shown in section 2.3.3, the ambiguity of the solution (2.13) can be eliminated based on additional physical considerations.

In the general case, the solution of the equation (2.12) can be obtained by its sequential scalar multiplication by the vectors $\mathbf{B}$, $\mathbf{E}$ and $\mathbf{E} \times \mathbf{B}$

$$\mathbf{v}_0\mathbf{B} = \frac{\mathbf{EB}}{\mathbf{v}_0\mathbf{E}}, \tag{2.15}$$

$$\mathbf{v}_0 \cdot \mathbf{E} \times \mathbf{B} = E^2 - (\mathbf{v}_0\mathbf{E})^2, \tag{2.16}$$

$$\mathbf{v}_0\mathbf{E} = -\sqrt{\frac{E^2 - B^2 + \sqrt{(E^2 - B^2)^2 + 4(\mathbf{EB})^2}}{2}}, \tag{2.17}$$

$$\mathbf{v}_0 \cdot \mathbf{E} \times [\mathbf{E} \times \mathbf{B}] = (\mathbf{v}_0\mathbf{E})(\mathbf{EB}) - (\mathbf{v}_0\mathbf{B})E^2. \tag{2.18}$$

Note that the right-hand side in the expression (2.17) is a Lorentz invariant. The sign "–" in the same expression is chosen on the basis of the following reasoning. In the case of $\mathbf{E} \cdot \mathbf{B} \neq 0$ and/or $E > B$, according to the Lorentz transformations, there exists a reference frame K' in which $\mathbf{E}' \parallel \mathbf{B}'$ and/or $B' = 0$. In this case, the electron trajectory asymptotically tends to a straight line parallel to the vector $\mathbf{E}'$, and the condition $\mathbf{v}' \cdot \mathbf{E}' < 0$ is satisfied. Note that the vectors $\mathbf{E}$, $\mathbf{E} \times \mathbf{B}$ and $\mathbf{E} \times [\mathbf{E} \times \mathbf{B}]$ form an orthogonal basis, so the expressions (2.16)–(2.18) uniquely define the vector $\mathbf{v}_0$.

The second note about the equation (2.12) is that its scalar multiplication by $\mathbf{v}_0$ results in $|\mathbf{v}_0| = 1$. This means that the solution $\mathbf{v}_0$ is not strictly physical, and in fact the electron is generally not able to move in the EM field and not experience transverse acceleration. In order to understand the connection of the radiation-free solution with the actual solution of the electron motion equations, let us consider the following. By definition, in the strongly radiation-dominated regime, the energy of an electron is significantly less than the energy of a certain hypothetical electron moving in the same EM field, but not experiencing radiation reaction. The energy of such a hypothetical electron is usually estimated in order of magnitude by the dimensionless electric field amplitude a_0. Thus, the energy of an electron experiencing extreme radiation losses satisfies the condition $\gamma \ll a_0$. When this condition is met, it follows from the equation (2.11) that the EM field orients the electron velocity vector on a time scale much smaller than the characteristic time of change of the EM field itself. Thus, on the scale of changes in the electron velocity, the EM field can be considered constant and uniform. And in a constant homogeneous EM field, the electron velocity asymptotically approaches the radiation-free direction $\mathbf{v}_0$. Neglecting the time of such an approach, one can construct the so-called asymptotic trajectory, which in a sense is an attractor for real electron trajectories

$$\frac{\mathrm{d}\mathbf{r}}{\mathrm{d}t} = \mathbf{v}_0\left(\mathbf{E}(\mathbf{r}, t), \mathbf{B}(\mathbf{r}, t)\right), \tag{2.19}$$

$$\mathbf{E} + \mathbf{v}_0 \times \mathbf{B} - \mathbf{v}_0(\mathbf{v}_0\mathbf{E}) = 0. \tag{2.20}$$

Thus, the order of the electron motion equations is reduced. Here and below, the solution of these equations $\mathbf{r}(t)$ will be called *asymptotic* trajectory, because firstly, this trajectory locally corresponds to the electron trajectory in the constant field approximation at asymptotically large times ($t \to \infty$), and secondly, it describes the electron trajectory in an asymptotically strong field ($a_0 \to \infty$).

2.3 Properties and examples of asymptotic trajectories

Let us consider the equations (2.19) and (2.20) and study the general properties of trajectories based on the known symmetry of Maxwell's equations. The following transformation

$$t' = -t, \tag{2.21}$$

$$\mathbf{E}' = -\mathbf{E}, \tag{2.22}$$

$$\mathbf{B}' = \mathbf{B}, \tag{2.23}$$

$$\rho' = -\rho, \tag{2.24}$$

$$\mathbf{j}' = \mathbf{j}. \tag{2.25}$$

does not change Maxwell's equations in the sense that it leads to the same equations for primed variables. In what follows, we denote the quantities $\mathbf{E}$, $\mathbf{B}$, $\mathbf{j}$, which change with time t, as the *initial* system, and $\mathbf{E}'$, $\mathbf{B}'$, $\mathbf{j}'$, changing over time t', as the *primed* system. The above symmetry is the relation between the system of currents that emit certain fields and the system of currents that absorb fields. This relation states that the Poynting vector, the scalar product $\mathbf{j} \cdot \mathbf{E}$ and the direction of time in the primed system are opposite to those in the initial system. According to the equation (2.20), in the primed system, the velocity field $\mathbf{v}_0'$ is related to the velocity field in the initial system $\mathbf{v}_0$ as follows

$$\mathbf{v}_0'(\mathbf{r}, t') = -\mathbf{v}_0(\mathbf{r}, -t'), \tag{2.26}$$

That is, in the primed system, the velocity field and the direction of time are opposite to those in the initial system, which leads to trajectories in the primed system $\mathbf{r}'(t')$ being the same as in the initial system, but passed by the electron in the opposite direction, $\mathrm{d}\mathbf{r}'/\mathrm{d}t' = \mathbf{v}_0'(\mathbf{r}', t') = -\mathbf{v}_0(\mathbf{r}', -t')$. Note the fundamental difference between the asymptotic trajectory described by the equations (2.19)–(2.20) and the ponderomotive description. The ponderomotive force is determined by the distribution of E^2 and B^2 and is accordingly invariant under the transformation (2.21)–(2.25), while this transformation reverses the direction of electron motion, described by the equations (2.19) and (2.20), which are valid in the regime of strong radiation reaction. Let us further demonstrate the difference between ponderomotive and asymptotic descriptions using the following example. Consider the scattering of an electron by two laser pulses counter propagating each other and located initially at some distance from each other. Let the first pulse propagate along the x axis, and the second one being obtained from the first one by transformation (2.21)–(2.23) and thus propagate against the x axis. Let the electron be closer to the first pulse. Then, according to the ponderomotive description, the first pulse scatters the electron to the side. In this case, the electron may be far from both pulses so that the second pulse will not affect the motion of the electron at all. However, if the electron radiates abundantly, then the asymptotic description of its motion is valid. In this case, the trajectory of the electron in the field of the second pulse should be the same as in the field of the first, but passed in the opposite direction. Therefore, in the strongly radiation-dominated regime, the electron, after moving in the field of the first pulse, returns to its original position, moving in the field of the second pulse. This behavior is very different from the behavior according to the ponderomotive description. Thus, the asymptotic description implies that the electrons do not scatter, but remain in the field of the laser beam for a long time. This conclusion is in good agreement with the results of theoretical considerations and numerical simulations, which show that the ponderomotive force can be significantly suppressed by radiation reaction [63, 161].

2.3.1 Asymptotic trajectories in standing waves

In this section, we will show that the equations (2.19) and (2.20) always lead to periodic trajectories in a wide class of fields, which are generally written in the following form

$$\mathbf{E} = \mathbf{f}(\mathbf{r}, t) - \mathbf{f}(\mathbf{r}, -t), \tag{2.27}$$

$$\mathbf{B} = \mathbf{g}(\mathbf{r}, t) + \mathbf{g}(\mathbf{r}, -t), \tag{2.28}$$

where $\mathbf{E} = \mathbf{f}(\mathbf{r}, t)$, $\mathbf{B} = \mathbf{g}(\mathbf{r}, t)$ are solutions of Maxwell's equations in free space ($\rho = 0$ and $\mathbf{j} = 0$). This representation means that the fields are the sum of the fields in some system and the fields in the corresponding primed system. In this case, the transformation (2.21)–(2.25) results in the same fields in the primed system as in the initial system, i.e. $\mathbf{E}'(\mathbf{r}, t') = \mathbf{E}(\mathbf{r}, t')$, $\mathbf{B}'(\mathbf{r}, t') = \mathbf{B}(\mathbf{r}, t')$, which leads to the same velocity field $\mathbf{v}'_0(\mathbf{r}, t') = \mathbf{v}_0(\mathbf{r}, t')$. Given the expression (2.26) we have

$$\mathbf{v}_0(\mathbf{r}, -t) = -\mathbf{v}_0(\mathbf{r}, t), \tag{2.29}$$

i.e. the velocity $\mathbf{v}_0$ is an odd function of time. If, among other things, the fields (2.27)–(2.28) are periodic functions of time, then the velocity field is also periodic in time with the same period T. Therefore, the average value of the velocity over the period is zero

$$\langle \mathbf{v}_0 \rangle_T = \int_0^T \mathbf{v}_0(t')\, dt' = \int_{-T}^0 \mathbf{v}_0(-t')\, dt' = -\int_0^T \mathbf{v}_0(t')\, dt' = -\langle \mathbf{v}_0 \rangle_T. \tag{2.30}$$

Thus,

$$\mathbf{r}(t+T) = \int_0^{t+T} \mathbf{v}_0(t')\, dt' = \int_0^t \mathbf{v}_0(t')\, dt' + \int_t^{t+T} \mathbf{v}_0(t')\, dt' = \mathbf{r}(t) + \langle \mathbf{v}_0 \rangle_T = \mathbf{r}(t). \tag{2.31}$$

Therefore, in periodic fields (2.27)–(2.28) within the framework of the asymptotic description, the electron periodically moves along the same path.

Below, we consider several specific examples of standing wave configurations, in which we compare the asymptotic trajectories and the numerical solution of the non-reduced motion equations.

2.3.2 Asymptotic trajectories in a linearly-polarized standing wave

The field configuration in a linearly-polarized standing wave is quite simple, so the asymptotic trajectories can be found explicitly. Let $\mathbf{E} = \mathbf{y}_0 \cos(t)\cos(x)$, $\mathbf{B} = \mathbf{z}_0 \sin(t)\sin(x)$, then

$$\mathbf{v}_0 = \begin{cases} \mathbf{x}_0 \operatorname{tg}(t)\operatorname{tg}(x) + \mathbf{y}_0\sqrt{1 - \operatorname{tg}^2(t)\operatorname{tg}^2(x)}, & \text{if } E > B; \\ \mathbf{x}_0 \operatorname{ctg}(t)\operatorname{ctg}(x), & \text{if } E < B. \end{cases} \tag{2.32}$$

Since the fields are uniform along the y axis, the movement along it is of little interest. The dependence $x(t)$ is determined from the equations

$$\begin{cases} \sin(x)\cos(t) = \sin(x_0)\cos(t_0), & \text{if } E > B; \\ \cos(x)\sin(t) = \cos(x_0)\sin(t_0), & \text{if } E < B. \end{cases} \tag{2.33}$$

Let the electron be initially ($t = 0$) located at the point $x = x_0$ such that $E > B$ (otherwise the electron will be at rest until this condition is met). The electron trajectory is determined by the first equation in (2.33) until it reaches the point where $E = B$; after that, the trajectory is determined by the second equation in (2.33) up to the next point where the condition $E = B$ is met, and so on. Such points are determined from the condition $\operatorname{tg}(x)\operatorname{tg}(t) = 1$. From here, one can explicitly find the point of change of the trajectory, which the electron will reach, starting at the moment $t = 0$ from the point x_0

$$\operatorname{ctg} x_1 = \operatorname{tg} t_1 = \sqrt{\frac{1}{\sin(x_0)} - 1} \tag{2.34}$$

It is easy to show that the electron will reach the next closest point of trajectory change at time $t_2 = \pi - t_1$ with coordinate $x_2 = x_1$, and the next one at $t_3 = \pi + t_1$ with coordinate $x_3 = x_1$ and after that the trajectory will repeat periodically. The trajectories of electrons starting from other points are found in a similar way. The explicit form of the $x(t)$ trajectories and their comparison with the numerical solution of the non-reduced motion equations are shown in Fig. 2.1. According to the reasoning in section 2.3.1, the asymptotic trajectories of an electron in a standing linearly polarized wave are periodic. However, it is known that the behavior of electrons in a strong standing wave is accompanied by the so-called *anomalous radiative trapping* [62], i.e. particles approach the magnetic node of the standing wave, which is an unstable equilibrium position without account of radiation reaction. The anomalous radiative trapping is caused by the electron drift between different asymptotic trajectories (2.33), which takes several field periods [62] and therefore is not described by the presented asymptotic theory. Note that in the case of $a_0 = 10^5$, the electron trajectories calculated numerically approach the magnetic field node with each successive period, which is exactly the effect of the anomalous radiative trapping (see Fig. 2.1).

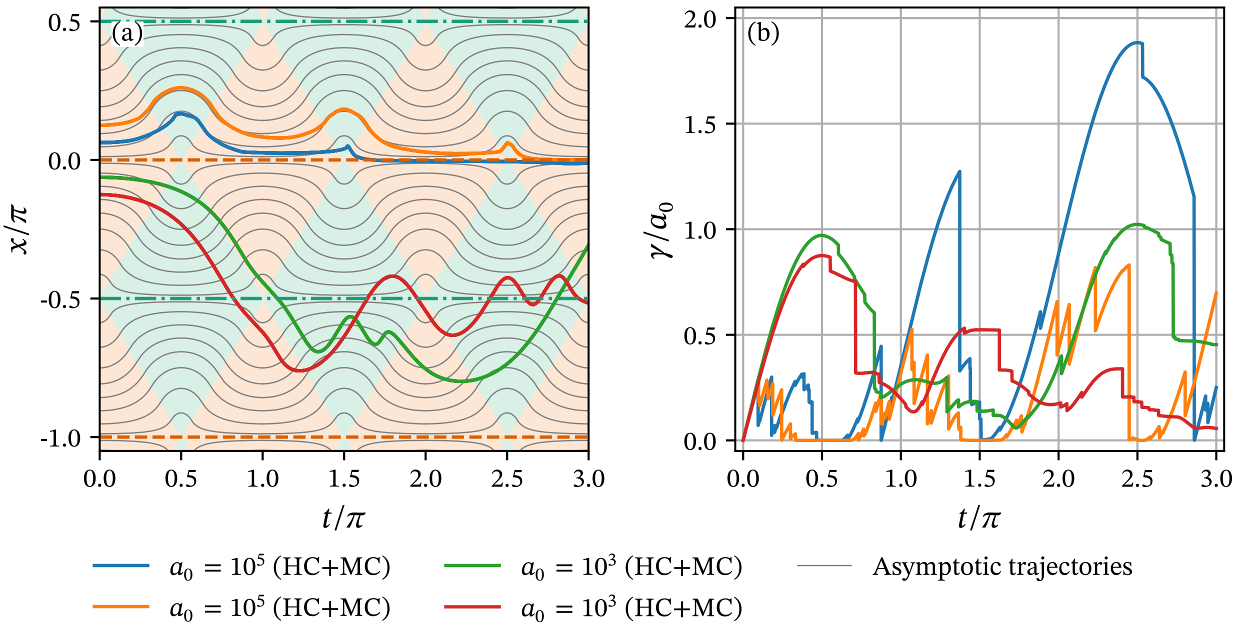

Figure 2.1: Electron dynamics in a linearly polarized standing electromagnetic wave. (a) Solid gray lines correspond to the asymptotic trajectories calculated from the equation (2.19). The areas of predominance of the electric (magnetic) fields are marked in light orange (green) colors. Solid colored lines correspond to the numerical trajectories calculated from the non-reduced motion equations with account of radiation reaction using the Monte Carlo method (see Appendix A) for $a_0 = 10^3$ and $a_0 = 10^5$ (starting from $x < 0$ and $x > 0$ respectively). The dashed orange lines correspond to the magnetic node of the standing wave ($B = 0$), the dash-dotted green lines correspond to the electrical node of the standing wave ($E = 0$). (b) Particle energy as a function of time for numerical trajectories, normalized to a_0.

2.3.3 Asymptotic trajectories in a laser beam of finite diameter

Let us show that a large number of electromagnetic field configurations can be represented as periodic fields with «emission-absorption» symmetry (2.21)–(2.25). We will also present one of the ways to resolve the ambiguity of the velocity field given by the equation (2.14).

Consider the TE11 mode of a rectangular metallic waveguide

$$E_x = 0, \tag{2.35}$$

$$E_y = a_0 \cos\left(k_y y\right) \sin(k_z z) \cos(t - k_x x), \tag{2.36}$$

$$E_z = -\frac{a_0 k_y}{k_z} \sin\left(k_y y\right) \cos(k_z z) \cos(t - k_x x), \tag{2.37}$$

$$B_x = \frac{a_0(k_z^2 + k_y^2)}{k_z} \cos\left(k_y y\right) \cos(k_z z) \sin(t - k_x x), \tag{2.38}$$

$$B_y = -k_x E_z, \tag{2.39}$$

$$B_z = k_x E_y, \tag{2.40}$$

where the angular frequency of the wave $\Omega = (k_x^2 + k_y^2 + k_z^2)^{1/2} = 1$ (we use the normalization frequency ω equal to the frequency of the wave and, as before, the time is normalized to $1/\omega$, coordinates — to c/ω, $\mathbf{k}$ — wave vector normalized to ω/c). These fields have metallic boundary conditions at $y = 0,\ \pm\ell_y,\ \pm2\ell_y, \dots (E_z = 0)$ and $z = 0,\ \pm\ell_z,\ \pm2\ell_z, \dots (E_y = 0)$, where $\ell_y = \pi/k_y$ and $\ell_z = \pi/k_z$ are the waveguide dimensions along the y and z axes respectively.

The fields (2.35)–(2.40) are solutions of the Maxwell equation not only inside the waveguide, but also in vacuum, because they can be represented as a sum of plane waves. We will consider these fields in the region $y \in [-\ell_y/2, \ell_y/2]$ and $z \in [0, \ell_z]$ as a model of a laser beam of a finite diameter. The asymptotic trajectory in such fields is shown in Fig. 2.2 (a), where $\xi = x - v_g t$, $v_g = k_x$ is the group velocity of the TE11 mode. The trajectory starts at $t = 0$ at the point $x = 0$, $y = 0.2$, $z = 0.55$ and ends at $t = 2\tau$, where τ is the characteristic timescale of the problem

$$\tau = \frac{2\pi}{k_x(v_\varphi - v_g)} = \frac{2\pi}{1 - k_x^2} \tag{2.41}$$

where $v_\varphi = 1/v_g$ is the wave phase velocity. It can be seen from Fig. 2.2 that the asymptotic trajectory is quasi-periodic, which agrees quite well with the trajectory of a real electron at $a_0 = 4 \cdot 10^3$, which remains in the strong field region for a long time. However, as will be shown below, along the asymptotic trajectories calculated in the laboratory frame of reference, the values of ξ and the period of the trajectory do not coincide well with those for real electron trajectories. This is due to the fact that the expression (2.14) is not a Lorentz invariant, therefore, by calculating the speed $\mathbf{v}_0$ using this expression in one frame of reference, in some other frame of reference, we get $\mathbf{v}_0{}' = \mathbf{E}' \times \mathbf{B}' + a\mathbf{B}'$, where a is some constant.

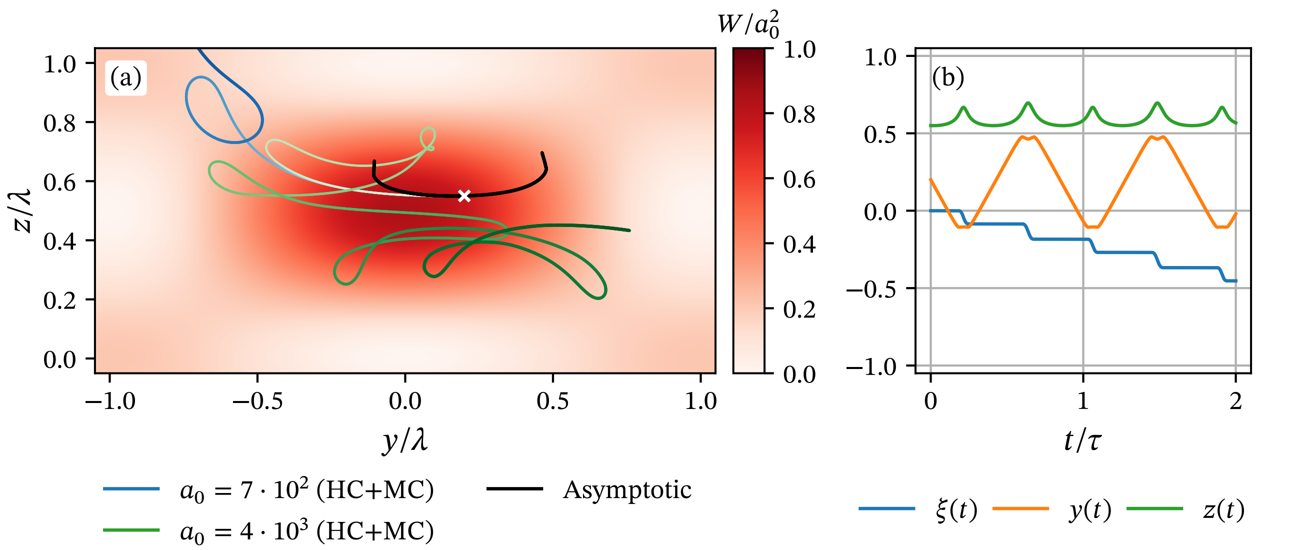

Figure 2.2: (a) Electromagnetic energy density $W = (E^2+B^2)/2$ of the TE11 waveguide mode (2.35)–(2.40) with dimensions $\ell_y = 2\lambda$, $\ell_z = \lambda$ in plane $x = 0$ at $t = 0$ (colormap). Trajectories of electrons calculated numerically (see Appendix A) starting from the point $x = 0$, $y = 0.2\,\lambda$, $z = 0.55\,\lambda$ (marked with white cross) ($\lambda = 1\,\mu\text{m}$, $t \in [0, 2\tau]$), for $a_0 = 700$ (blue line) and $a_0 = 4 \cdot 10^3$ (green line). Darker colors correspond to later times. Black line corresponds to asymptotic trajectory calculated from equations (2.14) and (2.15)–(2.18) (b) Asymptotic trajectory in the laboratory reference frame; $\xi = x - v_g t$, where v_g is the group velocity of the TE11 mode.

Consider the fields (2.35)–(2.40) in the reference frame K' moving along axis x with group velocity v_g

$$E'_y = a_0 k_\perp \cos(k_y y)\sin(k_z z)\cos(k_\perp t'), \tag{2.42}$$

$$E'_z = -\frac{a_0 k_\perp k_y}{k_z}\sin(k_y y)\cos(k_z z)\cos(k_\perp t'), \tag{2.43}$$

$$B'_x = \frac{a_0(k_z^2 + k_y^2)}{k_z}\cos(k_y y)\cos(k_z z)\sin(k_\perp t'), \tag{2.44}$$

$$E'_x = B'_x = B'_y = B'_z = 0, \tag{2.45}$$

where $k_\perp = \sqrt{1 - k_x^2}$. These fields do not depend on x' and for all electrons there is no Lorentz force component along the x' axis. Moreover, due to radiation losses, electrons «forget» their initial direction of motion, so we will assume that in fields (2.42)–(2.45) average electron velocity $v'_x = 0$. Therefore, in the laboratory reference frame K the average electron velocity is $v_x = v_g$ and hence $\xi = \text{const}$. Note that this statement is not true for asymptotic trajectories calculated in the laboratory reference frame (see Fig. 2.2 (b)), which in particular leads to a different value of the period of y and z coordinates.

The substitutions $t' \to t' + \pi/2k_\perp$ and $t' \to -t'$ indicate that electric field components (2.42)–(2.43) are odd functions of time, and magnetic field components (2.44) are even functions of time in K' and all the fields are periodic. In accordance with section 2.3.1, in this case, within the framework of the asymptotic description, the electron trajectories are also periodic with a period of $2\pi/k_\perp$ in K'. Thus, in the laboratory reference frame, the electrons move along the x axis with the group velocity of the laser and, and since $y' = y$ and $z' = z$, electron trajectories are periodic in the yz plane with period

$$T = \frac{2\pi}{k_\perp\sqrt{1 - v_g^2}} = \tau. \tag{2.46}$$

Therefore, the ambiguity of the velocity field in the asymptotic approach can be resolved by choosing the correct frame of reference.

So, we have shown that reduced motion equations (2.19) and (2.20) lead to periodic trajectories in a wide class of standing waves (for example, formed by laser beams of finite diameter) and the motion of electrons along the propagation axis of the laser pulse with its group velocity and periodic transverse motion. The latter can explain the effect of radiative trapping of particles induced by radiation reaction [63].

2.4 High-order corrections to the asymptotic description

The theory developed above makes it possible to describe the dynamics of an electron in the strongly radiation-dominated regime without specifying the expression for radiation friction force, and thus is a useful analytical tool with which we have obtained some new results. However, this approach has two significant limitations. First, as shown above, the real electron trajectories converge to the asymptotic ones fast enough only at extreme intensities exceeding 10^{25} W/cm^2 (at wavelength $\lambda = 1\,\mu$m). This is due to the fact that for most realistic EM field configurations, the characteristic time during which the electron velocity vector approaches the radiation-free direction is underestimated in our reasoning, which are given for a constant EM field. Secondly, it is impossible to calculate the energy and radiation losses of an electron when approaching the asymptotic trajectory, because the electron energy is assumed to be infinitely large, albeit much smaller than the dimensionless amplitude of the EM field. Despite these shortcomings, a similar approach was successfully applied to describe the dynamics of electrons in some astrophysical problems [89, 162, 163].

To get rid of the above drawbacks, we construct a perturbation theory, assuming that the electron velocity deviates from the radiation-free direction, but this deviation is small, i.e. we represent the electron velocity in the following form

$$\mathbf{v} = \left(1 - \frac{\delta^2}{2}\right)\mathbf{v}_0 + \mathbf{v}_1, \tag{2.47}$$

where $\mathbf{v}_1 \perp \mathbf{v}_0$ and δ can be found from the relation to the electron energy $|\mathbf{v}|^2 = 1 - \gamma^{-2}$ as follows

$$\delta^2 \approx v_1^2 + \gamma^{-2}. \tag{2.48}$$

Let us substitute this velocity representation into the equation (2.11) and expand it up to terms not higher than the second order in δ. We separately consider the term $\mathbf{F}_\perp$ in the rhs of the equation (2.11)

$$\mathbf{F}_\perp = -\frac{\delta^2}{2}[\mathbf{v}_0 \times \mathbf{B}] + [\mathbf{v}_1 \times \mathbf{B}] + \delta^2\mathbf{v}_0(\mathbf{v}_0\mathbf{E}) - \mathbf{v}_0(\mathbf{v}_1\mathbf{E}) - \mathbf{v}_1(\mathbf{v}_0\mathbf{E}) - \mathbf{v}_1(\mathbf{v}_1\mathbf{E}) + \mathcal{O}(\delta^3) \tag{2.49}$$

Let us transform the term $\mathbf{v}_1 \times \mathbf{B}$

$$\mathbf{v}_1 \times \mathbf{B} = -(\mathbf{v}_0\mathbf{B})[\mathbf{v}_0 \times \mathbf{v}_1] + \mathbf{v}_0(\mathbf{v}_0[\mathbf{v}_1 \times \mathbf{B}]). \tag{2.50}$$

Let us do a scalar multiplication of the equation (2.12) by $\mathbf{v}_1$

$$(\mathbf{v}_1\mathbf{E}) + \mathbf{v}_1[\mathbf{v}_0 \times \mathbf{B}] = 0. \tag{2.51}$$

After performing a cyclic permutation in the mixed product, we obtain

$$\mathbf{v}_0[\mathbf{v}_1 \times \mathbf{B}] = (\mathbf{v}_1\mathbf{E}). \tag{2.52}$$

Thus,

$$\mathbf{v}_1 \times \mathbf{B} = \mathbf{v}_0(\mathbf{v}_1\mathbf{E}) - [\mathbf{v}_0 \times \mathbf{v}_1](\mathbf{v}_0\mathbf{B}). \tag{2.53}$$

Performing similar actions, we can write the term $\mathbf{v}_0 \times \mathbf{B}$ in the following form

$$\mathbf{v}_0 \times \mathbf{B} = -\mathbf{v}_1\frac{(\mathbf{v}_1\mathbf{E})}{v_1^2} + [\mathbf{v}_0 \times \mathbf{v}_1]\frac{(\mathbf{v}_1\mathbf{B})}{v_1^2} \tag{2.54}$$

Thus, the transverse force $\mathbf{F}_\perp$ can be written as an expansion in the orthogonal basis $\mathbf{v}_0, \mathbf{v}_1, \mathbf{v}_0 \times \mathbf{v}_1$ as follows

$$\begin{aligned} \mathbf{F}_\perp = &\delta^2(\mathbf{v}_0\mathbf{E})\,\mathbf{v}_0 - \\ &-\left((\mathbf{v}_0\mathbf{E}) + (\mathbf{v}_1\mathbf{E})\frac{v_1^2-\gamma^{-2}}{2v_1^2}\right)\mathbf{v}_1 - \\ &-\left((\mathbf{v}_0\mathbf{B}) + (\mathbf{v}_1\mathbf{B})\frac{v_1^2+\gamma^{-2}}{2v_1^2}\right)[\mathbf{v}_0\times\mathbf{v}_1]. \end{aligned} \tag{2.55}$$

Consider the lhs of Eq. (2.11)

$$\frac{\mathrm{d}\mathbf{v}}{\mathrm{d}t} = \left(1-\frac{\delta^2}{2}\right)\frac{\mathrm{d}\mathbf{v}_0}{\mathrm{d}t} - \frac{\mathbf{v}_0}{2}\left(\frac{\mathrm{d}v_1^2}{\mathrm{d}t} + \frac{\mathrm{d}\gamma^{-2}}{\mathrm{d}t}\right) + \frac{\mathrm{d}\mathbf{v}_1}{\mathrm{d}t}. \tag{2.56}$$

To calculate the term $\mathrm{d}v_1^2/\mathrm{d}t$, we scalarly multiply the equation (2.11) by $\mathbf{v}_1$, taking into account that $\mathbf{v}_1\mathbf{v}_0 = 0$, and discarding terms of higher orders of smallness

$$\frac{1}{2}\frac{\mathrm{d}v_1^2}{\mathrm{d}t} = -\mathbf{v}_1\frac{\mathrm{d}\mathbf{v}_0}{\mathrm{d}t} + \frac{v_1^2(\mathbf{v}_0\mathbf{E})}{\gamma}. \tag{2.57}$$

Let us expand the term containing $\mathrm{d}\gamma^{-2}/\mathrm{d}t$ using the equation (2.11)

$$\frac{1}{2}\frac{\mathrm{d}\gamma^{-2}}{\mathrm{d}t} = -\frac{1}{\gamma^3}\frac{\mathrm{d}\gamma}{\mathrm{d}t} \approx \frac{\mathbf{v}_0\mathbf{E}}{\gamma^3}. \tag{2.58}$$

Thus,

$$\frac{1}{2}\frac{\mathrm{d}\delta^2}{\mathrm{d}t} = -\mathbf{v}_1\frac{\mathrm{d}\mathbf{v}_0}{\mathrm{d}t} + \delta^2\frac{(\mathbf{v}_0\mathbf{E})}{\gamma}. \tag{2.59}$$

Substituting the expressions (2.59) and (2.55) back into the equation (2.11), we get

$$\frac{\mathrm{d}\mathbf{v}_1}{\mathrm{d}t} = \frac{\mathbf{F}_1}{\gamma} - \left(1-\frac{\delta^2}{2}\right)\frac{\mathrm{d}\mathbf{v}_0}{\mathrm{d}t} - \mathbf{v}_0\left(\mathbf{v}_1\frac{\mathrm{d}\mathbf{v}_0}{\mathrm{d}t}\right), \tag{2.60}$$

$$\mathbf{F}_1 = \mathbf{v}_1\left((\mathbf{v}_0\mathbf{E}) + (\mathbf{v}_1\mathbf{E})\frac{v_1^2-\gamma^{-2}}{2v_1^2}\right) + [\mathbf{v}_0\times\mathbf{v}_1]\left((\mathbf{v}_0\mathbf{B}) + (\mathbf{v}_1\mathbf{B})\frac{\delta^2}{2v_1^2}\right). \tag{2.61}$$

Finally, let's find an expression for the QED parameter χ, based on its definition (2.2) and the above calculations

$$\chi = \frac{\gamma\delta}{a_S}\sqrt{\left[(\mathbf{v}_0\mathbf{E})^2 + (\mathbf{v}_0\mathbf{E})(\mathbf{v}_1\mathbf{E}) + (\mathbf{v}_0\mathbf{B})(\mathbf{v}_1\mathbf{B})\right] + \frac{\delta^2}{4v_1^2}\left[(\mathbf{v}_1\mathbf{E})^2 + (\mathbf{v}_1\mathbf{B})^2\right]}. \tag{2.62}$$

As a result, we have obtained the following system of general equations describing the dynamics of an electron in the strongly radiation-dominated regime

$$\frac{\mathrm{d}\mathbf{v}_1}{\mathrm{d}t} = \frac{\mathbf{F}_1}{\gamma} - \left(1 - \frac{\delta^2}{2}\right)\frac{\mathrm{d}\mathbf{v}_0}{\mathrm{d}t} - \mathbf{v}_0\left(\mathbf{v}_1\frac{\mathrm{d}\mathbf{v}_0}{\mathrm{d}t}\right), \tag{2.63}$$

$$\frac{\mathrm{d}\gamma}{\mathrm{d}t} = -\mathbf{v}_0\mathbf{E}\left(1 - \frac{\delta^2}{2}\right) - \mathbf{v}_1\mathbf{E} - F_{\mathrm{rr}}(\chi), \tag{2.64}$$

$$\mathbf{F}_1 = \mathbf{v}_1\left((\mathbf{v}_0\mathbf{E}) + (\mathbf{v}_1\mathbf{E})\frac{v_1^2 - \gamma^{-2}}{2v_1^2}\right) + [\mathbf{v}_0 \times \mathbf{v}_1]\left((\mathbf{v}_0\mathbf{B}) + (\mathbf{v}_1\mathbf{B})\frac{\delta^2}{2v_1^2}\right), \tag{2.65}$$

$$\chi = \frac{\gamma\delta}{a_{\mathrm{S}}}\sqrt{\left[(\mathbf{v}_0\mathbf{E})^2 + (\mathbf{v}_0\mathbf{E})(\mathbf{v}_1\mathbf{E}) + (\mathbf{v}_0\mathbf{B})(\mathbf{v}_1\mathbf{B})\right] + \frac{\delta^2}{4v_1^2}\left[(\mathbf{v}_1\mathbf{E})^2 + (\mathbf{v}_1\mathbf{B})^2\right]}. \tag{2.66}$$

Note that despite the fact that χ is proportional to the small parameter δ, it can be arbitrarily large due to the factor γ. Due to this, the term F_{rr} must be preserved in all expansion orders, which leads to the fact that the reduced motion equations remain nonlinear. It is also important to note that the total derivatives in the equations above must be understood in the sense of the derivative of the vector field $\mathbf{v}_0$ along the particle trajectory $\mathbf{r}(t)$, i.e.

$$\frac{\mathrm{d}\mathbf{v}_0}{\mathrm{d}t} = \frac{\partial\mathbf{v}_0}{\partial t} + (\mathbf{v}, \nabla)\mathbf{v}_0. \tag{2.67}$$

Consider the equation for the small parameter δ^2

$$\frac{1}{2}\frac{\mathrm{d}\delta^2}{\mathrm{d}t} = -\mathbf{v}_1\frac{\mathrm{d}\mathbf{v}_0}{\mathrm{d}t} + \frac{\delta^2(\mathbf{v}_0\mathbf{E})}{\gamma}. \tag{2.68}$$

From this equation, one can estimate the characteristic time of the electron trajectory approaching the asymptotic radiation-free trajectory in a constant EM field ($\mathrm{d}\mathbf{v}_0/\mathrm{d}t = 0$)

$$\tau_v = \frac{\gamma}{|\mathbf{v}_0\mathbf{E}|} \sim \frac{\gamma}{a_0}. \tag{2.69}$$

However, for a general EM field, the sign of the first term in the equation (2.68) can be arbitrary, and its value can be comparable to v_1, so the $\gamma \ll a_0$ condition alone is not enough to justify the asymptotic description of the electron dynamics in the zeroth order (2.19) in an arbitrary EM field. Thus, it is necessary to use the system of equations (2.63)–(2.64), which take into account the deviation of the velocity vector from the radiation-free direction. In addition, using these equations, one can find the energy of an electron and its radiation losses when moving in an EM field.

Let us explain the procedure carried out to obtain the reduced motion equations using simple steps. First, it was shown that there is a certain preferred radiation-free direction which the electron velocity approaches in a constant EM field. Decomposing the velocity vector in a basis in which one axis coincides with the radiation-free direction, we can split the equations of motion of an electron into two components. The motion along the radiation-free direction is essentially described by the energy of the particle, while the equations for the transverse velocity can be expanded into a series that obviously converges, since the length of the electron velocity vector is strictly less than unity.

Despite the fact that the resulting system of reduced equations remains non-linear and cannot be solved in a general form, examples will be considered below that show that this approach can be more productive than solving non-reduced motion equations. We also note that recently in the publication [164] a similar expansion was used to find equilibrium solutions to the equations (2.63)–(2.64).

Let us further consider specific examples of EM field configurations, in which the equations (2.63)–(2.64) can be explicitly solved in one form or another.

2.4.1 Generalized Zeldovich problem

Motion equations of an electron with account of radiation reaction can be analytically solved in a uniform rotating electric field, which was first demonstrated by Ya. B. Zeldovich [165]. Recently, in the Ref. [97], the Zeldovich solution was extended to the case when, in addition to the electric field, there is a uniform magnetic field parallel to it and rotating with the same frequency. This configuration of the EM field is of interest primarily because, with the exception of homogeneity, it is formed by the interference of two circularly polarized waves propagating towards each other. In particular, one of the first analytical solutions to the problem of QED cascade development was constructed precisely in this model field configuration [166, 167]. Let us construct a solution to the problem of the motion of an electron in such an EM field, using the theory we have developed. Let us assume that the electric and magnetic fields are uniform, parallel and rotate with the angular frequency $\mathbf{\Omega}$. The radiation-free direction in this case is opposite to the electric field: $\mathbf{v}_0 = -\mathbf{E}/E \equiv -\mathbf{e}$. We will be interested in the stationary solution, in which the electron velocity vector rotates synchronously with the electric and magnetic fields. In this case, in the equation (2.63) one can replace the time derivatives with the vector product $\mathbf{\Omega}\times$

$$\mathbf{\Omega} \times \mathbf{v}_1 = -\frac{E}{\gamma}\mathbf{v}_1 + \frac{B}{\gamma}\mathbf{e} \times \mathbf{v}_1 + \mathbf{\Omega} \times \mathbf{e} + v_1\mathbf{e}. \tag{2.70}$$

Using the fact that $\mathbf{v}_1 \perp \mathbf{v}_0$, the vector $\mathbf{v}_1$ can be decomposed into components as follows

$$\mathbf{v}_1 = v_\perp \mathbf{\Omega} \times \mathbf{e} + v_x \mathbf{\Omega}. \tag{2.71}$$

In this case, the equation (2.70) is split into a system of linear equations, the solution of which is easily found

$$v_x = \frac{\gamma B}{E^2 + B^2}, \tag{2.72}$$

$$v_\perp = \frac{\gamma E}{E^2 + B^2}, \tag{2.73}$$

$$v_1 = \frac{\gamma}{\sqrt{E^2 + B^2}}. \tag{2.74}$$

The stationarity of the solution also implies that the energy gain of an electron in an electric field is exactly compensated for by radiative losses, so $\mathrm{d}\gamma/\mathrm{d}t = 0$. In this case, the relation between the electron energy and the amplitude of the electric field is found from the following equation

$$E\left(1-\frac{\delta^2}{2}\right)=F_{\mathrm{rr}}\left(\frac{\gamma\delta E}{a_{\mathrm{S}}}\right), \tag{2.75}$$

$$\delta=\sqrt{v_1^2+\gamma^{-2}}=\sqrt{\frac{\gamma^2}{E^2+B^2}+\frac{1}{\gamma^2}}. \tag{2.76}$$

This result coincide exactly with the result obtained in the Ref. [97]. Let us separately consider the special case $B = 0$ investigated in the original publication by Zeldovich [165]. In this case, the solution is written in the following form

$$v_\perp=\frac{\gamma}{E}, \tag{2.77}$$

$$E\approx F_{\mathrm{rr}}\left(\frac{\gamma^2}{a_{\mathrm{S}}}\right). \tag{2.78}$$

Let us consider the classical radiation limit $\chi \ll 1$, in which the radiation power is given by $F_{\mathrm{rr}} = 2/3\alpha a_{\mathrm{S}}\chi^2$, then

$$E=\alpha\frac{2}{3}\frac{\gamma^4}{a_{\mathrm{S}}}. \tag{2.79}$$

In this case, the validity condition of the found solution, $v_\perp \ll 1$, can be rewritten in the following form

$$E\gg a_0^*\equiv\sqrt[3]{\frac{3}{2}\frac{a_{\mathrm{S}}}{\alpha}}. \tag{2.80}$$

This condition is often used as a definition of the strongly radiation-dominated regime regardless of the configuration of the EM field. This, however, is not always accurate, as will be shown below using the example of the problem of electron motion in plane waves.

Comparison of the obtained solution with the result of the numerical solution of non-reduced motion equations (2.10)–(2.11) with account the radiation reaction using both semiclassical and quantum approaches is presented in Fig. 2.3. The parameters of the EM field in this case were chosen so that the average value of the electron QED parameter χ was about 5. This choice was made to demonstrate the limits of applicability of our approach. In our theory, which is based on a semiclassical approach of describing radiation reaction, it is assumed that the value of the QED parameter χ does not differ significantly for electrons with similar initial conditions. In this case, we can assume that the radiative friction force averaged over the electron distribution function can be calculated as the friction force acting on the «average» electron, i.e. $\langle F_{\mathrm{rr}}(\chi)\rangle \approx F_{\mathrm{rr}}(\langle\chi\rangle)$, where angle brackets mean averaging over the electron distribution function. However, as can be seen from Fig. 2.3, the parameters of electrons with the same initial conditions acquire a significant spread during their motion, due to the stochastic nature of the radiation process. In connection with this and the character of the function $F_{\mathrm{rr}}(\chi)$ in the essentially quantum regime, the inequality $\langle F_{\mathrm{rr}}(\chi)\rangle < F_{\mathrm{rr}}(\langle\chi\rangle)$ is valid, which explains the difference between the values of v_x and $v_\perp$ obtained according to the analytical solution (2.72)–(2.73) and those obtained in the result of averaging over different runs of quantum numerical solutions, observed in Fig. 2.3 (b).

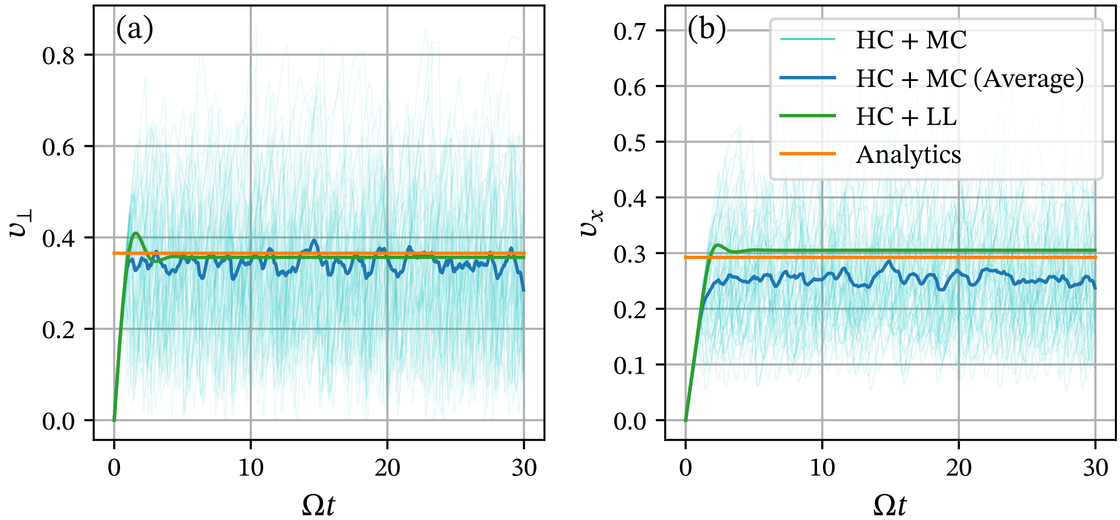

Figure 2.3: Dynamics of an electron in an electric field with a dimensionless amplitude $eE/mc\Omega = 2500$ and a parallel magnetic field with a dimensionless amplitude $eB/mc\Omega = 2000$, synchronously rotating with an angular frequency Ω corresponding to the wavelength $\lambda = 2\pi c/\Omega = 1\,\mu$m: (a) the electron velocity component across the electric field in the plane of rotation, (b) the electron velocity component along the angular vector speed $\mathbf{\Omega}$. Green (light blue) lines correspond to the numerical solution of non-reduced electron motion equations (2.10)–(2.11) with account of radiation reaction using the semiclassical (quantum) approach (see Appendix A), the dark blue lines correspond to values averaged over 100 runs of «quantum» solutions. The orange lines correspond to the analytical solution (2.72)–(2.73).

2.4.2 Model plasma accelerator

Let's consider a «toy model» of a plasma accelerator and find a known stable quasi-stationary solution in the radiation-dominated regime [54, 61] using the developed approach. To do this, we assume that the EM field is the sum of the uniform accelerating electric field $\mathbf{z}_0 E_{\text{acc}}$ and the focusing electric field $\mathbf{y}E_{\text{foc}}$ linearly dependent on the transverse coordinates, in which the electrons undergo betatron oscillations. To find a solution that corresponds to the constant radiation losses averaged over the period of betatron oscillations, we assume that an arbitrary function of the QED parameter χ is a strictly periodic function of time, i.e. its average value is constant. Mathematically, this condition is written as follows

$$\frac{\mathrm{d}\langle\chi^2\rangle}{\mathrm{d}t} = 0, \tag{2.81}$$

where the function χ^2 is used for the convenience of further reasoning. In the configuration of the EM field under consideration, it is easy to obtain an expression for χ from the equation (2.66)

$$\chi = \frac{\gamma\delta E}{a_{\text{S}}}. \tag{2.82}$$

Hereinafter, we will assume that the condition $\gamma \approx \langle\gamma\rangle$ is satisfied, i.e. the amplitude of oscillations of the electron energy is much less than the value of the energy itself. In this case, the energy γ can be taken out of the averaging sign in all calculations. Since we assume that the electron is accelerating, i.e. the value of γ increases with time, but the value of χ remains constant on average, then from the expression (2.82) it follows that the amplitude of oscillations of δ decreases with time. In this case, it is appropriate to assume that at large times the electron experiences predominantly an accelerating field, i.e. $E \approx E_{\text{acc}} = \text{const}$. The validity of both these assumptions is reliably confirmed by the numerical solution of the non-reduced motion equations and the final analytical solution obtained below. Using these assumptions, the equation (2.81) can be rewritten in the following form

$$\langle F_{\text{rr}} \rangle \langle \delta^2 \rangle + \gamma \left\langle \mathbf{v}_1 \frac{\mathrm{d}\mathbf{v}_0}{\mathrm{d}t} \right\rangle = 0. \tag{2.83}$$

Let us differentiate this expression

$$\frac{\langle F_{\text{rr}} \rangle}{\gamma} (3\langle F_{\text{rr}} \rangle - 2E_{\text{acc}}) \langle \delta^2 \rangle + \gamma \left\langle \mathbf{v}_1 \frac{\mathrm{d}^2\mathbf{v}_0}{\mathrm{d}t^2} - \left(\frac{\mathrm{d}\mathbf{v}_0}{\mathrm{d}t} \right)^2 \right\rangle = 0. \tag{2.84}$$

To calculate the last two terms in the expression above, we write the equations for the electron trajectory

$$\frac{\mathrm{d}\mathbf{r}}{\mathrm{d}t} = \mathbf{v}_0 + \mathbf{v}_1, \tag{2.85}$$

where

$$\mathbf{v}_0 = -\frac{-\mathbf{z}_0 E_{\text{acc}} + \mathbf{y} E_{\text{foc}}}{E} \approx \mathbf{z}_0 - \mathbf{y} \frac{E_{\text{foc}}}{E_{\text{acc}}} \equiv \mathbf{z}_0 - \varkappa \mathbf{y}. \tag{2.86}$$

Let us assume that the betatron oscillations are harmonic, i.e.

$$y = y_0 \cos \omega t, \tag{2.87}$$

then from the projection of the equation (2.85) onto the y axis we get

$$v_{1,y} = y_0 (\varkappa \cos \omega t - \omega \sin \omega t). \tag{2.88}$$

To calculate the average value of the sum of the last two terms in the equation (2.84), note that $\mathrm{d}\mathbf{v}_0/\mathrm{d}t = -\varkappa \mathrm{d}\mathbf{y}/\mathrm{d}t$

$$\left\langle \mathbf{v}_1 \frac{\mathrm{d}^2\mathbf{v}_0}{\mathrm{d}t^2} - \left(\frac{\mathrm{d}\mathbf{v}_0}{\mathrm{d}t} \right)^2 \right\rangle = y_0^2 \omega^2 \varkappa \left(\varkappa \left\langle \cos^2 \omega t - \sin^2 \omega t \right\rangle - \omega \left\langle \sin \omega t \cos \omega t \right\rangle \right) = 0. \tag{2.89}$$

As a result, we obtain the following relation for the model accelerator

$$\langle F_{\text{rr}} \rangle = \frac{2}{3} E_{\text{acc}}. \tag{2.90}$$

Thus, in the strongly radiation-dominated regime, the electron accelerates on average three times slower than in the case without account of radiation reaction, which is a known result [54, 61]. Fig. 2.4 demonstrates a good agreement between the obtained solution and the result of the numerical solution of non-reduced motion equations (2.10)–(2.11) . It should be noted that in our reasoning we did not explicitly use the expression for the power of radiation losses, although a more rigorous

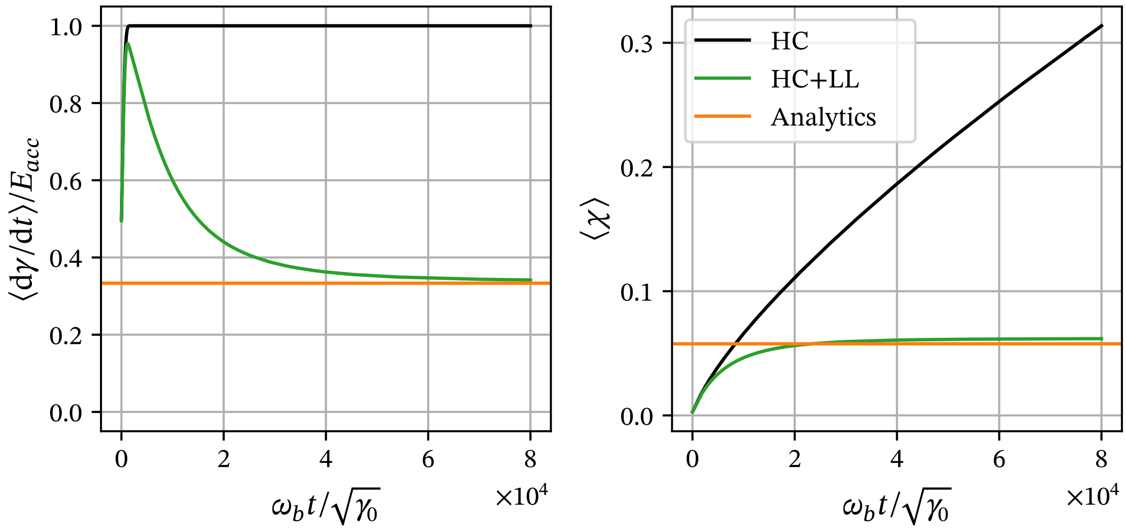

Figure 2.4: Dynamics of an electron in a model accelerator with an accelerating field $E_{\text{acc}} = 30\,\text{TV/m}$ and a focusing field E_{foc} linearly growing from 0 to $30\,\text{TV/m}$ at a transverse displacement of $0.1\,\mu\text{m}$: (a) average acceleration rate, (b) average value of the QED parameter χ. The time is normalized to the initial value of the reciprocal frequency of electron betatron oscillations $\omega_b/\sqrt{\gamma_0}$. The black line corresponds to the solution of the non-reduced motion equations averaged over the betatron oscillation period (2.10)–(2.11) without taking into account the radiation reaction; green line — with account of radiation reaction using semi-classical approach (see Appendix A). The orange line corresponds to the analytical solution (2.90)

derivation of the relation (2.90) shows that the result actually depends on the functional dependence of the radiation loss power on the parameter χ. In particular, according to the Ref. [61], in the quantum regime $\chi \gg 1$, when $F_{\text{rr}} \propto \chi^{2/3}$, the relation (2.90) is slightly modified

$$\langle F_{\text{rr}}\rangle = \frac{12}{19}E_{\text{acc}}, \tag{2.91}$$

which differs only by no more than 5% from the ratio (2.90), which is true in the classical $\chi \gg 1$ regime when $F_{\text{rr}} \propto \chi^2$. The above reasoning using the approach developed by us cannot accurately reproduce this insignificant difference due to the approximations used, in particular, neglecting the terms of the next orders of smallness in δ.

2.5 Motion in plane waves with account of radiation reaction

Let us apply the developed theory to solve the problem of electron motion in a plane EM wave with account of radiation reaction. For definiteness, consider the following plane wave configuration:

$$\mathbf{E} = \mathbf{y}_0 E_y(\varphi) + \mathbf{z}_0 E_z(\varphi), \tag{2.92}$$

$$\mathbf{B} = \mathbf{y}_0 E_z(\varphi) - \mathbf{z}_0 E_y(\varphi), \tag{2.93}$$

$$\varphi = t - x. \tag{2.94}$$

In this field configuration the radiation-free direction coincides with Poynting's vector and is constant

$$\mathbf{v}_0 = \frac{\mathbf{E}\times\mathbf{B}}{E^2}. \tag{2.95}$$

Let us write the reduced motion equations (2.63), (2.64)

$$\frac{\mathrm{d}\mathbf{v}_1}{\mathrm{d}t} = \frac{\mathbf{F}_1}{\gamma}, \tag{2.96}$$

$$\frac{\mathrm{d}\gamma}{\mathrm{d}t} = -\mathbf{v}_1\mathbf{E} - F_{\mathrm{rr}}. \tag{2.97}$$

Expression for $\mathbf{F}_1$ according to Eq. (2.65) is the following

$$\mathbf{F}_1 = \mathbf{v}(\mathbf{vE})\frac{v^2-\gamma^{-2}}{2v^2} + [\mathbf{v}_0\times\mathbf{v}](\mathbf{vB})\frac{\delta^2}{2v^2}, \tag{2.98}$$

where we omitted an index for $\mathbf{v}_1$. Note, that in this expression only terms of the second order of smallness in δ are present. Let us find an equation for v by scalar multiplication of Eq. (2.96) by $\mathbf{v}$

$$\frac{\mathrm{d}v}{\mathrm{d}t} = \frac{E\cos\psi}{2\gamma}\left(v^2 - \frac{1}{\gamma^2}\right), \tag{2.99}$$

where ψ is the angle between vector $\mathbf{v}$ and electric field of the plane wave $\mathbf{E}$, counted in such a way that when $\psi = +\pi/2$, velocity $\mathbf{v}$ is parallel to magnetic field of the wave $\mathbf{B}$, and thus $\mathbf{vB} = vB\sin\psi$. Let us also write an equation for product $\mathbf{vE}/E \equiv \mathbf{ve} = v\cos\psi$

$$\frac{\mathrm{d}}{\mathrm{d}t}(\mathbf{ve}) = \mathbf{e}\frac{\mathrm{d}\mathbf{v}}{\mathrm{d}t} + \mathbf{v}\frac{\mathrm{d}\mathbf{e}}{\mathrm{d}t}. \tag{2.100}$$

According to (2.98), the first term in the rhs of the above equation can be written as follows

$$\mathbf{e}\frac{\mathrm{d}\mathbf{v}}{\mathrm{d}t} = \frac{E\cos^2\psi}{2}\left(v^2 - \frac{1}{\gamma^2}\right) - \frac{E\sin^2\psi}{2}\left(v^2 + \frac{1}{\gamma^2}\right), \tag{2.101}$$

where we used the fact that $\mathbf{E}\perp\mathbf{B}$, $|E| = |B|$ in a plane wave. We can rewrite the second term in (2.100) the following way

$$\mathbf{v}\frac{\mathrm{d}\mathbf{e}}{\mathrm{d}t} = \mathbf{v}\frac{\mathrm{d}\mathbf{e}}{\mathrm{d}\varphi}\frac{\mathrm{d}\varphi}{\mathrm{d}t} = -v\sin\psi\Omega\frac{\mathrm{d}\varphi}{\mathrm{d}t}, \tag{2.102}$$

where it was assumed that direction of the electric field rotates with angular frequency $\Omega\mathbf{v}_0$. In this case, $\Omega = 0$ corresponds to linearly-polarized plane wave, $\Omega = \pm 1$ — to elliptically- or circularly-polarized plane wave (given a corresponding dependency $E(\varphi)$). Thus, Eq. (2.100) can be rewritten as follows

$$\frac{\mathrm{d}v}{\mathrm{d}t}\cos\psi - v\sin\psi\frac{\mathrm{d}\psi}{\mathrm{d}t} = \frac{E\cos^2\psi}{2}\left(v^2 - \frac{1}{\gamma^2}\right) - \frac{E\sin^2\psi}{2}\left(v^2 + \frac{1}{\gamma^2}\right) - v\sin\psi\Omega\frac{\mathrm{d}\varphi}{\mathrm{d}t}. \tag{2.103}$$

Using Eq. (2.99) we finally obtain

$$\frac{\mathrm{d}\psi}{\mathrm{d}t} - \Omega\frac{\mathrm{d}\varphi}{\mathrm{d}t} = \frac{E\sin\psi}{2v}\left(v^2 + \frac{1}{\gamma^2}\right). \tag{2.104}$$

Let us introduce a transverse momentum $p = \gamma v$ and write an equation for it using Eqs. (2.97) and (2.99)

$$\frac{\mathrm{d}p}{\mathrm{d}t} = \gamma\frac{\mathrm{d}v}{\mathrm{d}t} + v\frac{\mathrm{d}\gamma}{\mathrm{d}t} = -E\cos\psi\frac{1+p^2}{2\gamma^2} - F_{\mathrm{rr}}\frac{p}{\gamma}, \tag{2.105}$$

Let us change the integration variable to φ, considering the following

$$\frac{\mathrm{d}\varphi}{\mathrm{d}t} = 1 - v_x = 1 - \sqrt{1-\delta^2} \approx \frac{\delta^2}{2} = \frac{1+p^2}{2\gamma^2}, \tag{2.106}$$

and obtain the following system of equations

$$\frac{\mathrm{d}p}{\mathrm{d}\varphi} = -E\cos\psi - F_{\mathrm{rr}}\frac{2p\gamma}{1+p^2}, \tag{2.107}$$

$$\frac{\mathrm{d}\gamma}{\mathrm{d}\varphi} = -E\cos\psi\frac{2p\gamma}{1+p^2} - F_{\mathrm{rr}}\frac{2\gamma^2}{1+p^2}, \tag{2.108}$$

$$\frac{\mathrm{d}\psi}{\mathrm{d}\varphi} = \frac{E\sin\psi}{p} + \Omega. \tag{2.109}$$

Note, that

$$2p\gamma\frac{\mathrm{d}p}{\mathrm{d}\varphi} - (1+p^2)\frac{\mathrm{d}\gamma}{\mathrm{d}\varphi} = -2F_{\mathrm{rr}}(\chi)\gamma^2\frac{p^2-1}{p^2+1}. \tag{2.110}$$

Let us transform the lhs of this equation

$$2p\gamma\frac{\mathrm{d}p}{\mathrm{d}\varphi} - (1+p^2)\frac{\mathrm{d}\gamma}{\mathrm{d}\varphi} = \gamma^2\left(\frac{2p}{\gamma}\frac{\mathrm{d}p}{\mathrm{d}\varphi} - (1+p^2)\frac{1}{\gamma^2}\frac{\mathrm{d}\gamma}{\mathrm{d}\varphi}\right) = \gamma^2\frac{\mathrm{d}}{\mathrm{d}\varphi}\left(\frac{1+p^2}{\gamma}\right). \tag{2.111}$$

Thus,

$$\frac{\mathrm{d}}{\mathrm{d}\varphi}\left(\frac{1+p^2}{2\gamma}\right) = -F_{\mathrm{rr}}(\chi)\frac{p^2-1}{p^2+1}. \tag{2.112}$$

The rhs of this equations zeros out in classical limit and thus the value $p_- \equiv (1+p^2)/2\gamma$ is a constant of motion if radiation reaction is not accounted for. It is not difficult to see that p_- is nothing else that a well-known integral of motion $\gamma - p_x$ commonly called a *light-front momentum* [158]. Notably, without radiation reaction this quantity is conserved exactly even according to approximate equations. We can find an expression for χ according to (2.66)

$$\chi = \frac{\gamma|E|}{a_{\mathrm{S}}}\frac{1}{2}\left(v^2 + \frac{1}{\gamma^2}\right) = \frac{|E|}{a_{\mathrm{S}}}\frac{1+p^2}{2\gamma} = \frac{|E|}{a_{\mathrm{S}}}p_-. \tag{2.113}$$

Since value of p_- decreases when we account radiation reaction[2], so as χ decreases. Thus, after a finite time an electron with arbitrary initial conditions will reach the classical regime of radiation $\chi \ll 1$. We restrict ourselves to considering this limit case only, then

$$F_{\mathrm{rr}}(\chi) = \frac{2}{3}\alpha a_S \chi^2 = \frac{2}{3}\frac{\alpha}{a_S}E^2 p_-^2. \tag{2.114}$$

Equation for p_- is written as follows

$$\frac{\mathrm{d}p_-}{\mathrm{d}\varphi} = -\frac{2}{3}\frac{\alpha}{a_S}|E|^2 p_-^2 \frac{p^2-1}{p^2+1}. \tag{2.115}$$

Consider the last factor in the rhs of the equation

$$\frac{p^2-1}{p^2+1} = \frac{1-p^{-2}}{1+p^{-2}} = 1 - 2p^{-2} + \mathcal{O}(p^{-4}) \approx 1, \tag{2.116}$$

where the last equality is valid if

$$p^2 \gg 2. \tag{2.117}$$

If this condition is satisfied, Eq. (2.115) can be solved in quadratures

$$p_- = p_{-,0}\left(1 + \frac{2}{3}\frac{\alpha p_{-,0}E_0^2}{a_S}\int \frac{E^2}{E_0^2}\mathrm{d}\varphi\right)^{-1}. \tag{2.118}$$

Note, that

$$\frac{2}{3}\frac{\alpha p_{-,0}E_0^2}{a_S} = \frac{2}{3}\alpha\chi_0|E_0| \equiv \mathscr{A}, \tag{2.119}$$

and $\mathscr{A}$ is Lorentz-invariant in virtue of invariance of χ_0 and E_0. Let us introduce Φ the following way

$$\Phi \equiv \frac{1}{E_0^2}\int E^2 \mathrm{d}\varphi, \tag{2.120}$$

then

$$\frac{p_-}{p_{-,0}} = \frac{1}{1+\mathscr{A}\Phi}. \tag{2.121}$$

Note, that both sides of this relation are also Lorentz-invariant. The definition $p_- = (1+p^2)/2\gamma$ used above is valid only in limit $\gamma \gg 1 + p^2$. In general case p_- can be expressed as follows

$$p_- = \gamma - p_x = \gamma - \sqrt{\gamma^2 - 1 - p^2}. \tag{2.122}$$

Solving this in terms of γ we obtain

$$\gamma = \frac{1}{2}\left(\frac{1+p^2}{p_-} + p_-\right) = \frac{1}{2}\left(\frac{(1+p^2)(1+\mathscr{A}\Phi)}{p_{-,0}} + \frac{p_{-,0}}{1+\mathscr{A}\Phi}\right). \tag{2.123}$$

[2]This statement is true if $p > 1$. As will be shown below, the average value of p over a wave period can be estimated as a_0, thus the value p_- strictly decreases during each wave period.

Analogously, p_x is found as follows

$$p_x = \frac{1}{2}\left(\frac{1+p^2}{p_-} - p_-\right) = \frac{1}{2}\left(\frac{(1+p^2)(1+\mathscr{A}\Phi)}{p_{-,0}} - \frac{p_{-,0}}{1+\mathscr{A}\Phi}\right). \tag{2.124}$$

Let us rewrite equations for p and ψ accordingly

$$\frac{\mathrm{d}p}{\mathrm{d}\varphi} = -E\cos\psi - \frac{\mathscr{A}p}{1+\mathscr{A}\Phi}\frac{E^2}{E_0^2}, \tag{2.125}$$

$$\frac{\mathrm{d}\psi}{\mathrm{d}\varphi} = \frac{E\sin\psi}{p} + \Omega. \tag{2.126}$$

Let us also introduce variables $p_e = p\cos\psi$ and $p_b = p\sin\psi$ corresponding to projections of the electron momentum to electric and magnetic fields of the wave, respectively. Equations for these new variable have the following form

$$\frac{\mathrm{d}p_e}{\mathrm{d}\varphi} = -E - \Omega p_b - \frac{\mathscr{A}}{1+\mathscr{A}\Phi}\frac{E^2}{E_0^2}p_e, \tag{2.127}$$

$$\frac{\mathrm{d}p_b}{\mathrm{d}\varphi} = \Omega p_e - \frac{\mathscr{A}}{1+\mathscr{A}\Phi}\frac{E^2}{E_0^2}p_b. \tag{2.128}$$

Let us multiply these equations by $1+\mathscr{A}\Phi$ and note that $\mathrm{d}\Phi/\mathrm{d}\varphi \equiv E^2/E_0^2$. Then

$$(1+\mathscr{A}\Phi)\frac{\mathrm{d}p_e}{\mathrm{d}\varphi} + \mathscr{A}\frac{\mathrm{d}\Phi}{\mathrm{d}\varphi}p_e = -(E+\Omega p_b)(1+\mathscr{A}\Phi), \tag{2.129}$$

$$(1+\mathscr{A}\Phi)\frac{\mathrm{d}p_b}{\mathrm{d}\varphi} + \mathscr{A}\frac{\mathrm{d}\Phi}{\mathrm{d}\varphi}p_b = \Omega p_e(1+\mathscr{A}\Phi). \tag{2.130}$$

Introducing $\epsilon = (1+\mathscr{A}\Phi)p_e$ and $\beta = (1+\mathscr{A}\Phi)p_b$, we finally obtain

$$\frac{\mathrm{d}\epsilon}{\mathrm{d}\varphi} = -\Omega\beta - E(1+\mathscr{A}\Phi), \tag{2.131}$$

$$\frac{\mathrm{d}\beta}{\mathrm{d}\varphi} = \Omega\epsilon. \tag{2.132}$$

Thus, Eqs. (2.120), (2.121), and (2.131), (2.132) completely define electron motion in plane wave with account of radiation reaction. Note, that Eqs. (2.131), (2.132) is a system of *linear* differential equations. Although this system has general solution, it is of little interest. Instead, below we consider three special cases.

2.5.1 Constant crossed fields

Let us start by considering constant crossed fields, corresponding to $\Omega = 0$, $E = a_0 = \text{const}$. In that case

$$\Phi = \varphi, \tag{2.133}$$

$$p_- = \frac{p_{-,0}}{1 + \mathscr{A}\varphi}. \tag{2.134}$$

Let us rewrite Eqs. (2.131), (2.132), which become independent in that case

$$\frac{\mathrm{d}\epsilon}{\mathrm{d}\varphi} = -a_0(1 + \mathscr{A}\varphi), \tag{2.135}$$

$$\frac{\mathrm{d}\beta}{\mathrm{d}\varphi} = 0. \tag{2.136}$$

Solving these equations and transforming back to variables p_e, p_b, we get

$$p_e = \frac{p_{e,0} - a_0\varphi\left(1 + \frac{\mathscr{A}\varphi}{2}\right)}{1 + \mathscr{A}\varphi}, \tag{2.137}$$

$$p_b = \frac{p_{b,0}}{1 + \mathscr{A}\varphi} \tag{2.138}$$

Values of γ and p_x can be expressed via p_- and $p = \sqrt{p_e^2 + p_b^2}$, according to (2.123), (2.124).

Note, that since the fields are constant, then all the final expressions have to be written using the combinations which do not depend on nominal normalization frequency ω. According to definitions $\mathscr{A} \propto a_0 \propto \omega^{-1}$, $\varphi \propto \omega$, thus this requirement is met.

2.5.2 Monochromatic circularly-polarized plane wave

Let us next consider a monochromatic circularly-polarized plane wave, which corresponds to $\Omega = 1$, $E = a_0 = \text{const}$, where sign of Ω is chose for definiteness. In that case,

$$\Phi = \varphi, \tag{2.139}$$

$$p_- = \frac{p_{-,0}}{1 + \mathscr{A}\varphi}, \tag{2.140}$$

thus

$$\frac{\mathrm{d}\epsilon}{\mathrm{d}\varphi} = -\beta - a_0(1 + \mathscr{A}\varphi), \tag{2.141}$$

$$\frac{\mathrm{d}\beta}{\mathrm{d}\varphi} = \epsilon. \tag{2.142}$$

The equations above essentially describe a harmonic oscillator under linearly growing force, and the solution of these equations is known

$$\epsilon = -a_0\mathscr{A} - (\beta_0 + a_0)\sin\varphi + (\epsilon_0 + a_0\mathscr{A})\cos\varphi, \tag{2.143}$$

$$\beta = -a_0(1 + \mathscr{A}\varphi) + (\beta_0 + a_0)\cos\varphi + (\epsilon_0 + a_0\mathscr{A})\sin\varphi. \tag{2.144}$$

Finally, transforming to variables p_e and p_b, we get

$$p_e = \frac{-\mathscr{A}a_0 - (p_{b,0} + a_0)\sin\varphi + (p_{e,0} + a_0\mathscr{A})\cos\varphi}{1 + \mathscr{A}\varphi}, \tag{2.145}$$

$$p_b = -a_0 + \frac{(p_{b,0} + a_0)\cos\varphi + (p_{e,0} + a_0\mathscr{A})\sin\varphi}{1 + \mathscr{A}\varphi} \tag{2.146}$$

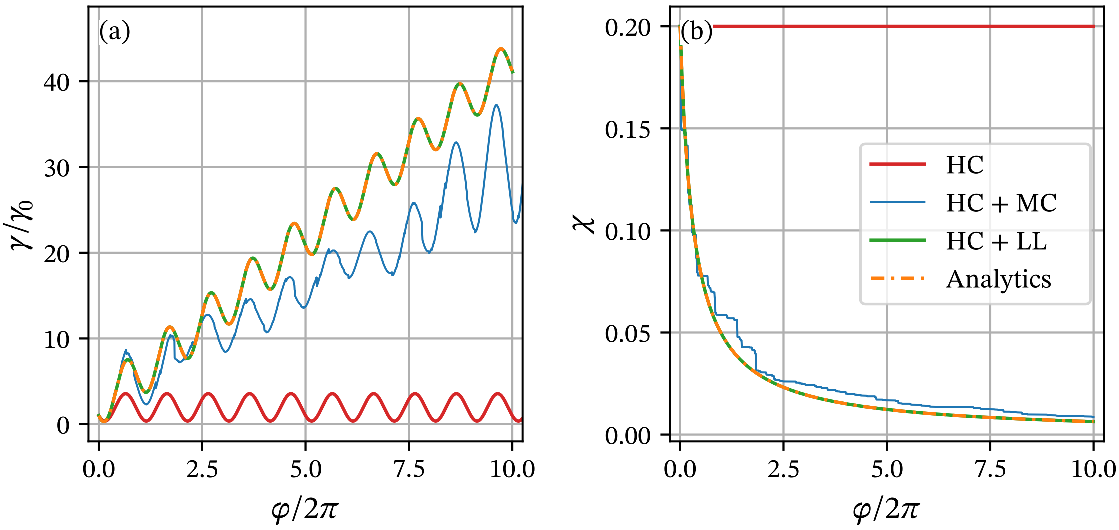

Figure 2.5: Dynamics of an electron with initial momentum $p_{x,0} = 400$, $p_{y,0} = p_{e,0} = 240$, $p_{z,0} = p_{b,0} = -320$ ($\gamma_0 \approx 568$) in a monochromatic circularly-polarized plane wave with dimensionless amplitude $a_0 = 500$ and wavelength $\lambda = 1\,\mu\text{m}$ ($\chi_0 = 0.2$, $\mathscr{A} \approx 0.5$) propagating along the x axis: (a) the electron energy normalized to its initial value, (b) the value of the QED parameter $\chi = a_0 p_-/a_S$. The red line corresponds to the classical solution without account of radiation reaction, the green (blue) line — to the numerical solution of non-reduced motion equations (2.10)–(2.11) with account of radiation reaction using the semiclassical (quantum) approach (see Appendix A). The orange dotted line corresponds to the analytical solution (2.140), (2.145), (2.146).

2.5.3 Monochromatic linearly-polarized plane wave

Finally, let us consider monochromatic linearly-polarized plane wave: $E_y = a_0\cos\varphi$, $E_z = 0$, $\Omega = 0$. In that case,

$$\Phi = \frac{1}{2}\left(\varphi + \frac{\sin 2\varphi}{2}\right), \tag{2.147}$$

$$p_- = \frac{p_{-,0}}{1 + \frac{\mathscr{A}}{2}\left(\varphi + \frac{\sin 2\varphi}{2}\right)}, \tag{2.148}$$

thus

$$\frac{\mathrm{d}\epsilon}{\mathrm{d}\varphi} = -a_0 \cos\varphi \left(1 + \frac{\mathscr{A}}{2}\left(\varphi + \frac{\sin 2\varphi}{2}\right)\right), \tag{2.149}$$

$$\frac{\mathrm{d}\beta}{\mathrm{d}\varphi} = 0. \tag{2.150}$$

Integrating these equations and writing the result in terms of the variables p_e, p_b, we get

$$p_e = \frac{p_{e,0} + a_0 \sin\varphi \left(1 + \frac{\mathscr{A}\varphi}{2}\right) - \frac{2\mathscr{A}a_0}{3}(2 + \cos\varphi)\sin^4\frac{\varphi}{2}}{1 + \frac{\mathscr{A}}{2}\left(\varphi + \frac{\sin 2\varphi}{2}\right)}, \tag{2.151}$$

$$p_b = \frac{p_{b,0}}{1 + \frac{\mathscr{A}}{2}\left(\varphi + \frac{\sin 2\varphi}{2}\right)}. \tag{2.152}$$

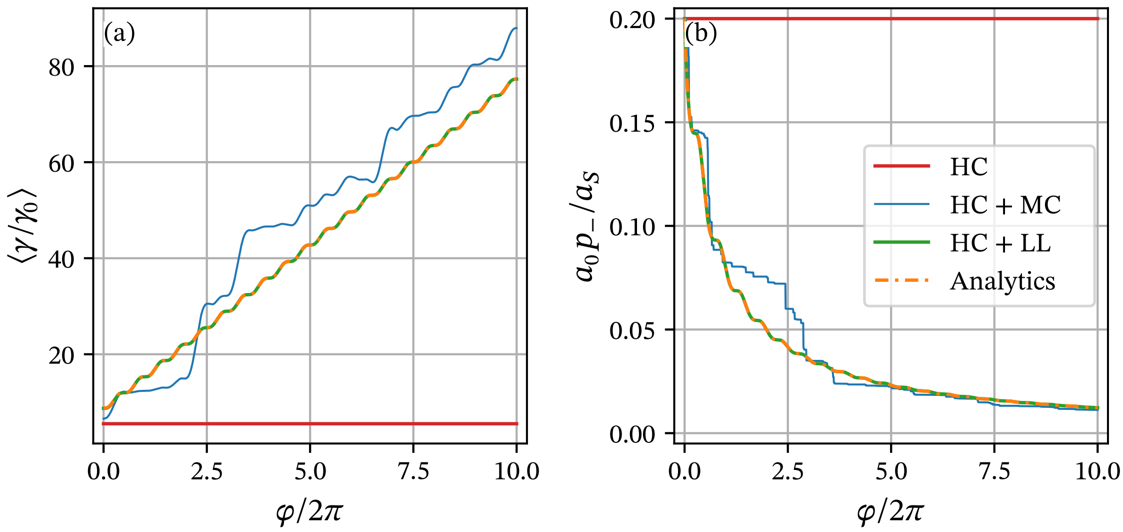

Figure 2.6: Dynamics of an electron with initial momentum $p_{x,0} = -81$, $p_{y,0} = p_{e,0} = -12$, $p_{z,0} = p_{b,0} = 16$ ($\gamma_0 \approx 84$) in a monochromatic linearly-polarized plane wave with dimensionless amplitude $a_0 = 500$ and wavelength $\lambda = 1\,\mu\mathrm{m}$ ($\chi_0 = 0.2$, $\mathscr{A} \approx 0.5$) propagating along the x axis: (a) the electron energy averaged over a wave period normalized to its initial value, (b) the maximum value of the QED parameter $\chi = a_0 p_- / a_S$ on a wave period. The red line corresponds to the classical solution without account of radiation reaction, the green (blue) line — to the numerical solution of non-reduced motion equations (2.10)–(2.11) with account of radiation reaction using the semiclassical (quantum) approach (see Appendix A). The orange dotted line corresponds to the analytical solution (2.148), (2.151), (2.152).

2.5.4 Discussion

We note that the exact solution of the non-reduced electron motion equations without account of radiation reaction in the considered special cases is well-known (see, for example, [158]) and it coincides with the solutions we obtained in the limit $\mathscr{A} = 0$. Moreover, in the publication [168], an exact solution of the electron motion equations with account of radiation in the Landau-Lifshitz form (which is also used in our solution) was found, but it is written in an implicit form, which is quite difficult for further analysis. The solution obtained with the help of the theory developed by us is written in a simple form and coincides with the exact solution in the limit $a_0 \gg 1$. We note a common property of the obtained solutions: the radiation reaction does not significantly change the transverse dynamics of an electron in a plane wave, but leads to an increase in the electron energy by a factor of $\mathscr{A}\varphi$ (up to a numerical factor) compared to the case without the radiation reaction. This leads to a rather unexpected result, that in a monochromatic plane wave (circularly or linearly polarized), the average value of the electron energy over the period of the wave, which is associated mainly with longitudinal motion, grows indefinitely. Despite the fact that this behavior has been known for quite some time (see [165, 168–173]) and it is confirmed by the numerical solution of non-reduced motion equations (2.10)–(2.11) (see Figs. 2.5–2.6), it doesn't seem to be widely acknowledged yet. Rather simple considerations can resolve the apparent inconsistency of this result. For this, it is more convenient to describe the radiation reaction from the quantum point of view. Repeating the arguments made in the introduction to this chapter, in a relativistically strong plane wave ($a_0 \gg 1$), the radiation formation length can be estimated as $\lambda/a_0 \ll \lambda$, from which it is concluded that the electron moves classically between almost instantaneous acts of radiation. Without taking into account the radiation reaction, the quantity $\gamma - p_x$ is a well-known constant of motion, where p_x is the electron momentum along the wave propagation direction (red line in Fig. 2.6 (b)) The emission probability depends on the value of the QED parameter χ, which in a plane wave can be expressed as follows

$$\chi = \frac{E(\varphi)}{a_\mathrm{S}} (\gamma - p_x) \,. \tag{2.153}$$

Since the radiation formation length is significantly less than the wavelength, we can assume that the radiation occurs in constant fields. In this case, it follows from the conservation of momentum and energy that the value of χ strictly decreases after radiation. This fact is well demonstrated by the blue line in Fig. 2.6 (b), which shows characteristic jumps corresponding to the emission of individual photons. Thus, we can conclude that when the radiation reaction is taken into account, the quantity $\gamma - p_x$ asymptotically tends to zero, which can be only achieved in the case when the longitudinal momentum p_x (and the energy γ, respectively) increase indefinitely.

This example is also very indicative in terms of the domain of applicability of our approach. The asymptotic theory developed above is initially based on the basic assumption that the electron velocity is «attracted» to the radiation-free direction faster than the EM field changes. This condition is fulfilled if inequality $\gamma \ll a_0$ is valid, which, in turn, is implied from an estimate of the characteristic energy of an electron in a plane wave without account of radiation reaction $\gamma \approx \sqrt{1 + a_0^2}$. However, as the solution obtained above shows, the energy of an electron in a plane wave, with account of radiation reaction, grows indefinitely, while the wave amplitude a_0 obviously remains constant. Therefore, after a finite time, the condition $\gamma \ll a_0$ ceases to be satisfied on most of the parts of the electron trajectory. Nevertheless, the solution we constructed coincides with the numerical solution with surprising accuracy. This disagreement can be resolved only by discarding the condition $\gamma \ll a_0$ as determining the applicability of the radiation-free description in the general case. Moreover, the only condition necessary for the validity of the resulting solution in a plane wave is the condition $a_0 \gg 1$, which also differs significantly from the applicability condition of, for example, the Zeldovich solution (2.80), which is written as $a_0 \gg a_0^*$, where $a_0^* \gg 1$ (at least for optical frequencies). Thus, apparently, the domain of applicability of the developed theory turns out to be broader than originally assumed and the question of the boundaries of this domain is still open. Some definiteness is given by the fact that the developed theory is nothing more than the expansion of the motion equations, written with respect to its velocity, in a series around some assumption $\mathbf{v}_0$. Since the magnitude of the electron velocity vector is strictly less than unity, the expansion around an arbitrary initial assumption $\mathbf{v}(\mathbf{r},\ t)$ converges. It turns out that in the strongly radiation-dominated regime, when the radiation-free direction $\mathbf{v}_0$ is chosen as the zeroth approximation, the series expansion converges most quickly, so in some problems expansion only to linear or quadratic terms is sufficient. We also note that in recent papers [164, 174] attempts were made to unify these conditions, but their reliability has not yet been verified on a large number of EM field configurations, in particular, those considered in this work.

2.6 Summary

To sum up, it was shown that in the strongly radiation-dominated regime, the velocity rather than its derivative of charged particles is determined by local EM field (2.20). This means that the electron trajectory can be found from the first order equation (2.19). We call this velocity direction *asymptotic*, since it coincides with the asymptotic ($t \to \infty$) electron velocity in the constant field approximation. The reason for reducing the order of the equation is that the energy of electrons in the regime of extreme radiation losses is small ($\gamma \ll a_0$), i.e. the electrons turn out to be «light» and are quickly turned by a strong field towards the asymptotic direction in a time much shorter than the characteristic time of the change of the EM field itself. The velocity field $\mathbf{v}_0(\mathbf{r}, t)$ corresponds to the absence of the transverse component of the Lorentz force and, accordingly, the force of radiative friction, therefore $\mathbf{v}_0$ is also called the radiation-free direction [175].

In several configurations of the electromagnetic field, numerical solutions of reduced and non-reduced electron motion equations with account of radiation reaction are found. Comparison of these solutions shows that the reduced equations can be used for a qualitative description of electron trajectories at a_0 larger or of the order of a thousand for optical wavelengths. In this regard, the constructed description is also asymptotic in terms of field strength, i.e. $a_0 \to \infty$.

It was also shown that the developed asymptotic theory is a useful analytical tool. For example, the asymptotic theory predicts periodic electron trajectories in a wide class of standing electromagnetic fields (including the case of counter-propagating sharply focused laser pulses, see section 2.3), which is fundamentally different from the results obtained in the ponderomotive approximation. This result is in good agreement with the work [161], which demonstrates a decrease in the ponderomotive force in the radiation-dominated regime. In addition, it was shown that in a certain configuration of a laser pulse in the radiation-dominated regime, electrons are not scattered, but trapped and carried away with the group velocity of the pulse. This result can possibly explain the radiative trapping of particles observed in numerical simulations in various configurations [62–67].

Thus, the ponderomotive approximation becomes inapplicable in the radiation-dominated regime and should be replaced by an asymptotic description. The latter also means that the velocities of all electrons in a small neighborhood practically coincide; therefore, their collective dynamics can be described in terms of the hydrodynamic approach. Such a hydrodynamic approach will be applied in the next chapter to describe the development of a QED cascade in the field of a plane wave.

Finally, high-order corrections to the asymptotic theory were found, with the help of which it is possible to describe dynamics of particles in the strongly radiation-dominated regime more accurately. It is noteworthy that the developed method makes it possible to obtain qualitatively new results in comparison with the «zeroth order» asymptotic theory. Application of this approach has been demonstrated in various electromagnetic field configurations. In particular, the solution of the generalized Zeldovich problem of the electron dynamics in rotating parallel electric and magnetic fields was reproduced [97, 165], a decrease in the average rate of electron acceleration in a model plasma accelerator was demonstrated [54, 61], and a little-known feature of the electron motion in strong plane waves was described, namely unlimited longitudinal acceleration [168–173].

Contributions of the author

The results obtained in this chapter are published in Refs. [176, 177]. In the publication [176] A. S. and E. N. worked together on the development of the asymptotic theory and obtaining general properties of the asymptotic trajectories. In publication [176] A. S. carried out the majority of the work.

Chapter 3

Interaction of extremely intensive laser radiation with a solid target

3.1 Introduction

In the previous chapter, it was shown that radiation reaction can significantly affect the particle dynamics in strong EM fields. In addition to radiation reaction, there is another important phenomena that can have a significant effect on the behavior of matter in extreme EM fields — development of QED *cascades* [46, 93–97, 105, 113–115, 129, 178]. They arise as a result of the emission of hard photons by ultrarelativistic particles, and the subsequent decay of the former into electron-positron pairs as a result of the nonlinear Breit-Wheeler process or the nonlinear trident process. Secondary particles become also involved in the emission of new generations of photons and photoproduction of pairs, which leads to an avalanche-like increase in the total number of particles. One of the main reasons why the development of QED cascades has not yet been experimentally demonstrated is the fact that this is a threshold phenomenon in terms of the intensity of the EM field. This, in turn, is due to the exponentially small probability of the Breit-Wheeler process and the trident process in the parameter range $\chi \lesssim 1$, where χ is the photon QED parameter defined as follows

$$\chi = \frac{\varepsilon}{a_S}\sqrt{(\mathbf{E} + \mathbf{v} \times \mathbf{B})^2 - (\mathbf{v}\mathbf{E})^2}, \tag{3.1}$$

where ε and $\mathbf{v} \equiv \mathbf{k}/k$ are the energy normalized to mc^2 and direction of the photon propagation, respectively, $\mathbf{k}$ is the wave vector of a photon. To estimate the parameters of laser radiation required to observe a QED cascade, it is usually assumed that the characteristic energy of an electron in the laser field is equal in order of magnitude to a_0. Thus, the condition $\chi > 1$ required for the development of a QED cascade can be written in terms of the laser parameters as $I[10^{23}\,\mathrm{W/cm^2}]\lambda[\mu\mathrm{m}] \gtrsim 5$. This estimate is quite optimistic in relation to the new-generation laser systems mentioned in the Introduction, which operate in the optical range $\lambda \approx 1\,\mu$m and which are expected to have intensities of the order of $I \sim 10^{24}\,\mathrm{W/cm^2}$. However, due to the threshold nature of the QED cascade, the rough estimate presented above is impractical, while more accurate estimates depend significantly on the interaction configuration. In this regard, an active search is currently underway for such optimal configurations at which the intensity threshold for the development of a QED cascade would be minimal [46, 68, 97–104, 179–193]. These configurations can be mainly divided into two groups: in the first one, the interaction of a laser beam with a preliminarily accelerated seed is considered, and in the second one, the use of a multi-beam laser configuration and interaction with an initially stationary seed is suggested. While both these configurations maximize QED parameter χ, there is a fundamental difference between these two approaches. In the first case, the cascade energy is limited by the initial energy of the seed, and such a cascade is called a *shower* or an S-type cascade. Air showers caused by cosmic rays are an example of such cascades [194]. In the second case, the cascade draws energy from the electromagnetic field, and is called *self-sustaining*, *avalanche* or an A-type cascade. It is important to note, that a single plane wave configuration is considered to be suboptimal for observing self-sustained QED cascade [96, 144, 186, 195], since the QED parameter χ is conserved during particle motion in a plane wave and is reduced at each emission of gamma photon, so each new generation of particles are less likely to produce the next generation, i.e. cascade is unable to sustain itself. When several and/or sharply focused laser beams are used, the configuration of the EM field differs significantly from the field of a single plane wave. This is also the case, e.g. for the field formed during the interaction of laser radiation with plasmas, in particular with solid targets. The influence of QED effects on the interaction of a laser with a solid target is mainly studied in the «hole boring» regime [23, 196], when the target thickness is much greater than the laser skin-depth. In particular, in numerical simulations, the formation of electron-positron plasma «cushions» is observed, which, however, do not stop the ion acceleration [57, 95, 97, 102, 197]. This regime of interaction is generally characterized by a significant reflection of the incident laser radiation, therefore, the development of a QED cascade in this configuration is in many respects analogous to the configuration with two counter-propagating pulses. If the target thickness does not exceed the depth of the skin layer, then the «light sail» regime is realized [20, 23, 27]. In this case, the foil is continuously accelerated as a whole, and laser reflection is insignificant. Although the light sail regime has attracted considerable interest in recent years as one of the most efficient schemes for laser ion acceleration [24, 27], it has been rather poorly studied in the region of extremely high laser radiation intensities, when QED effects play a key role.

Because of unstable nature of QED cascade and complex nonlinear interaction between the produced electron-positron plasma and EM field, analytical models describing the process usually consider significantly simplified EM configurations [166, 180, 187, 198], and its experimental observation is still impossible. Therefore, the most common tool for studying QED cascades is numerical simulation, among the methods of which the most fruitful is the *particle-in-cells* (PIC) method [199] with inclusion of stochastic QED processes using the Monte-Carlo method (see Ref. [200] and links therein). PIC modeling serves as the starting point for most of the current research in this area, and provides valuable information about the nature of QED cascade phenomenon. However, this method is extremely demanding on computational resources, so obtaining any phenomenological laws or scalings takes a lot of time, because this usually requires scanning over a multidimensional parameter space. Nevertheless, such findings are of great importance for designing and guiding experiments on new generation laser facilities.

This chapter is devoted to the description of a new discovered effect — propagation of a *vacuum breakdown* wave in the form of a self-sustaining QED cascade in an extremely intense plane wave, i.e. in a configuration usually considered unsuitable for the development of a QED cascade. Notably the wave field strength required to observe this effect turns out to be significantly lower than the Sauter-Schwinger threshold for pair production from vacuum [1, 2], and slightly higher than the threshold for the development of a self-sustaining cascade in a standing wave configuration [98]. The effect is observed in the QED-PIC simulation of the interaction of an extremely intensive laser pulse with a foil in the light sail regime. As a result of this interaction, the EM field configuration changes, which leads to the possibility of the development of a self-sustaining QED cascade. Opposite to the case of the interaction with a thick target, in the presented case, reflection is practically absent and the development of a QED cascade is possible due to the fact that the magnetic field inside the produced electron-positron plasma is greater than the electric one. Development of QED cascade ultimately leads to formation of a superdense electron-positron plasma «cushion» between the laser radiation and the moving foil. The front of this cushion propagates towards the radiation, which qualitatively resembles a breakdown wave propagating towards the microwave radiation source during a gas discharge [107, 108]. Moreover the produced electron-positron plasma efficiently absorbs laser radiation and separates it from the foil, thereby interrupting the ion acceleration. However, the QED cascade continues to develop even after the foil is separated from the laser field, which makes it possible to classify such a cascade as self-sustaining.

3.2 Effect of QED processes on interaction of laser radiation with foil

3.2.1 QED-PIC simulations

The interaction of laser radiation with a target is simulated using the QUILL code [201], which implements the particle-in-cell method and the Monte-Carlo method[1] for simulating probabilistic QED processes: nonlinear Compton scattering and the nonlinear Breit-Wheeler process. In simulations a circularly polarized laser pulse with wavelength $\lambda = 2\pi c/\omega_L = 1\,\mu$m, dimensionless amplitude $a_0 = eE/m_e c\omega_L$ propagated along the x axis and had the following field initial distribution

$$\mathbf{E}(x,y,z,t=0) = a_0 \cos^2\left(\frac{\pi}{2}\frac{x^4}{\sigma_x^4}\right)\cos^2\left(\frac{\pi}{2}\frac{y^4}{\sigma_y^4}\right)\cos^2\left(\frac{\pi}{2}\frac{z^4}{\sigma_z^4}\right)\times\left(0,\cos\left(\frac{x\omega_{\mathrm{L}}}{c}\right),\sin\left(\frac{x\omega_{\mathrm{L}}}{c}\right)\right), \qquad (3.2)$$

where the coordinates x, y, z are measured from the center of the laser pulse. The transverse dimensions of the pulse were $2\sigma_y = 2\sigma_z = 10.4\,\mu$m and pulse duration was 45 fs ($2\sigma_x = 13.4\,\mu$m). Since the laser pulse is quite wide, the field configuration is close to a plane wave. The target with thickness d and initial electron density n_e had transverse dimensions slightly larger than the transverse dimensions of the laser pulse. The simulation box with the size $20\lambda\times30\lambda\times30\lambda$ was divided into the $2000\times300\times300$ grid (along the x, y and z axes, respectively). A series of numerical simulations was

[1] See Ref. [167] for description of the event generator used in the code.

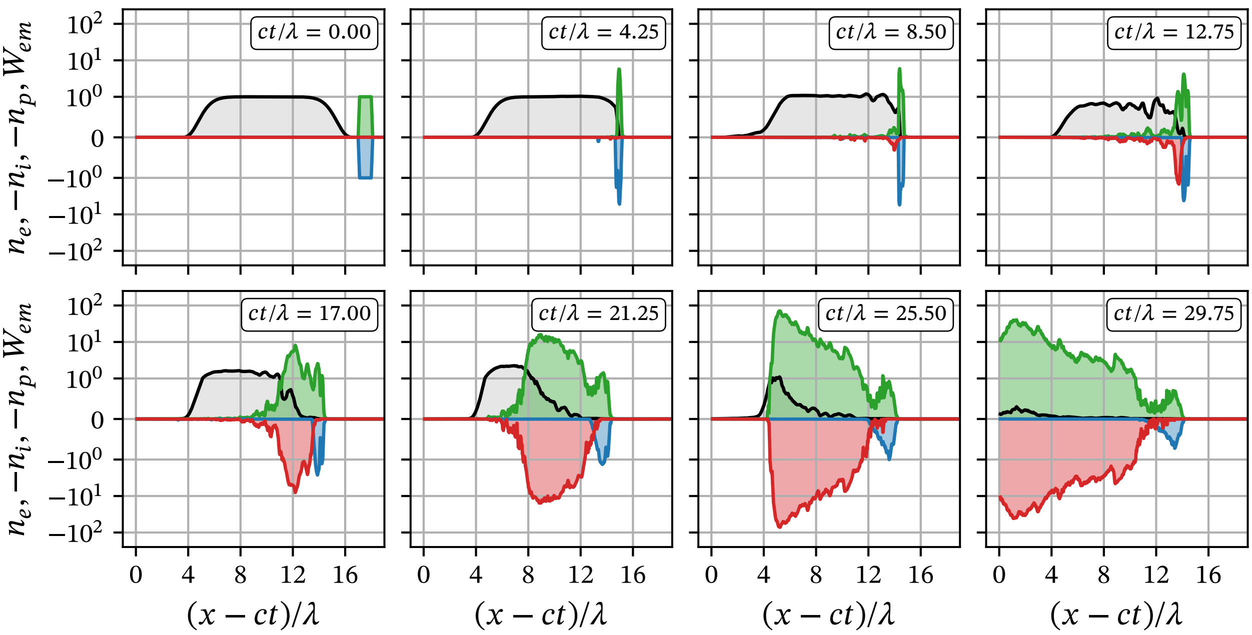

Figure 3.1: Density distribution of the electrons (green), ions (blue), positrons (red) and EM energy (black) along the x axis at different time instances in QED-PIC simulation with parameters $n_e = 5.9 \times 10^{23}\,\mathrm{cm}^{-3}$, $d = 1\,\mu\mathrm{m}$, $a_0 = 2500$. The values are normalized to its initial maxima. The vertical axis scale is linear in range $[-1, 1]$ and logarithmic outside this range.

carried out with different parameters a_0, n_e and d, satisfying the relation $a_0 = \eta n_e d \lambda r_e$, which is necessary for ion acceleration in the «light sail» regime (see for example [23]). Here, $r_e = e^2/m_e c^2$ is the classical electron radius, η is a numerical coefficient of the order of unity (in all simulations $\eta = 1.5$). Since the characteristic values of a_0 in our simulations are about 10^3, the characteristic value of the target electron density is $n_e \sim 10^{23}\,\mathrm{cm}^{-3}$, which corresponds to the characteristic density of solid material.

The temporal evolution of the particle density and electromagnetic energy is shown in Fig. 3.1 for the simulation with parameters: $n_e = 5.9 \times 10^{23}\,\mathrm{cm}^{-3} \approx 530\, n_{\mathrm{cr}}$ ($n_{\mathrm{cr}} = m_e \omega_L^2/4\pi e^2 \approx 10^{21}\,\mathrm{cm}^{-3}$ is the critical density), $d = 1\,\mu\mathrm{m}$, $a_0 = 2500$. It follows from the analysis of the results of the numerical simulation that during an interval $ct/\lambda \lesssim 8$ the target is compressed into a thin layer and accelerated in the longitudinal direction to a speed close to the speed of light, i.e. there is a typical acceleration of ions in the «light sail» regime (see blue line in Fig. 3.2). The number of electron-positron pairs formed during this time is insignificant. During the time interval $8 \lesssim ct/\lambda \lesssim 14$, an inhomogeneous electron-positron plasma starts to form, which partially absorbs radiation, which leads to a decrease in the efficiency of ion acceleration (see Fig. 3.2). During the time interval $14 \lesssim ct/\lambda \lesssim 28$, the QED cascade develops in a self-sustaining regime, i.e. without the participation of initial seed particles. In this case, the leading (with respect to the laser pulse) front of the electron-positron plasma moves with a speed v_{fr} less than the speed of light, while the trailing front moves ballistically together with the target at almost the speed of light.

Two series of numerical simulations were carried out: first with different values of a_0, equal to 1500, 2000, 2500, 3000, and a target with a fixed thickness of $d = 1\,\mu\mathrm{m}$, and second with different values of d, equal to $0.5\,\mu\mathrm{m}$, $1\,\mu\mathrm{m}$, and $2\,\mu\mathrm{m}$ and with a fixed value of $a_0 = 2500$. It can be seen

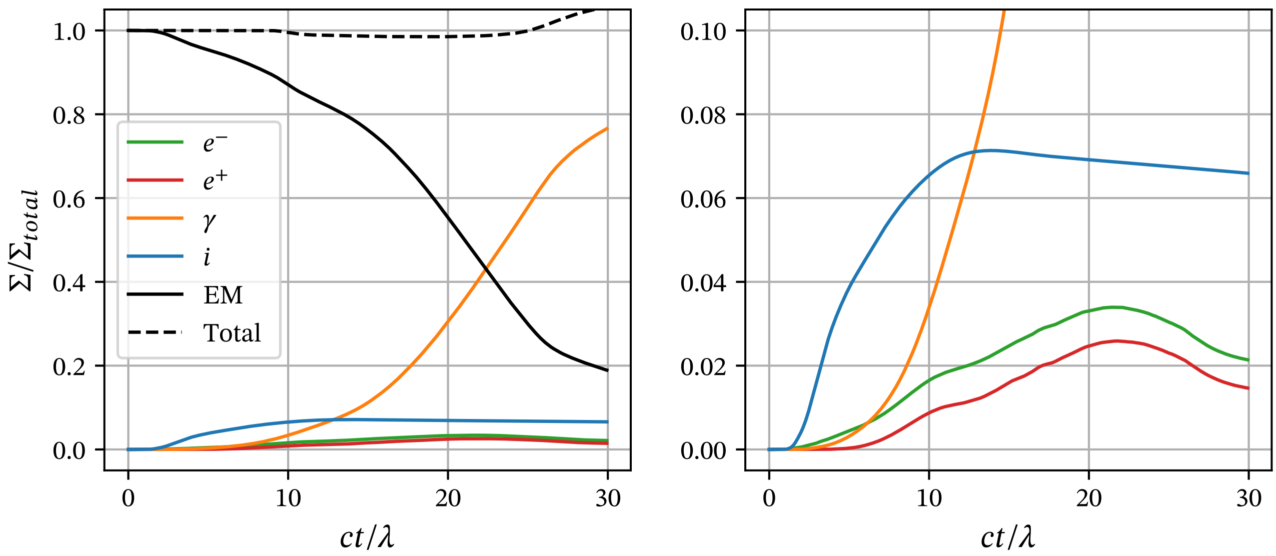

Figure 3.2: Distribution of the energy between EM field and particles as a function of time in QED-PIC simulation. The simulation parameters are the same as in Fig. 3.1. The right figure is a zoomed-in version of the left figure.

from Fig. 3.3 that the cascade front velocity weakly depends on the time and target thickness, while it strongly depends on the intensity of the laser pulse, decreasing (in the laboratory reference frame) with its growth. It is also worth noting that at the late stages of the interaction, the density of the electron-positron plasma is several times higher than the value of the relativistic critical concentration $a_0 n_{\mathrm{cr}}$. In all the calculations performed, the cascade develops efficiently, however, at $a_0 = 1500$, the plasma density reaches $0.6 a_0 n_{\mathrm{cr}}$ by the end of the simulation ($t = 30\lambda/c$). Therefore, we assume that the value $a_0 = 1500$ is a rough threshold value for the development of a self-sustaining cascade in a plane wave.

In order to determine the role of the ions of the initial target in the formation of a QED cascade, we simulated the interaction of a laser pulse with a supercritical electron-positron target. The geometry of the target and the pulse is the same as described above. The target thickness was $d = 1\,\mu\mathrm{m}$, the electron density was $n_e = 0.7 a_0 n_{\mathrm{cr}}$, $a_0 = 2500$. An analysis of the simulation results shows that the self-sustaining QED cascade develops in the same way as in the case of a seed in form of an electron-ion target. Moreover, the speed of the front of the cascade also coincides. From this, we can conclude that, with a certain choice of the seed and a sufficiently high intensity of the laser pulse, the development of an A-type QED cascade in a field with a configuration close to a plane wave is possible.

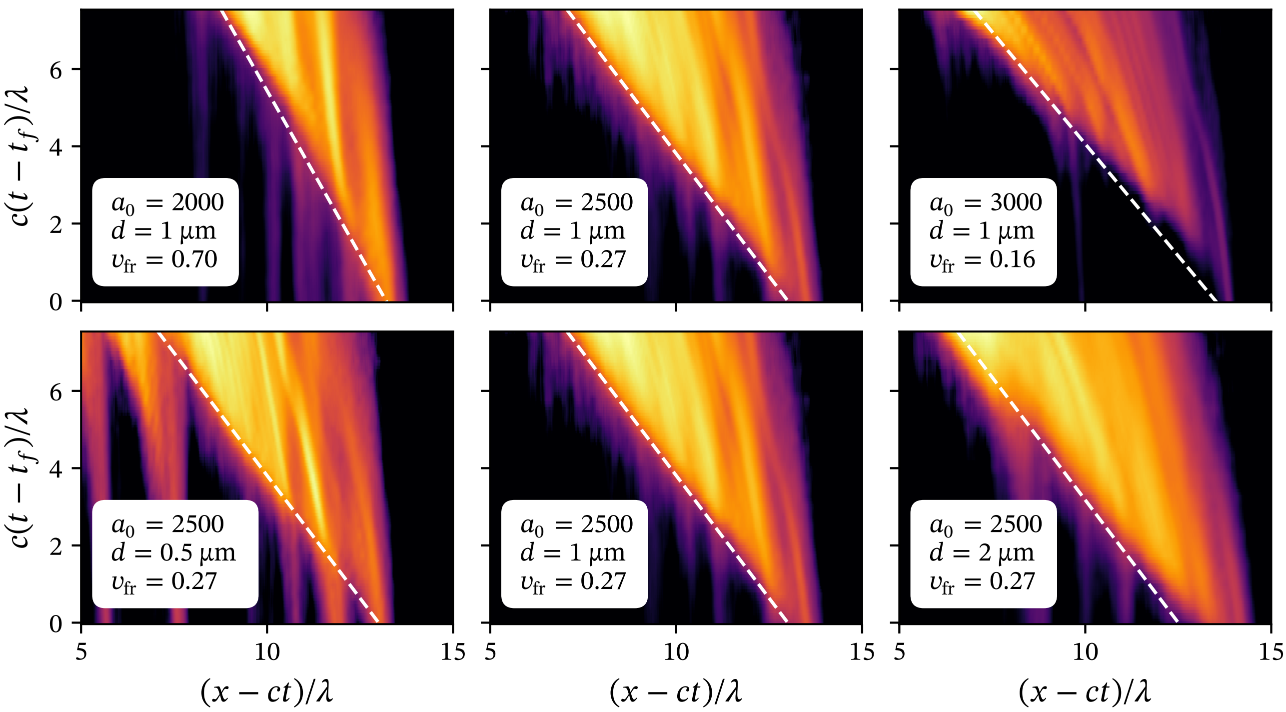

Figure 3.3: Positron distribution in $x - t$ plane (colormap, brighter color correspond to larger density). White dashed lines correspond to linear fit of the location of the distribution leading front $x = x_0 + v_{\text{fr}}(t - t_f)$, where t_f is an approximate time of the cushion formation. $ct_f/\lambda \approx 17.5$ for $a_0 = 2000$, $ct_f/\lambda \approx 15.0$ for $a_0 = 2500$, $ct_f/\lambda \approx 12.5$ for $a_0 = 3000$.

3.2.2 Key features and mechanism of QED cascade development

Let us investigate in more detail the distribution of the electromagnetic field and the dynamics of particles inside the electron-positron plasma in order to determine the mechanism of the cascade development. It follows from Fig. 3.4 (a) that the field structure is close to a circularly polarized wave with perpendicular electric and magnetic components, $\mathbf{E} \perp \mathbf{B}$, and the field decays in plasma on a scale of several wavelengths. The key feature of the field configuration is predominance of the magnetic field over the electric one, $B > E$. In such a field, electrons and positrons do not gain energy (see the $\overline{\gamma}/a_0$ line in Fig. 3.4 (b)), so the development of the cascade inside the plasma is suppressed. Moreover, in such a field the particle trajectories are helical (see Fig. 3.5 (a)). This is easily explained if we transform to a reference frame moving with the drift velocity $v_{\text{drift}} = [\mathbf{E} \times \mathbf{B}]_x / B^2$, in which the electric field is parallel to the magnetic field and less than it. In such a field, the particles rotate in a plane perpendicular to the magnetic field and may have a velocity component along the magnetic field. In a laboratory reference frame, electrons and positrons on average move along the x axis with the drift velocity v_{drift}. Since the cascade front always consists of new particles which are being constantly produced, it can propagate significantly slower than the particles comprising the plasma bulk. At the same time, due to the rotation of the particles, their instantaneous velocity along the x axis can occasionally be less than the front velocity (see Fig. 3.4 (b) and Fig. 3.5 (b)). At such time instants, particles can emit gamma quanta, which will reach the vacuum region (a large number of gamma quanta propagating slower than the front of the cascade and even directly towards the laser

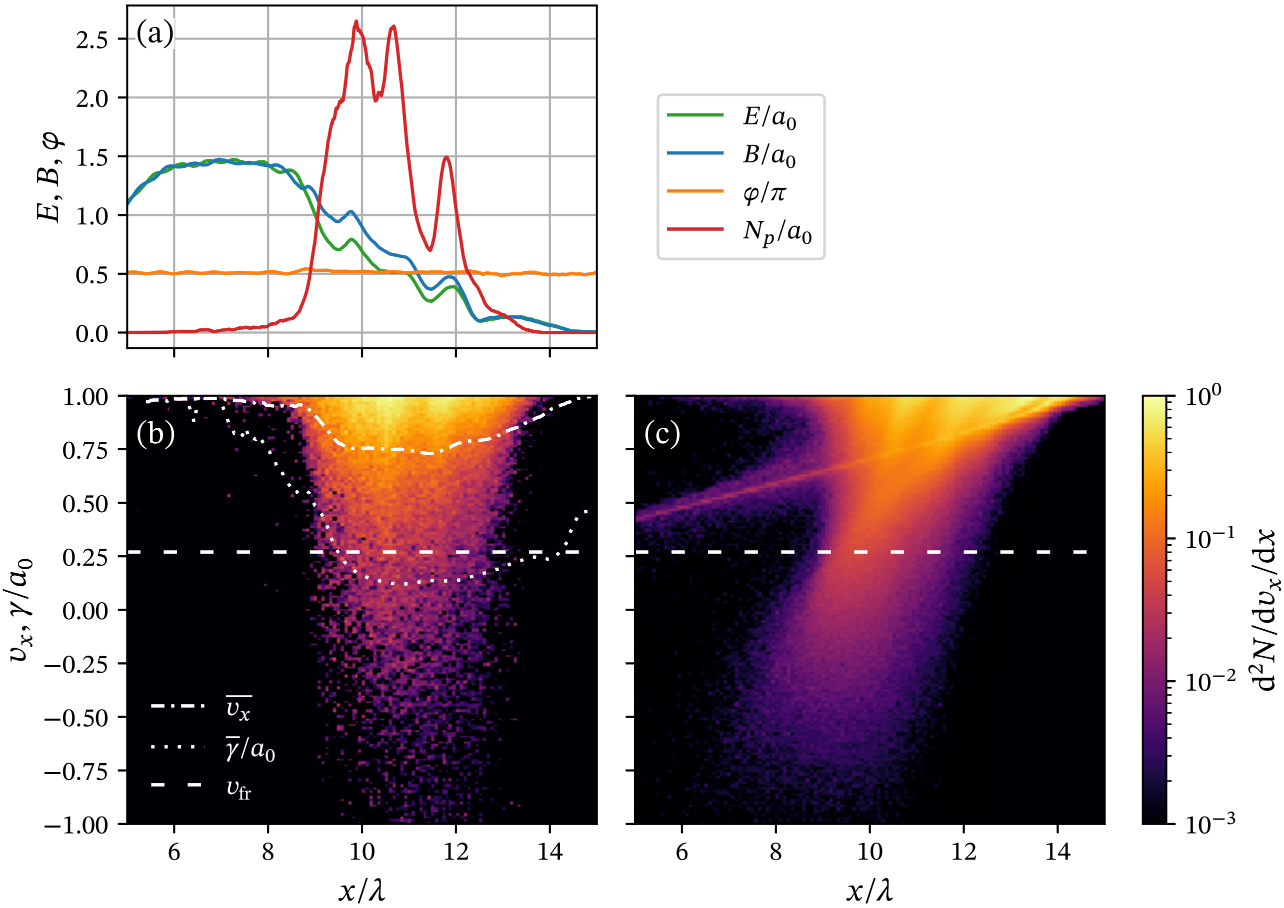

Figure 3.4: Results of QED-PIC simulations at $t = 20\lambda/c$. (a) Distribution of the magnitude of the electric field E, magnetic field B, angle φ between the latter and positron density N_p. Distribution of (b) positrons and (c) gamma-quanta in a phasespace $x - v_x$. White dash-dotted line correspond to average longitudinal velocity $\overline{v}_x$, white dotted line — to average Lorentz-factor $\overline{\gamma}$. White dashed line correspond to the cascade front velocity v_{fr}, equal to 0.27 in this simulation.

radiation is observed in numerical simulation, which is shown in Fig. 3.4 (c)) and form new electron-positron pairs in a strong laser field. These pairs are then accelerated by a laser field back into the plasma, where the magnetic field is greater than the electric field, and the process is repeated. Thus, the self-sustaining development of the cascade occurs at the interface between the vacuum and the electron-positron plasma. It is important to emphasize the fundamental difference between the *vacuum* and the *plasma* regions: in the former, electromagnetic energy is transferred to the cascade particles, while in the latter, particles are not accelerated, but they «release» the gained energy in the form of gamma radiation. Some of this radiation returns back to the vacuum region and provides the positive feedback necessary to maintain the cascade development. The mechanism for the QED cascade self-sustenance in a plane wave is schematically shown in Fig. 3.6.

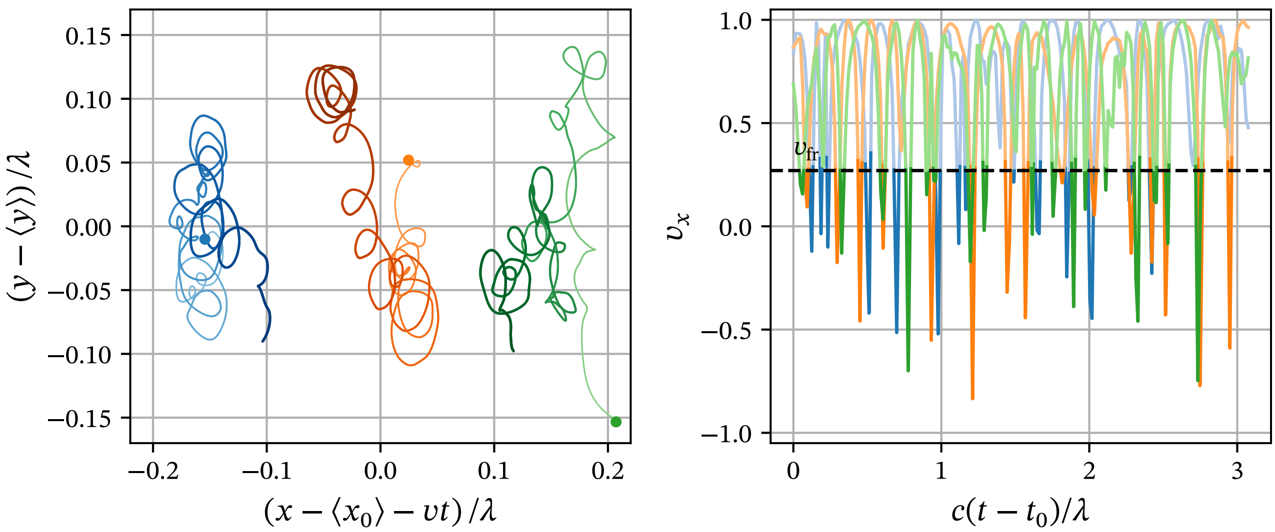

Figure 3.5: Dynamics of three electrons located inside the dense electron-positron plasma. (a) Electron trajectories in the *xy* plane in a reference frame moving with velocity 0.7*c* along the *x* axis with respect to the laboratory reference frame. Particle location at later time is marked with darker color; initial location is marked with a circle. (b) Longitudinal velocity in a laboratory reference frame as a function of time. Black dashed line correspond to the cascade front velocity $v_{\mathrm{fr}} = 0.27$.

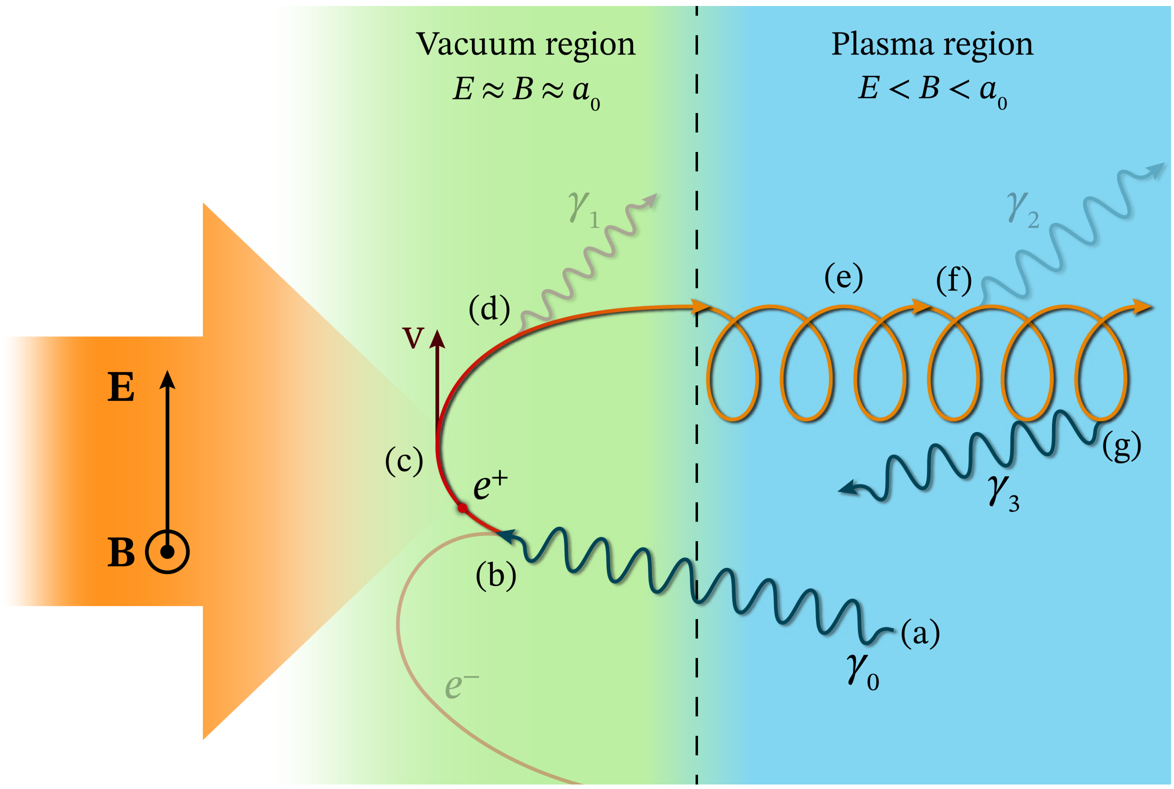

Figure 3.6: Scheme of the QED cascade self-sustenance. (a), (f), (g) Emission of an *active* (see below) gamma-quantum in the plasma region, (b) decay of an *active* gamma-quantum into an electron-positron pair in the vacuum region, (c) acceleration of the electron and the positron in the vacuum region, (d) emission of a *passive* gamma-quantum in the vacuum region, (e) positron motion along the helical trajectory in the plasma region.

3.3 Analytical model of self-sustaining QED cascade in a plane wave

Let us proceed to the analytical description of the processes considered above. Similarly to the Refs. [167, 180], we start from the kinetic equations for the electrons, the positrons, and the gamma quanta, assuming that the QED cascade is at the self-sustaining stage, so the seed particles, for example, the electrons and the ions of the initial target, do not affect its development. Kinetic equations together with Maxwell's equations (in the form of Poynting's theorem) are written in the following form

$$\frac{\partial f_{e^\pm}}{\partial t} + \mathbf{v}_{e^\pm}\nabla f_{e^\pm} \pm (\mathbf{E} + [\mathbf{v}_{e^\pm} \times \mathbf{B}])\frac{\partial f_{e^\pm}}{\partial \mathbf{p}} = \int f_\gamma(\mathbf{p}')w_{\mathrm{pair}}(\mathbf{p}',\mathbf{p})\mathrm{d}\mathbf{p}' + \int f_{e^\pm}(\mathbf{p}')w_{\mathrm{rad}}(\mathbf{p}',\mathbf{p})\mathrm{d}\mathbf{p}' - \int f_{e^\pm}(\mathbf{p})w_{\mathrm{rad}}(\mathbf{p},\mathbf{p}')\mathrm{d}\mathbf{p}', \tag{3.3}$$

$$\frac{\partial f_\gamma}{\partial t} + \mathbf{v}_\gamma\nabla f_\gamma = \int f_{e^\pm}(\mathbf{p}')w_{\mathrm{rad}}(\mathbf{p}',\mathbf{p}'-\mathbf{p})\mathrm{d}\mathbf{p}' - + \int f_\gamma(\mathbf{p})w_{\mathrm{pair}}(\mathbf{p},\mathbf{p}')\mathrm{d}\mathbf{p}', \tag{3.4}$$

$$\frac{\partial}{\partial t}\left(\frac{E^2+B^2}{2}\right) + \nabla[\mathbf{E}\times\mathbf{B}] = \int f_{e^-}(\mathbf{p})(\mathbf{v}_{e^-}\mathbf{E})\mathrm{d}\mathbf{p} - \tag{3.5}$$

$$- \int f_{e^+}(\mathbf{p})(\mathbf{v}_{e^+}\mathbf{E})\mathrm{d}\mathbf{p}, \tag{3.6}$$

where $f_{e^\pm,\gamma}(t,\mathbf{r},\mathbf{p})$ are the distribution functions of the electrons, the positrons and the gamma quanta, respectively, $\mathbf{v}$ is the particle velocity equal to $\mathbf{p}/\sqrt{1+p^2}$ for electrons and positrons and equal to $\mathbf{p}/p$ for gamma quanta, $w_{\mathrm{rad}}(\mathbf{p}',\mathbf{p})\mathrm{d}\mathbf{p}'$ is the probability of emission of a gamma quantum with momentum $\mathbf{p}'-\mathbf{p}$ by an electron or a positron with momentum $\mathbf{p}'$ per time unit, $w_{\mathrm{pair}}(\mathbf{p}',\mathbf{p})\mathrm{d}\mathbf{p}'$ is a probability of decay of a gamma quantum with momentum $\mathbf{p}'$ into an electron with momentum $\mathbf{p}$ and a positron with momentum $\mathbf{p}'-\mathbf{p}$ per time unit. Here we also use the relativistic normalization, in which the electric and magnetic fields are normalized to $m_e c\omega_{\mathrm{L}}/e$, the particle density — to the critical density $n_{\mathrm{cr}} = m_e\omega_{\mathrm{L}}^2/4\pi e^2$, energy and momentum — to $m_e c^2$ and $m_e c$ respectively, coordinates and time — to c/ω_{L} and $1/\omega_{\mathrm{L}}$ respectively.

3.3.1 General model assumptions

Let us apply a number of simplifications to the equations written above. First, since the interaction with a plane EM wave is studied, we assume the problem to be spatially one-dimensional. Moreover, we will consider the interaction with a circularly polarized wave and assume that the problem is symmetric with respect to rotation around the wave propagation axis (hereinafter, the x axis). These assumptions lead to the fact that the particle distribution functions become functions of only three variables (excluding time) instead of six, i.e. $f(t;\mathbf{r},\mathbf{p}) = f(t;x,p,\theta)/2\pi$, where p is the particle momentum, θ is the angle between the particle momentum and the x-axis.

Second, we suppose that the distribution functions are locally monoenergetic, i.e. $f \propto \delta(p-\overline{p}(x))/p^2$, where $\overline{p}(x)$ is the average momentum of particles located in a small vicinity of x. Let us denote the average energy of gamma quanta as ε_γ, and the average energy of electron-positron pairs as ε_p, assuming that they are ultrarelativistic, therefore $\varepsilon_p^2 = 1 + p_p^2 \approx p_p^2$. Despite the fact that the monoenergetic approximation is quite a strong assumption, we argue that the mechanism of QED cascade development described above is fundamentally independent of any specific features of the particle spectrum. Therefore, taking into account the evolution of energy spectra in our model will cause only quantitative rather than qualitative changes, while greatly complicating the equations. For gamma quanta, we also use a two-stream approximation, separating them into two groups: gamma quanta of the first group are emitted in the vacuum region and propagate mainly along the direction of the laser pulse propagation and thus do not contribute to the development of the cascade (we will denote them as *passive* gamma quanta), and gamma quanta of the second group are emitted in the plasma region in different directions and provide the positive feedback necessary for the development of the cascade (we designate them as *active* gamma quanta). As can be seen from Fig. 3.7, the energy spectrum of all gamma quanta is quite wide, but if passive gamma quanta are excluded, then the spectrum width decreases significantly, which justifies our assumption. Since passive gamma quanta affect the development of the cascade only by taking away a portion of the total energy, their spatial distribution is irrelevant for the cascade development.

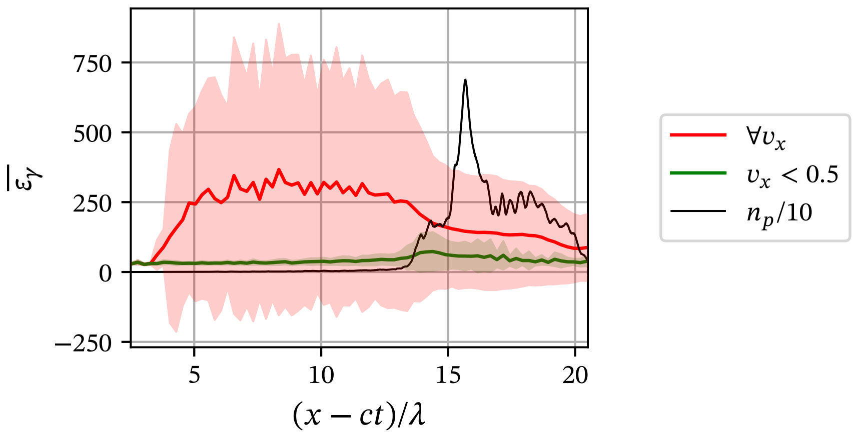

Figure 3.7: The average energy ε_γ of gamma quanta as a function of the coordinate x, calculated for all particles (red line) and only for particles with a velocity along the x axis not exceeding 0.5, which, according to our assumptions, includes only active gamma-quanta (green line). The filled colored areas represent the standard deviation of the energy. The black line corresponds to the electron-positron plasma density distribution. Data taken from PIC simulation results at $ct/\lambda = 18$. Simulation parameters are discussed in sec. 3.4.2. The initial conditions are the same as in Fig. 3.14.

In order to omit the integration over the energies and the azimuth angle φ (in the yz plane), we redefine the distribution functions f as follows

$$f(x,\varepsilon,\theta,\varphi) \to \int_0^\infty \int_0^{2\pi} f(x,\varepsilon,\theta,\varphi) 2\pi\varepsilon^2 \mathrm{d}\varphi \mathrm{d}\varepsilon = n(x)\Phi(\theta), \tag{3.7}$$

where $n(x)$ is the particle density, $\Phi(\theta)$ is the particle momentum distribution function over the angle θ, and

$$\int_{-\infty}^{+\infty} n(x)\mathrm{d}x = N, \tag{3.8}$$

$$\int_0^\pi \Phi(\theta)\sin\theta \mathrm{d}\theta = 1, \tag{3.9}$$

where N is the total number of particles.

Assumption of monoenergeticity corresponds to the transition from the kinetic to the hydrodynamic description, i.e. writing equations for the moments of the distribution functions. To write the hydrodynamic equations, we first introduce several additional quantities

$$W_{\mathrm{pair}}(\chi_\gamma,\varepsilon_\gamma) = \int w_{\mathrm{pair}}(\mathbf{p},\mathbf{p}')\mathrm{d}\mathbf{p}', \tag{3.10}$$

$$W_{\mathrm{rad}}(\chi_p,\varepsilon_p) = \int w_{\mathrm{rad}}(\mathbf{p},\mathbf{p}')\mathrm{d}\mathbf{p}', \tag{3.11}$$

$$I_{\mathrm{rad}}(\chi_p) = \int w_{\mathrm{rad}}(\mathbf{p},\mathbf{p}')(\varepsilon_p - \varepsilon_p')\mathrm{d}\mathbf{p}', \tag{3.12}$$

where $W_{\mathrm{pair}}, W_{\mathrm{rad}}, I_{\mathrm{rad}}$ are total probability of photoproduction of electron-positron pairs and total probability and radiation power of gamma quanta, respectively [33]. As mentioned above, these quantities depend on the Lorentz-invariant QED parameter χ

$$\chi = \frac{\varepsilon}{a_{\mathrm{S}}}\sqrt{(\mathbf{E}+\mathbf{v}\times\mathbf{B})^2 - (\mathbf{v}\cdot\mathbf{E})^2}, \tag{3.13}$$

where ε is the particle energy, $a_{\mathrm{S}} = eE_{\mathrm{S}}/m_e c\omega_{\mathrm{L}} = m_e c^2/\hbar\omega_{\mathrm{L}}$ and $E_{\mathrm{S}} = m_e^2 c^3/\hbar e$ is the Sauter-Schwinger field [32]. Generally, the hydrodynamic equations have a form of a continuity equation

$$\frac{\partial D_\alpha}{\partial t} + \frac{\partial F_\alpha}{\partial x} = \sum_\beta S[\alpha,\beta], \tag{3.14}$$

where D_α and F_α are the density and the flux of some physical quantity α, $S[\alpha,\beta]$ is the source leading to a change in the quantity α as a result of the process β. Note that despite the fact that we have determined the particle energy distribution function, to calculate the sources $S[\alpha,\beta]$ it is also necessary to know the particle angular distribution, which is discussed below. Based on the qualitative explanation of the mechanism for the development and sustenance of the QED cascade, described in section 3.2.2, we assume that the following system of equations describes this process quite fully

$$\frac{\partial}{\partial t} n_p + \frac{\partial}{\partial x}\left(v_x n_p\right) = S[n, \mathrm{pp}], \tag{3.15}$$

$$\frac{\partial}{\partial t}\left(\varepsilon_p n_p\right) + \frac{\partial}{\partial x}\left(v_x \varepsilon_p n_p\right) = S[\varepsilon, \mathrm{pp}] + S[\varepsilon, \mathrm{acc}]\psi_{\mathrm{vac}} - S[\varepsilon, \mathrm{rad_a}]\psi_{\mathrm{pl}} - S[\varepsilon, \mathrm{rad_p}]\psi_{\mathrm{vac}}, \tag{3.16}$$

$$\frac{\partial}{\partial t} n_\gamma + \frac{\partial}{\partial x}\left(\overline{v_{\gamma\parallel}} n_\gamma\right) = -S[n, \mathrm{pp}] + 2S[n, \mathrm{rad_a}]\psi_{\mathrm{pl}}, \tag{3.17}$$

$$\frac{\partial}{\partial t}\left(\overline{v_{\gamma\parallel}} n_\gamma\right) + \frac{\partial}{\partial x}\left(\overline{v_{\gamma\parallel}^2} n_\gamma\right) = -S[v, \mathrm{pp}] + 2S[v, \mathrm{rad_a}]\psi_{\mathrm{pl}}, \tag{3.18}$$

$$\frac{\partial}{\partial t}\left(\varepsilon_\gamma n_\gamma\right) + \frac{\partial}{\partial x}\left(\overline{v_{\gamma\parallel}} \varepsilon_\gamma n_\gamma\right) = -S[\varepsilon, \mathrm{pp}] + 2S[\varepsilon, \mathrm{rad_a}]\psi_{\mathrm{pl}}, \tag{3.19}$$

$$\frac{\partial}{\partial t}\left(\frac{E^2 + B^2}{2}\right) + \frac{\partial}{\partial x}[\mathbf{E} \times \mathbf{B}]_x = -2S[\varepsilon, \mathrm{acc}]\psi_{\mathrm{vac}} \equiv -\mathbf{jE}, \tag{3.20}$$

$$\frac{\partial \Sigma_\gamma}{\partial t} = 2\int\limits_0^\infty S[\varepsilon, \mathrm{rad_p}]\psi_{\mathrm{vac}} dx, \tag{3.21}$$

where $n_p = n_{e^+} = n_{e^-}$ is half the density of the electron-positron plasma under the assumption of its quasi-neutrality, v_x is the average longitudinal velocity of pairs, calculated in subsection 3.3.2, $\overline{v_{\gamma\parallel}}$ and $\overline{v_{\gamma\parallel}^2}$ are mean and mean square of the longitudinal velocity of gamma quanta. The latter are calculated from the angular distribution as follows

$$\overline{v_{\gamma\parallel}} = \int_0^\pi \Phi(\theta)\cos\theta\sin\theta d\theta, \tag{3.22}$$

$$\overline{v_{\gamma\parallel}^2} = \int_0^\pi \Phi(\theta)\cos^2\theta\sin\theta d\theta. \tag{3.23}$$

The equation (3.20) is basically the Poynting theorem, which describes transfer of the electromagnetic energy density. The sources $S[n,\beta]$, $S[v,\beta]$, and $S[\varepsilon,\beta]$ correspond to changes in density, longitudinal velocity, and energy of the particles, respectively; the sources $S[\alpha, \mathrm{pp}]$, $S[\alpha, \mathrm{acc}]$, $S[\alpha, \mathrm{rad_a}]$ and $S[\alpha, \mathrm{rad_p}]$ correspond to processes of pair photoproduction, acceleration of pairs in a plane wave, emission of active gamma quanta by pairs in the plasma region, and emission of passive gamma quanta by pairs in the vacuum region, respectively (marked respectively by letters (b), (c), (d) and (f) in Fig. 3.6), Σ_γ is the total energy of passive gamma quanta. The factor $\psi_{\mathrm{vac}}(\psi_{\mathrm{pl}})$ is considered to be equal to 1 in the vacuum (plasma) region and 0 in the plasma (vacuum) region. The calculation of these factors will be given below. Note that $\psi_{\mathrm{vac}} + \psi_{\mathrm{pl}} = 1$. For convenience, we will omit these factors when the region under consideration is obvious.

3.3.2 Electromagnetic field configuration

According to the results of the 3D QED-PIC simulation, the electric and magnetic fields in the plasma region remain almost perpendicular to each other, and the magnitude of the magnetic field everywhere exceeds the electric one: $B > E$. The spatial distribution of the EM field has a characteristic scale λ both in the vacuum and plasma regions. In such a field, charged particles drift in the direction perpendicular to both the electric and magnetic fields, i.e. along the x axis with the speed

$$v_x \approx E/B. \tag{3.24}$$

In the vacuum region, the EM field corresponds to the field of an incident plane wave. In this case, the electric and magnetic fields are mutually perpendicular and equal in magnitude. If the energy ε of a particle entering the vacuum region is less than the dimensionless field amplitude E, then, according to the asymptotic theory constructed in the previous chapter, on a timescale much shorter than the wave period, such a particle will be accelerated in the longitudinal direction almost to the speed of light. Thus, we can assume that the relation $v_x \approx 1 = E/B$ is satisfied in the vacuum region, i.e. the equation (3.24) is actually valid both in the plasma and the vacuum regions.

In this reasoning, we do not take into account the wave reflected from the e^-e^+ plasma boundary for several reasons. First, in the 3D QED-PIC simulation, there is no significant reflection during the development of the cascade at the stage of its self-sustenance. Second, the reflection that occurs at the initial stage of laser interaction with a thin solid target, according to the theory of relativity, is rapidly depleted as particles accelerate in the direction of laser pulse propagation and, thus, becomes insignificant for the later stages of cascade development. However, our model does not describe an electron-ion plasma, so we study the interaction of a laser pulse with a seed in the form of a counter-propagating gamma bunch (see Sec. 3.4.2), where reflection does not occur even at the initial stage of the interaction. In addition, reflection would slightly change the process of photoproduction of pairs due to the fact that gamma quanta counter-propagating the laser pulse have the highest probability of decay. So the fields of the co-propagating reflected wave do not increase the value of the QED-parameter χ of gamma quanta responsible for the development of QED cascade. Finally, in the vacuum region, where the laser field is strongest, there are mainly ultrarelativistic electrons and positrons produced from photons with the highest energy. Scattering of a relativistically strong laser field ($a_0 \gg 1$) by ultrarelativistic electrons and positrons ($\gamma \gg 1$) occurs both in the nonlinear and quantum regimes. Because of this, and also because the positions of the particles are uncorrelated, the resulting scattered radiation is incoherent and its frequency is strongly upshifted. Such radiation is best described by individual photons, as implemented in the QUILL code. Some of these photons propagating towards the laser pulse can indeed be considered as a reflection. Although such photons can increase the overall yield of electron-positron pairs and gamma quanta through higher-order QED processes, they are significantly less probable than non-linear Compton scattering and the Breit-Wheeler process, and therefore are not taken into account neither in QED-PIC simulations nor in our model. Note, however, that our model takes into account energy losses due to incoherent gamma radiation in both the vacuum and plasma regions.

3.3.3 Distribution function of active gamma-quanta

As described in section 3.2.2, active gamma quanta are emitted by pairs as they move along helical trajectories in the plasma region. Accordingly, their angular distribution is wide. We also assume that this distribution is smooth and can be described by a single parameter. This parameter is the velocity v of the instantaneous reference frame K', in which the angular distribution of photons located in a small vicinity of the coordinate x is practically isotropic, i.e.

$$\Phi'(\theta') \equiv \frac{\mathrm{d}N'}{\mathrm{d}\cos\theta'} = \frac{1}{2}, \tag{3.25}$$

where $\mathrm{d}N' = \mathrm{d}N$ is the number of particles with longitudinal velocity in the range $[\cos\theta', \cos\theta' + \mathrm{d}\cos\theta']$ and

$$\cos\theta' = \frac{\cos\theta - v}{1 - v\cos\theta}. \tag{3.26}$$

In the laboratory reference system, such a distribution looks like this [158]

$$\Phi(\theta, v) = \frac{\mathrm{d}N}{\mathrm{d}\cos\theta} = \frac{\mathrm{d}N'}{\mathrm{d}\cos\theta'}\frac{\mathrm{d}\cos\theta'}{\mathrm{d}\cos\theta} = \frac{1-v^2}{2\left(1 - v\cos\theta\right)^2}. \tag{3.27}$$

Thus, the distribution function of active gamma quanta has the following form

$$f_\gamma(t; x, \theta) = \Phi\left(\theta, v_{\gamma\parallel}(x,t)\right) n_\gamma(x,t). \tag{3.28}$$

The mean value $\overline{v_{\gamma\parallel}}$ and the mean square value $\overline{v_{\gamma\parallel}^2}$ of longitudinal velocity are calculated as follows

$$\overline{v_{\gamma\parallel}} = \int_0^\pi \Phi(\theta, v)\cos\theta\sin\theta \mathrm{d}\theta = \frac{1}{v_{\gamma\parallel}} - \frac{1 - v_{\gamma\parallel}^2}{v_{\gamma\parallel}^2}\mathrm{atanh}(v_{\gamma\parallel}), \tag{3.29}$$

$$\overline{v_{\gamma\parallel}^2} = \int_0^\pi \Phi(\theta, v)\cos^2\theta\sin\theta \mathrm{d}\theta = \frac{2\overline{v_{\gamma\parallel}}}{v_{\gamma\parallel}} - 1, \tag{3.30}$$

where $\mathrm{atanh}(x)$ is the inverse function of the hyperbolic tangent. Note that, according to the Lorentz transformations, the average velocity of gamma quanta $\overline{v_{\gamma\parallel}}$ differs slightly from the velocity $v_{\gamma\parallel}$ of the reference frame K', in which their distribution is isotropic. The results of QED-PIC simulations show that the expression (3.27) is a fairly good approximation of the angular distribution of active gamma quanta (see Fig. 3.8 (a), (b)).

The value of the QED parameter χ for gamma quanta in crossed electric and magnetic fields, which is true for both the vacuum and plasma regions, is calculated as follows

$$\chi_\gamma = \frac{\varepsilon_\gamma\left|B - E\cos\theta\right|}{a_\mathrm{S}} = \frac{\varepsilon_\gamma E}{a_\mathrm{S}}\frac{1 - v_x\cos\theta}{v_x}, \tag{3.31}$$

where the expression (3.24) was used.

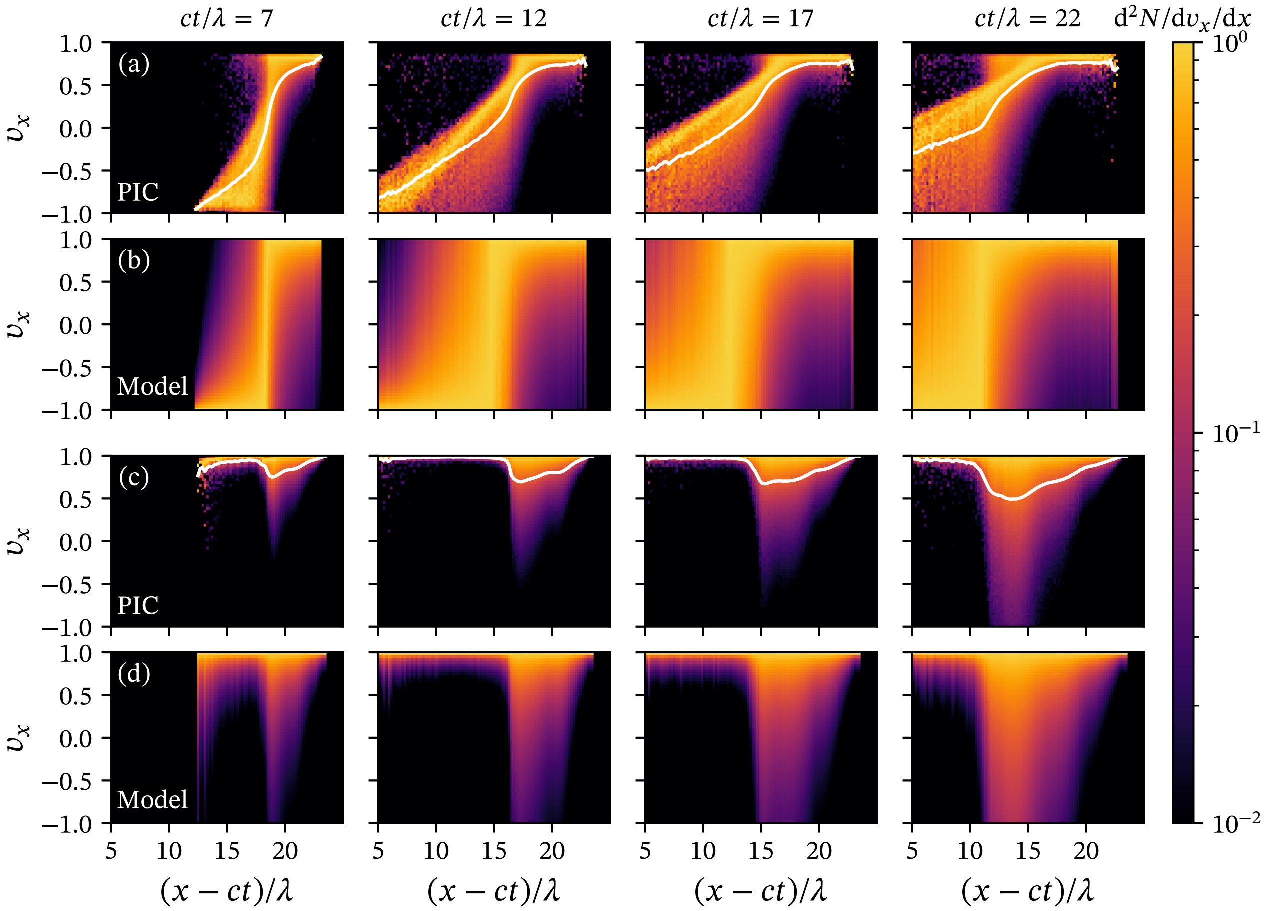

Figure 3.8: Verification of the approximation used to describe the angular distribution of particles. Angular distribution of (a) gamma quanta and (c) e^-e^+ pairs located in a small vicinity of the x coordinate (color map) and their average longitudinal velocity calculated from this distribution (white line) according to the results of numerical QED-PIC simulation at different time instances. (b), (d) — model angular distribution of gamma quanta and e^-e^+ pairs, respectively, reconstructed from the average longitudinal velocity using the expression (3.27).

Having completely determined the distribution function of gamma quanta, the sources $S[\alpha, \mathrm{pp}]$ corresponding to the process of pair photoproduction can be calculated

$$S[n, \mathrm{pp}] = n_\gamma \int_0^\pi \Phi(\theta, v_{\gamma\|}) W_{\mathrm{pair}}(\chi_\gamma, \varepsilon_\gamma) \sin\theta \mathrm{d}\theta \equiv \overline{W_{\mathrm{pair}}} n_\gamma, \tag{3.32}$$

$$S[\varepsilon, \mathrm{pp}] = \varepsilon_\gamma n_\gamma \int_0^\pi \Phi(\theta, v_{\gamma\|}) W_{\mathrm{pair}}(\chi_\gamma, \varepsilon_\gamma) \sin\theta \mathrm{d}\theta \equiv \overline{W_{\mathrm{pair}}} \varepsilon_\gamma n_\gamma, \tag{3.33}$$

$$S[v, \mathrm{pp}] = n_\gamma \int_0^\pi \Phi(\theta, v_{\gamma\|}) W_{\mathrm{pair}}(\chi_\gamma, \varepsilon_\gamma) \cos\theta \sin\theta \mathrm{d}\theta \equiv \overline{V_{\mathrm{pair}}} n_\gamma. \tag{3.34}$$

3.3.4 Dynamics of e^-e^+ pairs in the vacuum region

Let us consider electrons and positrons produced in the vacuum region, where their number is so small that the collective plasma effects can be neglected, and thus the EM field in this region is the field of an incident plane wave. The dynamics of a single electron in the field of an extremely intense plane wave is considered in detail in section 2.5.2 of this work. As mentioned above, to calculate the sources of $S[\alpha,\beta]$ in the rhs of the equations (3.15)–(3.20), it is necessary to know the angular distribution of particles. Despite the fact that the trajectories of electrons in a plane wave can be found analytically, the explicit calculation of the distribution function from these trajectories is practically infeasible, because particles are produced in this region at random times with different initial conditions. However, the following reasoning allows us to calculate the sources of $S[\alpha,\beta]$ based on a different approach. First, we note once again that a relativistically strong plane wave «pushes» particles in the direction of its propagation, i.e. in our case along the x axis. Therefore, regardless of the initial conditions, in a short period of time, the momentum of the particle is oriented almost along the x axis, and in the vacuum region we can assume $v_x \approx 1$. Neglecting the time of such an orientation, one can approximately calculate the flux of particles and energy simply by multiplying the density of these quantities by the velocity $v_x \approx 1$. Since by definition there are no collective effects in the vacuum region and QED cascade does not develop in it, the continuity equations in this region serve only to calculate the fluxes of particles and energy (including electromagnetic) at the cascade front. Thus, we only need to know the total contribution to these fluxes from each particle over the time interval from the moment of its production in the vacuum region up to the instance of it reaching the plasma edge. Thus we calculate the sources of $S[\varepsilon,\beta]$ as follows

$$S[\varepsilon,\beta] = \int_0^{\pi} f_\gamma(x,\theta) W_{\text{pair}}(\chi_\gamma,\varepsilon_\gamma)\Delta\varepsilon_\beta \sin\theta d\theta, \tag{3.35}$$

where $\Delta\varepsilon_\beta$ is the total energy change in the process β of a particle produced at a point with coordinate x at time t, for the entire time it spent in the vacuum region. Defining the source $S[\varepsilon,\beta]$ in this way is the same as assuming that the particle acquires a change in energy $\Delta\varepsilon_\beta$ immediately at the moment of its birth, and then, without further change in energy, moves at the speed of light to the boundary with the plasma region.

To calculate the change in particle energy when moving in a circularly polarized plane wave, we use the results of section 2.5.2.

$$\Delta\varepsilon_{\text{acc}} = \frac{2Ep_0}{p_{-,0}} \sin\frac{\Delta\varphi}{2}\left(\frac{E}{p_0}\sin\frac{\Delta\varphi}{2} - \sin\theta\sin\frac{\varphi+\varphi_0}{2}\right), \tag{3.36}$$

where we do not take into account the corrections associated with radiation reaction, which take effect at a large number of wave periods. Since particles are produced at arbitrary time instances and we consider the distribution of particles over the azimuthal angle to be isotropic, the expression (3.36) should be averaged over φ_0. In this case, we get

$$\Delta\varepsilon_{\text{acc}} = \frac{2E^2}{p_{-,0}}\sin^2\frac{\Delta\varphi}{2}. \tag{3.37}$$

To determine the value of $\Delta\varepsilon_{\mathrm{acc}}$, it is necessary to calculate the time the particles spend in the vacuum region. To do this, let us find the value of $\Delta\varphi$ corresponding to the condition that the longitudinal velocity of particles v_x reaches a certain threshold value v_{th} close to 1. In this case, after this threshold value is reached, the value of $\Delta\varphi$ and, accordingly, $\Delta\varepsilon_{\mathrm{acc}}$ practically do not change. We write this condition as follows

$$v_{\mathrm{th}} = v_x = \frac{p_x}{\gamma} = \frac{\gamma - p_-}{\gamma_0 + \Delta\varepsilon_{\mathrm{acc}}} \approx \frac{p_{x,0} + \Delta\varepsilon_{\mathrm{acc}}}{\gamma_0 + \Delta\varepsilon_{\mathrm{acc}}} \approx \frac{\gamma_0 \cos\theta + \Delta\varepsilon_{\mathrm{acc}}}{\gamma_0 + \Delta\varepsilon_{\mathrm{acc}}}, \tag{3.38}$$

where the penultimate equality used the fact that $p_- = \mathrm{const} = \gamma_0 - p_{x,0}$ without taking into account radiation reaction, and in the last it was assumed that $\gamma_0 \gg 1$, so $p_0 = \sqrt{\gamma_0^2 - 1} \approx \gamma_0$. Considering this expression as an equation for $\Delta\varepsilon_{\mathrm{acc}}$, we get

$$\Delta\varepsilon_{\mathrm{acc}} = 2\gamma_0\gamma_{\mathrm{th}}^2(1 - \cos\theta), \tag{3.39}$$

where $\gamma_{\mathrm{th}} = 1/\sqrt{1 - v_{\mathrm{th}}^2}$ is a sufficiently large number, so $v_{\mathrm{th}} = 1$ is assumed in the final expression. Note that during the photoproduction of an electron-positron pair, their average energy is equal to half the energy of the parent photon ε_γ, therefore $\gamma_0 = \varepsilon_\gamma/2$. Strictly speaking, the time the particle spends in the vacuum region is determined by its initial position and the dynamics of the cascade front. However, the velocity and position of the front cannot be calculated from the quantities our model operates with. Thus, to determine the dynamics of the front, either the construction of a separate independent model or the use of some heuristic approximation is required. Despite the fact that in section 3.4.1 we construct a simplified analytical solution of the model equations, from which we can determine the cascade front velocity, the use of this solution to determine the time the particles spend in the vacuum region is impractical. Moreover, the found solution was obtained in approximations, which in fact are rather poorly satisfied. Thus, we will assume that the change in the energy of a particle while in the vacuum region is described quite well by the expression (3.39), where the quantity γ_{th}^2 is a free parameter of our model, which we will denote as μ. The determination of the value of μ in this way is based on a comparison of the solution of the equations of our model with the results of a full-scale three-dimensional QED-PIC simulation. Moreover, it follows from the definition that $\mu \sim 1$–10. So,

$$\Delta\varepsilon_{\mathrm{acc}} = \varepsilon_\gamma\mu(1 - \cos\theta), \tag{3.40}$$

and thw final expression for $S[\varepsilon, \mathrm{acc}]$ takes the following form

$$S[\varepsilon, \mathrm{acc}] = \varepsilon_\gamma\mu n_\gamma \int_0^\pi \Phi(\theta, v_{\gamma\|}) W_{\mathrm{pair}}(\chi_\gamma, \varepsilon_\gamma)(1 - \cos\theta)\sin\theta d\theta \equiv \varepsilon_\gamma\mu\overline{G_{\mathrm{rad}}} n_\gamma. \tag{3.41}$$

Validation of the correctness of this approximate expression is shown in Fig. 3.9 (a). Note that the absorption of laser radiation is significant at the vacuum-plasma interface, and quite small in the dense plasma region, as discussed in section 3.2.2. Also note that the explicit form of the expression (3.41) is in fact not really significant for our model. This is due to the fact that in the vacuum region the unknown quantities are practically independent of the coordinate and time. Thus, the expression (3.41) can be completely denoted as a certain constant — free parameter of our model. In this regard, the accuracy of the assumptions used to determine the form of the expression (3.41) is also not essential. Indirect confirmation of this statement is also the fact that in the original publication [202], in which this model was developed, other expressions were used to calculate $\Delta\varepsilon_{\mathrm{acc}}$, however, the solutions of the model equations are practically identical to those presented in this thesis. The main reason for refining this expression is only that the free parameter μ has the meaning of a number independent of the initial parameters of the problem, such as the amplitude of the laser field, the energy of the photon beam, etc.

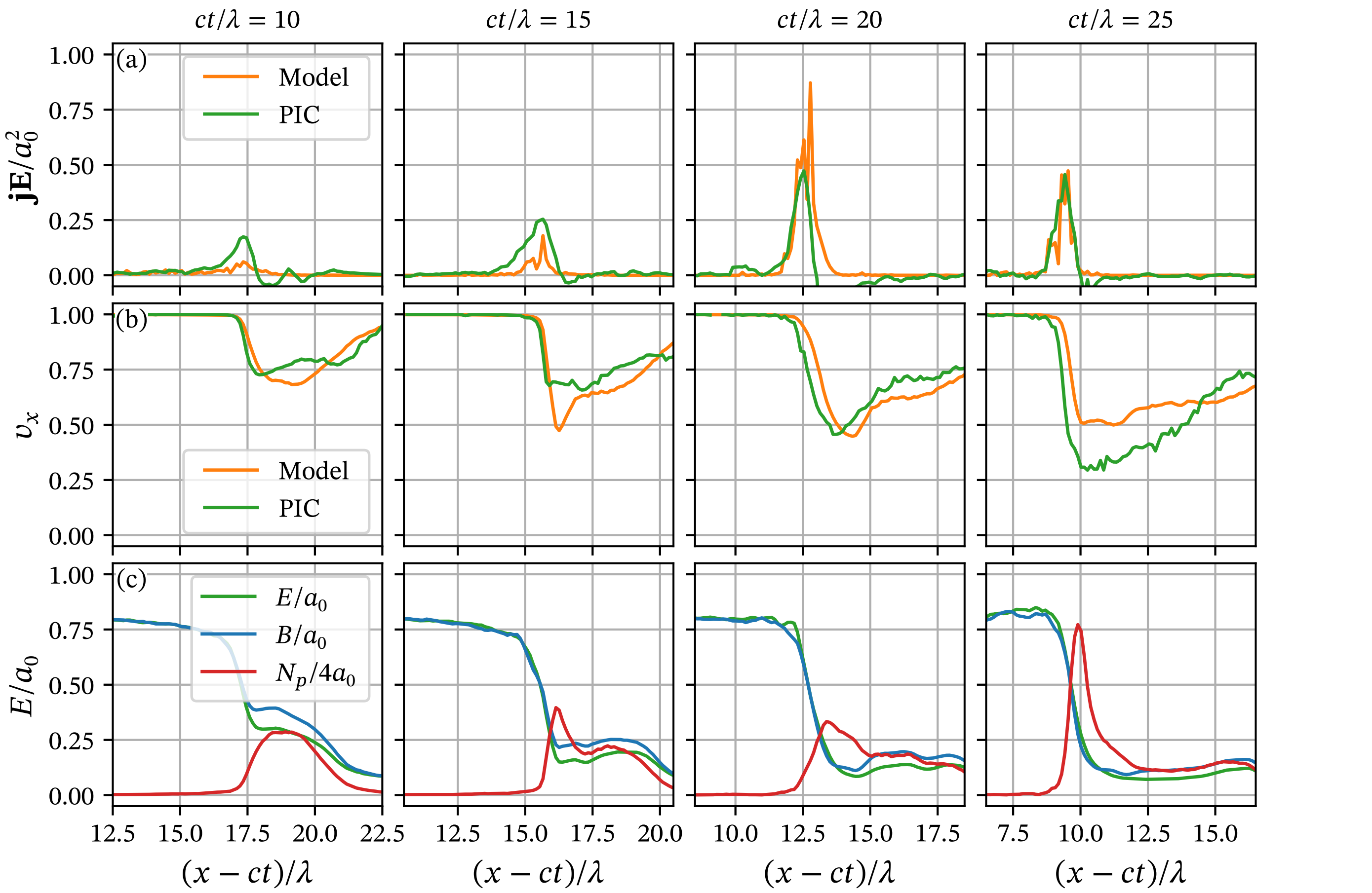

Figure 3.9: Validation of the model approximations. (a), (b) The value of **jE** and the average velocity of pairs v_x, calculated from the expressions (3.41) and (3.54), respectively (orange lines), and taken directly from the results of QED-PIC simulations (green lines) at various points in time. (c) Distribution of the amplitude of the electric (green lines) and magnetic (blue lines) fields and the e^-e^+ plasma density (red lines).

Assuming that the time the particle stays in the vacuum region is sufficiently short, so that radiation reaction does not significantly affect the dynamics of the particle, we assume that $\chi \approx \chi_0 =$ const. Then

$$\Delta\varepsilon_{\mathrm{rad}} = I_{\mathrm{rad}}(\chi_0)\Delta\varphi. \tag{3.42}$$

To calculate the value of $\Delta\varphi$, we use the expressions (3.37) and (3.40)

$$\mu\varepsilon_\gamma(1-\cos\theta) = \frac{E^2}{\varepsilon_\gamma(1-\cos\theta)}\sin^2\frac{\Delta\varphi}{2}, \tag{3.43}$$

from where we get

$$\Delta\varphi = \frac{2\varepsilon_\gamma(1-\cos\theta)}{E}\sqrt{\mu}. \tag{3.44}$$

Considering that $\chi_0 = \chi_\gamma/2$, the expression for the source $S[\varepsilon_p, \mathrm{rad}]$ is written as follows

$$S[\varepsilon, \mathrm{rad}] = \frac{2\varepsilon_\gamma n_\gamma\sqrt{\mu}}{E}\int_0^\pi \Phi(\theta, v_{\gamma\|})W_{\mathrm{pair}}(\chi_\gamma, \varepsilon_\gamma)I_{\mathrm{rad}}\left(\frac{\chi_\gamma}{2}\right)(1-\cos\theta)\sin\theta d\theta \equiv \overline{I_{\mathrm{vac}}}\frac{\varepsilon_\gamma n_\gamma\sqrt{\mu}}{E}. \tag{3.45}$$

3.3.5 Dynamics of e^-e^+ pairs in the plasma region

According to the reasoning in section 3.2.2, in the region of dense e^-e^+ plasma, at each point in space there exists an instantaneous reference frame K' moving with the speed $v_x(x,t) \approx E/B$, in which only the magnetic field is present. Due to the simplicity of the configuration of the EM field in K', it is convenient to carry out calculations in this reference frame. In K', electrons and positrons move along the magnetic field with the speed v'_B and also rotate in the plane perpendicular to the magnetic field with the speed $v'_\perp$ (see Fig. 3.10). Assume that the particles remain ultrarelativistic in the given reference frame (which is confirmed by the results of QED-PIC simulations), then the equality ${v'_\perp}^2 + {v'_B}^2 \approx 1$ is valid. Note that the movement of charged particles along a magnetic field can lead to the generation of a nonzero current, which must be taken into account in Maxwell's equations, while their rotation in a magnetic field does not, on average, create a current, but leads to the generation of copious gamma quanta. Let us calculate the QED value of the parameter χ, which is a Lorentz invariant, in K'

$$\chi_p = \frac{v'_\perp\varepsilon'_p B'}{a_S}. \tag{3.46}$$

The quantities in K' can be calculated from the corresponding quantities in the laboratory frame as follows: $B' = B\sqrt{1-(E/B)^2}$, $\varepsilon'_p = \varepsilon_p\sqrt{1-(E/B)^2}$, where we used the fact that the average particle momentum along the x axis is equal to γv_x and $v_x = E/B$. Thus the value of χ can be calculated as follows

$$\chi_p = \frac{v'_\perp\varepsilon_p E}{a_S}\frac{1-v_x^2}{v_x}. \tag{3.47}$$

Due to the rotation of particles in a magnetic field, it can be assumed that their angular distribution in K' is close to isotropic. In this case, similarly to the procedure with gamma quanta in Sec. 3.3.3, the distribution function of pairs in the laboratory frame of reference is written in the following form

$$f_p(t,x,\theta) = \Phi\left(\theta, v_x(x,t)\right) n_p(x,t). \tag{3.48}$$

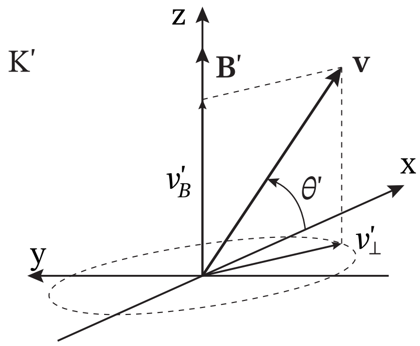

Figure 3.10: Geometric relation between the velocity and magnetic field in the reference frame K' moving with the speed $v_x = E/B$.

where Φ is defined in the same way as in equation (3.27)

$$\Phi(\theta, v) = \frac{1 - v^2}{2\left(1 - v\cos\theta\right)^2}.$$

The results of the QED-PIC simulations presented in Fig. 3.8 (c), (d) demonstrate that the expression (3.48) is a good approximation for calculating the angular distribution of the pairs. It will be shown below that the value of v_x can be approximately calculated from the local values of the electric field and the plasma density. Thus, we do not write the continuity equation for the quantity v_x, like the equation (3.18). Note also, that in the case of pairs, we neglect the difference between the velocity v of the reference frame in which the distribution of particles is isotropic and the average particle velocity $\overline{v}$ calculated from such a distribution, because their maximum difference does not exceed 0.2 according to the expression (3.29).

Since the value of χ_p does not depend on the angle θ, the sources of $S[\alpha, \mathrm{rad_a}]$ are calculated as follows

$$S[n, \mathrm{rad_a}] = n_p \int_0^\pi \Phi(\theta, v_x) W_{\mathrm{rad}}(\chi_p, \varepsilon_p) \sin\theta d\theta \equiv \overline{W_{\mathrm{pl}}} n_p, \tag{3.49}$$

$$S[\varepsilon, \mathrm{rad_a}] = n_p \int_0^\pi \Phi(\theta, v_x) I_{\mathrm{rad}}(\chi_p) \sin\theta d\theta \equiv \overline{I_{\mathrm{pl}}} n_p, \tag{3.50}$$

$$S[v, \mathrm{rad_a}] = n_p \int_0^\pi \Phi(\theta, v_x) \cos\theta W_{\mathrm{rad}}(\chi_p, \varepsilon_p) \sin\theta d\theta \equiv \overline{W_{\mathrm{pl}}} v_x n_p. \tag{3.51}$$

The total current density of the particles averaged over the characteristic Larmor rotation period $\tau_B = \varepsilon_p/B$ is calculated as follows

$$\mathbf{j} = 2n_p \frac{\mathbf{B}}{B} v_B \sqrt{1 - v_x^2}, \tag{3.52}$$

$$v_B = v'_B \frac{2}{\pi} \frac{\arccos\left(v_x\sqrt{1 - v_x^2}\right)}{\sqrt{1 - v_x^2(1 - v_x^2)}} \equiv \nu. \tag{3.53}$$

The factor 2 takes into account the fact that the currents of electrons and positrons are codirectional. This, in turn, is explained by the observation that in the laboratory reference frame, the electric and magnetic fields are not strictly perpendicular. Thus, in the reference frame K' there is a small electric field directed along or against the magnetic field (depending on the sign of the product $\mathbf{E} \cdot \mathbf{B}$). The presence of this field leads to the fact that the average velocity of electrons is opposite to it, and the average speed of positrons is co-directed to it. At the same time, the longitudinal drift of particles does not depend on the sign of the charge; therefore, the currents of electrons and positrons along the x axis compensate each other, and in the yz plane they are summed up. This fact also indicates that the electron-positron plasma is a conductive medium, so some absorption of electromagnetic energy also occurs in this region, although it is much less than the absorption in the vacuum region observed in QED-PIC simulations (see Fig. 3.9 (a)) and thus we don't include it in our model. The value of v_B averaged over particles, which we denoted as ν[2], is the second free parameter of our model. It can be roughly estimated by noting that for a single particle the value of v'_B can only slightly diverge from its initial value due to the presence of a weak electric field in K'. The particles enter the plasma region after being accelerated by a laser pulse with a predominantly longitudinal velocity, i.e. velocity along the x axis, so the initial projection of the particle velocity onto the magnetic field lying in the yz plane is a small value. Thus, we can expect that our model should give reliable results for smaller values of ν.

Calculation of the electrodynamic properties of a medium which response to a plane circularly-polarized EM wave consists in generating a current along the magnetic field is considered in the next section. The main conclusion is that the relationship between the electric and magnetic fields in such a medium can be expressed in terms of the density and amplitude of the electric field as follows

$$\frac{E}{B} = v_x = \sqrt{\frac{2}{1 + \sqrt{1 + \left(4n_p\nu/E\right)^2}}}. \tag{3.54}$$

The validity of the expression (3.54) is also confirmed by direct comparison with the results of the QED-PIC simulation shown in Fig. 3.9 (b).

[2]The value of the factor after v'_B in Eq. (3.53) is in the range 0.77–1.

3.3.6 Electrodynamical properties of e^-e^+ plasma

Let us consider the propagation of a plane circularly polarized EM wave along the x axis in a weakly inhomogeneous (also along the x axis) medium, the response of which to this wave consists in generating a current $\mathbf{j} = 2n_p\mathbf{v}$, along the magnetic field of the wave. To do this, we write Maxwell's equations

$$\frac{\partial E_z}{\partial x} = \frac{\partial B_y}{\partial t}, \tag{3.55}$$

$$\frac{\partial E_y}{\partial x} = -\frac{\partial B_z}{\partial t}, \tag{3.56}$$

$$\frac{\partial B_z}{\partial x} = -\frac{\partial E_y}{\partial t} - 2n_p v_y, \tag{3.57}$$

$$\frac{\partial B_y}{\partial x} = \frac{\partial E_z}{\partial t} + 2n_p v_z. \tag{3.58}$$

Let us switch to the following complex variables

$$\epsilon = E_y + iE_z, \tag{3.59}$$

$$\beta = B_z - iB_y, \tag{3.60}$$

$$v_y + iv_z = \frac{\epsilon}{|\epsilon|} i v_\perp, \tag{3.61}$$

and introduce a vector potential a the following way

$$\epsilon = -\frac{\partial a}{\partial t}, \tag{3.62}$$

$$\beta = \frac{\partial a}{\partial x}. \tag{3.63}$$

In the new variables, the equations (3.55)–(3.58) are rewritten as follows

$$\frac{\partial^2 a}{\partial x^2} = \frac{\partial^2 a}{\partial t^2} - 2n_p \frac{\partial a}{\partial t}\left|\frac{\partial a}{\partial t}\right|^{-1} iv_\perp. \tag{3.64}$$

We will look for a solution to this equation in the form of a quasi-monochromatic plane wave with an amplitude depending on the coordinate x

$$a = E(x)\exp\left\{i\int^x \kappa(x')\mathrm{d}x' - it\right\}, \tag{3.65}$$

where $E(x)$ and $\kappa(x)$ are real functions of the coordinate x, designating the amplitude and wavenumber of the wave, respectively. As a result, the equations have the following form

$$\frac{\partial^2 E}{\partial x^2} + E(1-\kappa^2) + 2n_p v_\perp = 0, \tag{3.66}$$

$$E\frac{\partial \kappa}{\partial x} + 2\kappa\frac{\partial E}{\partial x} = 0. \tag{3.67}$$

If the plasma is weakly inhomogeneous, then the WKB approximation can be applied to solve this equation. Assuming that the plasma inhomogeneity scale L significantly exceeds the wavelength λ, we can neglect the terms with the second derivative: $\partial^2 E/\partial x^2 \sim E/L^2 \ll \varkappa^2 E = (2\pi)^2 E/\lambda^2$. In that case we have

$$E(1-\varkappa^2) + 2n_p v_\perp = 0. \tag{3.68}$$

Solving this equation, we get

$$\varkappa \equiv \frac{B}{E} = \sqrt{1 + \frac{2n_p v_\perp}{E}}, \tag{3.69}$$

Let's use the expression (3.52) for $v_\perp$, i.e.

$$v_\perp = \nu\sqrt{1 - v_x^2}. \tag{3.70}$$

Note that for $\nu > 0$, $B > E$ according to (3.69), and therefore $1/\varkappa$ has the meaning of the drift velocity v_x. Thus,

$$\frac{1}{v_x} = \sqrt{1 + \frac{2n_p\nu}{E}\sqrt{1 - v_x^2}}. \tag{3.71}$$

The solution of this equation has the following form

$$v_x = \left(\frac{2}{1 + \sqrt{1 + S^2}}\right)^{1/2}, \tag{3.72}$$

$$S = \frac{4n_p\nu}{E}. \tag{3.73}$$

The comparison of the obtained solution with the numerical solution of the equations (3.66)–(3.67) is shown in Fig. 3.11 in both cases of either applicability or inapplicability of the WKB approximation. The solution (3.72) is obtained under the assumption that $v^2 = 1$, so it is valid in a reference frame where the particles are ultrarelativistic, in particular in the laboratory reference frame.

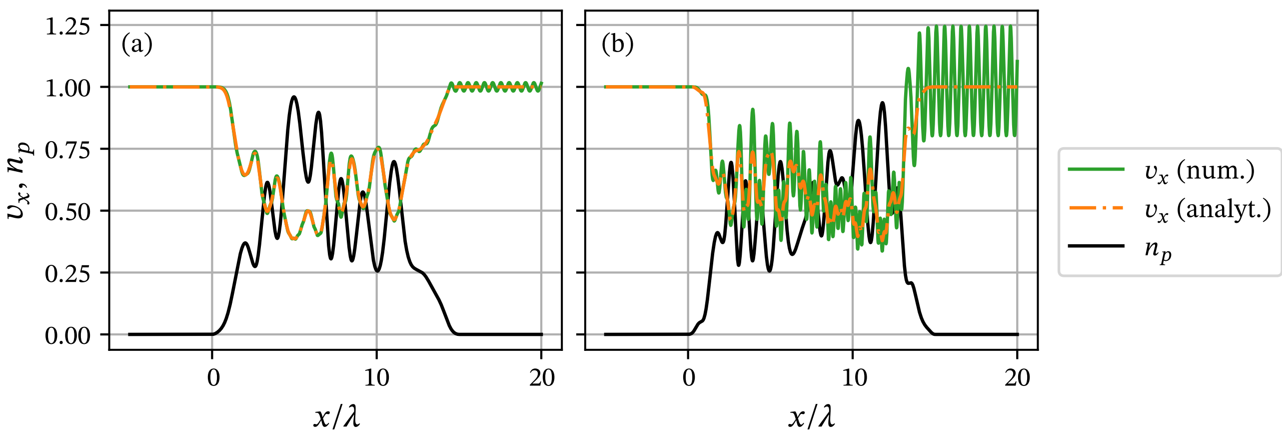

Figure 3.11: Drift velocity $v_x = E/B$ calculated from the numerical solution of the equations (3.66)–(3.67) (green line) and using the analytical expression (3.72) (orange line) for a randomly inhomogeneous plasma distribution (black line). The inhomogeneity scale exceeds the wavelength in subfigure (a), which makes the WKB approximation valid, and less than it in subfigure (b).

3.4 The model finalization and comparison with QED-PIC simulations

The last quantities left undefined are the factors ψ_{vac} and ψ_{pl}, which serve to separate the vacuum and plasma regions in space. Note that the longitudinal velocity of pairs v_x, determined according to the equation (3.54), makes it easy to distinguish between these regions: in vacuum $v_x \approx 1$, while in the plasma region $v_x < 1$. Therefore, ψ_{vac} and ψ_{pl} can be chosen as follows

$$\psi_{\text{vac}} = v_x^M, \tag{3.74}$$

$$\psi_{\text{pl}} = 1 - v_x^M, \tag{3.75}$$

where $M \sim 10$ is a fairly large constant. The value of this constant is selected on the basis of a certain threshold for v_x, above which it can be assumed that the plasma is quite rare and collective effects can be neglected. Further, we will assume that this threshold corresponds to 0.7, and $M = 8$.

Thus, the equations describing the development of a QED cascade in a plane wave have the following final form

$$\frac{\partial}{\partial t} n_p + \frac{\partial}{\partial x}\left(v_x n_p\right) = \overline{W_{\text{pair}}} n_\gamma, \tag{3.76}$$

$$\begin{aligned} \frac{\partial}{\partial t}\left(\varepsilon_p n_p\right) + \frac{\partial}{\partial x}\left(v_x \varepsilon_p n_p\right) &= \overline{W_{\text{pair}}} n_\gamma \frac{\varepsilon_\gamma}{2} + \mu \overline{G_{\text{rad}}} n_\gamma \varepsilon_\gamma \psi_{\text{vac}} - \\ &\quad - \frac{\sqrt{\mu}}{E} \overline{I_{\text{vac}}} n_\gamma \varepsilon_\gamma \psi_{\text{vac}} - \overline{I_{\text{pl}}} n_p \psi_{\text{pl}}, \end{aligned} \tag{3.77}$$

$$\frac{\partial}{\partial t} n_\gamma + \frac{\partial}{\partial x}\left(\overline{v_{\gamma\|}} n_\gamma\right) = -\overline{W_{\text{pair}}} n_\gamma + 2\overline{W_{\text{rad}}} n_p \psi_{\text{pl}}, \tag{3.78}$$

$$\frac{\partial}{\partial t}\left(\overline{v_{\gamma\|}} n_\gamma\right) + \frac{\partial}{\partial x}\left(\overline{v_{\gamma\|}^2} n_\gamma\right) = -\overline{V_{\text{pair}}} n_\gamma + 2\overline{V_{\text{rad}}} n_p \psi_{\text{pl}}, \tag{3.79}$$

$$\frac{\partial}{\partial t}\left(\varepsilon_\gamma n_\gamma\right) + \frac{\partial}{\partial x}\left(\overline{v_{\gamma\|}} \varepsilon_\gamma n_\gamma\right) = -\overline{W_{\text{pair}}} n_\gamma \varepsilon_\gamma + 2\overline{I_{\text{pl}}} n_p \psi_{\text{pl}}, \tag{3.80}$$

$$\frac{\partial}{\partial t}\left(\frac{E^2 + E^2/v_x^2}{2}\right) + \frac{\partial}{\partial x}\left(\frac{E^2}{v_x}\right) = -2\mu \overline{G_{\text{rad}}} n_\gamma \varepsilon_\gamma \psi_{\text{vac}}, \tag{3.81}$$

$$\frac{\partial}{\partial t}\Sigma_\gamma = \frac{2\sqrt{\mu}}{E} \overline{I_{\text{vac}}} n_\gamma \varepsilon_\gamma \psi_{\text{vac}}. \tag{3.82}$$

Note that the total energy is conserved in our model, i.e.,

$$\int \left(2 n_p \varepsilon_p + n_\gamma \varepsilon_\gamma + \frac{E^2 + B^2}{2}\right) dx + \Sigma_\gamma = \text{const.} \tag{3.83}$$

3.4.1 Analytical estimates

Before proceeding to the numerical solution of these equations and comparing it with the results of QED-PIC simulations, we will make some very rough, but analytical estimates. To do this, we will assume that electrons and positrons emit gamma quanta strictly opposite to the x axis. The distribution of laser intensity will be considered constant and uniform. In connection with the last assumption, the probabilities $\overline{W_{\rm pair}}$ and $\overline{W_{\rm rad}}$ will also be considered constant. In this case, the continuity equations for the plasma density n_p and photons n_γ are written as follows in the reference frame moving with the average plasma velocity v_x

$$\frac{\partial n_p}{\partial t} = W_{\rm pair} n_\gamma, \tag{3.84}$$

$$\frac{\partial n_\gamma}{\partial t} - \frac{\partial n_\gamma}{\partial x} = -W_{\rm pair} n_\gamma + 2W_{\rm rad} n_p. \tag{3.85}$$

If we neglect the term with ∂_x in (3.85), which characterizes the spatial dispersion, then the continuity equations turn into equations describing the QED cascade in a rotating electric field without spatial dynamics [98, 183]. The equations (3.84)–(3.85) can be solved using the one-sided Fourier transform [203], i.e. expanding of the solution into a sum of exponentials with real values k and complex values ω

$$n_{p,\gamma}(t,x) = \int\limits_{-\infty+i\sigma}^{+\infty+i\sigma} \mathrm{e}^{-i\omega t}\frac{d\omega}{2\pi}\int\limits_{-\infty}^{+\infty} \mathrm{e}^{ikx} n_{p,\gamma}(\omega,k)\frac{\mathrm{d}k}{2\pi}. \tag{3.86}$$

where

$$n_{p,\gamma}(\omega,k) = \int\limits_{0}^{+\infty} \mathrm{e}^{i\omega t}dt\int\limits_{-\infty}^{+\infty} \mathrm{e}^{-ikx} n_{p,\gamma}(t,x)\,\mathrm{d}x, \tag{3.87}$$

and σ is a real number such that the integration contour lies in the analyticity domain of $n_{p,\gamma}$. For initial density distributions of plasma and gamma quanta equal to $n_p(0,x)$ and $n_\gamma(0,x)$ respectively, the solution is found as follows

$$n_p(t,x) = \int\limits_{-\infty+i\sigma}^{+\infty+i\sigma} \frac{\mathrm{d}\omega}{2\pi}\int\limits_{-\infty}^{+\infty} \frac{\mathrm{d}k}{2\pi}\int\limits_{-\infty}^{+\infty} dx' \frac{W_{\rm pair} n_p(0,x') + i(\omega+k)\,n_\gamma(0,x')}{\Delta(\omega,k)} \mathrm{e}^{ik(x-x')-i\omega t}, \tag{3.88}$$

where $\Delta(\omega,k) = \omega^2 + \omega(k + iW_{\rm pair}) + 2W_{\rm pair}W_{\rm rad}$. Perturbations of the initial distribution propagate along the characteristics defined by the dispersion equation $\Delta(\omega,k) = 0$, which has the following solution

$$\omega = \frac{-k - iW_{\rm pair} \pm \sqrt{(k+iW_{\rm pair})^2 - 8W_{\rm pair}W_{\rm rad}}}{2}. \tag{3.89}$$

The group velocity of these perturbations is equal to $v_{\rm gr} = \partial \mathrm{Re}[\omega]/\partial k$. Analysis of the dispersion relation shows that perturbations with small wave numbers ($k \ll W_{\rm pair}$) are the most unstable and have the following instability increment

$$\Gamma \equiv \mathrm{Im}[\omega] = \frac{W_{\rm pair}}{2}\left(\sqrt{1+\frac{8W_{\rm rad}}{W_{\rm pair}}} - 1\right), \tag{3.90}$$

which coincides with the QED cascade growth rate in a rotating electric field [98, 183]. From (3.89) we obtain the dispersion relation for unstable perturbations

$$\omega \approx \frac{\mu - 1}{2} k + i\Gamma, \tag{3.91}$$

$$\mu = \frac{1}{\sqrt{1 + 8W_{\mathrm{rad}}/W_{\mathrm{pair}}}}. \tag{3.92}$$

In the limit $a_0 \to \infty$, $W_{\mathrm{rad}}/W_{\mathrm{pair}} \approx 4$ and $\mu \approx 0.17$ [32]. Therefore, perturbations with small wave numbers propagate at a speed of $v_{\mathrm{gr}} \approx -0.41$. This value coincides with the results of the numerical solution of the equations (3.84)–(3.85) with different forms of initial distributions of pairs and gamma quanta (see an example of such a solution in Fig. 3.12). In the frame of reference moving with the average longitudinal velocity of the plasma, the velocity of the cascade front v_{fr} coincides with the found group velocity $v_{\mathrm{gr}} \approx -0.41$. The transformation to the laboratory reference frame makes it possible to find the relation between the average longitudinal velocity of plasma particles and the velocity of the cascade front

$$v_{\mathrm{fr}} = \frac{v_x + v_{\mathrm{gr}}}{1 + v_x v_{\mathrm{gr}}/c^2}. \tag{3.93}$$

Solving this equation for v_x we get:

$$v_x = \frac{v_{\mathrm{fr}} - v_{\mathrm{gr}}}{1 - v_{\mathrm{gr}} v_{\mathrm{fr}}/c^2}. \tag{3.94}$$

This reasoning predicts $v_x = 0.61$ for $v_{\mathrm{fr}} = 0.27$ ($a_0 = 2500$, see Fig. 3.3), which is close enough to the average positron velocity ≈ 0.75 obtained from numerical simulations (see Fig. 3.4 (b)).

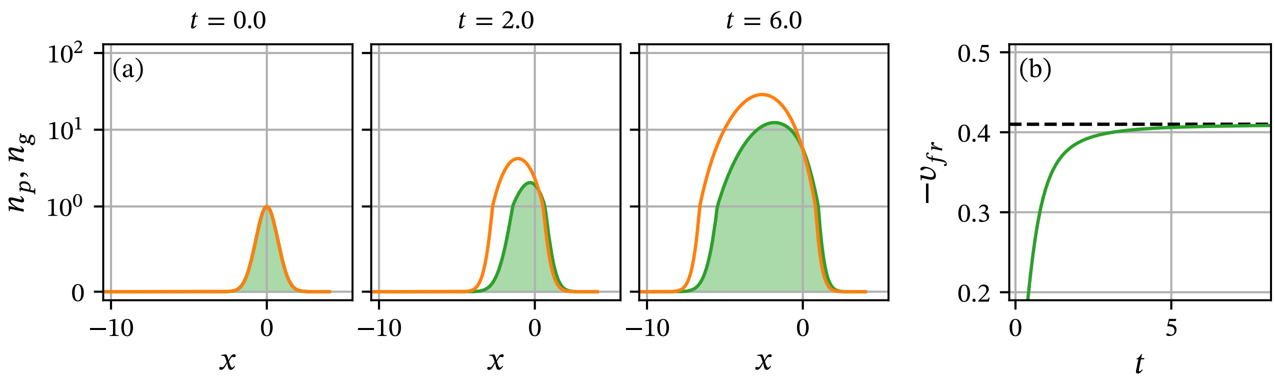

Figure 3.12: Numerical solution of Eqs.(3.84)–(3.85): (a) Density distribution of positrons n_p (green line) and gamma quanta n_γ (orange line) at different times. The scale of the vertical axis is linear in range $[-1, 1]$ and logarithmic outside this range. Coordinates, time and densities are normalized so that $W_{\mathrm{rad}} = 1.0$, $W_{\mathrm{pair}} = 0.25$. (b) The velocity of the density distribution front n_p, determined from the threshold $n_p = 0.1$, as a function of time.

3.4.2 Numerical solution

The numerical solution of the Eqs. (3.76)–(3.81) is found using the method of lines: the partial derivatives $\partial/\partial x$ are approximated by finite differences to obtain an ODE system, which is solved with using the explicit Runge-Kutta method. Since the Runge-Kutta method is not symplectic, the conservation of energy at each integration step is forced by manually clamping the derivative $\partial n_\gamma/\partial t$ so that the total energy does not increase. The relative error obtained as a result of this procedure turns out to be acceptably small. The free parameters were estimated manually by comparing the solution with the results of a 3D QED-PIC simulation based on two macroscopic parameters: the cascade front speed and the energy balance in the system. Model testing shows that there is a positive correlation between the parameter ν and the cascade front velocity. The parameter μ mainly determines the energy transfer from the laser to the cascade particles, therefore, by changing this parameter, one can control the characteristic laser energy absorption time. We have found the values of the free parameters of the model, at which there is good agreement with the simulation results with different initial conditions (see Figs. 3.13–3.15).

The 3D QED-PIC simulations were performed using the QUILL code [201], which allows the simulation of QED effects using the Monte-Carlo method. The initial distribution of EM fields has the form of a plane wave with a wavelength $\lambda = 2\pi c/\omega_L = 1\,\mu\text{m}$ and an amplitude a_0, propagating along the x axis with spatio-temporal envelope given by the following expression

$$a(x, y, z) = \cos^2\left(\frac{\pi}{2}\frac{x^4}{\sigma_x^4}\right)\cos^2\left(\frac{\pi}{2}\frac{\left(y^2+z^2\right)^2}{\sigma_r^4}\right). \tag{3.95}$$

The transverse spatial size of the laser pulse was $2\sigma_r = 18\,\mu\text{m}$, and the pulse duration was 60.5 fs ($2\sigma_x = 18.15\,\mu\text{m}$). The size of the simulation box was $30\lambda \times 30\lambda \times 30\lambda$, the number of cells was $3000 \times 300 \times 300$. As was discussed in section 3.2.2, the final stage of the development of the QED cascade in a single laser pulse is practically independent of the initial seed; therefore, a short gamma bunch propagating towards the laser pulse was set as the seed in the simulations in order not to take into account the interaction with the electron-ion plasma, which differs significantly from the interaction with produced electron-positron plasma. The initial seed in this form in our model can be specified by initializing $v_{\gamma\|}(t = 0) \approx -1$. The initial density distributions of gamma quanta in our model and PIC simulations coincide and are expressed by the following expression: $n_\gamma(t = 0) = n_0 \max\left\{0, 1 - (x - x_0)^2/w_\gamma^2\right\}$, where w_γ is the half-width of the bunch, and x_0 is the position of its center. The initial energy of gamma quanta was set equal to $200 m_e c^2$.

A direct comparison between the solutions of the equations (3.76)–(3.81) and the results of the QED-PIC simulation is shown in Figs. 3.13–3.15. Our model qualitatively agrees with the results of QED-PIC simulations in terms of particle distribution and electromagnetic field, as well as energy balance. The regimes of cascade development are also clearly distinguished both in our model and in the QED-PIC simulation.

The first regime (see Fig. 3.13) occurs when the value of a_0 of the laser pulse is not large enough or the gamma bunch is not dense enough. In this case, the density of the resulting electron-positron

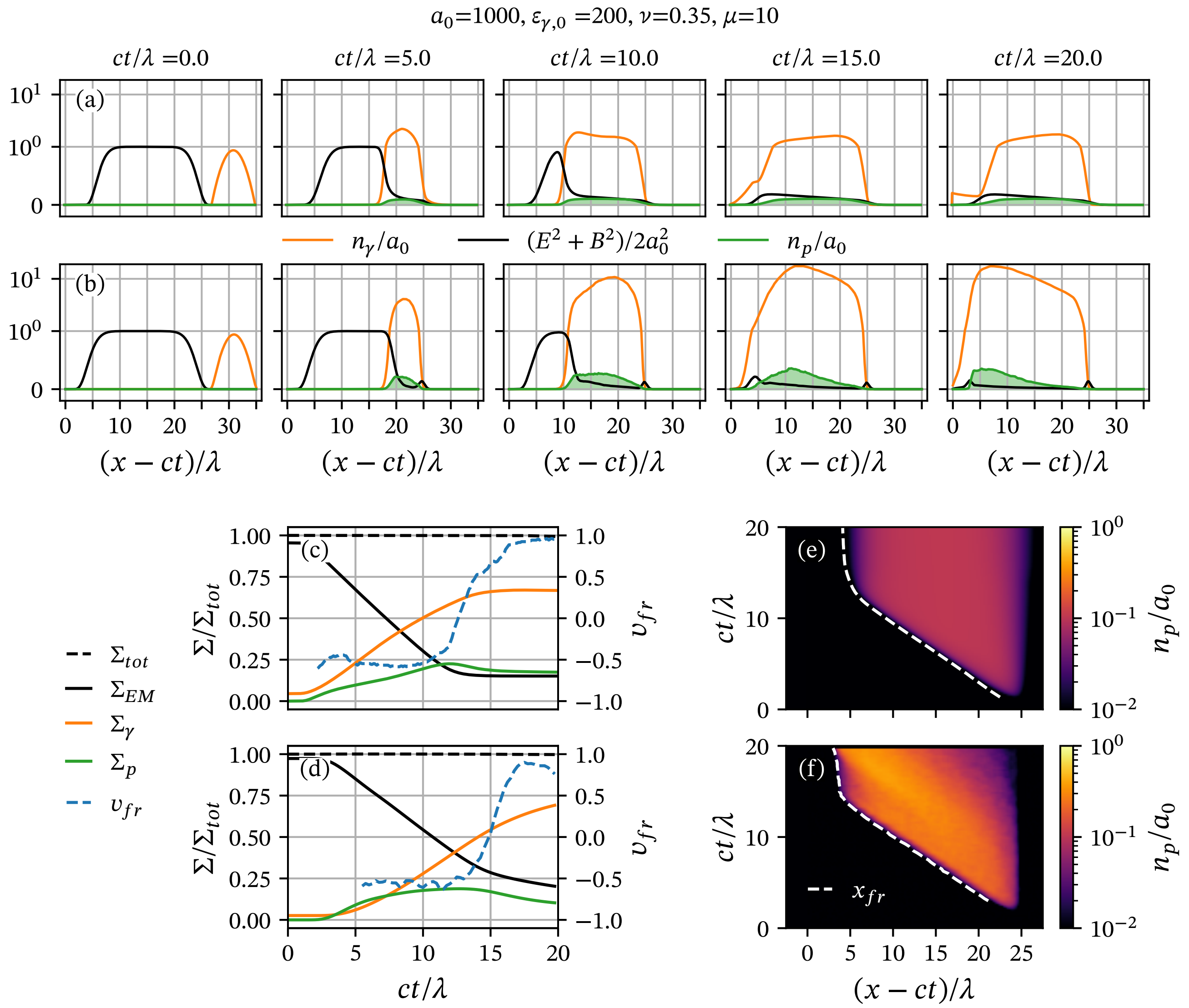

Figure 3.13: Comparison between (a, c, e) solution of Eqs. (3.76)–(3.81) and (b, d, f) QED-PIC simulation results for initial parameters $a_0 = 1000$, $n_{\gamma,0} = a_0 n_{\mathrm{cr}}$. (a, b) Distributions of gamma quanta density n_γ (orange line), EM energy density $(E^2+B^2)/2$ (black line) and plasma density n_p (green line) at various points in time. The vertical scale is linear in the range [0, 1] and logarithmic in the range [1, +∞]. (c, d) Energy balance in the system: total energy e^-e^+ of pairs Σ_p (green line), Σ_γ gamma quanta (orange line) and EM energy Σ_{EM} (black line) normalized to the total initial energy of the system Σ_{tot}; cascade front velocity v_{fr} (dashed blue line). (e, f) Distribution of e^-e^+ pairs in the $x-t$ plane and position of the cascade front x_{fr} (dashed white line). Values of free parameters: $\nu = 0.35$, $\mu = 10$.

plasma does not reach the relativistic critical density, so that $v_x \approx 1$, i.e. there are no collective plasma effects. In this case, there is no plasma region at all, and newly born particles move in a laser pulse field close to a plane wave. As discussed in the papers [96, 144, 186, 195] and the chapter 2 of this work, in this case the value of the χ parameter does not increase. Since after each act of gamma-quantum emission, the value of χ is split between the parent and child particles, after several generations its value for all the particles becomes sufficiently smaller than 1 and the development of the cascade stops. Thus, at sufficiently small a_0, the gamma quanta of the bunch decay into pairs, leaving a «trail» of electrons and positrons, which accelerate in a forward direction and propagate along with the laser pulse. Although the plasma density is low, the total number of pairs can be large enough to transfer a significant portion of the laser energy to them (see Fig. 3.13 (c), (d)). Since in this regime all particles propagate independently of each other, the cascade front propagates with an almost constant velocity $v_{\mathrm{fr}} \approx -0.5$.

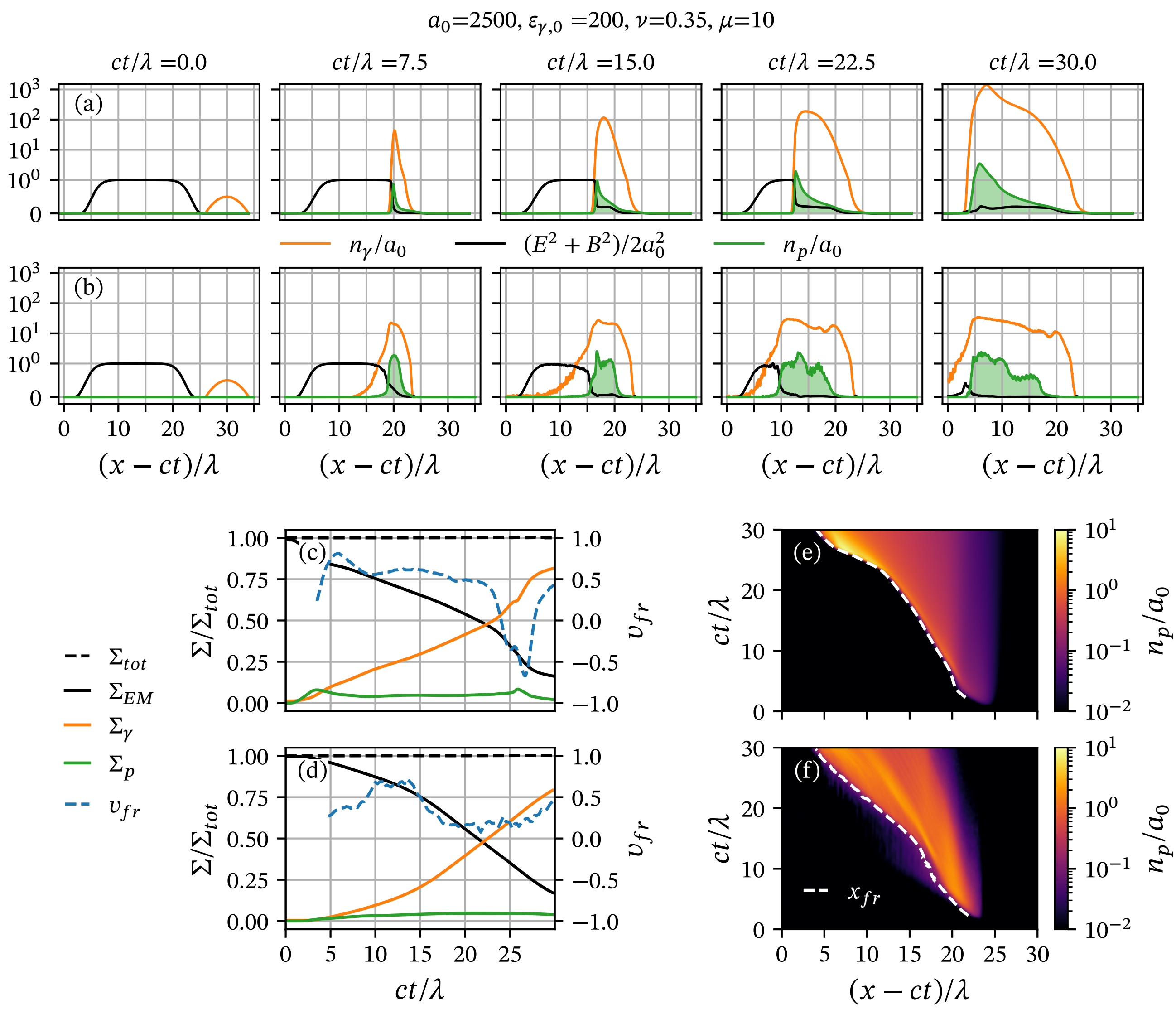

Figure 3.14: Same as in Fig. 3.13 for initial parameters $a_0 = 2500$, $n_{\gamma,0} = 0.5\, a_0 n_{\mathrm{cr}}$.

In the second regime (see Fig. 3.14), the cascade develops as discussed in Sec. 3.2.2. The peak of the pair density propagates towards the laser at a much lower speed (relative to the front edge of the laser pulse) than in the first regime. In this case, the plasma density increases with time, in contrast to the first regime, when the plasma density at each point remains practically unchanged after the initial gamma bunch passes through this point. As was mentioned in section 3.3.5, the dense electron-positron plasma practically does not absorb the laser energy, therefore, despite the fact that in this regime the total number of pairs is much higher than in the first regime, the energy transfer rates from the EM fields to the pairs are close to each other in both regimes.

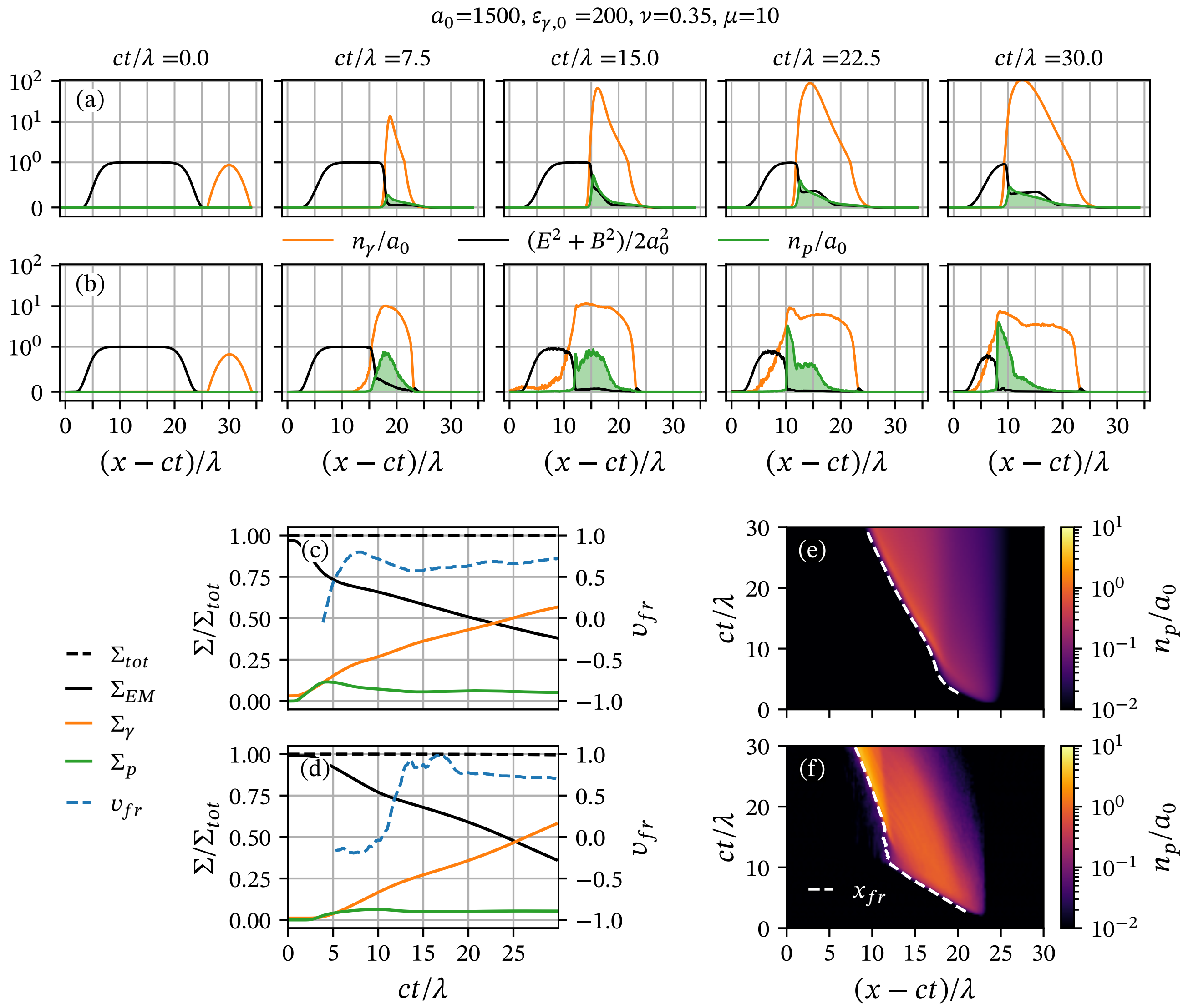

Figure 3.15: Same as in Fig. 3.13 for initial parameters $a_0 = 1500$, $n_{\gamma,0} = a_0 n_{\rm cr}$.

If a_0 lays in-between the values at which either the first or the second regimes are realized, at the initial stage the cascade resembles the S-type cascade which is clearly indicated by the negative value of the velocity of the cascade front (see blue dashed line in Fig. 3.15 (c), (d)). At some point the density of the pairs becomes large enough to alter the laser propagation and to shift the cascade dynamics to the self-sustained regime. The change between these two regimes is indicated by abrupt change in the velocity of the cascade front. The initial stage (stage of the S-type cascade) can also be seen for larger values of a_0 (see Fig. 3.14), though it is much shorter and is hardly pronounced in the results of the QED-PIC simulations.

We also validated the analytical estimate (3.94) developed above, from which the relation between the average longitudinal velocity of the cascade particles and the velocity of the cascade front was obtained. As shown in Fig. 3.16, the cascade front velocity calculated from this estimate based on the average particle velocity approximately coincides with the real front velocity observed in the model solution at the cascade self-sustaining stage. Since, as noted above, this stage never starts in the simulation at $a_0 = 1000$, this simplified model cannot be applied in this case.

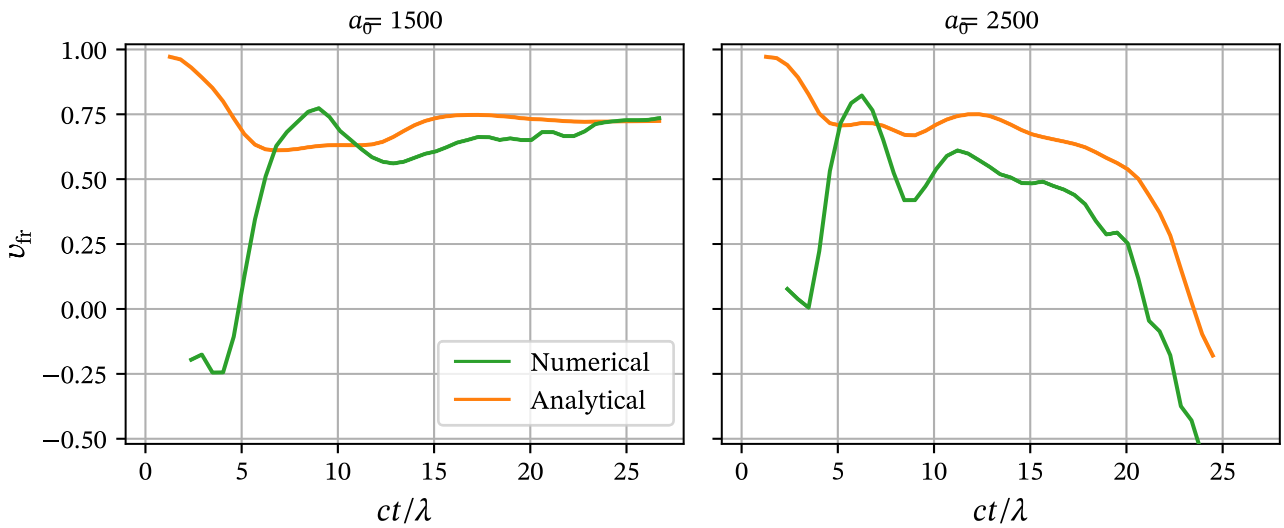

Figure 3.16: The cascade front velocity observed in the model solution (green line) and obtained from the analytical estimate (3.94) (orange line), calculated from the average velocity of particles located inside the electron-positron plasma at a depth of 2λ from the cascade front.

There are some features that are not captured by our model which are worth noting. For example, in the PIC simulation there is a distinct tail of the gamma-quanta spatial distribution counter-propagating to the laser pulse. These gamma-quanta have relatively low energy and thus are unable to photoproduce pairs. Our model predicts that the edge of the plasma and gamma-quanta distributions almost completely coincide. The total energy carried away by this sort of gamma-quanta is insignificant so this feature is not crucial for the cascade development. The reason that our model cannot capture this feature is the fact that we assume the distribution functions to be monoenergetic. Higher accuracy can be obtained if we would split the gamma-quanta into several groups with different energies and describe them separately; then this feature would be present in our solutions. But as already mentioned in Sec. 3.3.1 it would greatly complicate the model but will not lead to significant qualitative changes in the solutions.

3.5 Summary

To summarize, we have shown that a self-sustaining QED cascade can develop in a plane wave, contrary to a fairly common reasoning that such a field configuration is unsuitable for observing QED cascades [96, 144, 186]. Indeed, to observe such an effect, a sufficiently dense seed is required that can alter the propagation of this plane wave. The development of the QED cascade leads to the formation of a dense electron-positron «cushion», the front of which moves much slower than the speed of light, and which efficiently absorbs laser radiation. By analogy with ionization waves in gas discharge physics [107, 108], the propagation of the cascade QED front can be considered as a «vacuum breakdown» wave. It is important to note that for the development of such a QED cascade, the presence of a reflected wave is not fundamental, which makes it significantly different from a QED cascade in a standing wave, which is quite an actively studied configuration due to the relatively simple field configuration. In particular, the threshold value of the wave amplitude a_0, necessary for the development of a QED cascade in a standing wave, was calculated numerically in the publication [98], based on the condition of doubling the number of particles during a single laser period, and at a wavelength of 1 μm amounted to about 10^3. It follows from our calculations that the threshold for the development of a QED cascade in a plane wave corresponds approximately to $a_0 \sim 1500$, which is just a bit higher than the threshold for the development of a cascade in a standing wave, but still significantly below the Sauter-Schwinger critical field $a_S = mc^2/\hbar\omega_L \simeq 4 \times 10^5$ [1, 2]. The value $a_0 = 1500$ corresponds to an intensity near 6×10^{24} W/cm^2 at a wavelength 1 μm, which, as mentioned above, can potentially be achieve at future laser systems, albeit at the expense of sufficiently sharp focusing of the radiation. Nevertheless, the appearance of a vacuum breakdown wave and subsequent absorption of laser radiation can be considered as another fundamental limitation on the attainable intensity of laser radiation, first studied in publications [46, 166], for the case of weak focusing.

We also developed an analytical self-consistent model for the development of such a QED cascade. To obtain model equations for a computationally light model, a number of assumptions were made, the main of which are the transition to a quasi-one-dimensional hydrodynamic description, the use of locally monoenergetic particle distribution functions, and the plane wave approximation for laser radiation. The resulting system of equations is written in closed form and is also solved numerically. Despite the complexity and nonlinearity of the cascade dynamics, it turned out that a relatively simple one-dimensional model makes it possible to qualitatively predict its development, for example, the macroscopic space-time distribution of particles and the energy balance in the system. This justifies the analytical reasoning behind the model and hence our understanding of the phenomena involved. The methods used to develop this model can probably be used to build similar models that describe astrophysical phenomena, such as the development of QED cascades in the magnetospheres of neutron stars, also characterized by complex spatiotemporal dynamics and accompanied by the generation of vacuum breakdown waves [204].

Contributions of the author

The results obtained in this chapter are published in Refs. [202, 205]. In the publication [205] A. S. performed the PIC simulations and analyzed the results. All of the authors contributed to the development of the qualitative understanding of the QED cascade development. In the publication [202] A. S. developed the analytical model and performed PIC simulations. In the publication [193] all the authors discussed the idea of configuration with multiple beams. A. S. performed the simulations and analyzed the results. In the publications [27, 73] A. S. did most of the work. In the publication [70] A. S. helped with understanding the mechanism of QED cascading and writing the manuscript.

Chapter 4

Interaction of high-current beams of ultrarelativistic particles with matter

4.1 Introduction

Interaction of particle flows is a fundamental problem of plasma physics and high energy physics. On the one hand, it plays a key role in many astrophysical processes, for example, relativistic jets are associated with gamma ray bursts, tidal disruptions, active galactic nuclei and blazars. In the collapsar model of gamma ray bursts [206, 207], the jet interacts with the shell of the star formed after the collapse of the star. With the development of quantum electrodynamic (QED) cascades near the polar caps of neutron stars [113], the fluxes of generated electrons and positrons can interact with each other in the magnetosphere of a neutron star and significantly determine its dynamics [116]. On the other hand, colliders, which are the main research tool in the field of elementary particle physics, are based on the head-on collision of high-energy charged particle beams. Currently, there are several projects aimed at building high-energy lepton colliders with record parameters, such as ILC [118] and CLIC [119]. In the interaction region of such colliders, strong EM fields can be generated, thereby making possible manifestation of some strong-field phenomena such as *disruption* of beams [121–123], *beamstrahlung* [124–126], production of secondary electron-positron pairs [127, 128], and even effects of *nonperturbative* QED [129, 130]. As noted in the Introduction, it is expected that in the near future the main tool for studying the strong-field physics will be multi-PW laser facilities, such as ELI [3], SULF [5], Apollon [4], and in the future also 100-PW level facilities such as XCELS [7], SEL [6], etc. However, reaching ever-increasing laser intensities imposes increasingly stringent requirements on contrast, stability, and beam quality, which have not yet been achieved in practice [131]. In this regard, high-current high-energy colliders, which are distinguished by high beam quality and stability, can become an attractive «laserless» alternative for experiments in the strong-field physics. We note that relatively recently plasma acceleration has been considered as a promising alternative method for creating linear colliders with a large accelerating gradients [120]. The most actively discussed project in this context is FACET-II [129, 132, 133]. It is expected that this accelerator will make it possible to operate with electron (or positron) beams which own field amplitude is comparable to the field amplitude at the focus of an extremely intense multi-PW laser, i.e., only a few orders of magnitude less than the critical Schwinger field E_S. This chapter is devoted to the study of QED effects accompanying interaction of high-current beams of ultrarelativistic particles with each other and with plasma targets.

4.2 Effect of radiation reaction on disruption in beam-beam collision

When considering a head-on collision of beams in the ultrarelativistic regime, the dynamics of particles of each beam is predominantly determined by the EM fields of the counter-propagating beam, while the force from the own fields is negligible [208, 209]. In this approximation, the Lorentz force acting on a particle can be written in the following form

$$\mathbf{F} = q\mathbf{E} + (q/c)\,[\mathbf{v}\times\mathbf{B}] \simeq \pm m\omega_{\mathrm{b}}^2\mathbf{r}, \tag{4.1}$$

where $\mathbf{v}$ is the particle velocity, $\mathbf{E}$ and $\mathbf{B}$ are electric and magnetic fields of the counter-propagating beam, respectively, $q = \pm e$ is the particle charge, $\omega_{\mathrm{b}}^2 = 4\pi e^2 n_{\mathrm{b}}/m$ is the electron (positron) plasma frequency squared, n_{b} is the particle density of the counter-propagating beam, r is the particle distance from the beam axis. The positive sign in the equation (4.1) refers to the case of electron-electron or positron-positron collisions, when the resulting force causes defocusing of both beams. On the other hand, during electron-positron collisions, the beam particles perform transverse betatron oscillations with a frequency of $\omega_{\mathrm{b}}/\sqrt{\gamma}$ [123, 210], where γ is the Lorentz factor of a beam particle. In this case, the beam focusing time can be introduced as the time it takes for the particle to reach the beam axis, which is estimated up to a numerical factor as follows

$$T_D = \frac{\sqrt{2\gamma}}{\omega_{\mathrm{b}}}. \tag{4.2}$$

If the beam length σ_z satisfies the condition $\sigma_z/c > T_D$, then the beam radii change substantially during the interaction. Beam distortion in the interaction region can be quantified using the so-called *disruption parameter*, which is defined as follows

$$D_0 = \frac{\sigma_z^2}{c^2 T_D^2} = \frac{\omega_{\mathrm{b}}^2\sigma_z^2}{2\gamma c^2}, \tag{4.3}$$

for a beam with a uniform charge distribution of length σ_z and radius r_{b} [121]. Note that this expression gives a $\pi^{-1/2}2^{3/2} \approx 1.6$ times larger value than the disruption parameter for a beam with a Gaussian charge distribution having the same total charge, the root-mean-square length equal to σ_z and root-mean-square radius equal to r_{b} [121, 210]. The expression for D_0 can be generalized for other charge distributions and can also be used to characterize the interaction of beams of the same charge. Although a large value of the disruption parameter may be desirable to increase the brightness [211], at the same time it can lead to an increase in background noise and hinder precision measurements. For this reason, the condition $D_0 \ll 1$ is desirable for, e.g. the experimental study of nonperturbative QED [129].

Curvature of the particle trajectory at the interaction point is accompanied by synchrotron radiation, known in the community of collider physicists under the term *beamstrahlung* [125, 210]. The total power of losses due to photon emission depends on the QED parameter χ [32, 33, 135]

$$P_{\mathrm{rad}} = \frac{\alpha m^2 c^4}{3\sqrt{3}\pi\hbar} \int_0^\infty \frac{4u^3 + 5u^2 + 4u}{(1+u)^4} K_{2/3}\left(\frac{2u}{3\chi}\right) \mathrm{d}u, \tag{4.4}$$

$$\chi = \frac{\gamma}{E_S}\sqrt{(\mathbf{E} + \mathbf{v}\times\mathbf{B})^2 - (\mathbf{v}\cdot\mathbf{E})^2}, \tag{4.5}$$

where $\alpha = e^2/\hbar c$ is the fine structure constant, $\hbar$ is the Planck's constant, $E_S = m^2c^3/e\hbar$ is Sauter-Schwinger critical field [32], $K_\nu(z)$ is a modified Bessel function of the second kind [212]. In the classical ($\chi \ll 1$) and sufficiently quantum ($\chi \gg 1$) limits, the expression (4.4) can be reduced to simple power expressions

$$P_{\mathrm{rad}}(\chi \ll 1) \equiv P_C = \frac{2}{3}\frac{\alpha m^2 c^4}{\hbar}\chi^2, \tag{4.6}$$

$$P_{\mathrm{rad}}(\chi \gg 1) \equiv P_Q = 0.37\frac{\alpha m^2 c^4}{\hbar}\chi^{2/3}. \tag{4.7}$$

If the beam length is so small that during the interaction a particle emits only a few photons, then it is also necessary to take into account the quantum (i.e. stochastic) nature of synchrotron radiation even in the $\chi \ll 1$ limit.

In addition to beamstrahlung, other quantum effects are possible in the interaction region, such as the photoproduction of electron-positron pairs in strong electromagnetic fields, the trident process, etc. [127, 213]. Synergy between the emission of hard photons and the formation of pairs can lead to a very rapid increase of the total number of particles — an effect known as the QED cascade, which has attracted much attention lately (see Chapter 3). Thus, beamstrahlung and the formation of secondary particles as a result of QED processes can cause significant beam distortion due to energy depletion and, in general, play a negative role in the operation of the collider. Therefore, in the context of particle physics, colliders are usually designed to minimize these effects as much as possible. However, understanding the collective effects in the interaction region is critical not only for the optimal operation of the collider, but also in consideration of the experiments in strong-field physics. Thus, the regime of interaction of beams with strong beamstrahlung can be used, for example, to create bright sources of gamma radiation or to experimentally study QED [83, 130, 133]. Until now, analytical models of beam interactions have taken into account disruption and beamstrahlung independently of each other. In this section, we investigate the relationship between these two processes in order to find modified expressions for the disruption parameter that take into account radiation reaction in both the classical ($\chi \ll 1$) and quantum ($\chi \gg 1$) limits. The connection between these two processes is substantiated by the fact that beamstrahlung causes a loss of particle energy and, since the focusing time is proportional to $\sqrt{\gamma}$ (see equation (4.2)), leads to a decrease in the focusing time and, consequently, an increase of disruption parameter D. It is important to evaluate the strength of this effect not only qualitatively, but also quantitatively, regardless of whether the application of interest requires a small or large value of disruption parameter.

Further, the equations will be written in normalized quantities, where the plasma frequency (nonrelativistic) corresponding to the initial maximum density of beam particles ω_b is chosen as the normalization frequency. In this case, time is normalized to $1/\omega_b$, coordinates — to c/ω_b, momentum — to mc, EM fields — to $mc\omega_b/e$.

4.2.1 Formulation of the problem

Let us write the motion equations of ultra-relativistic particles taking into account radiation reaction

$$\frac{d\mathbf{p}}{d\tau} = -\mathbf{E} - \frac{\mathbf{p}}{\gamma} \times \mathbf{B} - P(\chi)\,\frac{\mathbf{p}}{\gamma}, \tag{4.8}$$

$$\frac{d\mathbf{r}}{d\tau} = \frac{\mathbf{p}}{\gamma}, \tag{4.9}$$

where P refers to the total radiation power in normalized units. These equations describe the classical motion of an electron in an electromagnetic field, taking into account the effect of radiation reaction in the semiclassical approximation (with QED corrections that reduce the total radiation power at large values of χ) (see section 2.1). Although the stochastic nature of the radiation causes individual particles to focus differently, the disruption effect applies to the beam as a whole and therefore must be calculated by averaging the distance from the axis over all particles. Such averaging even in the quantum regime essentially leads to the motion equations in the semiclassical approximation. It will be shown below that the results of QED-PIC simulations, in which the beam collision is modeled in a self-consistent way, taking into account the stochastic nature of quantum processes, agree quite well with the results of our analytical model, which also justifies the application of this approach.

For an analytical study of the effect of disruption in a head-on collision of electron and positron beams, we make additional assumptions. First, as mentioned in section 4.1, the self-force generated by the ultrarelativistic beam can be neglected in the equation (4.8), since it is proportional to the small value of γ^{-2} [208, 209]. Secondly, it is sufficient to study the transverse dynamics of particles located in the beam front, since they begin to experience the force from the counter-propagating beam earlier than others. And third, we further restrict our analysis to the particles at the periphery of the beam, that is, particles that experience the largest force and are therefore more likely to emit photons. Since radiation leads to a decrease in energy and, consequently, a decrease in the inertia of the particles, it is expected that it is the particles at the periphery and front of the beams that will experience the greatest focusing. The analysis of the motion of such particles is greatly simplified due to the fact that only the unperturbed part of the counter-propagating beam affects their dynamics. Finally, we assume that the electron and positron beams have the same initial parameters, in which case the beams develop symmetrically. In addition, beams are considered to have cylindrical symmetry. In this case, the beam density distribution can be written as $n(\xi_\pm, r) = n_0\eta_z(\xi_\pm)\eta_r(r)$, where n_0 is the maximum density of the beam, $\xi_\pm = z \pm \tau$ describes the longitudinal coordinate for beams moving at the speed of light, and the functions $\eta_{r,z}$ $(0 \le \eta_{r,z} \le 1)$ determine the density distribution profile. The electric field created by such a beam is mainly transverse and can be found using the Gauss's law in the reference frame co-moving with the beam and the subsequent Lorentz transformation to the laboratory reference frame

$$E_r = \frac{\eta_z(\xi_\pm)}{r} \int\limits_0^r \eta_r(r')r'\mathrm{d}r' = \frac{r_\mathrm{b}\eta_z(\xi_\pm)}{2}\,\mathcal{E}(\rho), \tag{4.10}$$

$$\mathcal{E}(\rho) \equiv \frac{2}{\rho} \int\limits_0^\rho \eta_r(r_\mathrm{b}\rho')\rho'\mathrm{d}\rho', \tag{4.11}$$

where $\rho = r/r_\mathrm{b}$ is the transverse coordinate, measured in units of the distance r_b, at which the electric field reaches its maximum. For electrons with $v_z = \text{const} = c$ we get $\xi_+ = 2\tau$. Given the above assumptions and redefining $\eta(\tau) \equiv \eta_z(2\tau)$, the motion equations are rewritten as follows

$$\frac{d^2\rho}{d\tau^2} = -\frac{\mathcal{E}(\rho)}{\gamma}\,\eta(\tau), \tag{4.12}$$

$$\frac{d\gamma}{d\tau} = -P(\chi), \tag{4.13}$$

$$\chi = \gamma\,\frac{\mathcal{E}(\rho)}{a_\mathrm{S}}\,r_\mathrm{b}\eta(\tau). \tag{4.14}$$

Here $a_\mathrm{S} = eE_\mathrm{S}/mc\omega_\mathrm{b} = mc^2/\hbar\omega_\mathrm{b}$ is the normalized Sauter-Schwinger field. When deriving these equations, it was assumed that the electric and magnetic components of the Lorentz force acting on the particle are almost equal to each other (hence the factor 1/2 in the equation (4.10) disappears), which is true if $v_z \simeq c \gg v_r$ and $\gamma \gg 1$. This also suggests that the radiation friction force acts predominantly along the z axis. Thus, it is not explicitly present in the equation for the transverse coordinate ρ. As mentioned above, we will be interested in particles experiencing the largest fields, i.e. particles which initial displacement r_0 from the beam axis is r_b and, therefore, $\rho_0 \equiv \rho(\tau = 0) = 1$.

Before solving the equations (4.12)–(4.13) it is useful to estimate the characteristic time scales present in the problem, namely, the time scale of the change in the electron trajectory τ_{D_0} and the time scale of energy losses due to radiation τ_BS which are defined as follows

$$\tau_{D_0} = \sqrt{2\gamma_0}, \tag{4.15}$$

$$\tau_\mathrm{BS} = \frac{\gamma_0}{P(\chi_0)}, \tag{4.16}$$

where $\chi_0 = r_\mathrm{b}\gamma_0\mathcal{E}(\rho_0)/a_\mathrm{S}$ and $\gamma_0 = \gamma(\tau = 0)$ are the initial values of the parameter χ and the Lorentz factor of the particles, respectively. We also introduce the parameter $\varkappa$ as follows

$$\varkappa = \frac{\tau_{D_0}}{\tau_\mathrm{BS}} = \sqrt{\frac{2}{\gamma_0}}P(\chi_0). \tag{4.17}$$

This parameter determines the regime of the collision. In the case of $\varkappa \gg 1$, considered in section 4.2.2, significant energy losses due to radiation occur on a timescale much shorter than the time required for the particle to reach the beam axis. In the opposite limit $\varkappa \ll 1$, considered in section 4.2.3, the beam energy changes significantly over a large number of betatron periods.

Using the relationship between γ_0 and χ_0 and given that $P(\chi) \equiv \alpha a_S \varphi(\chi)$, the $\varkappa$ parameter can also be expressed as follows

$$\varkappa = \alpha\sqrt{2r_b a_S}\,\frac{\varphi(\chi_0)}{\sqrt{\chi_0}}. \tag{4.18}$$

This shows that the effect of beamstrahlung is determined by two initial parameters of the interaction: the absolute value of the beam radius r_b[1] and the parameter χ_0. It will be shown below that these two parameters are sufficient to calculate the relative change in the disruption parameter caused by radiation. In classic and quantum regimes, definition (4.18) can be rewritten as follows

$$\varkappa \approx \alpha\sqrt{2r_b a_S} \times \begin{cases} 0.67\chi_0^{3/2}, & \chi_0 \ll 1, \\ 0.37\chi_0^{1/6}, & \chi_0 \gg 1. \end{cases} \tag{4.19}$$

4.2.2 Radiation-dominated regime

Constant force approximation

It is not possible to obtain a solution of the equations (4.12)–(4.13) in an explicit analytical form, therefore, first we will make some analytical estimates, resorting to the constant force approximation, which corresponds to the substitution of the coordinate ρ in the rhs of the equation (4.12) with its initial value $\rho_0 = 1$. In this case, the equations (4.12)–(4.13) become

$$\frac{d^2\rho}{d\tau^2} = -\frac{\mathcal{E}(\rho_0)}{\gamma}\eta(\tau), \tag{4.20}$$

$$\frac{d\gamma}{d\tau} = -P(\chi), \tag{4.21}$$

$$\chi = \chi_0\frac{\gamma}{\gamma_0}\eta(\tau). \tag{4.22}$$

According to the equations (4.6)–(4.7) both in the classical ($\chi \ll 1$) and quantum ($\chi \gg 1$) limits, the function P can be approximated as power function of χ

$$P(\chi) = \begin{cases} P_C(\chi) \approx 0.67\alpha a_S\chi^2, & \chi \ll 1, \\ P_Q(\chi) \approx 0.37\alpha a_S\chi^{2/3}, & \chi \gg 1. \end{cases} \tag{4.23}$$

[1]In dimensional terms, the product $r_b a_S$ is equal to the ratio of the beam radius to the Compton wavelength.

In this case, we can get the solution in quadratures

$$\gamma = \gamma_0 \left(1 - \frac{P_0(1-\nu)}{\gamma_0} \int\limits_0^{\tau} \eta^{\nu}(\tau')\mathrm{d}\tau' \right)^{\frac{1}{1-\nu}}, \tag{4.24}$$

$$\rho(\tau) = \rho_0 + \dot{\rho}_0 \tau - \mathscr{E}(\rho_0) \int\limits_0^{\tau} \mathrm{d}\tau' \int\limits_0^{\tau'} \frac{\eta(\tau'')}{\gamma(\tau'')} \mathrm{d}\tau'', \tag{4.25}$$

where $\nu = 2$ for the classical regime and $\nu = 2/3$ for the quantum regime, $P_0 = P(\chi_0)$, $\dot{\rho}_0 = \dot{\rho}(\tau = 0)$. Let us analyze the obtained solution for the homogeneous beam $\eta_z = \eta_r = \eta = 1$, for which $\mathscr{E}(\rho) = \rho$. In this case, all the integrals can be calculated explicitly. In particular, the solutions for γ and ρ have the following form

$$\gamma(\tau) = \gamma_0 \times \begin{cases} \left(1 + \varkappa \dfrac{\tau}{\tau_{D_0}}\right)^{-1}, & \chi \ll 1, \\ \left(1 - \dfrac{\varkappa}{3} \dfrac{\tau}{\tau_{D_0}}\right)^{3}, & \chi \gg 1, \end{cases} \tag{4.26}$$

$$\rho(\tau) = 1 - \frac{\tau^2}{\tau_{D_0}^2} \times \begin{cases} 1 + \dfrac{\varkappa}{3} \dfrac{\tau}{\tau_{D_0}}, & \chi \ll 1, \\ \left(1 - \dfrac{\varkappa}{3} \dfrac{\tau}{\tau_{D_0}}\right)^{-1}, & \chi \gg 1, \end{cases} \tag{4.27}$$

where $\dot{\rho}_0 = 0$ is assumed.

It is interesting to note that at the beginning of the interaction ($0 < \tau \ll \tau_{D_0}$) the dependence of the electron energy on time is the same for both the classical and quantum regimes

$$\gamma(\tau) \approx \gamma_0 \left(1 - \varkappa \frac{\tau}{\tau_{D_0}}\right). \tag{4.28}$$

If we introduce the time τ_γ after which the electron energy is halved due to radiation, then this time in the classical limit is about 1.6 times less than in the QED limit

$$\tau_\gamma(\chi \ll 1) = \tau_{\mathrm{BS}}, \tag{4.29}$$

$$\tau_\gamma(\chi \gg 1) = 3\left(1 - 2^{-1/3}\right)\tau_{\mathrm{BS}}. \tag{4.30}$$

This is an expected result, since the radiation losses according to the classical expression are greater than according to the quantum one. This fact shows that the collision of beams in the quantum regime can be preferable if it is necessary to reduce energy losses due to radiation [214].

The focusing time can be found from the condition $\rho(\tau = \tau_D) = 0$. Utilizing that $D \propto \tau_D^{-2}$, the expression for the disruption parameter with account of radiation reaction can be written in the

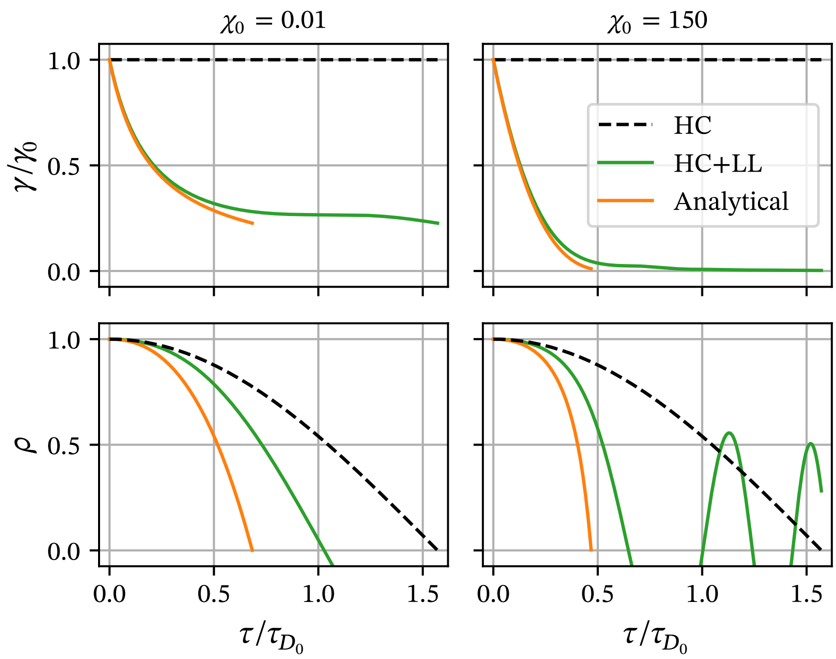

Figure 4.1: Comparison of an approximate solution (4.26)–(4.27) (orange line) with numerical solution of equations (4.12)–(4.13) (green line) (see Appendix A) with $\varkappa_0 = 5$. For the left column $\chi_0 = 0.01$, for the right one — $\chi_0 = 150$. The black dashed line corresponds to the solution of the equation (4.12) with constant particle energy γ.

following form

$$D \approx D_0 \begin{cases} (\varkappa/3)^{2/3}, & \chi \ll 1, \\ (\varkappa/3)^2, & \chi \gg 1. \end{cases} \tag{4.31}$$

By virtue of the equation (4.18), we can rewrite the equation (4.3) in the variables r_b and χ_0 as follows

$$D \approx D_0 \begin{cases} 2.4\sqrt[3]{r_b[\mu\text{m}]}\, \chi_0, & \chi \ll 1, \\ 4.2\, r_b[\mu\text{m}]\, \chi_0^{1/3}, & \chi \gg 1. \end{cases} \tag{4.32}$$

Fig. 4.1 shows that, although both solutions in the quantum and classical regimes describe energy losses quite well, the particle trajectory according to this solution differs quite strongly from the real trajectory, which overestimates the disruption parameter, so this simple model can only serve for rough estimates of the disruption parameter, which may be sufficient in cases where only its order of magnitude is of interest.

Corrections to the model

The accuracy of the analytical model can be significantly improved by two changes. First, we will use the average transverse coordinate of the particle μ in the rhs of the equation (4.12) instead of its initial value ρ_0,

$$\frac{d^2\rho}{d\tau^2} = -\frac{\mu}{\gamma}, \tag{4.33}$$

$$\frac{d\gamma}{d\tau} = -P\left(\mu\chi_0\frac{\gamma}{\gamma_0}\right), \tag{4.34}$$

$$\mu \equiv \frac{1}{\tau_D}\int_0^{\tau_D} \rho\left(\tau'\right) \mathrm{d}\tau' < 1. \tag{4.35}$$

Second, we «stich» solutions in quantum and classical regimes at the time instance τ_1, at which the particle parameter χ reaches a certain threshold value $\chi_1 \sim 1$, if its initial value was sufficiently large, i.e. $\chi_0 > \chi_1$. Then for $\tau < \tau_1$ the motion equations have the following solution

$$\gamma_Q(\tau) = \gamma_0\left(1 - \tilde{\varkappa}_0\frac{\tau}{\tau_{D_0}}\right)^3, \tag{4.36}$$

$$\rho_Q(\tau) = 1 - \frac{\tau^2}{\tau_{D_0}^2}\left(1 - \tilde{\varkappa}_0\frac{\tau}{\tau_{D_0}}\right)^{-1}, \tag{4.37}$$

$$\tilde{\varkappa}_0 = \sqrt{\frac{2}{9\gamma_0\mu}P_Q(\mu\chi_0)}. \tag{4.38}$$

Note that the variable $\tilde{\varkappa}_0$ (and also $\tilde{\varkappa}_1$ below) includes an additional factor 1/3 compared to the $\varkappa$ definition in equation (4.17), which slightly shortens the following expressions. Time τ_1 is found from the condition

$$\chi = \chi_0\frac{\gamma_Q(\tau_1)\rho_Q(\tau_1)}{\gamma_0} \equiv \chi_0\frac{\gamma_1\rho_1}{\gamma_0} = \chi_1. \tag{4.39}$$

To find an approximate solution to this equation, consider the following auxiliary equation for x

$$k_1 = \left(1 - \frac{x^2}{1-k_2x}\right)(1-k_2x)^3. \tag{4.40}$$

Since both factors in the rhs decrease as x increases, it is obvious that $x < x_{1,2}$, where $x_{1,2}$ satisfy the following equations

$$k_1 = (1-k_2x_1)^3, \tag{4.41}$$

$$k_1 = 1 - \frac{x_2^2}{1-k_2x_2}. \tag{4.42}$$

These equations have the following solutions

$$x_1 = \frac{1-\sqrt[3]{k_1}}{k_2}, \tag{4.43}$$

$$x_2 = \frac{k_2(1-k_1)}{2}\left(\sqrt{1 + \frac{4}{k_2^2(1-k_1)}} - 1\right). \tag{4.44}$$

Thus, the approximate solution of the equation (4.40) can be found as $x = \min\{x_1, x_2\}$. Finally, τ_1 is found by performing a substitution

$$x \to \frac{\tau_1}{\tau_{D_0}},\ k_1 \to \frac{\chi_1}{\chi_0} = \zeta,\ k_2 \to \tilde{\varkappa}_0. \tag{4.45}$$

From the equation (4.39), the ratio γ_1/γ_0 can be found as follows

$$\frac{\gamma_1}{\gamma_0} = \frac{\chi_1}{\chi_0}\frac{1}{\rho_1} \equiv \frac{\zeta}{\rho_1}, \tag{4.46}$$

where we introduced $\zeta = \chi_1/\chi_0$.

For $\tau > \tau_1$, by definition, it is necessary to use the classical formulas for the radiation power, so that the solution of the motion equations has the form

$$\gamma_C(\tau) = \gamma_1\left(1 + 3\tilde{\varkappa}_1\frac{\tau - \tau_1}{\tau_{D_1}}\right)^{-1}, \tag{4.47}$$

$$\rho_C(\tau) = \rho_1 + \dot{\rho}_1\frac{\tau - \tau_1}{\tau_{D_1}} - \frac{(\tau - \tau_1)^2}{\tau_{D_1}^2}\left(1 + \tilde{\varkappa}_1\frac{\tau - \tau_1}{\tau_{D_1}}\right), \tag{4.48}$$

where

$$\tau_{D_1} = \sqrt{2\gamma_1}, \tag{4.49}$$

$$\tilde{\varkappa}_1 = \sqrt{\frac{2}{9\gamma_1\mu}P_C(\mu\chi_1)}, \tag{4.50}$$

$$\dot{\rho}_1 = \tau_{D_1}\dot{\rho}_Q(\tau = \tau_1) = -\sqrt{\frac{\zeta}{\rho_1}\frac{\tau_1}{\tau_{D_0}}}\frac{2 - \tilde{\varkappa}_0\frac{\tau_1}{\tau_{D_0}}}{\left(1 - \tilde{\varkappa}_0\frac{\tau_1}{\tau_{D_0}}\right)^2}. \tag{4.51}$$

The focusing time can be calculated from the equation $\rho_C(\tau_D) = 0$, which has an explicit but too cumbersome solution. Let us find an approximate solution of this equation. To do this, consider another auxiliary equation for x

$$0 = k_1 + k_2 x - x^2\left(1 + k_3 x\right). \tag{4.52}$$

For large values of k_3, the solutions of this equation can be roughly estimated as follows

$$x_1 = \sqrt[3]{\frac{k_1}{k_3}}. \tag{4.53}$$

For smaller values of k_3, we can first find a solution by setting $k_3 = 0$, i.e.

$$0 = k_1 + k_2 x' - x'^2. \tag{4.54}$$

The above equation has a solution

$$x' = \frac{k_2}{2} + \sqrt{k_1 + \frac{k_2^2}{4}}. \tag{4.55}$$

Assuming that the solution of (4.52) is only slightly different from x', i.e. $x = x' + x''$, we can expand this equation in x'' and leave only linear terms

$$k_2 x'' + 2x''x'(1 + k_3 x') - k_3 x'^3 = 0. \tag{4.56}$$

From here we get that x can be approximately calculated as follows

$$x_2 = x' - \frac{k_3 x'^3}{k_2 + 2x'(1 + k_3 x')}. \tag{4.57}$$

Finally, the smallest of $x_{1,2}$ is chosen, i.e. $x = \min\{x_1, x_2\}$. To find τ_2, we perform the following substitution

$$x \to \frac{\tau_2}{\tau_{D_1}},\ k_1 \to \rho_1,\ k_2 \to \dot{\rho}_1,\ k_3 \to \tilde{\varkappa}_1. \tag{4.58}$$

Thus,

$$\frac{\tau_D}{\tau_{D_0}} = \tau_1 + \tau_2\sqrt{\frac{\zeta}{\rho_1}}, \tag{4.59}$$

$$\tau_1 = \min\left\{\frac{1 - \zeta^{1/3}}{\tilde{\varkappa}_0}\frac{\tilde{\varkappa}_0 (1 - \zeta)}{2}\left(\sqrt{1 + \frac{4}{\tilde{\varkappa}_0^2 (1 - \zeta)}} - 1\right)\right\}, \tag{4.60}$$

$$\tau_2 = \min\left\{\sqrt[3]{\frac{\rho_1}{\tilde{\varkappa}_1}}, \tau' - \frac{\tilde{\varkappa}_1 \tau'^3}{\dot{\rho}_1 + 2\tau' (1 + \tilde{\varkappa}_1 \tau')}\right\}, \tag{4.61}$$

$$\tau' = \sqrt{\rho_1 + \frac{\dot{\rho}_1^2}{4}} - \frac{\dot{\rho}_1}{2}. \tag{4.62}$$

In the case of $\chi_0 < \chi_1$, $\tau_1 \equiv 0$ and χ_1 must be replaced by χ_0 in expression for τ_2.

Analogously to the equation (4.18), the parameter that determines the significance of radiation can be expressed as follows

$$\tilde{\varkappa} = \alpha\sqrt{\frac{2}{9} r_b a_S} \times \begin{cases} (\mu\chi_0)^{2/3}, & \chi_0 < \chi_1, \\ (\mu\chi_0)^{1/6}, & \chi_0 > \chi_1, \end{cases} \tag{4.63}$$

and it is easy to show that $\tilde{\varkappa}_1$ can be expressed in terms of $\tilde{\varkappa}$. Thus, the disruption parameter with account of radiation reaction in the corrected model, is equal to

$$D = D_0 \left(\frac{\tau_{D_0}}{\tau_D}\right)^2. \tag{4.64}$$

The figure 4.2 shows that calculating the disruption parameter using this corrected model is significantly superior to using simple limit expressions (4.31). Note that although μ should be self-

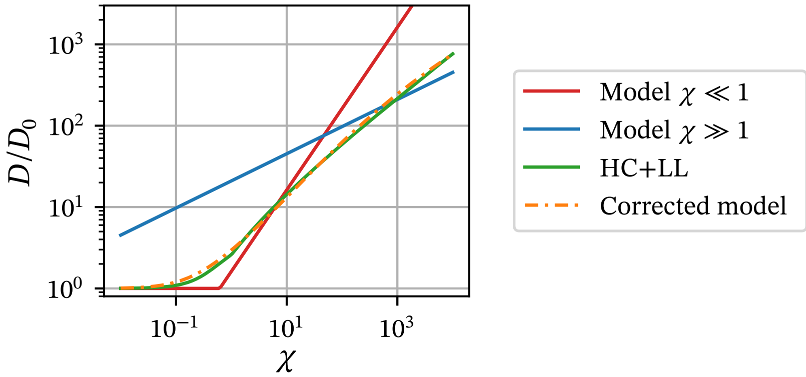

Figure 4.2: Comparison of the D/D_0 ratio calculated using the limit expression (4.31) (red line corresponds to the classical limit, blue — to the quantum), the corrected model (orange dash-dotted line) and from numerically solving the motion equations (4.12)–(4.13) (green line) (see Appendix A), as a function of χ for a fixed value $r_\mathrm{b} = 10\,\mu\mathrm{m}$.

consistently calculated from the solution obtained above, numerical analysis shows that the value of μ is close to 0.5. Thus, to find an analytical solution, we treat μ as a free parameter, which we set to 0.5. This is also confirmed by the fact that the variation of μ in the range 0.3–0.7 does not lead to a significant change in the final value of the disruption parameter. According to the equations (4.60)–(4.61), the ratio D/D_0 can be expressed as a function of only two initial parameters: the beam radius r_b and χ_0 values. This fact allows us to perform a parameter scan in a reasonable time using a full-scale 3D QED-PIC simulation and calculate the value of D/D_0 based on the results of such simulation (see Sec. 4.2.4).

4.2.3 Interaction of long beams

This section discusses the interaction of long uniform beams of oppositely charged particles when the number of betatron oscillations is large $\sigma_z/c\tau_{D_0} \gg 1$ and radiation losses are insignificant during a single period, which corresponds to the limit $\varkappa \ll 1$. Such a configuration may correspond to the interaction of beams with significantly different energy densities in the center-of-mass reference frame, which may arise due to the greater mass, Lorentz factor, or particle density of one beam compared to another in the laboratory reference frame. A characteristic example of such a scenario is the collision of electron and proton beams. In this case, the characteristic time scale of the evolution of a more energetic beam is much larger than that of the colliding beam; therefore, all particles of the colliding beam experience an almost unperturbed field, in contrast to the case considered in the previous section, when this statement is true only for particles at the beam front. For simplicity, we consider the interaction of homogeneous beams $\eta_z = \eta_r = \eta = 1$, for which $\mathscr{E}(\rho) = \rho$. In that case, it is convenient to introduce the following variables

$$a^2 = \rho^2 + \gamma\left(\frac{\mathrm{d}\rho}{\mathrm{d}\tau}\right)^2, \tag{4.65}$$

$$\varphi = \arctan\left(\frac{\mathrm{d}\rho}{\mathrm{d}\tau}\frac{\sqrt{\gamma}}{\rho}\right), \tag{4.66}$$

where a and φ are the amplitude and phase of betatron oscillations ($\rho = a\cos\varphi$), respectively. In the new variables, the equation (4.21) becomes

$$\frac{\mathrm{d}a}{\mathrm{d}\tau} = -\frac{a}{2\gamma}\sin^2\varphi\, P\left(\frac{\chi_0}{\gamma_0}a\gamma|\cos\varphi|\right). \tag{4.67}$$

To calculate the slowly varying amplitude of betatron oscillations, $A = \langle a\rangle$, we average the equation (4.67) over φ and neglect the fast components of the amplitude a and the energy γ

$$\frac{\mathrm{d}A}{\mathrm{d}\tau} = -\frac{A}{2\overline{\gamma}}f_1\left(\frac{\chi_0}{\gamma_0}A\overline{\gamma}\right), \tag{4.68}$$

$$\frac{\mathrm{d}\overline{\gamma}}{\mathrm{d}\tau} = -f_2\left(\frac{\chi_0}{\gamma_0}A\overline{\gamma}\right), \tag{4.69}$$

where

$$f_1(v) = \frac{1}{2\pi}\int_0^{2\pi}\sin^2\varphi\, P\left(v|\cos\varphi|\right)\mathrm{d}\varphi, \tag{4.70}$$

$$f_2(v) = \frac{1}{2\pi}\int_0^{2\pi} P\left(v|\cos\varphi|\right)\mathrm{d}\varphi, \tag{4.71}$$

and $\overline{\gamma} = \langle\gamma\rangle$. Introducing $\overline{\chi} = \langle\chi\rangle = \chi_0 A\overline{\gamma}/\gamma_0$, we obtain a system describing the electron dynamics averaged over betatron oscillations

$$\frac{d\overline{\chi}}{d\tau} = -\frac{\overline{\chi}}{2\overline{\gamma}}\left[f_1\left(\overline{\chi}\right) + 2f_2\left(\overline{\chi}\right)\right], \tag{4.72}$$

$$\frac{d\overline{\gamma}}{d\tau} = -f_2\left(\overline{\chi}\right). \tag{4.73}$$

This system has the following constant of motion

$$\ln\overline{\gamma} - \mathrm{g}(\overline{\chi}) = \mathrm{const}, \tag{4.74}$$

$$\mathrm{g}(v) = \int\frac{2f_2(v)\mathrm{d}v}{vf_1\left(v\right) + 2vf_2\left(v\right)}. \tag{4.75}$$

In the classical limit ($\chi \ll 1$) we have $f_2(v) = 4f_1(v) = P_C(v)/2$ and the constant of motion takes form

$$\overline{\gamma}^{-9/8}\overline{\chi} = \mathrm{const}. \tag{4.76}$$

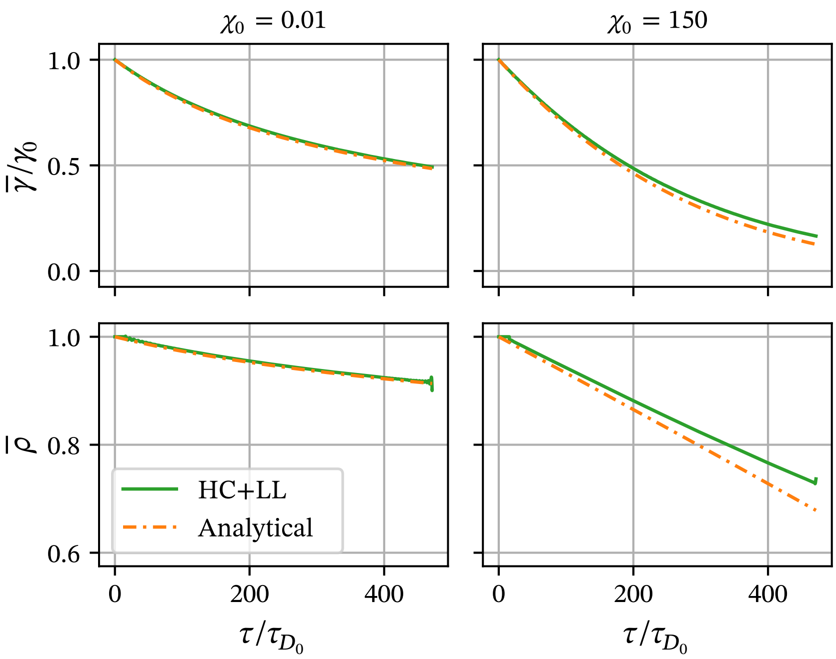

Figure 4.3: Comparison of the analytical solution (4.77)–(4.78) and (4.82)–(4.83) (orange dashed dotted line) and numerical solution of equations (4.12)–(4.13) (green line) (see Appendix A) with $\varkappa_0$ =0.005. In the left column $\chi_0 = 0.01$, in the right one $\chi_0 = 150$.

It follows from Eqs. (4.73) and (4.76) that

$$\overline{\gamma} = \gamma_0 S(\tau)^{-4/5}, \tag{4.77}$$

$$\overline{\rho} = \rho_0 S(\tau)^{-1/10}, \tag{4.78}$$

$$S(\tau) = 1 + \frac{5}{8}\left(\varkappa \frac{\tau}{\tau_{D_0}}\right). \tag{4.79}$$

In a quantum limit ($\chi \gg 1$) we have

$$f_2(v) = \frac{8}{3} f_1(v) = \frac{\Gamma(5/6)}{\Gamma(4/3)\sqrt{\pi}} P_Q(v), \tag{4.80}$$

and constant of motion takes form

$$\overline{\gamma}^{-19/16}\overline{\chi} = \text{const.} \tag{4.81}$$

Eqs. (4.73) and (4.81) have the following solutions

$$\overline{\gamma} = \gamma_0 S(\tau)^{24/5}, \tag{4.82}$$

$$\overline{\rho} = \rho_0 S(\tau)^{9/5}, \tag{4.83}$$

$$S(\tau) = 1 - \frac{5}{24\sqrt{\pi}} \frac{\Gamma(5/6)}{\Gamma(4/3)} \left(\varkappa \frac{\tau}{\tau_{D_0}}\right) \approx 1 - 0.149 \left(\varkappa \frac{\tau}{\tau_{D_0}}\right). \tag{4.84}$$

The figure 4.3 demonstrates good agreement between the numerical solution of the equations (4.12)–(4.14) and the analytical solution (4.77) and (4.82).

4.2.4 QED-PIC simulations

To confirm the predictions of the model developed in section 4.2.2, a full-scale three-dimensional QED-PIC simulations were performed using the code QUILL [201], which simulates QED processes taking into account their stochasticity via the Monte-Carlo method. Taking z as the beam propagation axis, the simulation parameters were $\Delta t = 0.6\Delta z$, $\Delta x = \Delta y = 2.5\Delta z$, $\Delta z = r_\mathrm{b}/20$. For all simulations performed, the time step Δt was much less than the average delay between successive QED processes (gamma quanta emission or electron-positron pair production). For the numerical solution of the Maxwell equations, a hybrid FDTD scheme was used, which is described in detail in section 4.4.1. Simulations were also performed using the VLPL [215–217] code in combination with a dispersionless scheme for solving the Maxwell equations — Rhombi in Plane (RIP) [218]. Differences between simulation results using two different codes were insignificant. Figure 4.4, which shows an example of simulation results, shows that at $\chi_0 = 10$ (see Figure 4.4 (c)) abundant production of secondary electrons and positrons occurs. Since this process does not affect the motion of beam particles at the front, the formation and development of such a cascade is not discussed in detail. We also note the development of the transverse kink instability in simulations taking into account QED processes, which will be described below.

We carried out a series of simulations with different values of the initial beam radius r_b and the value of χ_0. The beam length was chosen in such a way that for each simulation the disruption parameter without taking into account radiation reaction, i.e. D_0, was equal to 10. This was done in order to have a clear way to determine the focus time used in the calculation of the disruption parameter. In this regard, our QED-PIC simulations do not correspond to any specific experiment, which is possible, for example, at the FACET-II facility, since the latter requires a very short interaction time to suppress radiation losses [129]. Instead, QED-PIC simulation was used as a means to solve the equations of particle motion in a self-consistently calculated electromagnetic field and taking into account the stochastic nature of QED processes. For each simulation, we tracked several hundred particles located at the front and periphery of the electron beam, using their trajectories to calculate the average time of crossing the beam axis. Examples of such trajectories, numerical solution of equations (4.12)–(4.13) and approximate analytical solution are shown in Fig. 4.5. For each pair of r_b and χ_0 values, two simulations were carried out: with and without account of QED processes. Comparing the average focusing time in these two simulations, the ratio D/D_0 was calculated over a wide range of initial parameters, which is shown in Fig. 4.6 along with an estimate from the equations (4.59)–(4.61) (in which the free parameters $\mu = 0.5$, $\chi_1 = 1$ were used) and the result of the numerical solution of single-particle motion equations (4.12)–(4.13).

It is important to note that for large values of r_b and χ_0 (the area marked with a red frame in Fig. 4.6), an alternative criterion was used to calculate the disruption parameter. This is due to the fact that at such parameters, the energy losses due to radiation are so large that after some time the beam particles cease to be relativistic, and their longitudinal velocity becomes comparable with their

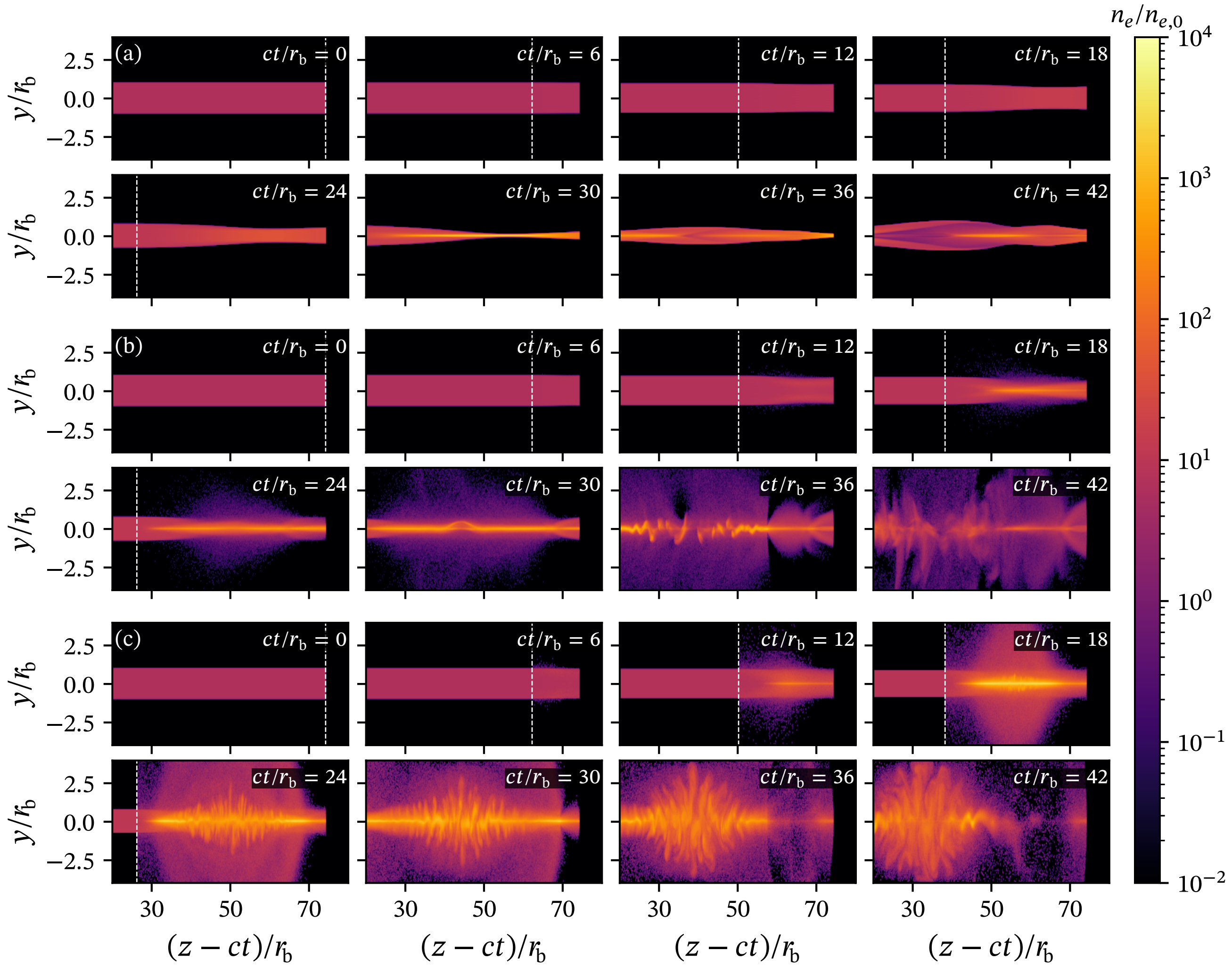

Figure 4.4: Electron density distribution at different time points in PIC simulations (a) without radiation reaction, and (b, c) with radiation reaction. The initial beam parameters are (b) $r = 10\,\mu$m, $\chi = 1$ (c) $r = 1\,\mu$m, $\chi = 10$. The density and duration of the beams correspond to the value of the disruption parameter D_0 equal to 10. The white dashed line corresponds to the position of the front of the counter-propagating positron beam.

transverse velocity, so that eventually the particles stop their directed motion and begin to rotate without crossing the beam axis. In such cases, to calculate the disruption parameter, instead of the time at which the particle reaches the beam axis, we used the time at which the longitudinal velocity of the particle reached $0.5c$. Since our analytical model assumes that the longitudinal velocity is always greater than the transverse velocity, it cannot be applied in these cases.

As mentioned above, our analytical model predicts that the ratio D/D_0 does not explicitly depend on the particle energy. To confirm this, we performed several QED-PIC simulations with different initial particle energies, but with the same values of χ_0 and r_b. The simulation results show that as long as the particle energy is high enough for the particles to remain ultrarelativistic until reaching the beam axis, the resulting ratio D/D_0 is independent of the particle energy.

Comparison of the predictions of the beam interaction model in the weak beamstrahlung limit ($\varkappa \ll 1$) with the results of QED-PIC simulation is not presented in this section, because this regime is largely associated with the interaction of beams with significantly different energy densities (in

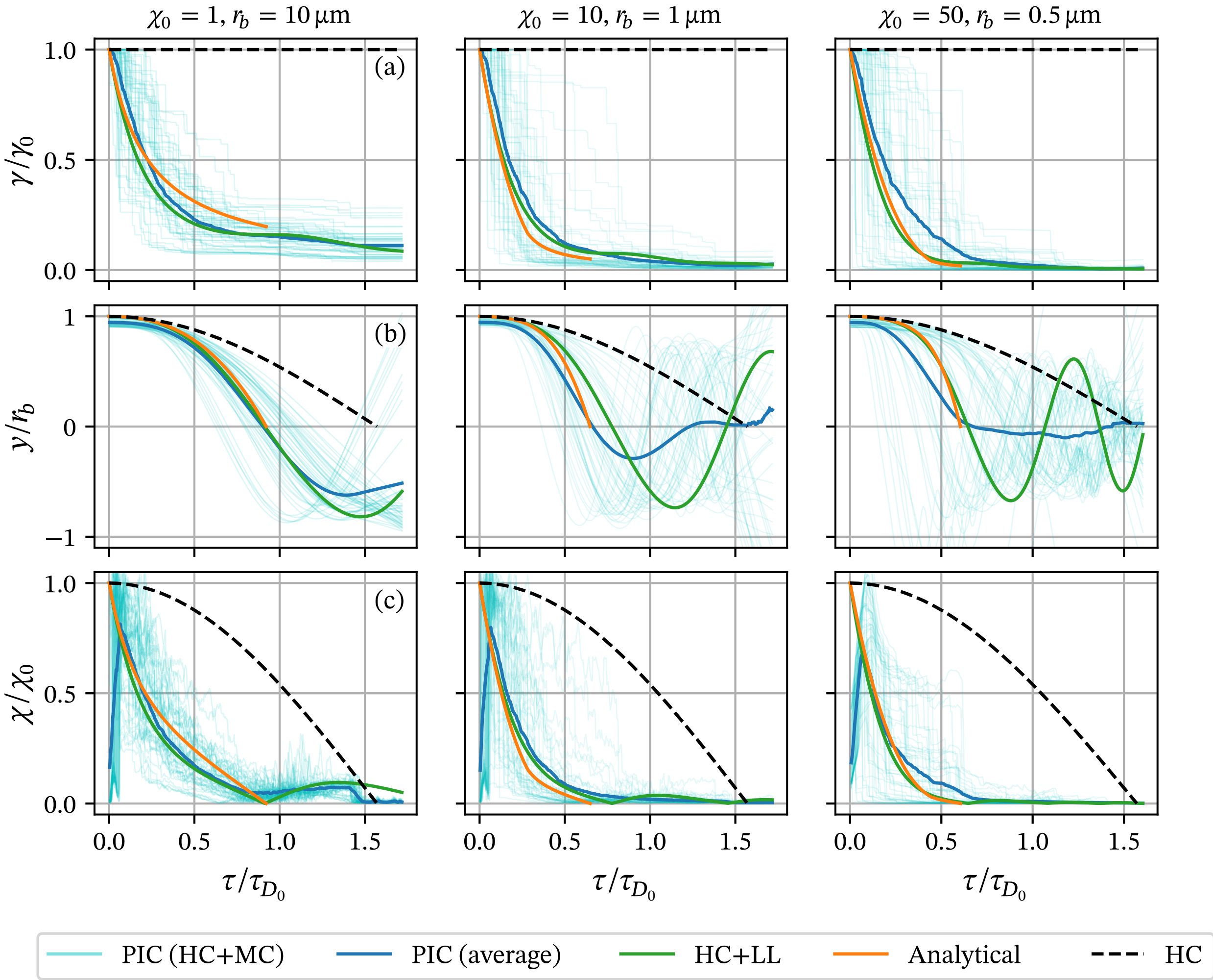

Figure 4.5: Dynamics of electrons in the field of a counter-propagating positron beam. (a) Electron energy, (b) displacement from the beam axis, and (c) value of the parameter χ as functions of time. The thin blue lines correspond to the trajectories of individual particles in the QED-PIC simulation, the solid blue line — to the values averaged over these particles, the green line — to the numerical solution of equations (4.12)–(4.13) (see Appendix A), orange line — to the analytic solution (4.36)–(4.37), (4.47)–(4.48), black dashed line — to the solution of the equation (4.12) without beamstrahlung taken into account, i.e. with constant energy γ. Different columns correspond to different initial parameters r_b and χ_0.

the center-of-mass system), in which the more energetic of them is practically not deformed, so this interaction can be quite accurately described by considering dynamics of a single particle in an unperturbed field. Nevertheless, in section 4.3 it will be shown that this model can be applied practically without changes to the problem of the interaction of a high-current beam of ultrarelativistic particles with plasma target. Comparison of the predictions of this model with the results of QED-PIC simulations is also presented in that section.

4.2.5 Discussion

The scheme discussed in the publication [129] for observing the effects of nonperturbative QED using a head-on collision of electron and positron beams requires collision with a very small disruption

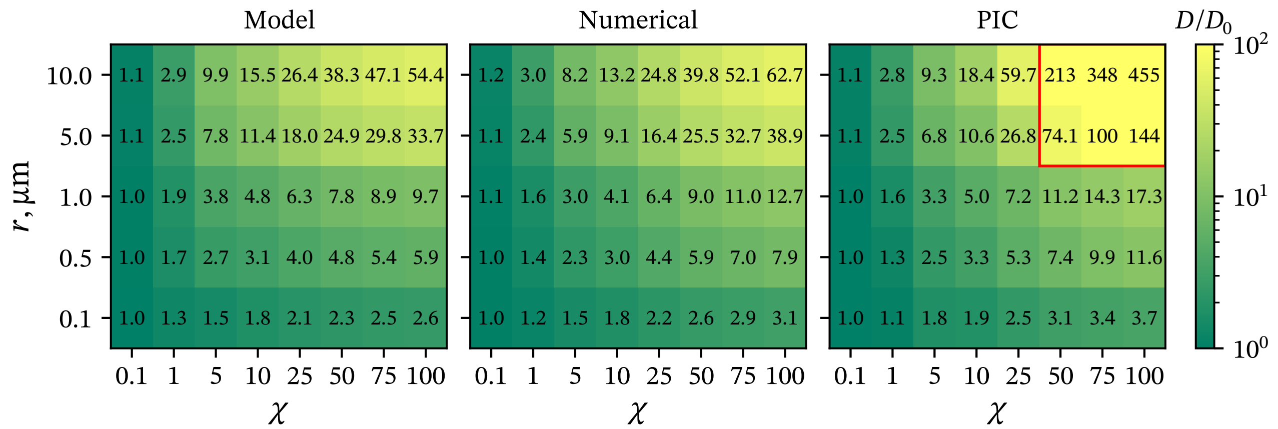

Figure 4.6: Ratio D/D_0 calculated (left column) from analytical solution (4.59)–(4.60), (middle column) from numerical solution of equations (4.12)–(4.13), (right column) derived from QED-PIC simulations. The red box indicates the area where the alternative disruption criterion was used (see text).

parameter. This requirement imposes severe restrictions on the length and diameter of the beam. However, as shown above, the disruption parameter is also affected by radiation reaction, which is not taken into account in the usual way of calculating the disruption parameter. Our analytical model shows that, for the beam parameters required to reach $\chi \sim 1600$ at the beam energy 125 GeV, the total charge 3 nC and radius 10 nm, the enhancement of the disruption parameter due beamstrahlung reaches 60%. For the future CLIC and ILC colliders, on the contrary, radiation reaction may somewhat relax the requirements on the beam parameters to achieve the desired brightness in the interaction region, which is partly achieved through the use of flat beams. Although we considered cylindrical beams when deriving the analytical estimate of the D/D_0 ratio, the results obtained can be applied to the flat beam configurations proposed for use in the CLIC and ILC facilities. For particles with an initial displacement lying along one of the beam main axes, the motion remains flat, and therefore the equations (4.12)–(4.13) remain valid. Thus, by calculating the values of χ_0 and r_b with respect to the beam charge distribution (see e.g. [219] for the distribution of electromagnetic fields for an elliptical Gaussian charge distribution), the disruption parameter can be calculated for a specific axis using our analytical model. Performing this procedure leads to the conclusion that for the expected beam parameters at the CLIC facility, the increase in the disruption parameter is approximately 35% for the longer axis and only 5% for the shorter one. For a round beam with the same total charge and cross-sectional area, the increase in the disruption parameter is about 35% in both axes, which confirms the fact that the use of flat beams reduces the influence of radiation reaction on beam collisions. For the parameters expected at the ILC facility, the increase in disruption does not exceed 5% in both axes due to the rather low value of χ.

Fig. 4.7 shows how radiation reaction affects beam disruption for various parameters. In particular, it is shown that the collision of beams with a sufficiently large total charge (> 10 nC) and small radii can be significantly affected by beamstrahlung. Another interesting relationship is that although increasing the particle energy and/or decreasing the beam length (while maintaining the same total charge) reduces the disruption parameter, it at the same time leads to an increase in the

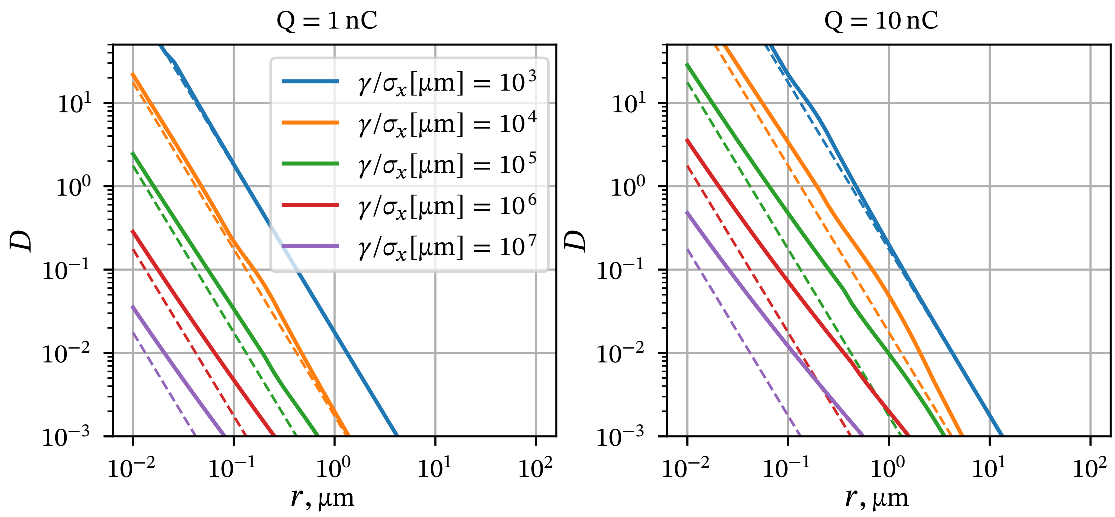

Figure 4.7: Disruption parameter calculated with (solid lines) and without (dashed lines) beamstrahlung taken into account for various beam parameters.

significance of the beamstrahlung. Thus, the ratio D/D_0 can be used to determine whether the effect of radiation radiation is significant for beam collision or not.

Collision of beams of the same charge sign

The model developed above, which describes the increase in the disruption parameter due to radiation reaction, can also be extended to the case of collision of beams with the same charge sign. In this case, the disruption parameter is the square of the ratio of the time during which the displacement of particles from the beam axis doubles to the time of interaction of the beams. The calculation of this parameter, taking into account radiation reaction, can be carried out using a similar method that was used above, i.e. by substituting in the rhs of the particle motion equations the instantaneous value of the force acting on the particle by its average value. Just as in the case of collision of oppositely charged beams, in this case the transverse displacement of the particle varies in a limited range from r_0 to $2r_0$, so this approximation is justified. This procedure also makes it possible to implicitly take into account the fact that the force acting on a particle outside the beam falls off according to the $1/r$ law. We note that when beams of the same charge sign interact, the particles move infinitely and do not oscillate; therefore, both regime of interaction, corresponding to the collision of either short or long beams, can be described by a single analytical model. Thus, it turns out that despite the different nature of particle motion in the case of collisions of identically or oppositely charged beams, the final expressions for calculating the disruption parameter, taking into account radiation reaction, are identical in both of these cases. Thus, the range of applicability of the proposed method for calculating the beam disruption parameter with account of radiation reaction extends to the case of interaction of beams of the same charge sign. We note that the experimental realization of the collision of, for example, two electron beams is a simpler task than the collision of an electron and positron beams; however, for example, from the point of view of achieving a nonperturbative regime of QED, such configurations are equivalent.

Enhancement of the yield of the secondary particles

The publication [220] studied the possibility of significantly increasing the yield of secondary particles during the collision of high-current beams due to the relative shift of their axes. The shift is determined in such a way that the axis of one beam is in the region of the maximum field of the counter-propagating beam. We have shown that in such a configuration, despite the smaller area of geometric overlap of the beams, the fraction of particles reaching the non-perturbative QED regime ($\alpha\chi^{2/3} > 1$) [129, 130] does not differ from that in the non-shifted configuration. The advantage of the shifted configuration is a more uniform distribution of secondary particles, since in this case all particles of the beam experience approximately the same field strength of the counter-propagating beam. In the case of the non-shifted configuration, the maximum field is experienced by particles at the periphery of the beam, which leads to a ring-shaped distribution of secondary particles. Numerical simulations also show an increase in the yield of the number of secondary particles in a displaced configuration up to 5-10%. A similar result is obtained when calculating the number of secondary particles using analytical estimates presented in publications [122, 127]. Since the implementation of such a configuration does not require any additional complications from an experimental point of view, its advantage over the unbiased configuration is obvious.

Kink instability

In addition to the emission of hard photons by particles in the collision of high-current beams, an important QED effect is the decay of emitted photons into secondary electron-positron pairs. Our full-scale QED-PIC simulation shows that in a sufficiently large range of initial parameters (the maximum initial value of the χ parameter for particles exceeds 1), the electron-positron plasma formed in this way has a significantly higher density than the density of initial particles. In such a plasma, due to the small spatial separation of the electron and positron components, the electric field of the initial beams is efficiently screened. Thus, the dynamics of the electron-positron plasma can be reduced to dynamics of neutral flows in an external magnetic field of the initial beams, which is one of the most common problems in astrophysics. It is known that a number of instabilities can develop in such case. Numerical simulation shows that the most pronounced is the kink instability of the plasma flow in an azimuthal magnetic field, which is the deviation of the center of mass of the beam from its average axis of symmetry (see Fig. 4.4 (b, c)).

We have determined the influence of secondary electron-positron pairs, formed as a result of the decay of hard photons emitted by the initial particles of the beam, on the development of this instability. The results of the full-scale 3D QED-PIC simulation show that production of secondary pairs does not significantly change the characteristic spatial scale of the instability and its growth rate. This result is explained by the fact that such particles do not lead to the generation of both magnetic fields, since the total current of the formed electron-positron pair is zero, and electrostatic ones, since they are compensated on average due to the symmetrical formation of a pair from the counter-propagating beam, creating the opposite field. Thus, secondary electron-positron pairs create a quasi-neutral background of a sufficiently high density. The simulation results with artificially disabled electron-positron pair production show that the seed for the kink instability is created as a result of the violation of the symmetry of the beam charge distribution caused by the stochastic emission of photons by the beam particles. The latter also leads to a significant broadening of the beam energy spectrum. Since particles with lower energy are more rapidly focused in the field of the colliding beam, this ultimately leads to the fact that the charge distribution in the beams acquires a random component.

We also estimated the characteristic temporal and spatial scales of the observed instability. For this, the long-developed theory of its linear stage was modified [122, 221]. According to this theory, these scales coincide in order of magnitude with the relativistic plasma frequency $\sqrt{4\pi e^2 n_\mathrm{b}/m\gamma}$, where n_b and γ are the density and Lorentz factor of the beam particles, respectively. An important difference between the problem we are studying and the model problem, which is used to describe the kink instability, is that the latter assumes the constancy of the particle energy and the beam charge distribution. Both of these assumptions turn out to be wrong in our case. The energy variability can be taken into account using the theory developed in section 4.2.2 which describes the increase in the beam disruption parameter when radiation reaction is taken into account. Since the relativistic plasma frequency is proportional to the square root of the disruption parameter, the ratio of the characteristic wavelength of the kink instability with radiation reaction taken into account to that without radiation reaction is equal to the square root of the ratio of the corresponding disruption parameters calculated using our theory, i.e.

$$\lambda_\mathrm{kink} \sim \sqrt{\frac{mc^2\gamma_0}{\pi e^2 n_\mathrm{b}}}\sqrt{\frac{D_0}{D}}, \tag{4.85}$$

where γ_0 is the initial Lorentz factor of beam particles. Focusing and the corresponding increase in the beam density leads to an additional increase in the plasma frequency. Due to the stochastic nature of the radiation, the maximum density of the focused beam is significantly less than in the case without taking into account radiation reaction. According to the simulation results, the ratio of the maximum beam density to the initial ν reaches values of the order of 10–100 (see Fig. 4.4 (b, c)). Thus, the characteristic scale of kink instability can be estimated in order of magnitude as follows

$$\lambda_\mathrm{kink} \sim \sqrt{\frac{mc^2\gamma_0}{\pi e^2 n_{b,0}}}\sqrt{\frac{D_0}{D}\frac{1}{\nu}} = \lambda_\mathrm{kink,0}\sqrt{\frac{D_0}{D}\frac{1}{\nu}}. \tag{4.86}$$

This estimate coincides in order of magnitude with the results of the full-scale QED-PIC simulation. We also note that, according to the theory of the linear stage of kink instability, it is considered that the threshold of its observation corresponds to a value of the disruption parameter of the order of 50. According to the theory developed above, due to an increase in the disruption parameter due to radiation reaction, the condition for the absence of kink instability obviously becomes more stringent. The QED-PIC simulation results are in good agreement with the corrected estimate. Such a large value of the disruption parameter is usually not achieved in colliders; nevertheless, further study of the kink instability in the collision of particle beams as a result of QED processes can probably be important from the point of view of astrophysical processes, which, however, lay outside of the scope of the present thesis.

4.3 Gamma radiation generation in beam-plasma interaction

Besides a technically difficult to implement configuration of a head-on collision of two high-current beams of ultrarelativistic particles, the observation of QED effects is possible in the configuration of the interaction of one such beam with a homogeneous plasma target. It is expected that the FACET-II facility will produce beams with an electron density above $10^{23}\,\mathrm{cm}^{-3}$, which corresponds to the characteristic electron density in solids. When such a beam propagates in a solid body, a strongly nonlinear wake wave, *bubble*, can be excited, formation of which is usually considered in much less dense media, for example, gas [10, 222]. In this section, using a full-scale 3D PIC simulation, we study the generation of gamma photons during the interaction of an ultrarelativistic electron beam with a thick plasma target. Numerical simulations were performed using the PIC code QUILL [201], in which the formation of secondary particles is taken into account using the Monte Carlo method. For the numerical solution of the Maxwell equations, a hybrid scheme was used, described in the section 4.4.1, which allows one to significantly reduce the increment of the numerical Cherenkov instability [199, 223, 224]. The beam parameters were chosen close to those expected at the FACET-II facility at the final stage of the project: the beam charge was equal to 3 nC, the rms beam diameter and length were 400 nm and 1 μm, respectively, the particle energy — 10 GeV. In the first series of simulations, the target density varied from $10^{21}\,\mathrm{cm}^{-3}$ to $5\times10^{23}\,\mathrm{cm}^{-3}$, thickness — from 1 to 100 μm. The maximum thickness of 100 μm is chosen based on the consideration that collisional processes, which lead to additional energy losses, should be insignificant (these processes are also not taken into account in the QUILL code, which was used for numerical simulation).

The simulation results show that beam propagation in the target is accompanied by the formation of a cavity that is almost completely devoid of electrons and propagates synchronously with the beam (Fig. 4.8). In such a strongly nonlinear wake wave, quasi-static radial electric and azimuthal magnetic fields are formed, in which the beam particles perform betatron oscillations with a frequency of $\omega_{\mathrm{pl}}/\sqrt{2\gamma}$, where the plasma frequency is ω_{pl} corresponds to the unperturbed target electron density, and γ is an instantaneous value of the Lorentz factor of the particle [225]. With such a motion, the radiation of electrons is incoherent and has a synchrotron nature. The generated beam of gamma quanta repeats the spatial distribution of electrons and has a fairly small divergence. Gamma radiation has a wide spectrum with a cutoff at the initial electron energy, 10 GeV, which practically does not change during the interaction. In addition to energy losses due to radiation, beam electrons are also slowed down due to the longitudinal field generated in the plasma cavity. However, for sufficiently dense targets, this effect is much less significant compared to radiation losses. It should be noted that as a result of the formation of a bubble, a secondary electron beam is formed in its rear part, similar to how it occurs in a rarefied plasma. The electrons of this secondary beam are in the accelerating longitudinal field and also perform betatron oscillations and radiate. The simulation results show that the cutoff energy of the secondary beam does not exceed 5 GeV, and the fraction of the total energy relative to the energy of the entire gamma radiation does not exceed 15%.

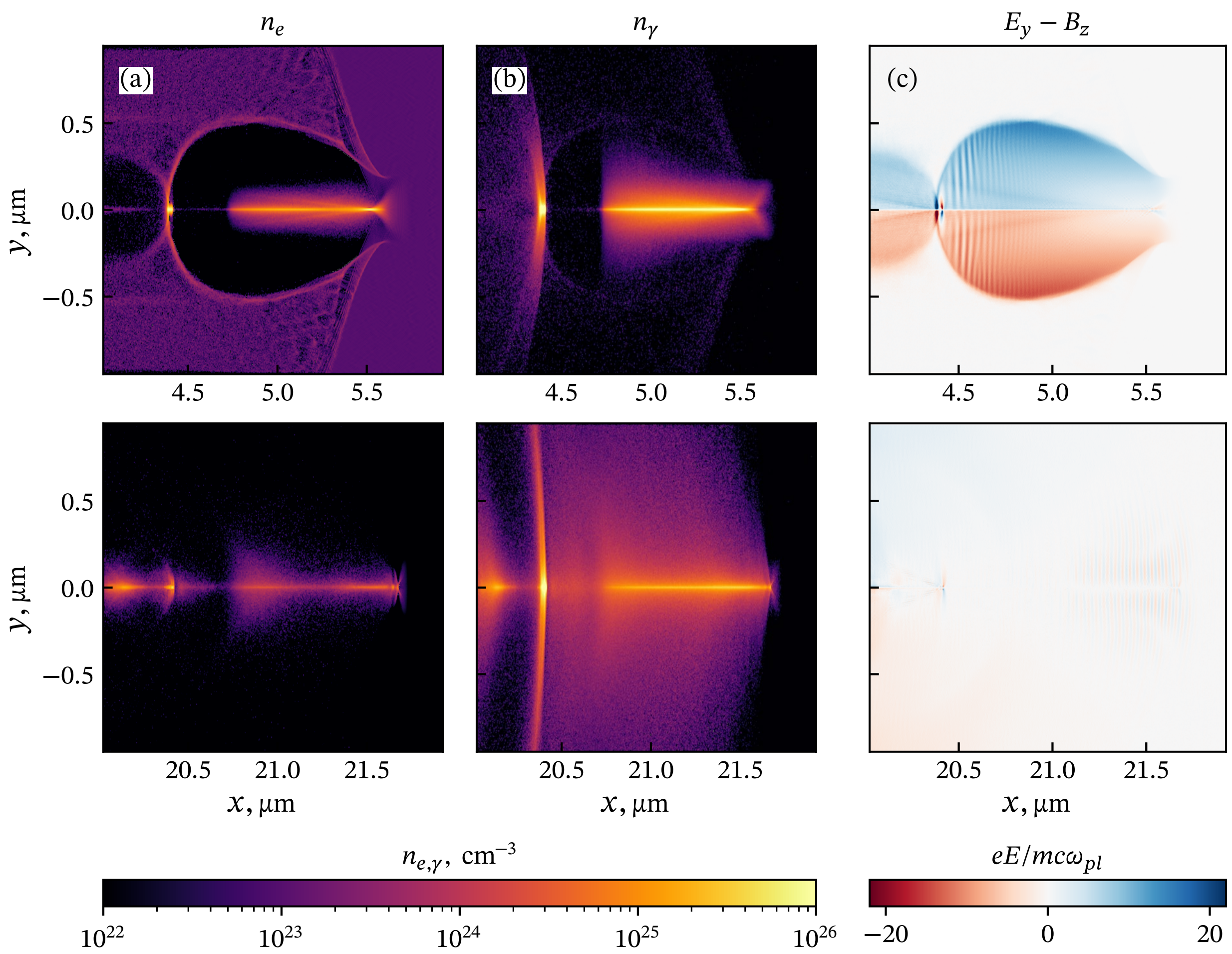

Figure 4.8: (a) Electron density distribution, (b) gamma photon density and (c) transverse force $E_y - B_z$ acting on beam electrons in simulation of high-current electron beam propagation in a solid target with density $n_e = 10^{23}$ cm^{-3} and thickness 10 μm. The top row corresponds to the penetration of the beam into the target to a depth of 5 μm, the bottom row corresponds to the moment the beam exits the target. The x coordinate is measured from the front boundary of the target.

Note that a similar scheme has recently been proposed for generating bright gamma beams, based on the collision of a high-current beam of ultrarelativistic particles with a sequence of thin metal films [226]. In this configuration, the effective field acting on beam electrons is associated with «reflection» of the beam's own field from a thin plasma layer, and is, in its meaning, a transition radiation field. Despite the differences in the physical mechanism of gamma radiation generation, the efficiency and the final spectrum are very similar in the configuration [226] and in the configuration under consideration.

As described above, the beam electrons perform betatron oscillations in the field of a strongly nonlinear wake wave, the structure of which is described, for example, in the publication [225]. It is important to note, that the focusing field depends linearly on the transverse coordinate. Thus, the configuration of the EM field inside the bubble coincides with the configuration of the field the particle experiences during a collision with a counter-propagating beam, considered in the previous section, except for the presence of a decelerating longitudinal field. Therefore, for an analytical description of the process of conversion of the beam energy into the gamma radiation energy, we can apply the theory developed in section 4.2.3. In that case, one can write

$$\frac{\mathrm{d}\rho}{\mathrm{d}t} = -\frac{\rho}{\Gamma}\frac{1}{4\pi}\int_0^{2\pi} P\left(\frac{\rho\Gamma}{2a_{\mathrm{S}}}|\cos\varphi|\right)\sin^2\varphi\mathrm{d}\varphi, \tag{4.87}$$

$$\frac{\mathrm{d}\Gamma}{\mathrm{d}t} = -\frac{1}{2\pi}\int_0^{2\pi} P\left(\frac{\rho\Gamma}{2a_{\mathrm{S}}}|\cos\varphi|\right)\mathrm{d}\varphi, \tag{4.88}$$

where ρ is the betatron oscillation amplitude, Γ is the electron energy, $a_{\mathrm{S}} = mc^2/\hbar\omega_{\mathrm{pl}}$. These equations use normalization to the plasma frequency ω_{pl}, corresponding to the unperturbed target electron density n_e: time is normalized to $1/\omega_{\mathrm{pl}}$, coordinates — to c/ω_{pl}, momentum — to mc, electromagnetic field strength — to $mc\omega_{\mathrm{pl}}/e$, power — to $mc^2\omega_{\mathrm{pl}}$. In the classical ($\chi_0 \ll 1$) and essentially quantum ($\chi_0 \gg 1$) cases, when the radiation loss power $P(\chi)$ is a power function of χ, these equations are solved analytically:

$$\frac{\Gamma(t)}{\gamma_0} \approx \begin{cases} (1+0.625P(\chi_0)t/\gamma_0)^{-4/5}, & \chi \ll 1 \\ (1-0.149P(\chi_0)t/\gamma_0)^{24/5}, & \chi \gg 1 \end{cases} \tag{4.89}$$

where $\chi_0 = r_0\gamma_0/2a_{\mathrm{S}}$, r_0 is the initial displacement of the electron from the beam axis. Taking into account the number of particles located inside the target, we can finally determine the dependence of the total beam energy on time

$$\Sigma_e(t) = \Sigma_0 - \int\limits_{-2\sigma_x}^{0}\int\limits_{0}^{r_{\mathrm{b}}} (\gamma_0 - \gamma(x+ct))\,\eta(r,x)\Theta(x+ct)2\pi r\mathrm{d}r\mathrm{d}x, \tag{4.90}$$

where $\Sigma_0 = N\gamma_0$, N is the number of electrons in the beam, the function $\eta(x,r) = n_{\mathrm{b}}(x,t)/N$ defines the charge distribution in a beam, $\Theta(x)$ is Heaviside step function. An example of comparing such an estimate with the results of QED-PIC simulation is shown in Fig. 4.9, 4.10.

Note, that this model does not take into account the presence of a longitudinal field in the plasma cavity, which additionally slows down the beam electrons. This partially explains the difference between the estimated beam energy (4.90) and its value in numerical simulations. Moreover, for the used beam parameters, even in a collision with a dense target, the efficiency of generation of electron-positron pairs from gamma quanta is low enough to significantly affect the collision process. This is why the formation of electron-positron pairs is not considered in detail.

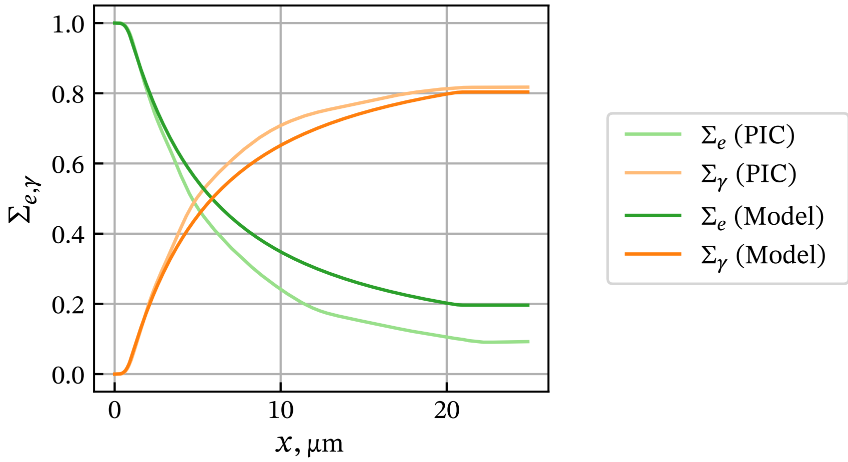

Figure 4.9: Time dependence of the total energy of electrons Σ_e and photons Σ_γ, normalized to the total initial electron energy. Lighter lines correspond to the results of QED-PIC simulation, darker lines correspond to the estimate (4.90) and the numerical solution of the equations (4.87), (4.88), respectively.

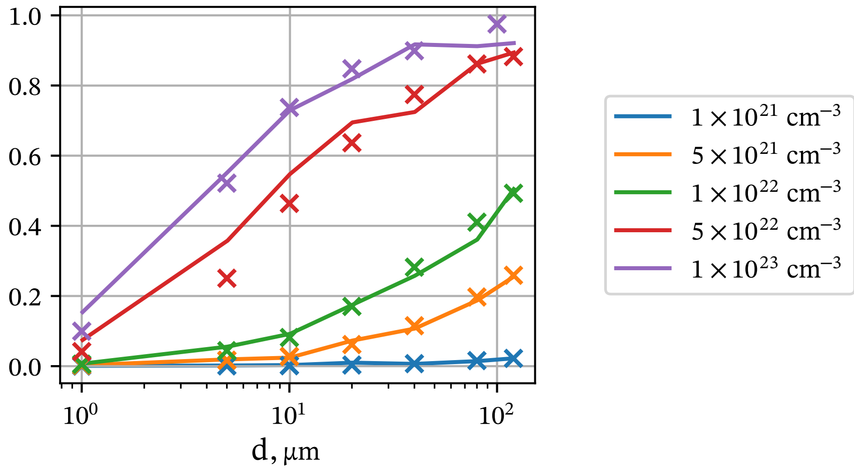

Figure 4.10: Conversion coefficient of the electron beam energy into gamma radiation energy depending on target concentration and thickness: solid lines correspond to QED-PIC simulation results, markers to the analytical estimate (4.90).

In addition to the influence of the target parameters, the influence of the geometrical dimensions of the beam on the efficiency of the conversion of the electron energy into the energy of gamma radiation was also studied. As the reference beam parameters, we chose the parameters implemented at the FACET-II facility to date, namely: beam charge from 0.5 to 3 nC, particle energy of 10 GeV, beam length l_b from 1 to 100 μm, beam radius r_b from 2.5 to 100 μm. As demonstrated above, the efficiency of beam energy conversion into gamma radiation energy increases with increasing target concentration and length. In this regard, the target density was chosen to be equal to 0.6 of the maximum electron density reached at the center of the beam. This choice is justified by the fact that at a given density ratio, the electron beam creates a cavity in the target that is free from electrons, i.e. bubble, in which a transverse charge separation field is created. In this case, the maximum target thickness was limited by the characteristic mean free path with respect to collisional processes, which lead to additional energy losses and are not studied in this work, in particular, bremsstrahlung of electrons on nuclei, the formation of electron-positron pairs from photons near nuclei, electron-electron scattering, etc., and was calculated from the relation

$$l_{\max} = 10^{-3}\lambda_\sigma = 10^{-3}\left(\sigma_{\max}n\right)^{-1}, \tag{4.91}$$

where $\lambda_\sigma = (\sigma_{\max}n)^{-1}$ is the mean free path with respect to the process with cross section $\sigma_{\max}$, n is the density of scatterers (nuclei, electrons), which was considered equal to the target electron density n_e. The characteristic maximum cross section $\sigma_{\max}$ was estimated by us as 10^{-22} cm^2, which corresponds, for example, to the bremsstrahlung cross section of electrons with energy 10 GeV on nuclei with charge number $Z \sim 50$ [32]. When the relation (4.91) holds, collisional processes can be considered insignificant. As demonstrated above, the energy loss of an electron beam due to the emission of hard photons depends on two dimensionless parameters: the initial value of the QED parameter χ_0 and the duration of interaction of the beam with the target in plasma periods $T = \omega_{\mathrm{pl}} l/c$. In this case, the value of χ_0 can be calculated as follows

$$\chi_0 = \gamma_0 n_e r_0 r_e \lambda_C, \tag{4.92}$$

where γ_0 is initial Lorentz factor of electrons, r_0 is beam diameter, r_e is classical electron radius, λ_C is Compton wavelength. Due to the fact that at the beam parameters achievable at the current stage of development of the FACET-II facility, the value of the parameter χ_0 does not exceed a value of about 0.2, radiation losses can be estimated using formulas corresponding to the classical radiation limit ($\chi_0 \ll 1$). In this case, according to (4.89), the efficiency of converting the energy of the electron beam into gamma radiation can be estimated as follows

$$\varkappa = \frac{\Sigma_\gamma}{\Sigma_{e,0}} \approx 1 - \left(1 + 0.625 P(\chi_0) T/\gamma_0\right)^{-4/5}, \tag{4.93}$$

where Σ_γ is total energy of gamma radiation, $\Sigma_{e,0}$ is initial energy of electron beam, $P(\chi_0) = 2/3\alpha a_{\mathrm{S}}\chi_0^2$ is total radiation power normalized to $mc^2\omega_{\mathrm{pl}}$, $\alpha = e^2/\hbar c$, $a_{\mathrm{S}} = mc^2/\hbar\omega_{\mathrm{pl}}$. Substituting into (4.93) the values of T and χ_0, expressed in terms of the maximum beam density, one can show that the value of $\varkappa$ is proportional to the maximum beam density n_{b}, as well as the value of χ_0, according to (4.92). Thus, from the estimate (4.93) it follows that in order to achieve the maximum conversion of the beam energy into the energy of gamma radiation, as well as the generation of radiation with the highest cutoff energy (since the maximum energy of the emitted the more photons, the larger the χ value), it is necessary to use the densest beam. For a fixed beam charge this corresponds to the minimum geometric dimensions of the beam. Since our estimate is quite simple and was obtained taking into account a number of assumptions, in order to more accurately determine the optimal geometric dimensions of the beam, we carried out a series of full-scale three-dimensional numerical simulations of the interaction of an electron beam with a homogeneous target using the particle-in-cell method with quantum electrodynamic effects taken

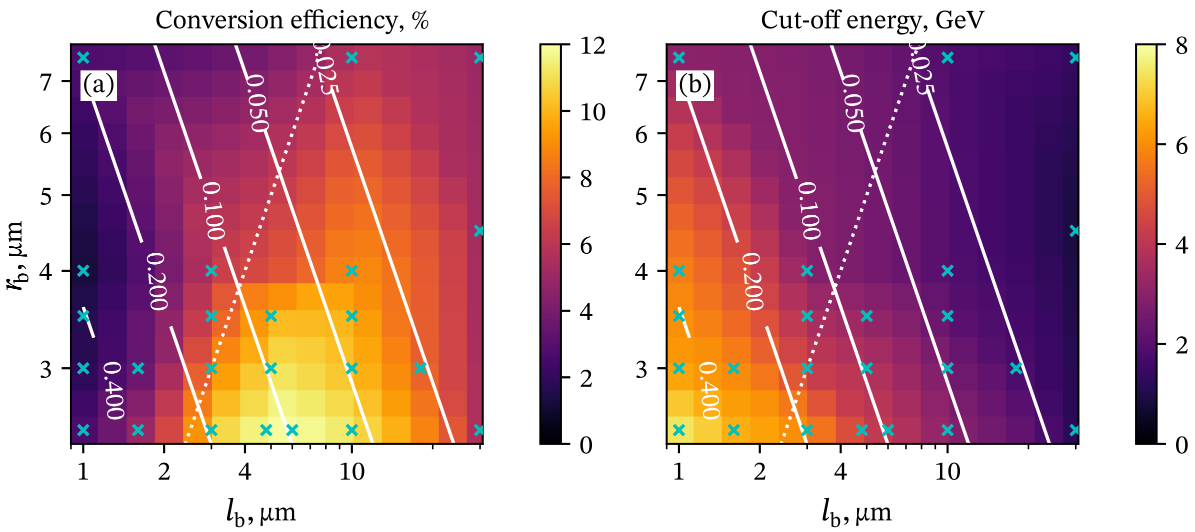

Figure 4.11: (a) Efficiency of the conversion of the electron beam energy into gamma radiation energy and (b) the cutoff energy in the gamma radiation spectrum on as function of the beam length and radius. The color map is obtained by linear interpolation between the values obtained from the PIC simulation (marked with blue crosses). The white dotted line corresponds to the ratio $l_b = r_b$, the white solid lines denote the levels of the constant value of χ_0, according to the estimate (4.92).

into account, implemented in the QUILL code [201]. The charge and energy were 3 nC and 10 GeV respectively. The results of the numerical simulation in the range of beam lengths from 1 to 30 μm and beam radii from 2.5 to 7.5 μm are shown in Fig. 4.11. According to the simulation results, the maximum conversion of beam energy into gamma radiation energy is achieved at the minimum beam radius (2.5 μm), but at a beam length greater than the minimum (6 μm) , and is about 12%. In this case, the maximum photon energy is 4.7 GeV.

To explain the reason for the discrepancy between the simulation results and our estimate, we have considered in detail the bubble formation process (see Fig. 4.12). In simulations with the smallest possible beam size (radius $r_b = 2.5$ μm, length $l_b = 1$ μm), its maximum density is 2.8×10^{21} cm^{-3}, and the target density is 1.7×10^{21} cm^{-3}. With these parameters, the estimate of the bubble radius according to the model developed in the publication [227] gives the value of 2.8 μm. Despite the fact that the transverse charge separation field inside the bubble is practically independent of the longitudinal coordinate [225], it obviously sharply decreases to zero when passing through the bubble boundary (see Fig. 4.12 (b)). Since the beam length is sufficiently less than the bubble radius, and the beam radius practically coincides with the latter, the beam electrons are located in the region where the transverse field strength is significantly less than in the main part of the bubble (see Fig. 4.12 (b)). This leads to the fact that the real value of the parameter χ of electrons turns out to be noticeably smaller than according to the estimate (4.92). In this regard, the emission of photons by electrons becomes inefficient. The simulation results show that, in general, during the interaction of an electron beam with a radius exceeding its length, the efficiency of gamma radiation generation is significantly reduced due to the effect described above (see dashed line in Fig. 4.11 (a)). When using a longer beam, a significant part of it is in the region of a strong transverse field, and the estimate (4.93) describes the energy conversion into gamma radiation pretty well.

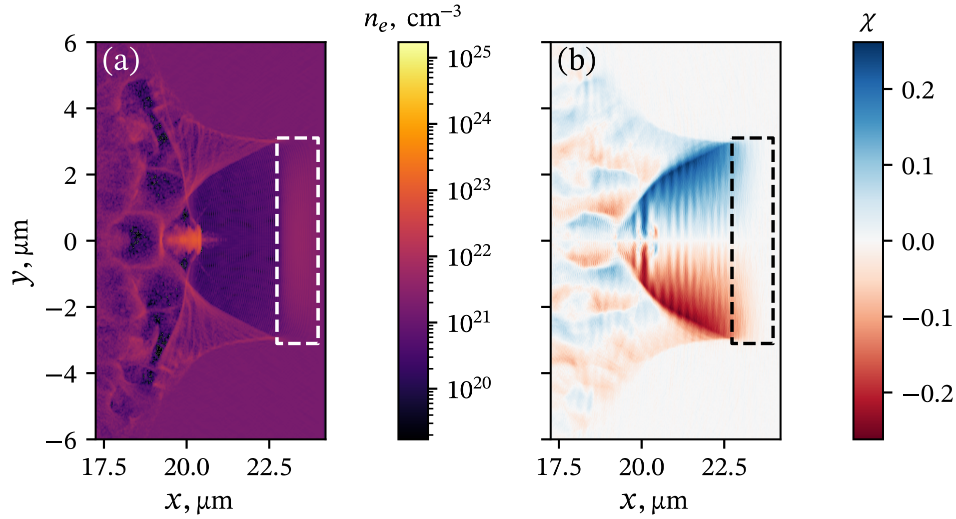

Figure 4.12: Peculiarities of the bubble generation by an electron beam with a diameter greater than its length ($l_b = 1\,\mu$m, $r_b = 2.5\,\mu$m). (a) Electron density distribution and (b) $\gamma_0 \left(E_y - B_z\right)/a_S$ equal to the value of the electron parameter χ. The x coordinate is measured from the beginning of the target. Dashed lines indicate the location of the electron beam.

It should be noted that despite the achievement of the maximum conversion efficiency at a beam length of 6 μm, from the point of view of applications of the resulting radiation, its spectral characteristics are also important. The simulation results show (see Fig. 4.11 (b)) that when using a beam with minimal geometric dimensions, by increasing the value of the parameter χ_0, the maximum energy of gamma photons is higher, than in the case of using a beam with optimal parameters, and reaches 7.5 GeV. However, the generation efficiency in this case turns out to be significantly lower — 3%.

4.4 Numerical simulation of ultrarelativistic beams using the PIC method

As described above, the development of charged particle accelerator technologies will make it possible in the foreseeable future to conduct unprecedented experiments on the interaction of high-current charged particle beams with matter to generate gamma radiation, study of strong-field QED processes, elementary particle physics, and even astrophysical processes. Due to the technical complexity of such experiments, an extremely important part of their planning is the search for optimal interaction configurations and obtaining various qualitative and quantitative estimates using numerical simulation. The most modern method for self-consistent modeling of plasma dynamics and electromagnetic fields is the *particles-in-cells* or PIC method. Despite the advantages of this method, it is not free from disadvantages, one of which is the dispersion of waves in vacuum, which occurs when using the standard scheme for solving Maxwell's equations — *Finite Differences in the Time Domain*, or FDTD. The dispersion of EM waves in vacuum, in particular, leads to the existence of waves which phase velocity is less than the speed of light. Thus, ultrarelativistic charged particles

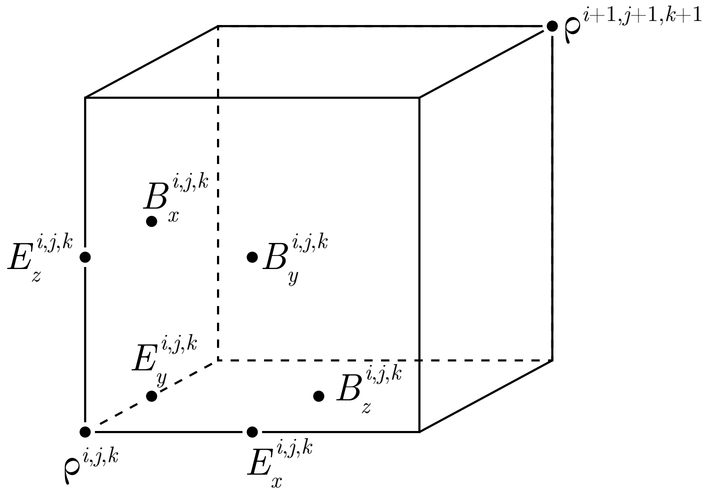

Figure 4.13: The location of the grid nodes of the electric and magnetic fields and the indices used in the QUILL code.

can satisfy the Cherenkov synchronism condition and resonantly excite such waves in vacuum — the effect known as *numerical Cherenkov instability* (NCI) [199, 223, 224], which may significantly reduce the reliability of the results obtained using numerical simulations.

Let us present a simplified analysis that indicates the cause of the appearance of the numerical Cherenkov instability (more rigorous reasoning, taking into account the interpolation of fields into particles, can be found, for example, in the papers [228, 229]). To do this, we will use the arrangement and indexing of fields on the grid, which is used in the QUILL code (see Fig. 4.13). The most common scheme for the numerical solution of Maxwell's equations is the FDTD scheme, in which the grids of the magnetic and electric fields are shifted by half a step in each direction of space and time, and the derivatives are replaced by finite differences. Thus, Maxwell's equations are written in the following form

$$\hat{\delta}_t B_x = \hat{\delta}_z E_y - \hat{\delta}_y E_z, \tag{4.94}$$
$$\hat{\delta}_t B_y = \hat{\delta}_x E_z - \hat{\delta}_z E_x, \tag{4.95}$$
$$\hat{\delta}_t B_z = \hat{\delta}_y E_x - \hat{\delta}_x E_y, \tag{4.96}$$
$$\hat{\delta}_t E_x = \hat{\delta}_y B_z - \hat{\delta}_z B_y + j_x, \tag{4.97}$$
$$\hat{\delta}_t E_y = \hat{\delta}_x B_x - \hat{\delta}_x B_z + j_y, \tag{4.98}$$
$$\hat{\delta}_t E_z = \hat{\delta}_z B_y - \hat{\delta}_y B_x + j_z, \tag{4.99}$$

where the finite difference operator $\hat{\delta}$ is used

$$\hat{\delta}_x F^{i+1/2,j,k} = \frac{F^{i+1,j,k} - F^{i,j,k}}{\Delta x}, \tag{4.100}$$

which approximates the derivative up to terms of order Δx^2. The operators $\hat{\delta}_y$, $\hat{\delta}_z$, $\hat{\delta}_t$ are defined similarly. Let us find the dispersion relation for waves in vacuum ($\mathbf{j} = 0$). To do this, we will look for solutions of the equations (4.94)–(4.99) in the form of plane waves, i.e. $\mathbf{E}$, $\mathbf{B} \propto \exp(-i\omega t + i\mathbf{kr})$.

To do this, it suffices to define the action of the operator $\hat{\delta}$ on the expression $\exp(-i\omega t + i\mathbf{kr})$

$$\hat{\delta}_\alpha e^{-i\omega t+i\mathbf{kr}} = \frac{1}{\Delta\alpha}\left(e^{ik_\alpha\Delta\alpha/2} - e^{-ik_\alpha\Delta\alpha/2}\right)e^{-i\omega t+i\mathbf{kr}} = \frac{2i}{\Delta\alpha}\sin\frac{k_\alpha\Delta\alpha}{2}e^{-i\omega t+i\mathbf{kr}}, \tag{4.101}$$

$$\hat{\delta}_t e^{-i\omega t+i\mathbf{kr}} = \frac{1}{\Delta t}\left(e^{-i\omega\Delta t/2} + e^{-i\omega\Delta t/2}\right)e^{-i\omega t+i\mathbf{kr}} = -\frac{2i}{\Delta t}\sin\frac{\omega\Delta t}{2}e^{-i\omega t+i\mathbf{kr}}, \tag{4.102}$$

where $\alpha = x, y, z$. Thus, the equations (4.94)–(4.99) in vacuum for plane waves are rewritten in the following form

$$A_t B_{x0} = A_y E_{z0} - A_z E_{y_0}, \tag{4.103}$$

$$A_t B_{y_0} = A_z E_{x0} - A_x E_{z0}, \tag{4.104}$$

$$A_t B_{z0} = A_x E_{y_0} - A_y E_{x0}, \tag{4.105}$$

$$A_t E_{x0} = A_z B_{y_0} - A_y B_{z0}, \tag{4.106}$$

$$A_t E_{y_0} = A_x B_{z0} - A_z B_{x0}, \tag{4.107}$$

$$A_t E_{z0} = A_y B_{x0} - A_x B_{y_0}, \tag{4.108}$$

where

$$A_\alpha = \frac{1}{\Delta\alpha}\sin\frac{k_\alpha\Delta\alpha}{2},\ \alpha = x, y, z, \tag{4.109}$$

$$A_t = \frac{1}{\Delta t}\sin\frac{\omega\Delta t}{2}. \tag{4.110}$$

Equating the determinant of the system (4.103)–(4.108) to zero and performing simple algebraic transformations, we obtain the following dispersion relation

$${A_t}^2 = {A_x}^2 + {A_y}^2 + {A_z}^2, \tag{4.111}$$

$$\omega = \pm\frac{2}{\Delta t}\arcsin\left(\Delta t\sqrt{{A_x}^2 + {A_y}^2 + {A_z}^2}\right). \tag{4.112}$$

This numerical scheme is stable (ω has no complex part) under the condition

$$\frac{1}{\Delta t^2} > \frac{1}{\Delta x^2} + \frac{1}{\Delta y^2} + \frac{1}{\Delta z^2}. \tag{4.113}$$

The phase and group wave velocities in the FDTD scheme are shown in Fig. 4.15 (b), (e). It can be seen that indeed all waves propagate with a phase velocity less than the speed of light. This means that particles propagating at near-light speeds can move synchronously with such waves and generate them. The generation of such waves is also observed in numerical simulations of electron beam propagation in vacuum. Figure 4.14 shows the results of such a simulation with the following parameters: $\Delta t = 0.025\lambda/c$, $\Delta x = 0.05\lambda$, $\Delta y = \Delta z = 0.25\lambda$, where λ is a normalization wavelength equal to 1/15 of the beam length, beam electron energy $E_\mathrm{b} = 10\,\mathrm{GeV}$. The Fourier spectrum of the y component of the electric field (see Fig. 4.14 (d)) shows that the most pronounced harmonic is indeed in Cherenkov resonance with beam particles $\omega/k_x = v_\mathrm{b} = \sqrt{1-\gamma^{-2}}$.

In the next section, we propose a scheme for the numerical solution of Maxwell's equations, in which the phase velocity of the waves is strictly greater (but insignificantly) than the speed of light, which makes it possible to effectively eliminate the numerical Cherenkov instability.

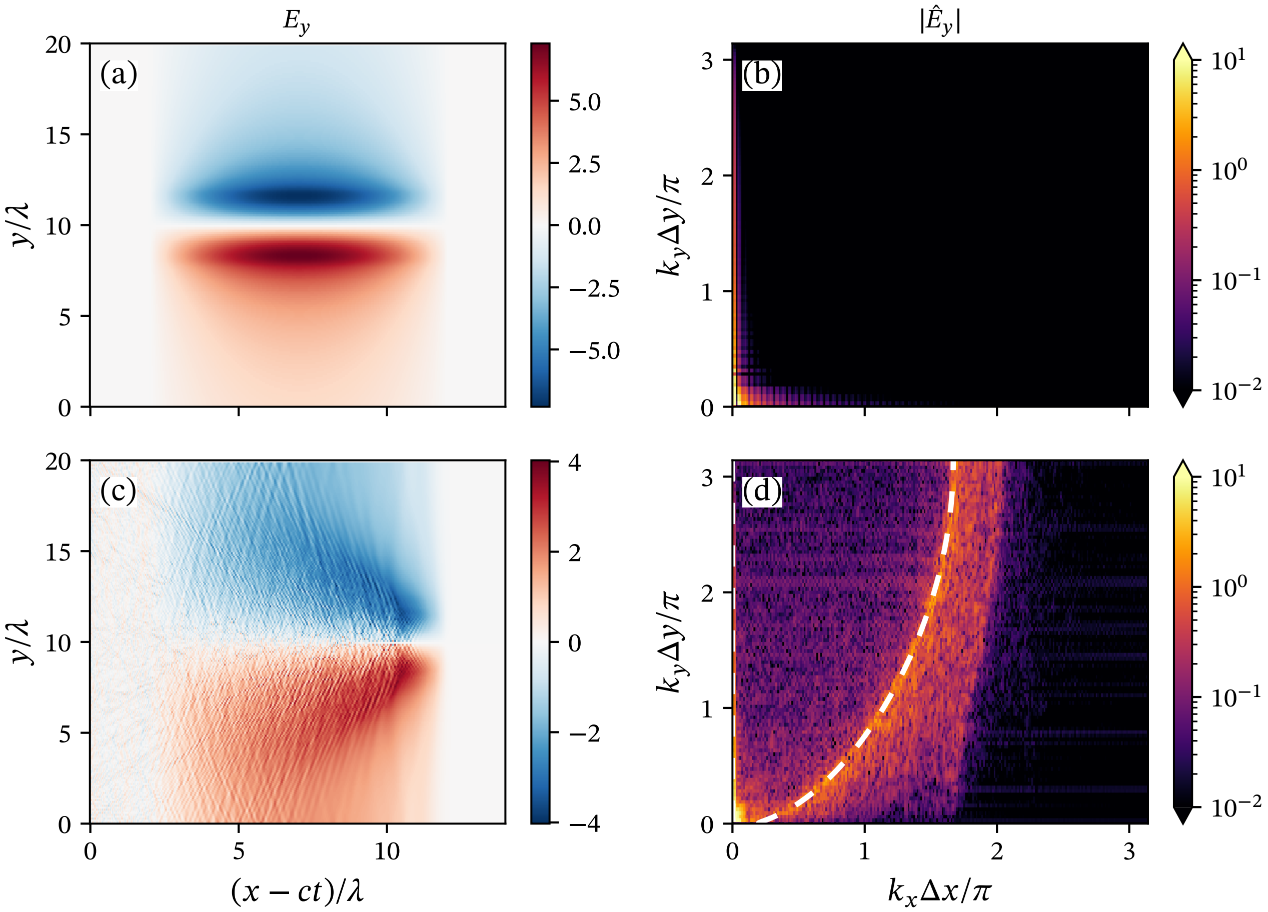

Figure 4.14: Results of numerical simulation of propagation of an ultrarelativistic ($\gamma = 10^3$) electron beam in vacuum using the FDTD scheme. (a) Distribution of the y component of the electric field, and (b) its Fourier spectrum at the initial time. (c), (d) — the same after 3×10^4 simulation steps. The white dashed line corresponds to the Cherenkov resonance $v_{\mathrm{ph},x} = \sqrt{1-\gamma^{-2}}$.

4.4.1 Mitigating numerical Cherenkov instability

There are several ways to suppress NCI, for example, using higher-order approximations for spatial derivatives [230–232], applying filters to fields and currents on a grid [233], or using a spectral approach to solving Maxwell's equations in Fourier space [234], each with its own advantages and use cases. We propose an NCI reduction scheme that can be easily implemented in existing PIC codes and is based on the following modification of the FDTD scheme stencil

$$\hat{\delta}_t B_x = (a_{0,z} + a_{1,z}\hat{\mu}_z)\hat{\delta}_z E_y - (a_{0,y} + a_{1,y}\hat{\mu}_y)\hat{\delta}_y E_z, \tag{4.114}$$
$$\hat{\delta}_t B_y = (a_{0,x} + a_{1,x}\hat{\mu}_x)\hat{\delta}_x E_z - (a_{0,z} + a_{1,z}\hat{\mu}_z)\hat{\delta}_z E_x, \tag{4.115}$$
$$\hat{\delta}_t B_z = (a_{0,y} + a_{1,y}\hat{\mu}_y)\hat{\delta}_y E_x - (a_{0,x} + a_{1,x}\hat{\mu}_x)\hat{\delta}_x E_y, \tag{4.116}$$
$$\hat{\delta}_t E_x = (a_{0,y} + a_{1,y}\hat{\mu}_y)\hat{\delta}_y B_z - (a_{0,z} + a_{1,z}\hat{\mu}_z)\hat{\delta}_z B_y - j_x, \tag{4.117}$$
$$\hat{\delta}_t E_y = (a_{0,z} + a_{1,z}\hat{\mu}_z)\hat{\delta}_z B_x - (a_{0,x} + a_{1,x}\hat{\mu}_x)\hat{\delta}_x B_z - j_y, \tag{4.118}$$
$$\hat{\delta}_t E_z = (a_{0,x} + a_{1,x}\hat{\mu}_x)\hat{\delta}_x B_y - (a_{0,y} + a_{1,y}\hat{\mu}_y)\hat{\delta}_y B_x - j_z, \tag{4.119}$$
$$a_{0,\alpha} + a_{1,\alpha} = 1,\ \alpha = x, y, z, \tag{4.120}$$

where

$$\hat{\mu}_\alpha F^{j_\alpha} = \frac{F^{j_\alpha+1} + F^{j_\alpha-1}}{2}. \tag{4.121}$$

The operator $\hat{\mu}_\alpha$ is essentially an averaging operator along the α axis. It is easy to show that the operator $\hat{\mu}_\alpha \hat{\delta}_\alpha$ approximates the derivative of ∂/∂_α with quadratic accuracy, thus under the condition (4.120) $(a_{0,\alpha} + a_{1,\alpha}\hat{\mu}_\alpha)\hat{\delta}_\alpha \to \partial/\partial\alpha$ for $\Delta\alpha \to 0$. Solutions in vacuum in the form of plane waves of the equations (4.114)–(4.119) are written in the same form as the equations (4.103)–(4.108) , but the coefficients A_α have a different form

$$A_\alpha = \frac{1}{\Delta\alpha} \sin \frac{k_\alpha \Delta\alpha}{2} \left(a_{0,\alpha} + a_{1,\alpha} \cos\left(k_\alpha \Delta\alpha\right)\right). \tag{4.122}$$

The dispersion of waves in such a scheme already depends on the parameters $a_{1,\alpha}$. Consider the expression for the phase velocity of waves propagating strictly along the α coordinate axis

$$v_{\mathrm{ph},\alpha} = 2\frac{\Delta\alpha}{\Delta t}\frac{1}{k_\alpha \Delta\alpha} \arcsin\left[\frac{\Delta t}{\Delta\alpha} \sin\frac{k_\alpha\Delta\alpha}{2} \left(a_{0,\alpha} + a_{1,\alpha}\cos\left(k_\alpha\Delta\alpha\right)\right)\right]. \tag{4.123}$$

From the analysis of this function, it can be established that an increase in the coefficient $a_{1,\alpha}$ leads to an increase in the modulus $v_{\mathrm{ph},\alpha}$ for all values of $k_\alpha\Delta\alpha$ in the first Brillouin zone ($|k_\alpha\Delta\alpha| \le \pi$). Therefore, we can find the coefficients $a_{1,\alpha}$, for example, based on the requirement that the phase velocity in the entire first Brillouin zone be greater than the speed of light and be equal to it at the boundaries, then

$$1 = \frac{\Delta\alpha}{\Delta t}\frac{2}{\pi} \arcsin\left[\frac{\Delta t}{\Delta\alpha}\left(1 - 2a_{1,\alpha}\right)\right]. \tag{4.124}$$

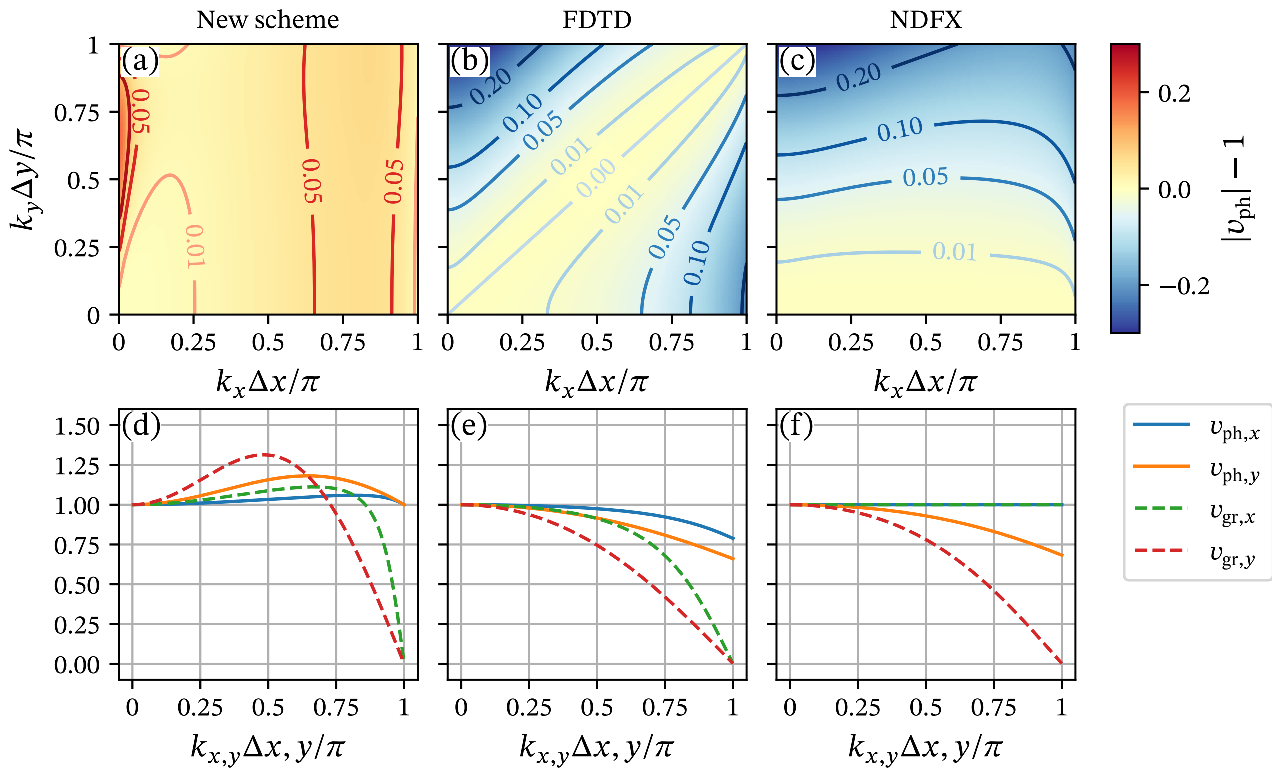

Figure 4.15: (a)–(c) Magnitude of phase velocity of waves with $k_z = 0$ as a function of wave numbers k_x and k_y, (d)–(f) dependence of phase and group velocity of waves with $k_z = k_y(k_x) = 0$ on the wave number $k_x(k_y)$ in various numerical schemes.

The solution of this equation is written in the following form

$$a_{1,\alpha} = \frac{1}{2}\left(1 - \frac{\Delta\alpha}{\Delta t}\sin\left[\frac{\pi}{2}\frac{\Delta t}{\Delta\alpha}\right]\right). \tag{4.125}$$

Let us calculate the maximum possible value of the coefficients A_α in this case

$$A_{\alpha\max} = \frac{1}{\Delta t}\sin\left(\frac{\pi}{2}\frac{\Delta t}{\Delta\alpha}\right). \tag{4.126}$$

Then the scheme is certainly stable under the condition

$$\sin^2\left(\frac{\pi}{2}\frac{\Delta t}{\Delta x}\right) + \sin^2\left(\frac{\pi}{2}\frac{\Delta t}{\Delta y}\right) + \sin^2\left(\frac{\pi}{2}\frac{\Delta t}{\Delta z}\right) < 1. \tag{4.127}$$

A comparison of the dependencies of the phase and group velocities of waves in various numerical schemes is shown in Fig. 4.15, from which it can be seen that, indeed, in the proposed scheme, waves propagate at a speed greater than the speed of light, so we can expect a decrease in the numerical Cherenkov instability. In addition to the comparison with the standard FDTD scheme, a comparison with the NDFX scheme (*Numerical Dispersion Free in X direction*) [216] is also presented, which is also based on an extension of the FDTD scheme stencil, but such a selection of coefficients that the phase velocity is precisely equal to the speed of light for all waves propagating along a single coordinate axis. Note, that the most significant deviation of the phase and group wave velocities

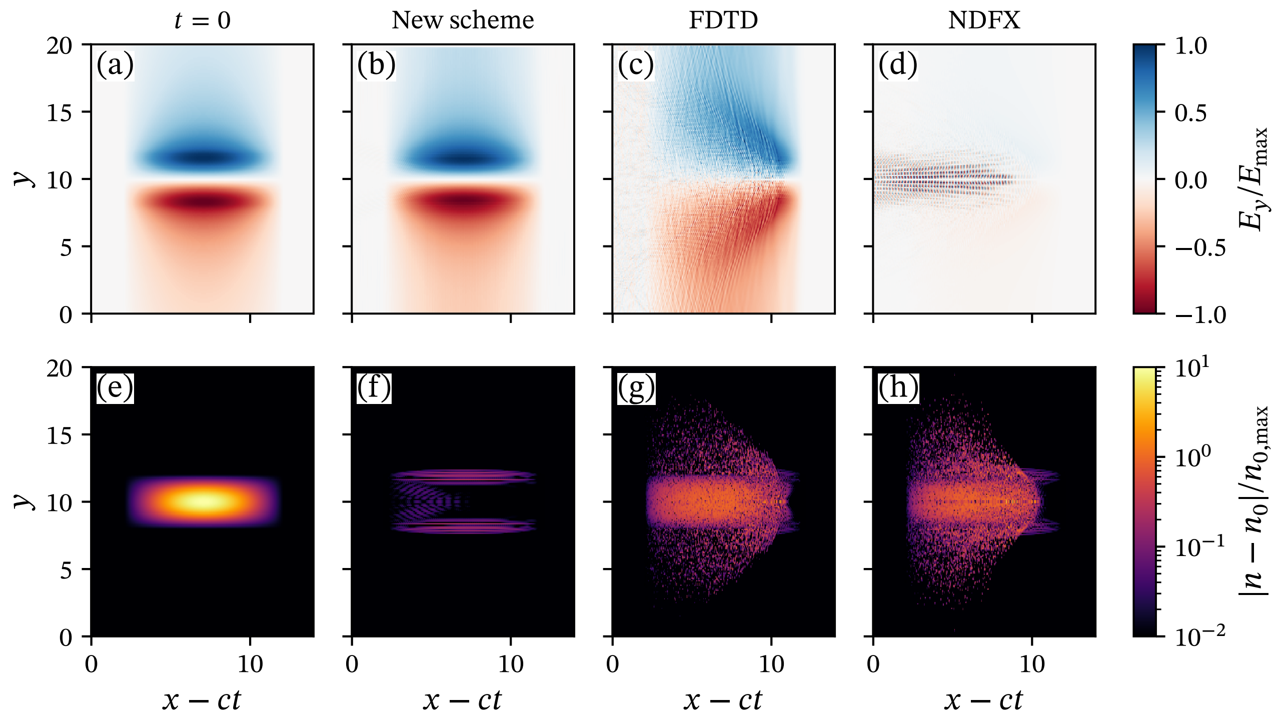

Figure 4.16: Results of numerical simulation of ultrarelativistic electron beam propagation in vacuum using various numerical schemes. (a) Initial distribution of the y-component of the electric field, (b)–(d) distribution of the y-component of the electric field after 3×10^4 simulation steps, (e) initial distribution of the electron density, (f)–(h) relative deviation of the electron density from the initial density after 3×10^4 simulation steps.

from the speed of light in all the schemes is present in the high-frequency range, i.e. for waves that are poorly resolved on the grid. Since the waves in the frequency range of interest must be resolved with a large number of grid steps for the simulation results to be reliable, the dispersion deviation can be small enough, for example, to correctly simulate laser radiation. The deviation of the dispersion in the proposed scheme coincides in order of magnitude with the FDTD or NDFX schemes and is also most significant in the high frequency region, so the accuracy of the simulation results obtained using this scheme is at least as good as that for other schemes. We also compared the results of identical numerical simulations of the propagation of an ultrarelativistic electron beam in vacuum using different schemes. The simulation was carried out using the QUILL [201] code, the cell sizes were 0.003 µm, 0.01 µm, 0.01 µm at coordinates x, y and z respectively. The time step Δt was set to $0.6\Delta x/c$ for the proposed scheme and the FDTD scheme and $\Delta x/c$ for the NDFX scheme. The comparison of the results are shown in Fig. 4.16. As expected, the Cherenkov instability grows most rapidly in the FDTD scheme. In the NDFX scheme, despite the exact vacuum dispersion of the waves propagating along the beam propagation axis, there is also instability. This happens, firstly, due to the generation of waves propagating at a small angle to the axis, having a phase velocity less than the speed of light, and, secondly, due to the effect of *frequency aliasing* [199]. This effect comes from the fact that schemes for the numerical solution of Maxwell's equations based on difference schemes always operate with a limited volume in space, so the dependence $\omega(\mathbf{k})$ for the waves in such schemes is always periodic, i.e. $\omega(\mathbf{k} + \mathbf{x}_\alpha N_\alpha 2\pi/\Delta\alpha) = \omega(\mathbf{k})$, where N_α is an integer, $\mathbf{x}_\alpha$ is a unit vector in the direction k_α, $\alpha = x, y, z$. This means that even if in the first Brillouin zone ($|k_\alpha \Delta\alpha| \leq \pi$) the phase velocity of waves is equal to or slightly greater than the speed of light, then there will always be such a Brillouin zone in which the phase velocity will certainly be less than the speed of light. An analysis of this effect shows that the interaction of particles and waves in the first Brillouin zone is a linear effect, while the effects associated with resonance in more distant zones is nonlinear and depend not only on the scheme used for solving the Maxwell equations, but also on the shape of particles, the method of interpolation of fields on particles, the method of calculating the current in the grid nodes, etc. [228, 229]. Despite the fact that the Cherenkov resonance in higher Brillouin zones cannot be completely eliminated in schemes based on the finite differences, it is much less noticeable than in the fundamental Brillouin zone, and therefore it affects the simulation only at a sufficiently large number of simulation steps. It follows from Fig. 4.16 that in our proposed scheme, there is no numerical Cherenkov instability for a sufficiently large number of simulation steps ($N = 3 \times 10^4$).

Since the proposed scheme only modifies the FDTD scheme stencil, it can be easily implemented in the existing PIC code, compared to, for example, the recently proposed RIP scheme [218], which requires quite a significant restructuring of the code. Thus, it can be argued that the proposed scheme is well suited for simulating the interaction of dense charged beams with stationary targets, laser pulses, or other beams, the experimental implementation of which is expected at the FACET-II facility in the future, as well as for modeling laser-plasma interaction, in which beam of relativistic charged particles are formed. The PIC simulation results presented in sections 4.2 and 4.3 and obtained using the developed scheme do not have signs of the presence of numerical Cherenkov instability and agree with the analytical results, which also confirms the reliability of this scheme.

4.5 Summary

Thus, in the configuration of a head-on collision of two beams, the interrelation between the process of focusing (or defocusing) of beams and beamstrahlung was considered. An analytical model was developed that allows calculating the disruption parameter taking into account radiation reaction. It was shown that the increase in disruption due to beam radiation for the future CLIC and ILC colliders can reach several tens of percent and lead to an additional increase in brightness. In the application to the FACET-II accelerator, whose prospects for studying the effects of nonperturbative QED due to beam collisions are discussed in the paper [129], an increase in the disruption parameter leads to even more stringent requirements on the beam parameters for precision measurements. It was shown that the region of applicability of the constructed model also extends to the case of collision of beams of the same charge. An analytical model has also been developed that describes the interaction of long oppositely charged beams in the weak beamstrahlung regime, when beam particles perform a large number of betatron oscillations during the interaction time. The dependencies of the energy and amplitude of the betatron oscillations of the particle are calculated both in the classical regime and in essentially quantum regimes.

Apart from collision of beams with each other, a more technically simple alternative for observing QED effects on the FACET-II facility is the collision of a single beam with a thick target. With the help of full-scale three-dimensional numerical simulation, we found that when a high-current beam of ultrarelativistic electrons collides with a plasma target, two short bunches of gamma quanta photons are generated. The first of them corresponds to the radiation by the electrons of the initial beam, and the second one corresponds to the radiation by the electrons injected into the plasma cavity created by the initial beam. The efficiency of conversion of the energy of the electron beam into the energy of gamma photons can reach 90%. The studied scheme for obtaining gamma radiation is promising in terms of ease of experimental implementation and extremely high efficiency. Simulations and analytical estimates carried out for the currently achieved beam parameters at the FACET-II facility show that the actually achievable conversion efficiency turns out to be significantly lower, however, it still reaches more than ten percent. It has also been demonstrated that using a beam in the form of a disk, i.e. with a beam diameter exceeding its length is inefficient even when a higher beam density is reached, which is due to the fact that in this case only a small fraction of the particles is located in the region of a strong plasma field.

We also developed and implemented in the QUILL code an alternative scheme for the numerical solution of Maxwell's equations on a rectangular grid with sufficiently reduced numerical Cherenkov instability. The above numerical simulations of the interaction of high-current beams of ultrarelativistic particles with each other and with a plasma target were carried out using this scheme.

Contributions of the author

The results obtained in this chapter are published in Refs. [235–237]. In the publication [235] A. S. and A. P. worked together on the idea of the alternative scheme. A. S. implemented the scheme in the code QUILL. In the publication [236] A. S. and I. Yu. worked together on the development of the model for the calculation of disruption parameter and obtaining solution of averaged equations. A. S. and M. F. conducted PIC simulations using codes QUILL and VLPL, respectively. In the publication [220] A. S. discussed the idea of shifting beams for increased yield of the secondary particles, helped with the analytical estimates and writing the manuscript. In the publication [237] A. S. did most of the work.

Chapter 5

Conclusion

In this work we investigated effects of nonlinear quantum electrodynamics, such as Compton scattering and the Breit-Wheeler process, on interaction of strong electron-magnetic fields with matter in several configurations. In the first chapter a brief introduction was given to parameters determining regimes of QED. A qualitative description of processes in the nonlinear regime of QED and a brief literature overview on their effect on interaction of strong fields with matter were given. The aims of the current work were established.

In chapter 2, a so-called asymptotic theory of a charged particle motion in the strongly radiation-dominated regime was developed. The theory is based on an observation that a particle velocity is quickly oriented along a certain direction by EM field if its strength is sufficiently larger than the particle energy, which is the case in radiation-dominated regime, in which particle losses a lot of energy due to abundant radiation. This direction coincides with the direction of the electric field in an instant reference frame where the electric and the magnetic fields are parallel and corresponds to vanishing of both transverse Lorentz-force and radiation friction force acting on the particle and is thus called radiation-free. Since particle velocity can be approximately determined by local EM field, the order of the motion equation reduces by one. An interesting general property of a particle motion according to this asymptotic radiation-free description was discovered, namely, periodic trajectories in periodic EM fields. It was demonstrated that this seemingly simple discovery might explain a known effect of radiative trapping of particles in the region of strong field, which cannot be interpreted in the framework of ponderomotive description, which is widely used when strong EM fields are considered. Further, based on this asymptotic theory a general method of obtaining approximate solution of the motion equations with account of radiation reaction was developed. Utilizing this approach several known solutions were reproduced, such as solution of the so-called Zeldovich problem of an electron dynamics in the uniform rotating parallel electric and magnetic fields, a quasi-stationary solution in the model fields of a linear accelerator and solution of the electron motion equations in plane waves. In the latter case a peculiar feature of the solution — unlimited longitudinal acceleration — is revealed.

In chapter 3, effects of nonlinear QED processes on collective dynamics of particles in configuration of interaction of extremely intensive laser pulse with thin solid target was studied. An effect of development of a self-sustained QED cascade was discovered and qualitatively explained. It was shown that due to dielectric properties of electron-positron plasma, propagation of a laser pulse through such plasma is altered in such a way that the resulting configuration of the electromagnetic field is sufficiently different from the configuration of a single traveling plane wave and is favorable for production of electron-positron pairs. Development of thq QED cascade leads to an avalanche-like multiplication of the particles and expansion of the electron-positron plasma towards the laser radiation, which ceases only after the laser pulse is completely depleted. Further, a relatively simple one-dimensional hydrodynamical analytical model of the development of a QED cascade in a plane wave was proposed which is able to reproduce the behavior observed in the full-scale three-dimensional QED-PIC simulations.

In chapter 4, interaction of high-current beams of ultrarelativistic particles, which field strength is high enough to the reach nonlinear regime of QED, with matter was considered. First, the head-on collision of identical electron and positron beams was studied and a model was developed for calculating disruption parameter which accounts beamstrahlung. The results of the model were validated through comparison with the results of full-scale three-dimensional QED-PIC simulations. Implications of the enhancement of disruption due to radiation reaction were discussed with regard to projects of the next generation colliders, such as ILC, CLIC and FACET-II. Next, an efficient generation of gamma radiation was demonstrated in the interaction of a high-current beam of ultrarelativistic electrons with a thick plasma target. A model was developed for calculating the conversion efficiency of the beam energy to the energy of gamma radiation. Beam parameters optimal at the current state of FACET-II facility for generation of gamma radiation were found. Finally, an alternative numerical scheme for solving Maxwell's equations on a rectangular grid was developed and implemented in PIC code QUILL, which is distinguished by sufficiently mitigated numerical Cherenkov instability, present in the commonly used schemes. This scheme allows to simulate interaction of ultrarelativistic particle flows with matter accurately for large amount of numerical steps.

A particular aspect was intentionally left outside the scope of this work, namely dependence of the probabilities of QED processes on polarization state of either leptons or photons, although it is worth noting that research is currently being actively conducted on, e.g., obtaining highly-polarized particle beams as a result of QED processes [75–85]. Since a few very promising results have already been obtained, it makes it possible to assume that this still infant topic will receive a special attention in further research of the strong field physics.

Appendix A

Numerical solution of relativistic motion equations of a charged particle

The relativistic motion equations of an electron in an external EM field with radiation reaction taken into account, are written in the following form

$$\frac{\mathrm{d}\gamma}{\mathrm{d}t} = -\mathbf{vE} - F_{\mathrm{rr}} v^2, \tag{A.1}$$

$$\frac{\mathrm{d}\mathbf{p}}{\mathrm{d}t} = -\mathbf{E} - \mathbf{v} \times \mathbf{B} - F_{\mathrm{rr}} \mathbf{v}, \tag{A.2}$$

where the electron momentum $\mathbf{p}$ is normalized to mc, time t — to $1/\omega$, electric and magnetic fields — to $mc\omega/e$, F_{rr} — total radiation power normalized to $mc^2\omega$. For the numerical solution of the equations (A.1)–(A.2) without taking into account radiation reaction ($F_{\mathrm{rr}} = 0$), there are several methods, such as the Boris scheme [238], Vay scheme [239], and Higuera-Cary (HC) scheme [240]. The last of these schemes most accurately preserves the Hamiltonian of the system (and hence the phase volume), so this scheme is used in this work to solve the equations of motion of a single particle in given fields. The numerical algorithm corresponding to the scheme is explicitly written as follows

$$\mathbf{r}_{i+1} = \mathbf{r}_i + \Delta t \frac{\mathbf{p}_{i+1/2}}{\gamma_{i+1/2}}, \tag{A.3}$$

$$\mathbf{p}_{i+1/2} = 2\left(\tilde{\mathbf{p}} + \frac{\tilde{\mathbf{p}} \times \boldsymbol{\beta}}{\hat{\gamma}} + \boldsymbol{\beta}\frac{\tilde{\mathbf{p}} \cdot \boldsymbol{\beta}}{\hat{\gamma}^2}\right)\left(1 + \frac{\beta^2}{\hat{\gamma}^2}\right)^{-1} - \mathbf{p}_{i-1/2}, \tag{A.4}$$

$$\hat{\gamma}^2 = \frac{\tilde{\gamma}^2 - \beta^2}{2} + \sqrt{\frac{\left(\tilde{\gamma}^2 + \beta^2\right)^2}{4} + \left(\tilde{\mathbf{p}} \cdot \boldsymbol{\beta}\right)^2}, \tag{A.5}$$

where $\tilde{\mathbf{p}} = \mathbf{p}_{i-1/2} + \boldsymbol{\epsilon}$, $\tilde{\gamma} = \sqrt{1 + \tilde{\mathbf{p}} \cdot \tilde{\mathbf{p}}}$, $\boldsymbol{\epsilon} = -\mathbf{E}\Delta t/2$, $\boldsymbol{\beta} = -\mathbf{B}\Delta t/2$ (the sign "−" corresponds to the electron). Note that the coordinates (and the EM field) and momenta of the electron are determined at time moments shifted by half the step Δt relative to each other, which explains the half-integer indices of the momenta.

Two different approaches are used to take into account effect of radiation reaction. In the first, semiclassical approach (denoted in the figures by the abbreviation LL), radiative friction is considered a continuous force, which is added to the numerical scheme using the Euler method as follows:

first, a step is taken according to the Higuera-Cary scheme to calculate the momentum $\mathbf{p}_{\mathrm{HC},i+1/2}$, then the final momentum of the electron is determined as follows

$$\mathbf{p}_{i+1/2} = \mathbf{p}_{\mathrm{HC},i+1/2} - \Delta t F_{\mathrm{rr}}(\bar{\chi})\frac{\bar{\mathbf{p}}}{\bar{\gamma}}, \tag{A.6}$$

$$\bar{\chi} = \frac{1}{a_{\mathrm{S}}}\sqrt{(\bar{\gamma}\mathbf{E} + \bar{\mathbf{p}} \times \mathbf{B})^2 - (\bar{\mathbf{p}} \cdot E)^2}, \tag{A.7}$$

$$\bar{\mathbf{p}} = \frac{\mathbf{p}_{i-1/2} + \mathbf{p}_{\mathrm{HC},i+1/2}}{2}, \tag{A.8}$$

$$\bar{\gamma} = \sqrt{1 + \bar{\mathbf{p}} \cdot \bar{\mathbf{p}}}, \tag{A.9}$$

where $a_{\mathrm{S}} = mc^2/\hbar\omega$ is a normalized Sauter-Schwinger critical field. The second approach (denoted in the figures by the abbreviation MC) takes into account the quantum (stochastic) nature of radiation using the Monte Carlo method in a similar way to the method implemented in the QUILL code [167, 201]: at each step, two uniformly distributed in the interval $[0, 1]$ random numbers r_0 and r_1 are generated; then the probability W of an electron emitting a photon with energy $r_0\bar{\gamma}$ over a time interval Δt is calculated; if the inequality $r_1 < W$ is satisfied, then the value $r_0\bar{\mathbf{p}}$ is subtracted from the final electron momentum $\mathbf{p}_{\mathrm{HC},i+1/2}$, otherwise, the final momentum of the electron does not change. The value of W is calculated as follows [33]

$$W = \Delta t \frac{\alpha a_{\mathrm{S}}}{\sqrt{3}\pi\bar{\gamma}}\left(\frac{r_0^2 - 2r_0 + 2}{1 - r_0}K_{2/3}(y) - \int_y^{+\infty} K_{1/3}(x)\mathrm{d}x\right), \tag{A.10}$$

$$y = \frac{2}{3\bar{\chi}}\frac{r_0}{1 - r_0}, \tag{A.11}$$

where $K_\nu(x)$ is the modified Bessel function of the second kind.

Other various differential equations in this work are solved using the 8th order adaptive Runge-Kutta method (DOP853 [241]), unless otherwise is stated.

Acknowledgments

First, I would like to thank Prof. Igor Kostyukov from Institute of Applied Physics of Russian Academy of Sciences who has been my supervisor for the large portion of the conducted research and the head of the group where my professional career as a researcher has started. The present work would not be possible without his advice and support throughout the years. I thank Prof. Alexander Pukhov for providing me the opportunity to finish this work in his lab. A significant fraction of the presented work has been done in collaboration with his group, including Christoph Baumann, Marko Filipovic, Lars Reichwein and himself, which proved to be extremely interesting, helpful and fruitful. I would like to specially thank Lars Reichwein for helping me with the process of preparing the thesis for the defense and Eugen Braun for the technical assistance. I also thank both of them for providing advise that helped me settle in a new place, which ultimately made it possible to finish the thesis in a short period of time.

I also expresses deep gratitude to Evgeny Nerush for his valuable advice, assistance in the development of numerical models, important discussions of the results and his supervision during my Bachelor's degree. Thank you to Anton Golovanov for interesting and valuable discussions on both academic and non-academic topics. I thank both Evgeny Nerush and Anton Golovanov for developing the PIC code Quill, which was used in obtaining a significant part of the results, as well as for their valuable help in modifying this code.

Finally, I thank my family for invaluable support throughout my whole life and especially the past year.

Declaration of Authorship

I declare under oath that I have produced my thesis independently and without any undue assistance by third parties under consideration of the 'Principles for the Safeguarding of Good Scientific Practice at Heinrich Heine University Düsseldorf'

Düsseldorf, 10.04.2024

Alexander Samsonov

Bibliography

[1] F. Sauter, "*Uber das Verhalten eines Elektrons im homogenen elektrischen Feld nach der relativistischen Theorie Diracs*", Zeitschrift für Physik A **69**, 742–764 (1931).

[2] J. Schwinger, "*On Gauge Invariance and Vacuum Polarization*", Physical Review **82**, 664–679 (1951).

[3] *The Extreme Light Infrastructure (ELI): http://www.eli-laser.eu*.

[4] J. Zou et al., "*Design and current progress of the Apollon 10 PW project*", High Power Laser Science and Engineering **3**, e2 (2015).

[5] Z. Gan et al., "*The Shanghai Superintense Ultrafast Laser Facility (SULF) Project*", in Progress in Ultrafast Intense Laser Science XVI (Springer, 2021), pp. 199–217.

[6] B. Shao et al., "*Broad-bandwidth high-temporal-contrast carrier-envelope-phase-stabilized laser seed for 100 PW lasers*", Optics Letters **45**, 2215–2218 (2020).

[7] E. Khazanov et al., "*Exawatt Center for Extreme Light Studies (XCELS)*", High Power Laser Science and Engineering, 1–77 (2023).

[8] V. Veksler, "*The principle of coherent acceleration of charged particles*", The Soviet Journal of Atomic Energy **2**, 525–528 (1957).

[9] T. Tajima and J. M. Dawson, "*Laser electron accelerator*", Physical Review Letters **43**, 267 (1979).

[10] A. Pukhov and J. Meyer-ter-Vehn, "*Laser wake field acceleration: the highly non-linear broken-wave regime*", Applied Physics B **74**, 355–361 (2002).

[11] A. Pukhov et al., "*A laser–plasma accelerator producing monoenergetic electron beams*", Nature **431**, 541–544 (2004).

[12] E. Esarey, C. B. Schroeder, and W. P. Leemans, "*Physics of laser-driven plasma-based electron accelerators*", Reviews of modern physics **81**, 1229 (2009).

[13] C. E. Clayton et al., "*Self-guided laser wakefield acceleration beyond 1 GeV using ionization-induced injection*", Physical Review Letters **105**, 105003 (2010).

[14] I. Yu. Kostyukov and A. M. Pukhov, "*Plasma-based methods for electron acceleration: current status and prospects*", Physics-Uspekhi **58**, 81 (2015).

[15] M. Wen, M. Tamburini, and C. H. Keitel, "*Polarized laser-wakefield-accelerated kiloampere electron beams*", Physical Review Letters **122**, 214801 (2019).

[16] J. Palastro et al., "*Dephasingless laser wakefield acceleration*", Physical Review Letters **124**, 134802 (2020).

[17] T. Tajima, X. Yan, and T. Ebisuzaki, "*Wakefield acceleration*", Reviews of Modern Plasma Physics **4**, 1–72 (2020).

[18] M. E. Veisman, I. R. Umarov, D. V. Pugacheva, and N. E. Andreev, "*Multistage laser-plasma acceleration of ultrashort electron and positron bunches*", Quantum electronics **53**, 182–188 (2023).

[19] S. Wilks et al., "*Energetic proton generation in ultra-intense laser–solid interactions*", Physics of Plasmas **8**, 542–549 (2001).

[20] T. Esirkepov, M. Borghesi, S. V. Bulanov, G. Mourou, and T. Tajima, "*Highly efficient relativistic-ion generation in the laser-piston regime*", Physical Review Letters **92**, 175003 (2004).

[21] J. Fuchs et al., "*Laser-driven proton scaling laws and new paths towards energy increase*", Nature physics **2**, 48–54 (2006).

[22] S. Bulanov et al., "*Accelerating monoenergetic protons from ultrathin foils by flat-top laser pulses in the directed-Coulomb-explosion regime*", Physical Review E **78**, 026412 (2008).

[23] A. Macchi, M. Borghesi, and M. Passoni, "*Ion acceleration by superintense laser-plasma interaction*", Reviews of Modern Physics **85**, 751 (2013).

[24] S. Steinke et al., "*Stable laser-ion acceleration in the light sail regime*", Physical Review Special Topics - Accelerators and Beams **16**, 011303 (2013).

[25] V. Y. Bychenkov, A. V. Brantov, E. A. Govras, and V. F. Kovalev, "*Laser acceleration of ions: recent results and prospects for applications*", Physics-Uspekhi **58**, 71B (2015).

[26] A. Brantov, E. Govras, V. Kovalev, and V. Y. Bychenkov, "*Synchronized ion acceleration by ultraintense slow light*", Physical Review Letters **116**, 085004 (2016).

[27] A. S. Samsonov and I. Yu. Kostyukov, "*Acceleration of ions by the force of radiation pressure during the interaction of an extremely intense pulse of circularly polarized laser radiation with a solid target*", Bulletin of the Lebedev Physics Institute **50**, S749–S754 (2023).

[28] J. Vieira and J. Mendonça, "*Nonlinear laser driven donut wakefields for positron and electron acceleration*", Physical Review Letters **112**, 215001 (2014).

[29] S. Gessner et al., "*Demonstration of a positron beam-driven hollow channel plasma wakefield accelerator*", Nature communications **7**, 11785 (2016).

[30] J. Zhao et al., "*All-optical quasi-monoenergetic GeV positron bunch generation by twisted laser fields*", Communications Physics **5**, 15 (2022).

[31] L. Reichwein, A. Pukhov, A. Golovanov, and I. Yu. Kostyukov, "*Positron acceleration via laser-augmented blowouts in two-column plasma structures*", Physical Review E **105**, 055207 (2022).

[32] V. B. Berestetskii, E. M. Lifshitz, and L. P. Pitaevskii, *Quantum Electrodynamics* (Pergamon, New York, 1982).

[33] V. N. Baier, V. M. Katkov, and V. M. Strakhovenko, *Electromagnetic processes at high energies in oriented single crystals* (World Scientific, 1998).

[34] P. A. Dirac, "*Discussion of the infinite distribution of electrons in the theory of the positron*", in *Mathematical Proceedings of the Cambridge Philosophical Society*, Vol. 30, 2 (Cambridge University Press, 1934), pp. 150–163.

[35] R. Serber, "*Linear modifications in the Maxwell field equations*", Physical Review **48**, 49 (1935).

[36] E. A. Uehling, "*Polarization effects in the positron theory*", Physical Review **48**, 55 (1935).

[37] W. Heisenberg and H. Euler, "*Folgerungen aus der diracschen theorie des positrons*", Zeitschrift für Physik **98**, 714–732 (1936).

[38] G. W. Bennett et al., "*Final report of the E821 muon anomalous magnetic moment measurement at BNL*", Physical Review D **73**, 072003 (2006).

[39] D. Hanneke, S. Fogwell, and G. Gabrielse, "*New measurement of the electron magnetic moment and the fine structure constant*", Physical Review Letters **100**, 120801 (2008).

[40] "*Evidence for light-by-light scattering in heavy-ion collisions with the ATLAS detector at the LHC*", Nature physics **13**, 852–858 (2017).

[41] W. Furry, "*On bound states and scattering in positron theory*", Physical Review **81**, 115 (1951).

[42] D. M. Wolkow, "*Über eine klasse von lösungen der diracschen gleichung*", Zeitschrift für Physik **94**, 250–260 (1935).

[43] A. Fedotov et al., "*Advances in QED with intense background fields*", Physics Reports **1010**, 1–138 (2023).

[44] G. Breit and J. A. Wheeler, "*Collision of two light quanta*", Physical Review **46**, 1087 (1934).

[45] H. Hu, C. Müller, and C. H. Keitel, "*Complete QED theory of multiphoton trident pair production in strong laser fields*", Physical review letters **105**, 080401 (2010).

[46] A. R. Bell and J. G. Kirk, "*Possibility of Prolific Pair Production with High-Power Lasers*", Physical Review Letters **101**, 200403 (2008).

[47] C. Bula et al., "*Observation of nonlinear effects in Compton scattering*", Physical Review Letters **76**, 3116 (1996).

[48] D. Burke et al., "*Positron production in multiphoton light-by-light scattering*", Physical Review Letters **79**, 1626 (1997).

[49] K. Poder et al., "*Experimental signatures of the quantum nature of radiation reaction in the field of an ultraintense laser*", Physical Review X **8**, 031004 (2018).

[50] J. Cole et al., "*Experimental evidence of radiation reaction in the collision of a high-intensity laser pulse with a laser-wakefield accelerated electron beam*", Physical Review X **8**, 011020 (2018).

[51] S. Meuren, "*Probing strong-field QED at FACET-II (SLAC E-320)*", in *Third conference on extremely high intensity laser physics (ExHILP)*, Vol. 7 (2019).

[52] M. Tamburini, F. Pegoraro, A. D. Piazza, C. H. Keitel, and A. Macchi, "*Radiation reaction effects on radiation pressure acceleration*", New Journal of Physics **12**, 123005 (2010).

[53] M. Tamburini, T. V. Liseykina, F. Pegoraro, and A. Macchi, "*Radiation-pressure-dominant acceleration: Polarization and radiation reaction effects and energy increase in three-dimensional simulations*", Physical Review E **85**, 016407 (2012).

[54] I. Yu. Kostyukov, E. N. Nerush, and A. G. Litvak, "*Radiative damping in plasma-based accelerators*", Physical Review Special Topics - Accelerators and Beams **15**, 111001 (2012).

[55] R. Capdessus, E. d'Humières, and V. T. Tikhonchuk, "*Modeling of radiation losses in ultrahigh power laser-matter interaction*", Physical Review E **86**, 036401 (2012).

[56] R. Capdessus and P. McKenna, "*Influence of radiation reaction force on ultraintense laser-driven ion acceleration*", Physical Review E **91**, 053105 (2015).

[57] E. N. Nerush and I. Yu. Kostyukov, "*Laser-driven hole boring and gamma-ray emission in high-density plasmas*", Plasma Physics and Controlled Fusion **57**, 035007 (2015).

[58] E. G. Gelfer, A. M. Fedotov, and S. Weber, "*Theory and simulations of radiation friction induced enhancement of laser-driven longitudinal fields*", Plasma Physics and Controlled Fusion **60**, 064005 (2018).

[59] E. Gelfer, N. Elkina, and A. Fedotov, "*Unexpected impact of radiation friction: enhancing production of longitudinal plasma waves*", Scientific Reports **8**, 6478 (2018).

[60] E. G. Gelfer, A. M. Fedotov, and S. Weber, "*Radiation induced acceleration of ions in a laser irradiated transparent foil*", New Journal of Physics **23**, 095002 (2021).

[61] A. A. Golovanov, E. N. Nerush, and I. Yu. Kostyukov, "*Radiation reaction-dominated regime of wakefield acceleration*", New Journal of Physics **24**, 033011 (2022).

[62] A. Gonoskov et al., "*Anomalous Radiative Trapping in Laser Fields of Extreme Intensity*", Physical Review Letters **113**, 014801 (2014).

[63] L. L. Ji, A. Pukhov, I. Yu. Kostyukov, B. F. Shen, and K. Akli, "*Radiation-Reaction Trapping of Electrons in Extreme Laser Fields*", Physical Review Letters **112**, 145003 (2014).

[64] X.-L. Zhu et al., "*Enhanced electron trapping and γ ray emission by ultra-intense laser irradiating a near-critical-density plasma filled gold cone*", New Journal of Physics **17**, 053039 (2015).

[65] J. Kirk, "*Radiative trapping in intense laser beams*", Plasma Physics and Controlled Fusion **58**, 085005 (2016).

[66] M. Vranic, R. A. Fonseca, and L. O. Silva, "*Extremely intense laser-based electron acceleration in a plasma channel*", Plasma Physics and Controlled Fusion **60**, 034002 (2018).

[67] Z. Gong, F. Mackenroth, X. Yan, and A. Arefiev, "*Radiation reaction as an energy enhancement mechanism for laser-irradiated electrons in a strong plasma magnetic field*", Scientific reports **9**, 1–11 (2019).

[68] T. Grismayer, M. Vranic, J. L. Martins, R. A. Fonseca, and L. O. Silva, "*Laser absorption via quantum electrodynamics cascades in counter propagating laser pulses*", Physics of Plasmas **23**, 056706 (2016).

[69] P. Zhang, C. P. Ridgers, and A. G. R. Thomas, "*The effect of nonlinear quantum electrodynamics on relativistic transparency and laser absorption in ultra-relativistic plasmas*", New Journal of Physics **17**, 043051 (2015).

[70] M. A. Serebryakov, A. S. Samsonov, E. N. Nerush, and I. Yu. Kostyukov, "*Abnormal absorption of extremely intense laser pulses in relativistically underdense plasmas*", Physics of Plasmas **30**, 113303 (2023).

[71] T. V. Liseykina, S. V. Popruzhenko, and A. Macchi, "*Inverse Faraday effect driven by radiation friction*", New Journal of Physics **18**, 072001 (2016).

[72] T. V. Liseykina, A. Macchi, and S. V. Popruzhenko, "*Quantum effects on radiation friction driven magnetic field generation*", The European Physical Journal Plus **136**, 170 (2021).

[73] A. S. Samsonov, E. N. Nerush, and I. Yu. Kostyukov, "*Effect of electron–positron plasma production on the generation of a magnetic field in laser-plasma interactions*", Quantum Electronics **51**, 861 (2021).

[74] T. Liseykina, E. Peganov, and S. Popruzhenko, "*The Inverse Faraday Effect Induced by Radiation Friction during Irradiation of Dense Plasma with Crossed Multipetawatt Laser Beams*", Bulletin of the Lebedev Physics Institute **50**, S700–S705 (2023).

[75] D. Del Sorbo et al., "*Spin polarization of electrons by ultraintense lasers*", Physical Review A **96**, 043407 (2017).

[76] D. Del Sorbo, D. Seipt, A. G. R. Thomas, and C. P. Ridgers, "*Electron spin polarization in realistic trajectories around the magnetic node of two counter-propagating, circularly polarized, ultra-intense lasers*", Plasma Physics and Controlled Fusion **60**, 064003 (2018).

[77] Y. Chen, P. He, R. Shaisultanov, K. Z. Hatsagortsyan, and C. H. Keitel, "*Polarized Positron Beams via Intense Two-Color Laser Pulses*", Physical Review Letters **123**, 174801 (2019).

[78] D. Seipt, D. Del Sorbo, C. P. Ridgers, and A. G. R. Thomas, "*Ultrafast polarization of an electron beam in an intense bichromatic laser field*", Physical Review A **100**, 061402 (2019).

[79] Y. Wu et al., "*Polarized electron-beam acceleration driven by vortex laser pulses*", New Journal of Physics **21**, 073052 (2019).

[80] Y.-F. Li et al., "*Ultrarelativistic electron-beam polarization in single-shot interaction with an ultraintense laser pulse*", Physical Review Letters **122**, 154801 (2019).

[81] Y. Li, Y. Chen, W. Wang, and H. Hu, "*Production of Highly Polarized Positron Beams via Helicity Transfer from Polarized Electrons in a Strong Laser Field*", Physical Review Letters **125**, 044802 (2020).

[82] F. Wan et al., "*Ultrarelativistic polarized positron jets via collision of electron and ultraintense laser beams*", Physics Letters B **800**, 135120 (2020).

[83] H.-H. Song, W.-M. Wang, and Y.-T. Li, "*Generation of polarized positron beams via collisions of ultrarelativistic electron beams*", Physical Review Research **3**, 033245 (2021).

[84] Z. Gong, K. Z. Hatsagortsyan, and C. H. Keitel, "*Retrieving transient magnetic fields of ultrarelativistic laser plasma via ejected electron polarization*", Physical Review Letters **127**, 165002 (2021).

[85] K.-H. Zhuang, Y.-Y. Chen, Y.-F. Li, K. Z. Hatsagortsyan, and C. H. Keitel, "*Laser-driven lepton polarization in the quantum radiation-dominated reflection regime*", Physical Review D **108**, 033001 (2023).

[86] F. Aharonian, A. Belyanin, E. Derishev, V. Kocharovsky, and V. V. Kocharovsky, "*Constraints on the extremely high-energy cosmic ray accelerators from classical electrodynamics*", Physical Review D **66**, 023005 (2002).

[87] M. V. Medvedev, "*Constraint on electromagnetic acceleration of highest energy cosmic rays*", Physical Review E **67**, 045401 (2003).

[88] Y. Yuan, K. Nalewajko, J. Zrake, W. E. East, and R. D. Blandford, "*Kinetic study of radiation-reaction-limited particle acceleration during the relaxation of unstable force-free equilibria*", The Astrophysical Journal **828**, 92 (2016).

[89] B. Finkbeiner, H. Herold, T. Ertl, and H. Ruder, "*Effects of radiation damping on particle motion in pulsar vacuum fields*", Astronomy & Astrophysics **225**, 479–487 (1989).

[90] G. Cao and X. Yang, "*Three-dimensional dissipative pulsar magnetospheres with Aristotelian electrodynamics*", The Astrophysical Journal **889**, 29 (2020).

[91] D. A. Uzdensky, "*Radiative magnetic reconnection in astrophysics*", Magnetic Reconnection: Concepts and Applications, 473–519 (2016).

[92] A. M. Beloborodov, "*Radiative magnetic reconnection near accreting black holes*", The Astrophysical Journal **850**, 141 (2017).

[93] E. N. Nerush and I. Yu. Kostyukov, "*Radiation emission by extreme relativistic electrons and pair production by hard photons in a strong plasma wakefield*", Physical Review E **75**, 057401 (2007).

[94] E. N. Nerush et al., "*Laser Field Absorption in Self-Generated Electron-Positron Pair Plasma*", Physical Review Letters **106**, 035001 (2011).

[95] C. P. Ridgers et al., "*Dense Electron-Positron Plasmas and Ultraintense γ-rays from Laser-Irradiated Solids*", Physical Review Letters **108**, 165006 (2012).

[96] N. B. Narozhny and A. M. Fedotov, "*Quantum-electrodynamic cascades in intense laser fields*", Physics-Uspekhi **58**, 95 (2015).

[97] I. Yu. Kostyukov and E. N. Nerush, "*Production and dynamics of positrons in ultrahigh intensity laser-foil interactions*", Physics of Plasmas **23**, 093119 (2016).

[98] T. Grismayer, M. Vranic, J. L. Martins, R. A. Fonseca, and L. O. Silva, "*Seeded QED cascades in counterpropagating laser pulses*", Physical Review E **95**, 023210 (2017).

[99] M. Jirka, O. Klimo, M. Vranic, S. Weber, and G. Korn, "*QED cascade with 10 PW-class lasers*", Scientific Reports **7**, 15302 (2017).

[100] W. Luo et al., "*QED cascade saturation in extreme high fields*", Scientific Reports **8**, 8400 (2018).

[101] T. Yuan et al., "*Spatiotemporal distributions of pair production and cascade in solid targets irradiated by ultra-relativistic lasers with different polarizations*", Plasma Physics and Controlled Fusion **60**, 065003 (2018).

[102] D. Del Sorbo et al., "*Efficient ion acceleration and dense electron–positron plasma creation in ultra-high intensity laser-solid interactions*", New Journal of Physics **20**, 033014 (2018).

[103] Y. Lu et al., "*Enhanced copious electron–positron pair production via electron injection from a mass-limited foil*", Plasma Physics and Controlled Fusion **60**, 125008 (2018).

[104] W. Luo et al., "*Enhanced electron-positron pair production by two obliquely incident lasers interacting with a solid target*", Plasma Physics and Controlled Fusion **60**, 095006 (2018).

[105] E. S. Efimenko et al., "*Laser-driven plasma pinching in e^-e^+ cascade*", Physical Review E **99**, 031201 (2019).

[106] Y. P. Raizer and J. E. Allen, *Gas discharge physics*, Vol. 1 (Springer, 1991).

[107] W. M. Bollen, C. L. Yee, A. W. Ali, M. J. Nagurney, and M. E. Read, "*High-power microwave energy coupling to nitrogen during breakdown*", Journal of Applied Physics **54**, 101–106 (1983).

[108] V. Semenov, "*Breakdown wave in the self-consistent field of an electromagnetic wave beam*", Soviet Journal of Plasma Physics **8**, 347–350 (1982).

[109] G. V. Dunne, "*THE HEISENBERG–EULER EFFECTIVE ACTION: 75 YEARS ON*", International Journal of Modern Physics A **27**, 1260004 (2012).

[110] E. S. Efimenko et al., "*Extreme plasma states in laser-governed vacuum breakdown*", Scientific reports **8**, 2329 (2018).

[111] H. J. Bhabha and W. Heitler, "*The passage of fast electrons and the theory of cosmic showers*", Proceedings of the Royal Society of London. Series A-Mathematical and Physical Sciences **159**, 432–458 (1937).

[112] P. Meszaros, "*Gamma-ray bursts*", Reports on Progress in Physics **69**, 2259 (2006).

[113] P. Sturrock, "*A model of pulsars*", The Astrophysical Journal **164**, 529 (1971).

[114] M. Ruderman and P. G. Sutherland, “*Theory of pulsars-Polar caps, sparks, and coherent microwave radiation*”, The Astrophysical Journal **196**, 51–72 (1975).

[115] J. Daugherty and A. Harding, “*Electromagnetic cascades in pulsars*”, The Astrophysical Journal **252**, 337–347 (1982).

[116] A. A. Philippov, B. Cerutti, A. Tchekhovskoy, and A. Spitkovsky, “*Ab initio pulsar magnetosphere: the role of general relativity*”, The Astrophysical Journal Letters **815**, L19 (2015).

[117] S. Bulanov et al., “*On the problems of relativistic laboratory astrophysics and fundamental physics with super powerful lasers*”, Plasma Physics Reports **41**, 1–51 (2015).

[118] C. Adolphsen et al., *The International Linear Collider Technical Design Report - Volume 3.II: Accelerator Baseline Design*, 2013, arXiv:1306.6328 [physics.acc-ph].

[119] M. Aicheler et al., *A Multi-TeV Linear Collider Based on CLIC Technology: CLIC Conceptual Design Report*, CERN Yellow Reports: Monographs (CERN, Geneva, 2012).

[120] C. Schroeder, E. Esarey, C. Geddes, C. Benedetti, and W. Leemans, “*Physics considerations for laser-plasma linear colliders*”, Physical Review Special Topics - Accelerators and Beams **13**, 101301 (2010).

[121] R. Hollebeek, “*Disruption limits for linear colliders*”, Nuclear Instruments and Methods **184**, 333–347 (1981).

[122] K. Yokoya and P. Chen, “*Beam-beam phenomena in linear colliders*”, in Frontiers of Particle Beams: Intensity Limitations (Springer, 1992), pp. 415–445.

[123] P. Chen and K. Yokoya, “*Disruption effects from the interaction of round e^+e^- beams*”, Physical Review D **38**, 987 (1988).

[124] R. J. Noble, “*Beamstrahlung from colliding electron-positron beams with negligible disruption*”, Nuclear Instruments and Methods in Physics Research Section A: Accelerators, Spectrometers, Detectors and Associated Equipment **256**, 427–433 (1987).

[125] R. Blankenbecler and S. D. Drell, “*Quantum treatment of beamstrahlung*”, Physical Review D **36**, 277 (1987).

[126] M. Bell and J. S. Bell, “*Quantum beamstrahlung*”, in Quantum Mechanics, High Energy Physics And Accelerators: Selected Papers Of John S Bell (With Commentary) (World Scientific, 1995), pp. 99–104.

[127] P. Chen and V. I. Telnov, “*Coherent pair creation in linear colliders*”, Physical Review Letters **63**, 1796 (1989).

[128] J. Esberg, U. Uggerhøj, B. Dalena, and D. Schulte, “*Strong field processes in beam-beam interactions at the Compact Linear Collider*”, Physical Review Special Topics - Accelerators and Beams **17**, 051003 (2014).

[129] V. Yakimenko et al., “*Prospect of studying nonperturbative QED with beam-beam collisions*”, Physical Review Letters **122**, 190404 (2019).

[130] M. Tamburini and S. Meuren, "*Efficient high-energy photon production in the supercritical QED regime*", Physical Review D **104**, L091903 (2021).

[131] C. N. Danson et al., "*Petawatt and exawatt class lasers worldwide*", High Power Laser Science and Engineering **7**, e54 (2019).

[132] *Technical Design Report for the FACET-II Project at SLAC National Accelerator Laboratory* (2016).

[133] F. Del Gaudio, T. Grismayer, R. Fonseca, W. Mori, and L. Silva, "*Bright γ rays source and nonlinear Breit-Wheeler pairs in the collision of high density particle beams*", Physical Review Special Topics - Accelerators and Beams **22**, 023402 (2019).

[134] A. Nikishov and V. Ritus, "*Quantum processes in the field of a plane electromagnetic wave and in a constant field. I*", Soviet Physics JETP **19**, 529–541 (1964).

[135] V. Ritus, "*Quantum effects of the interaction of elementary particles with an intense electromagnetic field*", Journal of Soviet Laser Research **6**, 497–617 (1985).

[136] M. K. Khokonov and H. Nitta, "*Standard radiation spectrum of relativistic electrons: Beyond the synchrotron approximation*", Physical Review Letters **89**, 094801 (2002).

[137] A. Di Piazza, M. Tamburini, S. Meuren, and C. H. Keitel, "*Improved local-constant-field approximation for strong-field QED codes*", Physical Review A **99**, 022125 (2019).

[138] A. Ilderton, B. King, and D. Seipt, "*Extended locally constant field approximation for nonlinear Compton scattering*", Physical Review A **99**, 042121 (2019).

[139] T. Heinzl, B. King, and A. MacLeod, "*Locally monochromatic approximation to QED in intense laser fields*", Physical Review A **102**, 063110 (2020).

[140] E. Gelfer, A. Fedotov, A. Mironov, and S. Weber, "*Nonlinear Compton scattering in time-dependent electric fields beyond the locally constant crossed field approximation*", Physical Review D **106**, 056013 (2022).

[141] T. Podszus and A. Di Piazza, "*High-energy behavior of strong-field QED in an intense plane wave*", Physical Review D **99**, 076004 (2019).

[142] I. I. Artemenko, E. N. Nerush, and I. Yu. Kostyukov, "*Quasiclassical approach to synergic synchrotron-Cherenkov radiation in polarized vacuum*", New Journal of Physics **22**, 093072 (2020).

[143] J. G. Kirk, A. Bell, and I. Arka, "*Pair production in counter-propagating laser beams*", Plasma Physics and Controlled Fusion **51**, 085008 (2009).

[144] S. Bulanov, C. Schroeder, E. Esarey, and W. Leemans, "*Electromagnetic cascade in high-energy electron, positron, and photon interactions with intense laser pulses*", Physical Review A **87**, 062110 (2013).

[145] T. Z. Esirkepov et al., "*Attractors and chaos of electron dynamics in electromagnetic standing wave*", Physics Letters A **379**, 2044 (2015).

[146] F. Niel, C. Riconda, F. Amiranoff, R. Duclous, and M. Grech, "*From quantum to classical modeling of radiation reaction: A focus on stochasticity effects*", Physical Review E **97**, 043209 (2018).

[147] A. Gonoskov, T. Blackburn, M. Marklund, and S. Bulanov, "*Charged particle motion and radiation in strong electromagnetic fields*", Reviews of Modern Physics **94**, 045001 (2022).

[148] C. Shen and D. White, "*Energy straggling and radiation reaction for magnetic bremsstrahlung*", Physical Review Letters **28**, 455 (1972).

[149] R. Duclous, J. G. Kirk, and A. R. Bell, "*Monte Carlo calculations of pair production in high-intensity laser–plasma interactions*", Plasma Physics and Controlled Fusion **53**, 015009 (2010).

[150] C. Harvey, A. Gonoskov, A. Ilderton, and M. Marklund, "*Quantum quenching of radiation losses in short laser pulses*", Physical Review Letters **118**, 105004 (2017).

[151] N. Neitz and A. Di Piazza, "*Stochasticity effects in quantum radiation reaction*", Physical Review Letters **111**, 054802 (2013).

[152] C. Ridgers et al., "*Signatures of quantum effects on radiation reaction in laser–electron-beam collisions*", Journal of Plasma Physics **83**, 715830502 (2017).

[153] W. Gerlach and O. Stern, "*Der experimentelle nachweis der richtungsquantelung im magnetfeld*", Zeitschrift für Physik **9**, 349–352 (1922).

[154] L. H. Thomas, "*The motion of the spinning electron*", Nature **117**, 514–514 (1926).

[155] V. Bargmann, L. Michel, and V. Telegdi, "*Precession of the polarization of particles moving in a homogeneous electromagnetic field*", Physical Review Letters **2**, 435 (1959).

[156] S. Mane, Y. M. Shatunov, and K. Yokoya, "*Spin-polarized charged particle beams in high-energy accelerators*", Reports on Progress in Physics **68**, 1997 (2005).

[157] D. Seipt, C. P. Ridgers, D. Del Sorbo, and A. G. R. Thomas, "*Polarized QED cascades*", New Journal of Physics **23**, 053025 (2021).

[158] L. D. Landau, *The classical theory of fields*, Vol. 2 (Elsevier, 2013).

[159] H. Heintzmann and E. Schrüfer, "*Exact solutions of the Loretnz-Dirac equations of motion for charged particles in constant electromagnetic fields*", Physics Letters A **43**, 287–288 (1973).

[160] A. Gonoskov and M. Marklund, "*Radiation-dominated particle and plasma dynamics*", Physics of Plasmas **25**, 093109 (2018).

[161] A. M. Fedotov, N. V. Elkina, E. G. Gelfer, N. B. Narozhny, and H. Ruhl, "*Radiation friction versus ponderomotive effect*", Physical Review A **90**, 053847 (2014).

[162] A. Gruzinov, *Aristotelian electrodynamics solves the pulsar: lower efficiency of strong pulsars*, 2013, arXiv:1303.4094.

[163] J. Pétri, "*Particle acceleration and radiation reaction in a strongly magnetised rotating dipole*", Astronomy & Astrophysics **666**, A5 (2022).

[164] Y. Cai, S. E. Gralla, and V. Paschalidis, "*Dynamics of ultrarelativistic charged particles with strong radiation reaction. I. Aristotelian equilibrium state*", Physical Review D **108**, 063018 (2023).

[165] Y. B. Zel'dovich, "*Interaction of free electrons with electromagnetic radiation*", Soviet Physics Uspekhi **18**, 79 (1975).

[166] A. Fedotov, N. Narozhny, G. Mourou, and G. Korn, "*Limitations on the attainable intensity of high power lasers*", Physical Review Letters **105**, 080402 (2010).

[167] N. V. Elkina et al., "*QED cascades induced by circularly polarized laser fields*", Physical Review Special Topics - Accelerators and Beams **14**, 054401 (2011).

[168] A. Di Piazza, "*Exact solution of the Landau-Lifshitz equation in a plane wave*", Letters in Mathematical Physics **83**, 305–313 (2008), eprint: 0801.1751v2.

[169] J. E. Gunn and J. P. Ostriker, "*On the Motion and Radiation of Charged Particles in Strong Electromagnetic Waves. I. Motion in Plane and Spherical Waves*", The Astrophysical Journal **165**, 523 (1971).

[170] M. Grewing, E. Schrüfer, and H. Heintzmann, "*Acceleration of charged particles and radiation reaction in strong plane and spherical waves. II*", Zeitschrift für Physik A Hadrons and nuclei **260**, 375–384 (1973).

[171] K. Thielheim, "*Particle acceleration in extremely strong electromagnetic wave fields*", in *Proceedings of International Conference on Particle Accelerators* (IEEE, 1993), pp. 276–278.

[172] Y. Hadad et al., "*Effects of radiation reaction in relativistic laser acceleration*", Physical Review D **82**, 096012 (2010).

[173] R. Ekman, T. Heinzl, and A. Ilderton, "*Exact solutions in radiation reaction and the radiation-free direction*", New Journal of Physics **23**, 055001 (2021).

[174] Y. Cai, S. E. Gralla, and V. Paschalidis, "*Dynamics of ultrarelativistic charged particles with strong radiation reaction. II. Entry into Aristotelian equilibrium*", Physical Review D **108**, 063019 (2023).

[175] A. Gonoskov and M. Marklund, "*Radiation-dominated particle and plasma dynamics*", Physics of Plasmas **25**, 093109 (2018).

[176] A. S. Samsonov, E. N. Nerush, and I. Yu. Kostyukov, "*Asymptotic electron motion in the strongly-radiation-dominated regime*", Physical Review A **98**, 053858 (2018).

[177] A. S. Samsonov, E. N. Nerush, and I. Yu. Kostyukov, "*High-order corrections to the radiation-free dynamics of an electron in the strongly radiation-dominated regime*", Matter and Radiation at Extremes **8**, 014402 (2022).

[178] E. N. Nerush, D. A. Serebryakov, and I. Yu. Kostyukov, "*Weibel Instability in Hot Plasma Flows with the Production of Gamma-Rays and Electron–Positron Pairs*", The Astrophysical Journal **851**, 129 (2017).

[179] S. S. Bulanov, V. D. Mur, N. B. Narozhny, J. Nees, and V. S. Popov, "*Multiple colliding electromagnetic pulses: a way to lower the threshold of e^+e^- pair production from vacuum*", Physical Review Letters **104**, 220404 (2010).

[180] E. Nerush, V. Bashmakov, and I. Yu. Kostyukov, "*Analytical model for electromagnetic cascades in rotating electric field*", Physics of Plasmas **18**, 083107 (2011).

[181] I. Gonoskov, A. Aiello, S. Heugel, and G. Leuchs, "*Dipole pulse theory: Maximizing the field amplitude from 4π focused laser pulses*", Physical Review A **86**, 053836 (2012).

[182] A. Gonoskov et al., "*Probing nonperturbative QED with optimally focused laser pulses*", Physical Review Letters **111**, 060404 (2013).

[183] V. F. Bashmakov, E. N. Nerush, I. Yu. Kostyukov, A. M. Fedotov, and N. B. Narozhny, "*Effect of laser polarization on quantum electrodynamical cascading*", Physics of Plasmas **21**, 013105 (2014).

[184] A. A. Muraviev et al., "*Generation of current sheets and giant quasistatic magnetic fields at the ionization of vacuum in extremely strong light fields*", JETP Letters **102**, 148–153 (2015).

[185] E. G. Gelfer et al., "*Optimized multibeam configuration for observation of QED cascades*", Physical Review A **92**, 022113 (2015).

[186] A. Mironov, A. Fedotov, and N. Narozhny, "*Observable Features of QED Cascades in Collisions of GeV Electrons with Intense Laser Pulses*", in *Journal of Physics: Conference Series*, Vol. 826, 1 (IOP Publishing, 2017), p. 012029.

[187] I. Yu. Kostyukov, I. Artemenko, and E. Nerush, "*Growth rate of QED cascades in a rotating electric field*", Problems of Atomic Science and Technology, 259–263 (2018).

[188] B. Martinez, M. Lobet, R. Duclous, E. d'Humières, and L. Gremillet, "*High-energy radiation and pair production by Coulomb processes in particle-in-cell simulations*", Physics of Plasmas **26**, 103109 (2019).

[189] P. Zhang, S. S. Bulanov, D. Seipt, A. V. Arefiev, and A. G. R. Thomas, "*Relativistic plasma physics in supercritical fields*", Physics of Plasmas **27**, 050601 (2020).

[190] F. Salgado et al., "*Towards pair production in the non-perturbative regime*", New Journal of Physics **23**, 105002 (2021).

[191] M. Filipovic and A. Pukhov, "*QED effects at grazing incidence on solid-state targets*", The European Physical Journal D **76**, 187 (2022).

[192] A. Golub, S. Villalba-Chávez, and C. Müller, "*Nonlinear Breit-Wheeler pair production in collisions of bremsstrahlung γ quanta and a tightly focused laser pulse*", Physical Review D **105**, 116016 (2022).

[193] A. S. Samsonov, I. Yu. Kostyukov, M. Filipovic, and A. Pukhov, "*Generation of electron–positron pairs upon grazing incidence of a laser pulse on a foil*", Bulletin of the Lebedev Physics Institute **50**, S693–S699 (2023).

[194] M. V. S. Rao and B. V. Sreekantan, *Extensive air showers* (World scientific, 1998).

[195] A. Di Piazza, C. Müller, K. Hatsagortsyan, and C. H. Keitel, "*Extremely high-intensity laser interactions with fundamental quantum systems*", Reviews of Modern Physics **84**, 1177 (2012).

[196] S. Wilks, W. Kruer, M. Tabak, and A. Langdon, "*Absorption of ultra-intense laser pulses*", Physical Review Letters **69**, 1383 (1992).

[197] J. G. Kirk, A. R. Bell, and C. P. Ridgers, "*Pair plasma cushions in the hole-boring scenario*", Plasma Physics and Controlled Fusion **55**, 095016 (2013).

[198] A. Mironov, E. Gelfer, and A. Fedotov, "*Onset of electron-seeded cascades in generic electromagnetic fields*", Physical Review A **104**, 012221 (2021).

[199] C. K. Birdsall and A. B. Langdon, *Plasma physics via computer simulation* (CRC press, 2018).

[200] A. Gonoskov et al., "*Extended particle-in-cell schemes for physics in ultrastrong laser fields: Review and developments.*", Physical Review. E, Statistical, Nonlinear, and Soft Matter Physics **92**, 023305 (2015).

[201] *QUILL code — https://github.com/QUILL-PIC/Quill*.

[202] A. S. Samsonov, I. Yu. Kostyukov, and E. N. Nerush, "*Hydrodynamical model of QED cascade expansion in an extremely strong laser pulse*", Matter and Radiation at Extremes **6**, 034401 (2021).

[203] L. P. Pitaevskii and E. Lifshitz, *Physical Kinetics*, Vol. 10 (Butterworth-Heinemann, 2012).

[204] A. N. Timokhin, "*Time-dependent pair cascades in magnetospheres of neutron stars–I. Dynamics of the polar cap cascade with no particle supply from the neutron star surface*", Monthly Notices of the Royal Astronomical Society **408**, 2092–2114 (2010).

[205] A. S. Samsonov, E. N. Nerush, and I. Yu. Kostyukov, "*Laser-driven vacuum breakdown waves*", Scientific reports **9**, 11133 (2019).

[206] A. MacFadyen and S. Woosley, "*Collapsars: Gamma-ray bursts and explosions in "failed supernovae"*", The Astrophysical Journal **524**, 262 (1999).

[207] S. Woosley and A. MacFadyen, "*Central engines for gamma-ray bursts*", Astronomy & Astrophysics Supplement Series **138**, 499–502 (1999).

[208] R. C. Davidson and Q. Hong, *Physics of intense charged particle beams in high energy accelerators* (World Scientific, 2001).

[209] T. Katsouleas, J. Su, W. Mori, and J. Dawson, "*Plasma physics at the final focus of high-energy colliders*", Physics of Fluids B: Plasma Physics **2**, 1384–1389 (1990).

[210] P. Chen, "*An introduction to beamstrahlung and disruption*", in *Frontiers of Particle Beams* (1988), pp. 495–532.

[211] N. Phinney, *SLC Final Performance and Lessons* (2000).

[212] M. Abramowitz and I. A. Stegun, *Handbook of mathematical functions with formulas, graphs, and mathematical tables*, Vol. 55 (US Government printing office, 1964).

[213] A. Hartin, "*Strong field QED in lepton colliders and electron/laser interactions*", International Journal of Modern Physics A **33**, 1830011 (2018).

[214] M. Xie, "*Quantum suppression of beamstrahlung for future e^+e^- linear colliders: An evaluation of QED backgrounds*", in *AIP Conference Proceedings*, Vol. 472, 1 (American Institute of Physics, 1999), pp. 290–299.

[215] A. Pukhov, "*Three-dimensional electromagnetic relativistic particle-in-cell code VLPL (Virtual Laser Plasma Lab)*", Journal of Plasma Physics **61**, 425–433 (1999).

[216] A. Pukhov, "*Particle-In-Cell Codes for Plasma-based Particle Acceleration*", CERN Yellow Reports **1**, 10.5170/CERN-2016-001.181 (2016).

[217] C. Baumann and A. Pukhov, "*Influence of e^-e^+ creation on the radiative trapping in ultraintense fields of colliding laser pulses*", Physical Review E **94**, 063204 (2016).

[218] A. Pukhov, "*X-dispersionless Maxwell solver for plasma-based particle acceleration*", Journal of Computational Physics **418**, 109622 (2020).

[219] M. Bassetti et al., "*Properties and possible use of beam-beam synchrotron radiation*", IEEE Transactions on Nuclear Science **30**, 2182–2184 (1983).

[220] M. Filipovic, C. Baumann, A. Pukhov, A. S. Samsonov, and I. Yu. Kostyukov, "*Effect of transverse displacement of charged particle beams on quantum electrodynamic processes during their collision*", Quantum Electronics **51**, 807 (2021).

[221] Y. H. Chin, *Stability of a colliding Beam in a Linear Collider*, tech. rep. (DESY, 1987).

[222] J. Rosenzweig, B. Breizman, T. Katsouleas, and J. Su, "*Acceleration and focusing of electrons in two-dimensional nonlinear plasma wake fields*", Physical Review A **44**, R6189 (1991).

[223] M. D. Meyers, C.-K. Huang, Y. Zeng, S. Yi, and B. J. Albright, "*On the numerical dispersion of electromagnetic particle-in-cell code: Finite grid instability*", Journal of Computational Physics **297**, 565–583 (2015).

[224] A. Blinne et al., "*A systematic approach to numerical dispersion in Maxwell solvers*", Computer Physics Communications **224**, 273–281 (2018).

[225] I. Kostyukov, A. Pukhov, and S. Kiselev, "*Phenomenological theory of laser-plasma interaction in "bubble" regime*", Physics of Plasmas **11**, 5256–5264 (2004).

[226] A. Sampath et al., "*Extremely Dense Gamma-Ray Pulses in Electron Beam-Multifoil Collisions*", Physical Review Letters **126**, 064801 (2021).

[227] A. A. Golovanov, I. Yu. Kostyukov, L. Reichwein, J. Thomas, and A. Pukhov, "*Excitation of strongly nonlinear plasma wakefield by electron bunches*", Plasma Physics and Controlled Fusion **63**, 085004 (2021).

[228] X. Xu et al., "*Numerical instability due to relativistic plasma drift in EM-PIC simulations*", Computer Physics Communications **184**, 2503–2514 (2013).

[229] B. B. Godfrey and J.-L. Vay, "*Numerical stability of relativistic beam multidimensional PIC simulations employing the Esirkepov algorithm*", Journal of Computational Physics **248**, 33–46 (2013).

[230] Y. Lu et al., *An O(N) Maxwell solver with improved numerical dispersion properties*, 2019, arXiv:1907.13088 [physics.plasm-ph].

[231] X. Xu et al., "*On numerical errors to the fields surrounding a relativistically moving particle in PIC codes*", Journal of Computational Physics **413**, 109451 (2020).

[232] F. Li et al., "*A new field solver for modeling of relativistic particle-laser interactions using the particle-in-cell algorithm*", Computer Physics Communications **258**, 107580 (2021).

[233] A. D. Greenwood, K. L. Cartwright, J. W. Luginsland, and E. A. Baca, "*On the elimination of numerical Cerenkov radiation in PIC simulations*", Journal of Computational Physics **201**, 665–684 (2004).

[234] P. Yu et al., "*Mitigation of numerical Cerenkov radiation and instability using a hybrid finite difference-FFT Maxwell solver and a local charge conserving current deposit*", Computer Physics Communications **197**, 144–152 (2015).

[235] A. Samsonov, A. Pukhov, and I. Kostyukov, "*Superluminal phase velocity approach for suppression of Numerical Cherenkov Instability in Maxwell solver*", Journal of Physics: Conference Series **1692**, 012002 (2020).

[236] A. S. Samsonov et al., "*Beamstrahlung-enhanced disruption in beam-beam interaction*", New Journal of Physics **23**, 103040 (2021).

[237] A. S. Samsonov and I. Yu. Kostyukov, "*Simulation of Gamma-Ray Generation in Interaction of High-Current Ultrarelativistic Particle Beams with Plasma*", Optics and Spectroscopy **130**, 219–223 (2022).

[238] J. P. Boris et al., "*Relativistic plasma simulation-optimization of a hybrid code*", in *Proc. Fourth Conf. Num. Sim. Plasmas* (1970), pp. 3–67.

[239] J.-L. Vay, "*Simulation of beams or plasmas crossing at relativistic velocity*", Physics of Plasmas **15**, 056701 (2008).

[240] A. V. Higuera and J. R. Cary, "*Structure-preserving second-order integration of relativistic charged particle trajectories in electromagnetic fields*", Physics of Plasmas **24**, 052104 (2017).

[241] E. Hairer, S. P. Nørsett, and G. Wanner, *Solving ordinary differential equations. 1, Nonstiff problems* (Springer-Vlg, 1993).